

https://dspace.org/

Molecular detection of atypical bacteria and viruses linked to community-acquired pneumonia

Gumede, Nomathemba Michell

2009-09-22T10:50:00Z
http://hdl.handle.net/10539/7311

Downloaded from a DSpace repository. https://dspace.org/

MOLECULAR DETECTION OF ATYPICAL BACTERIA AND VIRUSES LINKED TO COMMUNITY-ACQUIRED PNEUMONIA

Nomathemba Michell Gumede

Degree of Master of Science in Medicine by research only

Dissertation submitted to the Faculty of Health Sciences, University of the Witwatersrand, Johannesburg, in fulfilment of the requirements for the degree of Master of Science in Medicine

Johannesburg, 2009

DECLARATION

I, Nomathemba Michell Gumede, declare that this dissertation is my own unaided work. It is being submitted for the degree of Master of Science in Medicine to the University of the Witwatersrand, Johannesburg. It has not been submitted before for any degree or examination at this or any other university.

…….. (Signature of candidate)

Signed this…… day of ……. 2009

DEDICATION

To Wandile T. Gumede, my loving son,

Ndabezinhle Dube, my pillar of strength

and

In loving memory of my late brother, Bukhosi M. Gumede

PRESENTATIONS

1. University of Witwatersrand Faculty Research Day, Parktown, South Africa, 20 August 2008. Multiplex real-time PCR for the detection of pathogens causing community-acquired pneumonia. Nomathemba Gumede, Olga Perovic, Adriano Duse, Else Marais.

ABSTRACT

Community-acquired pneumonia (CAP) is a major cause of morbidity and mortality worldwide. Knowledge of the predominant agents associated with CAP locally is essential, as it represents the basis for empiric antibiotic treatment. The objective of this study was to establish polymerase chain reaction (PCR)-based methods that could be used to identify CAP pathogens. Real-time PCR assays were developed to detect 10 viral and 5 non-viral pathogens as well as 2 internal controls using SYBR Green I and TaqMan probes, in singleplex and multiplex reactions. Six multiplex assays, with sensitivities of 1-10 copies/µl, were successfully developed to simultaneously detect 12 organisms. These reactions were used to test a limited number of patient and simulated samples. Data from the real-time PCR methods compared favourably to those from commercially available conventional PCR kits. These detection methods could be used to complement each other in prevalence studies and in selected diagnostic applications.

ACKNOWLEDGEMENTS

Supervisors:

My cordial thankfulness to my supervisor, **Dr Elsé Marais**, for her constant leadership and support throughout this very challenging project and to my co-supervisor, **Dr Olga Perovic**, for her invaluable input during this period.

Funding:

My earnest gratitude to the **Belgian Technical Cooperation** for awarding me a student fellowship to support the proceedings of this project.

General:

I am grateful to the **National Institute for Communicable Diseases** (NICD) and **Craig Corcoran** (University of Cape Town) for supplying positive controls in the form of viral culture supernatants, direct culture and nucleic acids for this project and to my **laboratory colleagues** (Department of Clinical Microbiology and Infectious Diseases, University of the Witwatersrand) for their valuable assistance. I acknowledge the assistance of **Kubendran Naidoo** and the Department of Molecular Medicine Haematology (University of the Witwatersrand) for allowing me to use their NanoDrop spectrophotometer for quantification purposes.

I am also thankful to my **sister, mother and father** for all their endeavours towards the completion of my degree; and to my son who kept me going and gave me the will to achieve.

Finally, to my soul mate and husband, **Ndabezinhle Dube**, whose constant love and encouragement has made these two years far less gruesome, I thank you.

TABLE OF CONTENTS

Page

DECLARATION ii
DEDICATION iii
PRESENTATIONS iv
ABSTRACT v
ACKNOWLEDGEMENTS vi
TABLE OF CONTENTS vii
LIST OF FIGURES xiii
LIST OF TABLES xxix
LIST OF ABBREVIATIONS AND ACRONYMS xxx

CHAPTER 1: INTRODUCTION

1.1. Community-acquired pneumonia----1

1.2. Diagnosis of CAP----3

1.3. PCR----4

1.4. Real-time PCR----5

1.4.1 Non-specific detection chemistries----8

1.4.2 Specific detection chemistries----11

1.5. Real-time PCR platform----13

1.6. Multiplex real-time PCR ----14

1.7. Dual Priming Oligonucleotide (DPO) system ----15

1.8. Brief description of organisms investigated----19

1.8.1. Viruses----19

. *1.8.1.1.* Influenza (Flu) A and B viruses----20

1.8.1.2. Human metapneumovirus (hMPV)----------22

1.8.1.3. Parainfluenza viruses (PIV) 1, 2 and 3----------24

1.8.1.4. Respiratory syncytial virus (RSV) ----------26

1.8.1.5. Adenovirus (AdV) ----------28

1.8.1.6. Cytomegalovirus (CMV)----------30

1.8.1.7. Epstein-Barr virus (EBV) ----------31

1.8.2 Bacteria ----------33

1.8.2.1. Chlamydia pneumoniae and *Chlamydia psittaci*----------33

1.8.2.2. Mycoplasma pneumoniae----------35

1.8.2.3. Legionella pneumophila----------37

1.8.3. Fungi ----------39

1.8.3.1. Pneumocystis jirovecii----------39

1.8.4. Glyceraldehyde-3-phosphate dehydrogenase (GAPDH)----------41

1.9. Statement of the problem ----------42

1.10. Justification of the study ----------42

1.11. Objectives----------44

Table of Contents

CHAPTER 2: MATERIALS AND METHODS

2.1.Bacterial and viral controls----------45

2.2. Sample collection----------45

2.3. DNA/RNA extraction----------46

2.3.1. Positive control extraction----------47

2.3.2. Specimen extraction----------48

2.4. Reverse Transcription----------49

2.5. Real-time PCR----------49

2.5.1. Primer sequences----------51

2.5.2. Probe sequences----------52

2.5.3. Singleplex reactions----------52

2.5.3.1. SYBR® Green I----------52

2.5.3.2. TaqMan probes----------54

2.5.4. Multiplex reactions----------55

2.6. Interpretation of real-time PCR data----------57

2.7. Agarose gel electrophoresis----------57

2.8. Seeplex detection kits----------57

2.9. Cloning----------58

2.10. Glycerol stock preparation----------61

2.11. Sensitivity assays----------61

CHAPTER 3A: RESULTS- REAL-TIME PCR ASSAYS (POSITIVE CONTROLS)

3.1. Singleplex reactions----------62

3.1.1. SYBR® Green I----------62

3.1.2. TaqMan probes----------71

3.2. Multiplex reactions----------78

3.3. Efficiency of reactions----------85

CHAPTER 3B: RESULTS- CLONING

3.4. Cloning----------87

CHAPTER 3C: RESULTS- SENSITIVITY ASSAYS

3.5. Singleplex reactions----------88

3.5.1. TaqMan probes----------89

3.5.2. SYBR® Green I----------95

3.6. Multiplex reactions----------97

3.7. Summary of sensitivities of real-time PCR assays----------104

CHAPTER 3D: RESULTS- PATIENT SAMPLES AND SIMULATED SAMPLES

3.8. Pathogen detection using Seeplex kits----------106

3.8.1. Seeplex® Pneumobacter ACE detection kit----------106

3.8.2. Seeplex® RV5 ACE detection kit----------107

3.9. Pathogen detection using real-time PCR assays----------110

3.9.1. Pathogen detection in simulated samples----------110

3.9.1.1. Singleplex reactions----------110

3.9.1.2. Multiplex reactions----------113

3.9.2. Pathogen detection in CAP patient samples----------113

3.10. Pathogen detection using microbiological methods----------116

CHAPTER 4: DISCUSSION

4.1. NucliSens miniMag System (miniMag) for nucleic acid extraction----------117

4.2. Molecular Methods----------119

4.2.1. Real-time PCR assays----------119

4.2.2. Seeplex detection kits----------119

4.3. Sensitivity of real-time PCR assays using TaqMan probes----------120

4.4. Fluorescence intensity is dependant on the dye attached to the probe----------120

4.5. TaqMan probes for real-time PCR assays----------121

4.6. Multiplex real-time PCR reactions----------123

4.7. Bacterial and viral detection on patient samples and simulations----------124

4.8. Limitations of study----------127

CHAPTER 5: CONCLUSION----------128

CHAPTER 6: REFERENCES----------130

CHAPTER 7: APPENDICES

Appendix A: Buffers, Media and Stains----------142

Appendix B: Agarose gels of singleplex real-time PCR reactions: positive controls and sensitivity assays----------144

Appendix C: Agarose gels of multiplex real-time PCR reactions: positive controls and sensitivity assays----------159

Appendix D: Agarose gels of real-time PCR reactions performed on patient samples and simulations ----------162

Appendix E: Real-time PCR results for patient samples and simulations----------167

Appendix F: Ethics clearance certificate----------183

LIST OF FIGURES

Figure 1.1: The PCR temperature cycle----------6

Figure 1.2: The PCR amplification curve indicating the different phases of PCR Amplification----------8

Figure 1.3: Real-time PCR SYBR Green I technology----------10

Figure 1.4: Melting curve analysis----------10

Figure 1.5: Real-time PCR 5' nuclease probe technology----------12

Figure 1.6: Fluorescence spectra of the Chromo4 real-time detection system----------13

Figure 1.7: The structure of DPO----------16

Figure 1.8: Diagrammatic illustration of the change in shape of the polydeoxyinosine linker into a bubble-like shape----------17

Figure 1.9: Diagrammatic illustration of the first priming reaction involving DPO----------17

Figure 1.10: Diagrammatic illustration of the second priming PCR reaction involving DPO----------18

Figure 1.11: Difference in conventional and DPO priming systems----------18

Figure 1.12: Shapes of human viral pathogens and the families they belong to----------20

Figure 1.13: Diagrammatic representation of influenza virus----------22

Figure 1.14: Structure of parainfluenza virus and respiratory syncytial virus----------26

Figure 3.1: Melting curve analysis of FluA generated when using SYBR Green I----------63

Figure 3.2: Melting curve analysis of FluB generated when using SYBR Green I----------63

Figure 3.3: Melting curve analysis of hMPV generated when using SYBR Green I----------64

Figure 3.4: Melting curve analysis of PIV1 generated when using SYBR Green I----------64

Figure 3.5: Melting curve analysis of PIV2 generated when using SYBR Green I----------65

Figure 3.6: Melting curve analysis of PIV3 generated when using SYBR Green I----------65

Figure 3.7: Melting curve analysis of AdV generated when using SYBR Green I----------66

Figure 3.8: Melting curve analysis of RSV generated when using SYBR Green I----------66

Figure 3.9: Melting curve analysis of CMV generated when using SYBR Green I----------67

Figure 3.10: Melting curve analysis of EBV generated when using SYBR Green I----------67

Figure 3.11: Melting curve analysis of *M. pneumoniae* generated when using SYBR Green I----------68

Figure 3.12: Melting curve analysis of *L. pneumophila* generated when using SYBR Green I----------68

Figure 3.13: Melting curve analysis of *C. pneumoniae* generated when using SYBR Green I----------69

Figure 3.14: Melting curve analysis of GAPDH (DNA) generated when using SYBR Green I----------69

Figure 3.15: Melting curve analysis of GAPDH (RNA) generated when using SYBR Green I----------70

Figure 3.16: Melting curve analysis of *P. jirovecii* generated when using SYBR Green I----------70

Figure 3.17: Melting curve analysis of *C. psittaci* generated when using SYBR Green I----------71

Figure 3.18: Real-time PCR singleplex analysis of FluA using a TaqMan probe----------72

Figure 3.19: Real-time PCR singleplex analysis of FluB using a TaqMan probe----------72

Figure 3.20: Real-time PCR singleplex analysis of hMPV using a TaqMan probe----------73

Figure 3.21: Real-time PCR singleplex analysis of PIV1 using a TaqMan probe----------73

Figure 3.22: Real-time PCR singleplex analysis of PIV3 using a TaqMan probe----------74

Figure 3.23: Real-time PCR singleplex analysis of AdV using a TaqMan probe----------74

Figure 3.24: Real-time PCR singleplex analysis of RSV using a TaqMan probe----------75

Figure 3.25: Real-time PCR singleplex analysis of CMV using a TaqMan probe----------75

Figure 3.26: Real-time PCR singleplex analysis of EBV using a TaqMan probe----------76

Figure 3.27: Real-time PCR singleplex analysis of *M. pneumoniae* using a TaqMan probe----------76

Figure 3.28: Real-time PCR singleplex analysis of *L. pneumophila* using a TaqMan probe----------77

Figure 3.29: Real-time PCR singleplex analysis of *C. pneumoniae* using a TaqMan probe----------77

Figure 3.30: Real-time PCR singleplex analysis of GAPDH (DNA) using a TaqMan probe----------78

Figure 3.31a: Real-time PCR analysis of PIV1 in a multiplex reaction using a TaqMan probe----------79

Figure 3.31b: Real-time PCR analysis of PIV3 in a multiplex reaction using a TaqMan probe----------79

Figure 3.32a: Real-time PCR analysis of RSV in a multiplex reaction using a TaqMan probe----------80

Figure 3.32b: Real-time PCR analysis of AdV in a multiplex reaction using a TaqMan probe----------80

Figure 3.33a: Real-time PCR analysis of EBV in a multiplex reaction using a TaqMan probe----------81

Figure 3.33b: Real-time PCR analysis of CMV in a multiplex reaction using a TaqMan probe----------81

Figure 3.34a: Real-time PCR analysis of *M. pneumoniae* in a multiplex reaction using a TaqMan probe----------82

Figure 3.34b: Real-time PCR analysis of *L. pneumophila* in a multiplex reaction using a TaqMan probe----------82

Figure 3.35a: Real-time PCR analysis of GAPDH (DNA) in a multiplex reaction using a TaqMan probe----------83

Figure 3.35b: Real-time PCR analysis of *C. pneumoniae* in a multiplex reaction using a TaqMan probe----------83

Figure 3.36a: Real-time PCR analysis of FluA in a multiplex reaction using a TaqMan probe----------84

Figure 3.36b: Real-time PCR analysis of FluB in a multiplex reaction using a TaqMan probe----------84

Figure 3.36c: Real-time PCR analysis of hMPV in a multiplex reaction using a TaqMan probe----------85

Figure 3.37: Bar chart illustrating the difference in amplification efficiencies between TaqMan probes and SYBR Green I for each organism----------86

Figure 3.38: Blue-white screening of transformed cells plated out on LB agar supplemented with ampicillin, X-gal and IPTG----------87

Figure 3.39: Fluorescence of FluA plasmid serial dilutions demonstrating the sensitivity of the TaqMan assay----------89

Figure 3.40: Fluorescence of FluB plasmid serial dilutions demonstrating the sensitivity of the TaqMan assay----------89

Figure 3.41: Fluorescence of hMPV plasmid serial dilutions demonstrating the sensitivity of the TaqMan assay----------90

Figure 3.42: Fluorescence of PIV1 plasmid serial dilutions demonstrating the sensitivity of the TaqMan assay----------90

Figure 3.43: Fluorescence of PIV3 plasmid serial dilutions demonstrating the sensitivity of the TaqMan assay----------91

Figure 3.44: Fluorescence of AdV plasmid serial dilutions demonstrating the sensitivity of the TaqMan assay----------91

Figure 3.45: Fluorescence of RSV plasmid serial dilutions demonstrating the sensitivity of the TaqMan assay----------92

Figure 3.46: Fluorescence of CMV plasmid serial dilutions demonstrating the sensitivity of the TaqMan assay----------92

Figure 3.47: Fluorescence of EBV plasmid serial dilutions demonstrating the sensitivity of the TaqMan assay----------93

Figure 3.48: Fluorescence of *M. pneumoniae* plasmid serial dilutions demonstrating the sensitivity of the TaqMan assay----------93

Figure 3.49: Fluorescence of *L. pneumophila* plasmid serial dilutions demonstrating the sensitivity of the TaqMan assay----------94

Figure 3.50: Fluorescence of *C. pneumoniae* plasmid serial dilutions demonstrating the sensitivity of the TaqMan assay----------94

Figure 3.51: Fluorescence of GAPDH (DNA) plasmid serial dilutions demonstrating the sensitivity of the TaqMan assay----------95

Figure 3.52: Fluorescence of *P. jirovecii* plasmid serial dilutions demonstrating the sensitivity of the SYBR Green I assay----------95

Figure 3.53: Fluorescence of *C. psittaci* plasmid serial dilutions demonstrating the sensitivity of the SYBR Green I assay----------96

Figure 3.54: Fluorescence of PIV2 plasmid serial dilutions demonstrating the sensitivity of the SYBR Green I assay----------96

Figure 3.55a: Fluorescence graph of RSV multiplex reaction indicating sensitivity of the TaqMan assay----------97

Figure 3.55b: Fluorescence graph of AdV multiplex reaction indicating sensitivity of the TaqMan assay----------98

Figure 3.56a: Fluorescence graph of EBV multiplex reaction indicating sensitivity of the TaqMan assay----------98

Figure 3.56b: Fluorescence graph of CMV multiplex reaction indicating sensitivity of the TaqMan assay----------99

Figure 3.57a: Fluorescence graph of GAPDH (DNA) multiplex reaction indicating sensitivity of the TaqMan assay----------99

Figure 3.57b: Fluorescence graph of *C. pneumoniae* multiplex reaction indicating sensitivity of the TaqMan assay----------100

Figure 3.58a: Fluorescence graph of *M. pneumoniae* multiplex reaction indicating sensitivity of the TaqMan assay----------100

Figure 3.58b: Fluorescence graph of *L. pneumophila* multiplex reaction indicating sensitivity of the TaqMan assay----------103

Figure 3.59a: Fluorescence graph of PIV1 multiplex reaction indicating sensitivity of the TaqMan assay----------101

Figure 3.59b: Fluorescence graph of PIV3 multiplex reaction indicating sensitivity of the TaqMan assay----------102

Figure 3.60a: Fluorescence graph of FluA multiplex reaction indicating sensitivity of the TaqMan assay----------102

Figure 3.60b: Fluorescence graph of FluB multiplex reaction indicating sensitivity of the TaqMan assay----------103

Figure 3.60c: Fluorescence graph of hMPV multiplex reaction indicating sensitivity of the TaqMan assay----------103

Figure 3.61: PCR results obtained using Seeplex® Pneumobacter ACE detection kit----------107

Figure 3.62: PCR results obtained using Seeplex® RV5 ACE detection kit----------109

Figure 3.63: Analysis of real-time PCR results obtained from nasopharyngeal swabs spiked with different viral cultures simulating multiple viral infections in a patient----------111

Figure 3.64: Analysis of real-time PCR results obtained from cystic fibrosis patient sputum samples spiked with bacterial cultures of *C. pneumoniae* and *C. psittaci* and a colony of *L. pneumophila* simulating multiple bacterial infections in a patient----------112

Figure B1A: Agarose gel electrophoresis of CMV positive control using SYBR Green I------144

Figure B1B: Agarose gel electrophoresis of CMV positive control using TaqMan probes-----144

Figure B1C: Agarose gel electrophoresis of CMV sensitivity assay performed on plasmids using TaqMan probes----------144

Figure B2A: Agarose gel electrophoresis of EBV positive control using SYBR Green I-------145

Figure B2B: Agarose gel electrophoresis of EBV positive control using TaqMan probes------145

Figure B2C: Agarose gel electrophoresis of EBV sensitivity assay performed on plasmids using TaqMan probes----------145

Figure B3A: Agarose gel electrophoresis of PIV1 positive control using SYBR Green I-------146

Figure B3B: Agarose gel electrophoresis of PIV1 positive control using TaqMan probes-----146

Figure B3C: Agarose gel electrophoresis of PIV1 sensitivity assay performed on plasmids using TaqMan probes----------146

Figure B4A: Agarose gel electrophoresis of AdV positive control using SYBR Green I-------147

Figure B4B: Agarose gel electrophoresis of AdV positive control using TaqMan probes------147

Figure B4C: Agarose gel electrophoresis of AdV sensitivity assay performed on plasmids using TaqMan probes----------147

Figure B5A: Agarose gel electrophoresis of PIV3 positive control using SYBR Green I--------148

Figure B5B: Agarose gel electrophoresis of PIV3 positive control using TaqMan probes------148

Figure B5C: Agarose gel electrophoresis of PIV3 sensitivity assay performed on plasmids using TaqMan probes----------148

Figure B6A: Agarose gel electrophoresis of RSV positive control using SYBR Green I--------149

Figure B6B: Agarose gel electrophoresis of RSV positive control using TaqMan probes-------149

Figure B6C: Agarose gel electrophoresis of RSV sensitivity assay performed on plasmids using TaqMan probes----------149

Figure B7A: Agarose gel electrophoresis of hMPV positive control using SYBR Green I------150

Figure B7B: Agarose gel electrophoresis of hMPV positive control using TaqMan probes-----150

Figure B7C: Agarose gel electrophoresis of hMPV sensitivity assay performed on plasmids using TaqMan probes----------150

Figure B8A: Agarose gel electrophoresis of positive controls of FluA and FluB using SYBR Green I----------151

Figure B8B: Agarose gel electrophoresis of positive control of FluB using TaqMan probes----------151

Figure B8C: Agarose gel electrophoresis of positive control of FluA using TaqMan probes----------151

Figure B8D: Agarose gel electrophoresis of sensitivity assay of FluA performed on plasmids using TaqMan probes----------151

Figure B8E: Agarose gel electrophoresis of sensitivity assay of FluB performed on plasmids using TaqMan probes----------152

Figure B9A: Agarose gel electrophoresis of positive controls of *M. pneumoniae* and *L. pneumophila* using SYBR Green I----------153

Figure B9B: Agarose gel electrophoresis of positive control of *M. pneumoniae* using TaqMan probes----------153

Figure B9C: Agarose gel electrophoresis of positive control of *L. pneumophila* using TaqMan probes----------153

Figure B9D: Agarose gel electrophoresis of sensitivity assay of *L. pneumophila* performed on plasmids using TaqMan probes----------153

Figure B9E: Agarose gel electrophoresis of sensitivity assay of *M. pneumoniae* performed on plasmids using TaqMan probes----------154

Figure B10A: Agarose gel electrophoresis of positive control of GAPDH (DNA) using SYBR Green I----------155

Figure B10B: Agarose gel electrophoresis of positive control of GAPDH (RNA) using SYBR Green I----------155

Figure B10C: Agarose gel electrophoresis of positive control of GAPDH (DNA) using TaqMan probes----------155

Figure B10D: Agarose gel electrophoresis of GAPDH (DNA) sensitivity assay performed on plasmids using TaqMan probes----------155

Figure B11A: Agarose gel electrophoresis of *C. pneumoniae* positive control using SYBR Green I----------156

Figure B11B: Agarose gel electrophoresis of *C. pneumoniae* positive control using TaqMan probes----------156

Figure B11C: Agarose gel electrophoresis of *C. pneumoniae* sensitivity assay performed on plasmids using TaqMan probes----------157

Figure B12A: Agarose gel electrophoresis of *P. jirovecii* positive control using SYBR Green I----------157

Figure B12B: Agarose gel electrophoresis of *P. jirovecii* sensitivity assay performed on plasmids using SYBR Green I----------157

Figure B13A: Agarose gel electrophoresis of *C. psittaci* positive control using SYBR Green I----------157

Figure B13B: Agarose gel electrophoresis of *C. psittaci* sensitivity assay performed on plasmids using SYBR Green I----------157

Figure B14A: Agarose gel electrophoresis of PIV2 positive control using SYBR Green I----------158

Figure B14B: Agarose gel electrophoresis of PIV2 sensitivity assay performed on plasmids using SYBR Green I----------158

Figure C1A: Agarose gel of CMV and EBV multiplex reaction obtained using TaqMan probes on positive controls----------159

Figure C1B: Agarose gel of CMV and EBV multiplex reaction obtained using TaqMan probes on plasmids at the lowest detectable concentration----------159

Figure C2A: Agarose gel of AdV and RSV multiplex reaction obtained using TaqMan probes on positive controls----------159

Figure C2B: Agarose gel of AdV and RSV multiplex reaction obtained using TaqMan probes on plasmids at the lowest detectable concentration----------159

Figure C3A: Agarose gel of FluA, FluB and hMPV multiplex reaction obtained using TaqMan probes on positive controls----------160

Figure C3B: Agarose gel of FluA, FluB and hMPV multiplex reaction obtained using TaqMan probes on plasmids at the lowest detectable concentration----------160

Figure C4A: Agarose gel of PIV1 and PIV3 multiplex reaction obtained using TaqMan probes on positive controls----------160

Figure C4B: Agarose gel of PIV1 and PIV3 multiplex reaction obtained using TaqMan probes on plasmids at the lowest detectable concentration----------160

Figure C5A: Agarose gel of *L. pneumophila* and *M. pneumoniae* multiplex reaction obtained using TaqMan probes on positive controls----------161

Figure C5B: Agarose gel of *L. pneumophila* and *M. pneumoniae* multiplex reaction obtained using TaqMan probes on plasmids at the lowest detectable concentration----------161

Figure C6A: Agarose gel of *C. pneumoniae* and GAPDH (DNA) multiplex reaction obtained using TaqMan probes on positive controls----------161

Figure C6B: Agarose gel of *C. pneumoniae* and GAPDH (DNA) multiplex reaction obtained using TaqMan probes on plasmids at the lowest detectable concentration----------161

Figure D1: Agarose gel of *C. pneumoniae* real-time PCR product obtained from simulated sputum samples----------162

Figure D2: Agarose gel of *C. psittaci* real-time PCR product obtained from simulated sputum samples----------162

Figure D3: Agarose gel of CMV real-time PCR product obtained from simulated nasopharyngeal swabs----------162

Figure D4: Agarose gel of FluA real-time PCR product obtained from simulated nasopharyngeal swabs----------162

Figure D5: Agarose gel of GAPDH (DNA) real-time PCR product obtained from simulated sputum samples----------163

Figure D6: Agarose gel of *L. pneumophila* real-time PCR product obtained from simulated sputum samples----------163

Figure D7: Agarose gel of *C. pneumoniae* and GAPDH (DNA) multiplex reaction obtained from simulated sputum samples----------163

Figure D8: Agarose gel of PIV1 real-time PCR product obtained from simulated nasopharyngeal swabs----------163

Figure D9: Agarose gel of PIV2 real-time PCR product obtained from simulated nasopharyngeal swabs----------164

Figure D10: Agarose gel of RSV real-time PCR product obtained from simulated nasopharyngeal swabs----------164

Figure D11: Agarose gel of *C. psittaci* real-time PCR product obtained from CAP patient sputum samples----------164

Figure D12: Agarose gel of *P. jirovecii* real-time PCR product obtained from CAP patient sputum samples----------164

Figure D13: Agarose gel of PIV2 real-time PCR product obtained from CAP patient nasopharyngeal swabs----------165

Figure D14: Agarose gel of AdV and RSV multiplex real-time PCR product obtained from CAP patient nasopharyngeal swabs----------165

Figure D15: Agarose gel of FluA, FluB and hMPV multiplex real-time PCR product obtained from CAP patient nasopharyngeal swabs----------165

Figure D16: Agarose gel of PIV1 and PIV3 multiplex real-time PCR product obtained from CAP patient nasopharyngeal swabs----------165

Figure D17: Agarose gel of *C. pneumoniae* and GAPDH (DNA) multiplex real-time PCR product obtained from CAP patient sputum samples----------166

Figure D18: Agarose gel of CMV and EBV multiplex real-time PCR product obtained from CAP patient nasopharyngeal swabs----------166

Figure D19: Agarose gel of *M. pneumoniae* and *L. pneumophila* multiplex real-time PCR product obtained from CAP patient sputum samples----------166

Figure E1: Fluorescence graph of GAPDH (DNA) singleplex reaction performed on nucleic acids extracted from spiked sputum samples----------167

Figure E2: Fluorescence graph of FluA singleplex reaction performed on nucleic acids extracted from spiked nasopharyngeal swabs----------168

Figure E3: Fluorescence graph of PIV1 singleplex reaction performed on nucleic acids extracted from spiked nasopharyngeal swabs----------168

Figure E4: Fluorescence graph of RSV singleplex reaction performed on nucleic acids extracted from spiked nasopharyngeal swabs----------169

Figure E5: Fluorescence graph of CMV singleplex reaction performed on nucleic acids extracted from spiked nasopharyngeal swabs----------169

Figure E6: Fluorescence graph of *L. pneumophila* singleplex reaction performed on nucleic acids extracted from spiked sputum samples----------170

Figure E7: Fluorescence graph of *C. pneumoniae* singleplex reaction performed on nucleic acids extracted from spiked sputum samples----------170

Figure E8: Melting curve analysis of *C. psittaci* singleplex reaction performed on nucleic acids extracted from spiked sputum samples----------171

Figure E9: Melting curve analysis of PIV2 singleplex reaction performed on nucleic acids extracted from spiked nasopharyngeal swabs----------171

Figure E10a: Fluorescence graph of GAPDH (DNA) multiplex reaction performed on nucleic acids extracted from spiked sputum samples----------172

Figure E10b: Fluorescence graph of *C. pneumoniae* multiplex reaction performed on nucleic acids extracted from spiked sputum samples----------172

Figure E11: Fluorescence graph of GAPDH (DNA) singleplex reaction performed on nucleic acids extracted from sputum samples taken from CAP patients----------173

Figure E12: Fluorescence graph of GAPDH (DNA) singleplex reaction performed on nucleic acids extracted from nasopharyngeal swabs taken from CAP patients----------173

Figure E13: Melting curve analysis of GAPDH (RNA) singleplex reaction performed on nucleic acids extracted from sputum samples taken from CAP patients----------174

Figure E14: Melting curve analysis of *P. jirovecii* singleplex reaction performed on nucleic acids extracted from sputum samples taken from CAP patients----------174

Figure E15: Melting curve analysis of *C. psittaci* singleplex reaction performed on nucleic acids extracted from sputum samples taken from CAP patients----------175

Figure E16: Melting curve analysis of PIV2 singleplex reaction performed on nucleic acids extracted from nasopharyngeal swabs taken from CAP patients----------175

Figure E17a: Fluorescence graph of PIV1 multiplex reaction performed on nucleic acids extracted from nasopharyngeal swabs taken from CAP patients----------176

Figure E17b: Fluorescence graph of PIV3 multiplex reaction performed on nucleic acids extracted from nasopharyngeal swabs taken from CAP patients----------176

Figure E18a: Fluorescence graph of CMV multiplex reaction performed on nucleic acids extracted from nasopharyngeal swabs taken from CAP patients----------177

Figure E18b: Fluorescence graph of EBV multiplex reaction performed on nucleic acids extracted from nasopharyngeal swabs taken from CAP patients----------177

Figure E19a: Fluorescence graph of *M. pneumoniae* multiplex reaction performed on nucleic acids extracted from sputum samples taken from CAP patients----------178

Figure E19b: Fluorescence graph of *L. pneumophila* multiplex reaction performed on nucleic acids extracted from sputum samples taken from CAP patients----------178

Figure E20a: Fluorescence graph of RSV multiplex reaction performed on nucleic acids extracted from nasopharyngeal swabs taken from CAP patients----------179

Figure E20b: Fluorescence graph of AdV multiplex reaction performed on nucleic acids extracted from nasopharyngeal swabs taken from CAP patients----------179

Figure E21a: Fluorescence graph of GAPDH (DNA) multiplex reaction performed on nucleic acids extracted from sputum samples taken from CAP patients----------180

Figure E21b: Fluorescence graph of *C. pneumoniae* multiplex reaction performed on nucleic acids extracted from sputum samples taken from CAP patients----------180

Figure E22a: Fluorescence graph of FluA multiplex reaction performed on nucleic acids extracted from nasopharyngeal swabs taken from CAP patients----------181

Figure E22b: Fluorescence graph of FluB multiplex reaction performed on nucleic acids extracted from nasopharyngeal swabs taken from CAP patients----------181

Figure E22c: Fluorescence graph of hMPV multiplex reaction performed on nucleic acids extracted from nasopharyngeal swabs taken from CAP patients----------182

LIST OF TABLES

Table 1.1: Functions performed by GAPDH in mammalian cells----------43

Table 2.1: Primer sequences and final concentrations used for real-time PCR assays and product sizes----------51

Table 2.2: TaqMan probe sequences and final concentrations used for real-time PCR assays----------52

Table 2.3: Real-time PCR thermocycling conditions for FluA, FluB and hMPV----------53

Table 2.4: Real-time PCR thermocycling conditions for *P. jirovecii*----------54

Table 3.1: Comparison of results obtained from real-time PCR assays and Seeplex® Pneumobacter ACE detection kit----------114

Table 3.2: Comparison of results obtained from real-time PCR assays and Seeplex® RV5 ACE detection kit----------115

Table 3.3: Diagnosis of patients 1, 2 and 3----------116

LIST OF ABBREVIATIONS AND ACRONYMS

AIDS	Acquired Immunodeficiency Syndrome
ACE	auto-capillary electrophoresis
AdV	adenovirus
ASE	auto-sequencer electrophoresis
ATP	adenosine triphosphate
BAL	bronchoalveolar lavage
BBQ	BlackBerry quencher
BHQ1, 2 and 3	Black hole quencher 1, 2 and 3
bp	base pair
CAP	community-acquired pneumonia
CFU/µl	colony forming units per microliter
C_t	threshold cycle
Cy3	indocarbocyanine
Cy5	tetramethyl-indodicarbocyanine
CMV	cytomegalovirus
DNA	deoxyribonucleic acid
dNTPs	deoxy-nucleotide triphosphates
DMSO	dimethyl sulfoxide
DPO	dual priming oligonucleotide
°C	degrees Celsius
EDTA	ethylenediaminetetraacetic acid
EBV	Epstein-Barr virus
F	fusion
FAM	6-carboxyfluorescein
Fe_3O_4	iron oxide
FKBP	FK506 binding protein
FluA	influenza A virus
FluB	influenza B virus
G	attachment glycoprotein
GAPDH	glyceraldehyde-3-phosphate dehydrogenase

H_2O	water
HAART	highly active antiretroviral therapy
hMPV	human metapneumovirus
HEX	hexachloro-6-carboxyfluoroscein
HIV	Human Immunodeficiency Virus
hrs	hours
JOE	2′,7′-dimethoxy-4′5′-dichloro-6-carboxyfluoresce in
kb	kilo base
kDa	kilo daltons
Kbp	kilobase pairs
L	polymerase
LB	Luria-Bertani
LNA	locked nucleic acid
LRTI	lower respiratory tract infections
MES	morpholine-4-ethanesulfonic acid
mg	milligrams
MGB	minor groove binding
min	minute
mip	macrophage infectivity potentiator
µl	microliters
ml	milliliters
µM	micromolar
MOMP	major outer membrane protein
mtLSU rRNA	mitochondrial large subunit rRNA
N	neuraminidase
Neu5Ac	N-acetyl neuraminic acid
NICD	National Institute for Communicable Diseases
nm	nanometre
NS1 and NS2	non-structural proteins 1 and 2
NP	nucleoprotein
NTC	no template controls
OmpA	outer membrane protein
P	phosphoprotein

PCR	Polymerase Chain Reaction
PIV1	parainfluenza virus 1
PIV2	parainfluenza virus 2
PIV3	parainfluenza virus 3
RAPD	random amplification of polymorphic DNA
RFLP	restriction fragment length polymorphism
RNA	ribonucleic acid
ROX	6-carboxy-X-rhodamine N-succinimidyl ester
Rpm	revolutions per minute
RPMS1	repetitive peripheral magnetic stimulation
RSV	respiratory syncytial virus
SDS	sodium dodecyl sulfate
sec	second
SH	small hydrophobic protein
SNP	single nucleotide polymorphism
spp	species
TAE	Tris-acetate EDTA buffer
TAMRA	6-carboxy-tetramethyl-rhodamine
Taq	*Thermus aquaticus*
TE	Tris EDTA buffer
TET	6-carboxy-4,7,2',7'-tetrachloro-fluorescein
$\mathbf{T_m}$	melting temperature
V	volts
UV	ultraviolet
x *g*	times relative centrifugal force
X-gal	5-bromo-4-chloro-3-indole-β-D-galactopyranoside
$^{\mathbf{32}}\mathbf{P}$	chromic phosphate
∞	infinity
%	percentage
ΔC_t	change in C_t value
/	per
~	approximately

CHAPTER 1: INTRODUCTION

1.1. Community-acquired pneumonia

Pneumonia is an inflammatory response of the host to uncontrolled multiplication of pathogenic organisms in the distal airways and alveoli (Woodhead, 2002). It is an infection resulting from microbial invasion of the normally sterile lower respiratory tract and lung tissue. It may be caused by bacteria, viruses or parasites and is clinically characterised by pulmonary or extrapulmonary signs and symptoms. On chest radiography, the inflammation within and around the alveolar spaces of the lung can be visualized as an infiltrate, which distinguishes pneumonia from other lower respiratory tract diseases. However, it is not possible to distinguish between different types of pneumonia on clinical or biochemical parameters alone and the diagnosis has to be microbiological.

Community-acquired pneumonia (CAP), which is pneumonia not acquired from a hospital or a long-term care facility (Lutfiyya *et al.,* 2006), is a major cause of morbidity and mortality worldwide. Symptoms commonly found in patients with CAP include coughing, sputum production, breathlessness, chest pain and haemoptysis (coughing up blood) amongst others (Woodhead, 2002). Two types of CAP are commonly recognised - typical and atypical. Typical pneumonia is usually caused by bacteria such as *Streptococcus pneumoniae, Haemophilus influenza* and *Moraxella catharralis*, whilst atypical pneumonia can be caused by respiratory viruses, *Mycoplasma pneumoniae*, *Chlamydia pneumoniae* and *Legionella pneumophila*.

CAP remains a serious illness that can have a significant impact on patients as well as society. Risk factors for CAP are: age over 60 years, alcoholism, immunosuppression, asthma and institutionalization. The microbial patterns in CAP differ considerably across studies, depending on the geographic area studied, the patient population included, and the nature and extent of the diagnostic techniques used (Garcia-Sastre *et al.,* 1998). Knowledge of the major microbial patterns in CAP is essential, as it represents the basis for initial decisions about its antimicrobial treatment. Empiric antimicrobial treatment must be initiated based on clinical symptoms, radiographic and laboratory findings, and specific epidemiologic risk factors. As early intervention with appropriate antibiotics has been shown to improve mortality and may decrease transmission of infection, more rapid and sensitive tests would greatly improve the care of patients with pneumonia (Leroy *et al.,* 1995) by identifying causative organisms and providing knowledge of their regional and geographic distribution.

Changes have occurred in the demographics of the patient population vulnerable to CAP in South Africa, with increasing numbers of individuals over the age of 65 and HIV positive persons bearing the burden of the disease. This shift has increased not only the total number of individuals at risk of pneumonia, but also the variety of pathogens found in association with the infections (Templeton *et al.,* 2005). The patient's age may be a major discriminating factor between typical and atypical pneumonia. Young adults are more prone to atypical causes, and very young and older persons are more predisposed to typical causes. This is however not the case with patients with HIV/ AIDS and other immunocompromised conditions (Lutfiyya *et al.,* 2006).

1.2. Diagnosis of CAP

Early diagnosis of pneumonia is important and timeous initiation of appropriate antimicrobial treatment is associated with a better outcome of patients with CAP, while delayed therapy is associated with an increased risk of death (Metlay and Fine, 2003). The microbiological diagnosis of CAP is usually made by microscopy and culture of sputum and blood, or by serological examinations which include detection of urine antigens for pneumococcus and *Legionella* spp., and antibodies for *M. pneumoniae*. The diagnostic value of positive blood culture is high; however its sensitivity can be low. Diagnosis of viral respiratory tract infections using viral culture, antigen detection or serology is either too slow or too insensitive to be applicable in clinical practice (Gunson *et al.,* 2005). It should also be noted that sputum samples from pneumonia patients are routinely used for bacteriological tests whilst nasopharyngeal aspirates and swabs are standard specimens for respiratory viral and atypical (mycoplasmal and chlamydial) diagnosis (Kok and Higgins, 1997).

Restriction fragment length polymorphism (RFLP) was one of the first molecular methods applied to the identification of pneumonia (Singh *et al.,* 2006) whereby restriction enzymes were used to digest DNA to generate different size fragments and fragments were then analyzed by gel electrophoresis. However RFLP requires growth of the organism in culture and is more useful in the examination of disease transmission and strain identification rather than clinical identification (Chan and Morris, 2007). Most currently used molecular techniques are based on polymerase chain reaction (PCR) technology (Yang and Rothman, 2004). PCR methods are more reliable, specific and sensitive, however, they have not yet been accepted as the first choice for routine diagnosis due to the high cost particularly when several agents are targeted (Brittain-Long *et al.,* 2008). Nevertheless, methods such as real-time PCR, which

combines nucleic acid amplification with amplicon detection, have revolutionized the way clinical microbiological laboratories identify human pathogens.

1.3. PCR

PCR is a revolutionary method developed by Kary Mullis in the 1980s (Mullis, 1990) and PCR-based approaches have allowed molecular biology to advance greatly by allowing researchers to manipulate DNA effortlessly, thereby facilitating procedures such as cloning and enabling endeavors such as the Human Genome Project. PCR is typically performed on a DNA template, which is either single or double-stranded. The basic steps of PCR in a clinical microbiology setting include extraction of DNA or RNA from either a cultured pathogen or from a patient sample. In the case of RNA, reverse transcription must be carried out to transform the RNA to complementary DNA (cDNA). For most applications, at least a partial DNA sequence of the organism must be known to design primers that flank that region and can thus hybridize to the target DNA sequence. A heat-stable DNA polymerase, most commonly derived from the thermophilic bacterium *Thermus aquaticus* and called *Taq*, is also required, along with magnesium ions in the buffer and deoxynucleotide triphosphates (dNTPs). The reaction is performed by temperature cycling in a thermocycler and can be summarized in three steps: (i) A High temperature of >90°C is applied to denature (melt) the strands of the double stranded DNA. The required melting temperature and period of melting depends on the length and occasionally the sequence of the template as well as the instrument used, (ii) The temperature is then lowered (50-75°C) to allow primers to anneal to the template, and (iii) finally the temperature is set at approximately 72°C, which is optimum for the *Taq* polymerase to extend the primers by incorporating dNTPs thereby creating a DNA complementary strand (Figure 1.1) (Mackay *et al.,* 2002). A typical PCR reaction lasts about

30 to 50 cycles and the amount of DNA theoretically doubles with each cycle in the exponential phase provided there is a sufficient amount of nucleotides and primers. Gel electrophoresis, typically using ethidium bromide to visualize the amplification products, is frequently used to estimate the size of the amplicon and this is both cheap and simple to implement.

1.4. Real-time PCR

Real-time PCR refers to amplification of DNA (by PCR) that is monitored while the amplification is taking place (Valasek and Repa, 2005). It symbolizes yet another technological leap forward that has unlocked new and powerful applications for researchers worldwide. PCR has advanced from detection of products at the end point of the reaction in conventional PCR to real-time PCR where detection is done while the reaction is occurring (Parashar *et al.,* 2006).

In real-time PCR, fluorescent reporter molecules are used to monitor the production of amplification products at each cycle of the PCR reaction obviating the need for gel electrophoresis to detect amplification products (Bustin, 2005). The detection of products is made possible by including fluorescent molecules in the reaction that report increases in the amount of DNA by a proportional increase in the fluorescent signal.

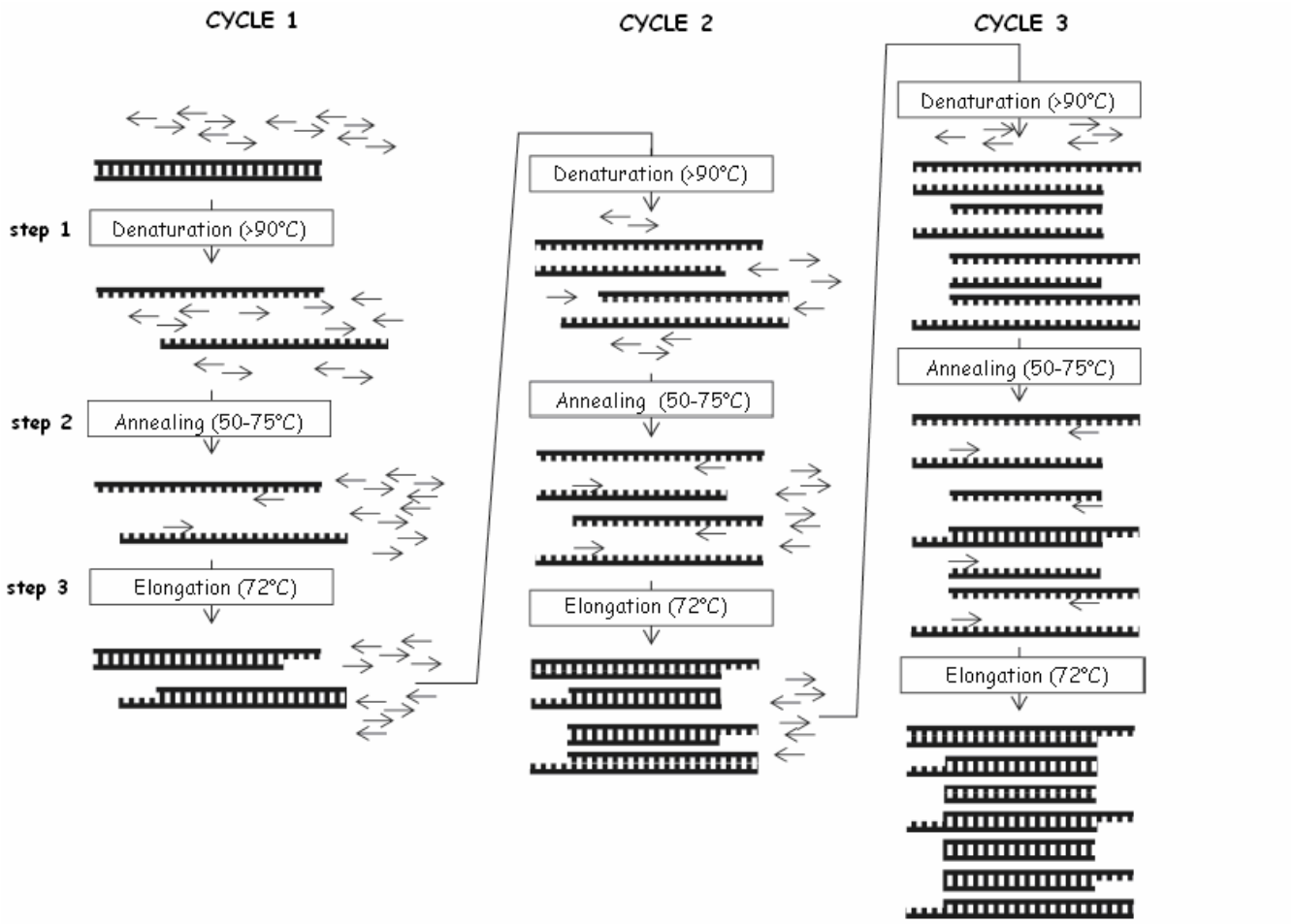

Figure 1.1: The PCR temperature cycle. Step 1: Temperature is raised to 90°C or more to denature the double-stranded DNA strands; Step 2: Temperature is lowered significantly to allow the primers to anneal to the template; Step 3: temperature is set at 72°C to allow the *Taq* polymerase enzyme to extend the primers. DNA theoretically doubles after each cycle provided the nucleotides and primers are not limiting. Adapted from Mulhardt and Beese (2006).

Real-time PCR can be divided into four major phases (Figure 1.2) and these are: the linear ground phase, early exponential phase, log-linear (known also as exponential) phase, and plateau phase (Tichopad *et al.,* 2003). For the duration of the linear ground phase which is typically the first 10–15 cycles, PCR is just beginning, and fluorescence emission at each cycle has not yet exceeded the background. Baseline fluorescence is calculated at this stage. During the early exponential phase, the amount of fluorescence has reached a threshold where

it is considerably higher than background levels. The cycle at which this occurs is known as C_t (threshold) (Heid *et al.,* 1996). During the log-linear phase, PCR attains its most favourable amplification period with the PCR product doubling after every cycle in ideal reaction circumstances thus allowing researchers to amplify specific pieces of DNA more than a billion-fold (Figure 1.1) (Mullis, 1990). Lastly, the plateau stage is reached when reaction components become limiting and the fluorescence intensity is no longer useful for data calculation (Bustin, 2000).

Real-time PCR is considerably faster than conventional PCR with standard detection methods, hence for some time this technology was referred to as rapid-cycle real-time PCR (Espy *et al.,* 2006). Also, the sensitivity of assays is often improved and the hands-on time is significantly reduced (van de Pol *et al.,* 2006). Since the nucleic acid amplification and detection steps are performed in the same closed vessel, the risk for release of amplified product into the environment, and resultant contamination of subsequent analyses, is minimal compared with agarose based end-point PCR methods. Overall, the combination of excellent sensitivity and specificity, low contamination risk, ease of performance and speed has made real-time PCR an appealing alternative to other methods for diagnosing infectious diseases (Morozumi *et al.,* 2006).

There are various chemistries available to obtain a fluorescent signal from the synthesis of product in real-time PCR. These are basically grouped into two groups namely non-specific and specific detection chemistries.

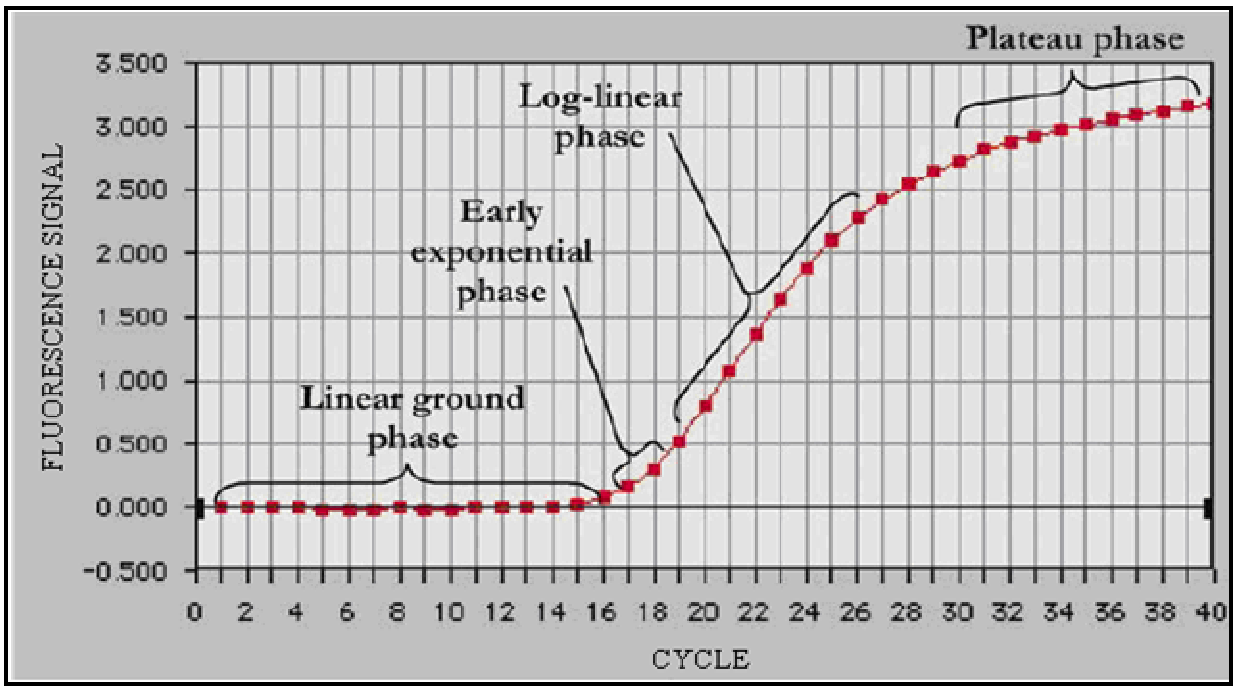

Figure 1.2: PCR amplification curve indicating the different phases of PCR amplification. The PCR amplification curve charts the accumulation of fluorescence signal at each reaction cycle. The curve can be divided into four different phases: the linear ground, early exponential, log-linear, and plateau phases. Data collected from these phases are vital for calculating background signal, cycle threshold (C_t), and amplification efficiency. Adapted from Wong and Medrano (2005).

1.4.1. Non-specific detection chemistries

Nonspecific detection uses intercalating dyes such as SYBR Green I, which binds non-specifically to double stranded DNA and has an excitation and emission maxima of 494 nm and 521nm, respectively (Soheili and Samiei, 2005). SYBR Green I displays little fluorescence when free in solution, but this fluorescence increases up to 1000-fold when the dye is bound to double-stranded DNA thus overall fluorescence is proportional to the amount of double-stranded DNA present (Valasek and Repa, 2005) (Figure 1.3). Melting-curve analysis is thereafter used to identify different products, including non-specific ones. This curve is generated by increasing the temperature in small increments. The highest level of fluorescence is observed when the DNA is double-stranded and as the double-stranded DNA

denatures, the fluorescence decreases. A signature peak is observed at the amplicon melting temperature (T_m, the temperature at which 50% of the base pairs of a double stranded DNA molecule are separated) and this differentiates it from other products which melt at different temperatures (Figure 1.4) such as primer-dimers (Valasek and Repa, 2005). However, it should be noted that T_m values may vary as the reagent concentrations (DMSO, magnesium chloride, template DNA and SYBR Green I) change. Also, the rate of temperature transition during the melting analysis has an effect on the T_m value generated (Giglio *et al.,* 2003). The area under the peak is proportional to the amount of product produced ((Wilhelm and Pingoud, 2003). Therefore, melting curve analysis may be used for quantification. Primer-dimers are typically shorter than the target product and as a result, they have a melting temperature lower than that of the product and can be easily distinguished using a melting curve. The melting temperature is a property of the amplicon that is dependent on the concentration of double-stranded DNA, its length and nucleotide composition (Mackay *et al.,* 2002).

Advantages displayed by assays using DNA-binding dyes are: (1) their ability to be integrated without much difficulty into optimized and long-established protocols, and (2) their affordability, as there is no probe-related cost. As a result, they are very useful for optimizing a PCR reaction; for instance, when testing any interaction between the primers by melt curve analysis, and running initial, investigative screens of multiple amplicons before using a probe-based protocol, as was done in this study.

Despite their advantages, DNA-binding dye assays have disadvantages that include (1) their indiscriminate binding to any double-stranded DNA, which may result in fluorescence coming up in the "no template controls" (NTC) owing to dye molecules binding to primer dimers, (2)

the mandatory use of melting curves since these assays are no more specific than conventional PCR making data analysis more complex (Bustin and Nolan, 2004), and (3) difficulty in establishing multiplex reactions due to preferential binding of DNA-binding dyes, particularly SYBR Green I, to selected amplicons.

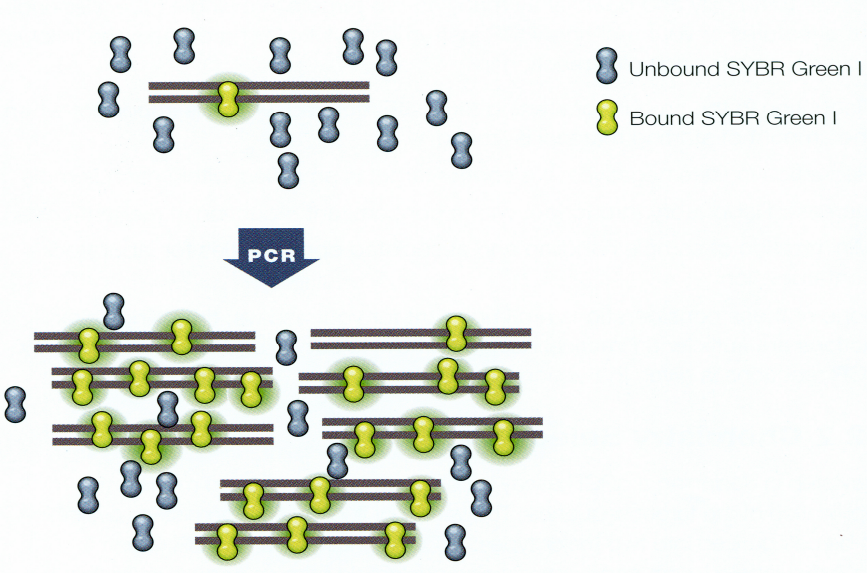

Figure 1.3: Real-time PCR SYBR Green I Technology. Taken from Bio-Rad (2007).

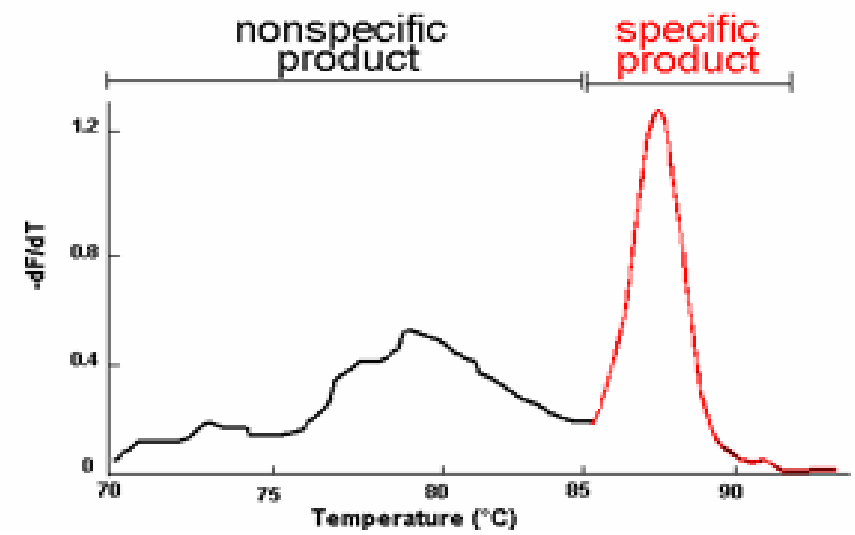

Figure 1.4: Melting curve analysis. Melting temperature helps distinguish specific and non-specific product. Taken from Wittwer *et al* (1998).

1.4.2. Specific detection chemistries

Specific detection chemistries include dual labeled probes (exemplified by TaqMan™ probes, also known as 5' nuclease probes), minor groove binding (MGB) probes, molecular beacons, and more newly developed fluorescent labeled primers: Lux™, Sunrise™ and Scorpion™ primers (Gunson *et al.,* 2006). Originally, 5' nuclease-based formats used a 5'-^{32}P-labelled probe and the release of the ^{32}P-label was used to measure probe hydrolysis (Holland *et al.,* 1991). Subsequently, dual labeled probes were used. Essentially, the TaqMan probe is a short, sequence-specific oligonucleotide that contains a 5' fluorescent dye and a 3'quenching dye. When the fluorescent and reporter are in close proximity, that is to say, they are both attached to the same short oligonucleotide, the quencher absorbs the signal from the reporter and at this stage, no signal is observed. To produce a light signal, the TaqMan probe binds to a complementary strand of DNA at 72°C. At this temperature, *Taq* polymerase is active and cleaves the 5' end of the TaqMan probe (5' nuclease activity), separating the fluorescent dye from the quenching dye (Figure 1.5) (Espy *et al.,* 2006). The cleaved fluorescent dye accumulates after each temperature cycle and can be measured at any time during the PCR cycling.

The major advantage of using specific chemistries is that specificity no longer resides with the primers; instead, the probe introduces an added level of specificity and as a result, nonspecific amplification due to mispriming or primer–dimer artifacts is not noted by the fluorescence detector and no signal is produced. This eliminates the need for melting curves, or sequence analysis to verify the identity of the amplicon (Bustin and Nolan, 2004). In addition, the fact that probes can be labeled with different, distinguishable reporter dyes allows for the detection of amplification products from several distinct sequences in a single PCR multiplex reaction

(Bustin and Nolan, 2004). However, the main disadvantage with specific chemistries is that because of its specificity, inhibitors that impede amplification efficiency go unnoticed. Consequently, dyes such as SYBR Green I should be used to optimize primers and reaction conditions prior to any experiments to make certain that amplification inhibitors are absent. Also, because primer-dimers cannot be detected by probes, it is important to check for their presence by gel electrophoresis especially when high C_t values are obtained. Another disadvantage is that the cost associated with these chemistries is high because each target requires its own specific probe. This becomes particularly expensive when amplifying multiple targets, as costs escalate very rapidly (Bustin and Nolan, 2004).

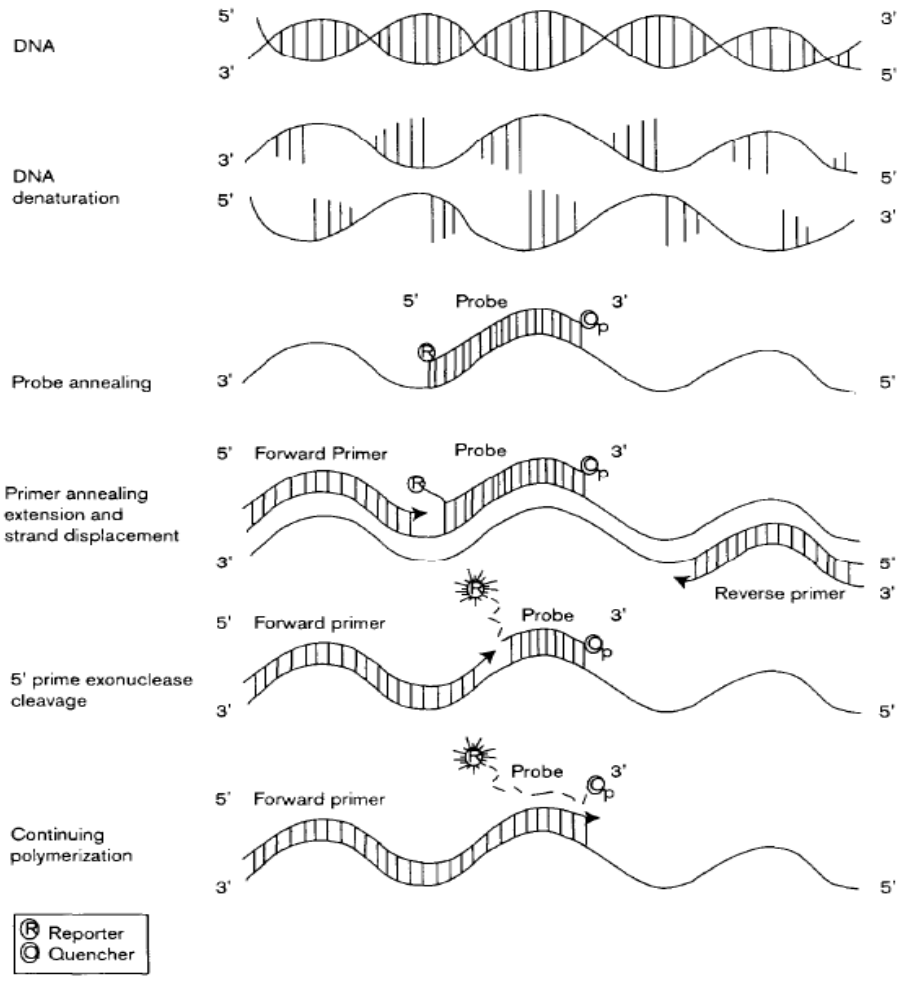

Figure 1.5: Real-time PCR 5' nuclease probe technology. Taken from Lie and Petropoulos (1998).

1.5. Real-time PCR platform

As the use of real-time PCR becomes popular, a range of real-time PCR instruments are becoming available, ranging from the iCycler (Bio-Rad), the SmartCycler (Cepheid) and the Sentinel (Stratagene) amongst others. The real-time PCR instrument used in this study is the Chromo4 (Bio-Rad).

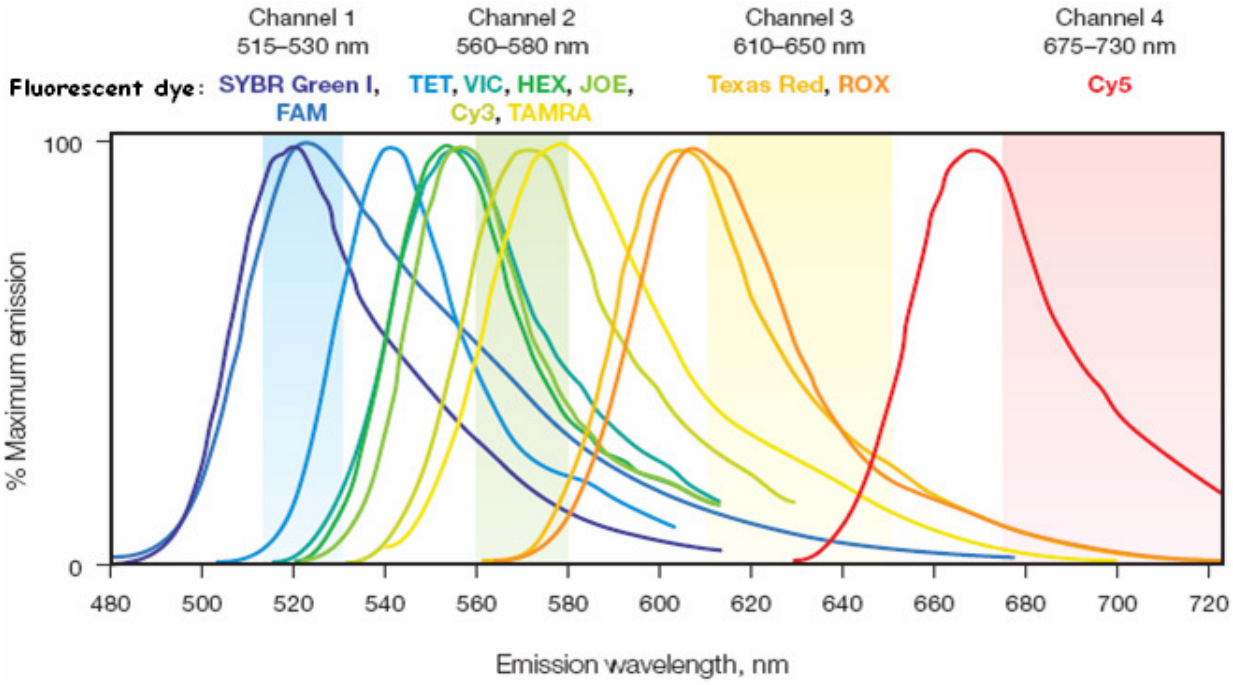

Figure 1.6: Fluorescence spectra of the Chromo4 real-time detection system. The standard photonics shuttle has 4 colour channels. The fluorescent dyes detected in each channel as well as the detection wavelengths are indicated above the spectra. The emission wavelength of each of the fluorescent dyes is indicated on the x-axis. Adapted from Bio-Rad (2008). (**FAM**: 6-carboxyfluorescein; **TET**: 6-carboxy-4,7,2',7'-tetrachloro-fluorescein; **VIC**; **ROX**: 6-carboxy-X-rhodamine N-succinimidyl ester; **HEX**: hexachloro-6-carboxyfluoroscein; **Cy3**: indocarbocyanine; **TAMRA**: (6-carboxy-tetramethyl-rhodamine); **Cy5**: tetramethyl-indodicarbocyanine; **JOE**: 2′,7′-dimethoxy-4′5′-dichloro-6-carboxyfluoresce in).

The photonics shuttle is the heart of the Chromo4 detector. It is a compact unit that contains all the components for real-time excitation and detection. This shuttle has four channels

meaning it can detect up to four colours in the same reaction vessel. These channels are shown in figure 1.6 along with the respective fluorescent dyes that have detection wavelengths that fall within the range of these channels.

General fundamentals of fluorescent dyes are that they should sufficiently excite and emit energy at different wavelengths without any overlap, they must bind easily to DNA molecules, must be detectable at low concentrations and must be still functional after long term storage (Mackay, 2007). There are a number of quenchers available. Examples of the most common are black hole quencher 1, 2 and 3 (BHQ1, 2 and 3), BlackBerry quencher (BBQ) and minor groove binding (MGB) quencher.

1.6. Multiplex real-time PCR

Multiplex real-time PCR is a modification of real-time PCR in which two or more target sequences can be amplified by including more than one pair of primers and probes in a single reaction vessel, saving time and effort in the laboratory (Markoulatos *et al.,* 2002). This allows for colour multiplexing where probes labeled with different fluorescent dyes are present. Dyes like SYBR Green I cannot be used in multiplex reactions because they are not sequence specific (Wittwer *et al.,* 2001), they have been shown to inhibit PCR (Gudnason *et al.,* 2007), bind preferentially to GC-rich sequences (Giglio *et al.,* 2003) and have an effect on melting curve analysis in that the melting temperature has been shown to be highly dependent on the dye (Ririe *et al.,* 1997) and DNA concentration (Xu *et al.,* 2000). It is important to carefully select the fluorescence dyes one will use when multiplexing and to make sure that they are spectrally well separated and there is no bleed-through into other dye layers which will result in false positives (Figure 1.6).

The utilization of multiplex assays reduces overall testing costs in that a lower sample volume is required. This is particularly an advantage in a clinical setting when the volume of a sample received is low. In addition to this, less reagents and consumables are required and turn around times are reduced permitting a high throughput (Cirino *et al.,* 2007). The development of multiplex real-time PCR has been a complicated process because of the limited number of existing fluorophores as well as the great deal of trial and error required. While excitation by a single wavelength results in bright emissions from a suitably receptive fluorophore being produced, the number of fluorophores that can be excited by that wavelength is limited (Mackay, 2004). In order to optimize the multiplex assay, each separate PCR reaction must be optimized separately before being assessed when added together.

A problem inherent in multiplex reactions is that PCR efficiencies may decrease with the inclusion of multiple primer sets and probes due to preferential amplification of certain specific targets (Markoulatos *et al.,* 2002). Differences in starting target template concentrations can also cause one reaction to out-compete the other resulting in false negative results (Exner and Lewinski, 2002) and this is why careful planning of the multiplex reaction is essential to minimize the chances of primer-dimer formation and reduced reaction efficiency.

1.7. Dual Priming Oligonucleotide (DPO) system

Proper priming between an oligonucleotide primer and its DNA template is essential for a successful PCR reaction. However, even with rigid primer design and optimization of PCR reaction conditions, a high level of non-specific priming and amplification of non-specific product is still present. The DPO technology is a novel principle developed to counteract the

effects of mismatched priming that cannot be avoided in the currently used PCR system (Chun *et al.,* 2007). Two separate priming regions joined by a polydeoxyinosine linker, which is not involved in priming, constitute the DPO (Figure 1.7). The linker joining the 2 priming regions has a low melting temperature thus changes into a bubble-like shape at high temperatures. Its function is to physically separate the long DPO primer (34-42 nucleotides) into two priming sites resulting in them having two different annealing properties.

The 5'end fragment in the DPO system is longer (18-25 nucleotides) than the 3'end fragment (6-12 nucleotides) and the linker is 3 to 8 deoxyinosines long (Figure 1.7).

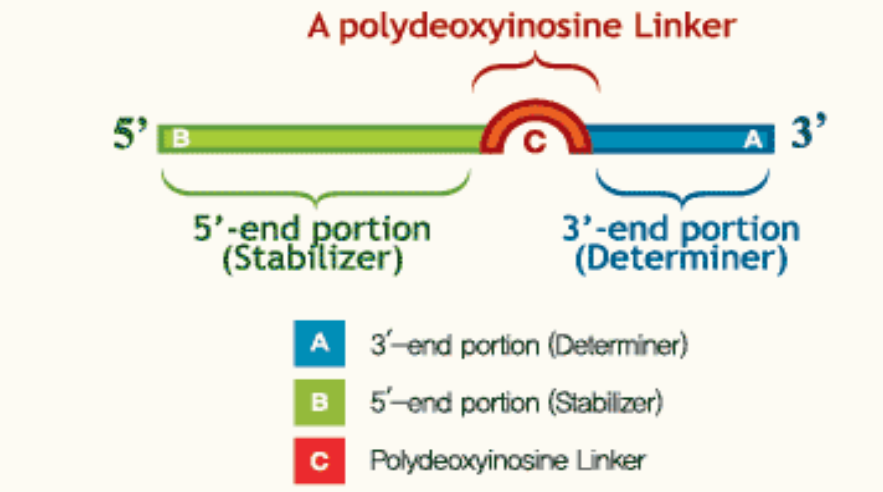

Figure 1.7: The structure of DPO. The 5'end portion (B) is longer than the 3' end portion (A). The polydeoxyinosine linker is not involved in the priming process and forms a bubble-like structure at high temperatures. Taken from Seegene, (http://www.seegene.com).

Basically, the first step of the reaction involves the linker activation step during which, due to its weak hydrogen bonds, the linker conforms a bubble-like shape at a certain temperature, and as the result, the initial single primer, changes into two functional priming regions (Figure 1.8).

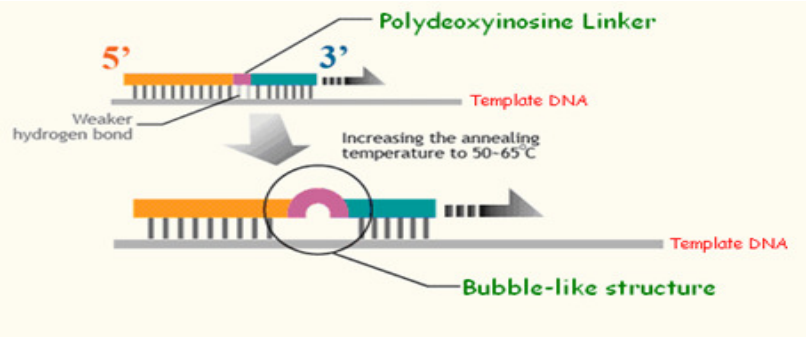

Figure 1.8: Diagrammatic illustration of the change in shape of the polydeoxyinosine linker into a bubble-like shape. The linker has weak hydrogen bonds and as a result, it has a low melting temperature. At high annealing temperatures, its hydrogen bonds break resulting in it forming a bubble-like shape. The initial single primer changes into two separate entities as a result. Adapted from Seegene, (www.seegene.com, 2008).

The first priming PCR reaction involves preferential binding of the longer priming fragment (5'end) to its target region forming a stable structure (Figure 1.9).

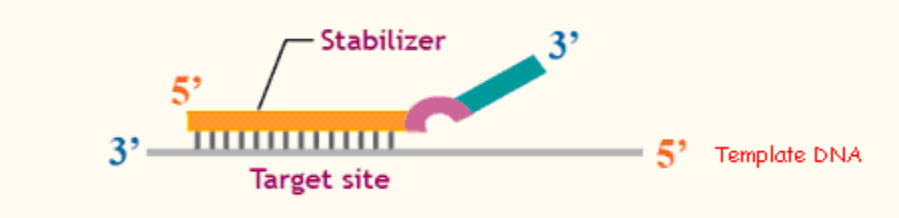

Figure 1.9: Diagrammatic illustration of the first priming PCR reaction involving DPO. The longer 5'end region acts as a stabilizer and binds preferentially to the target region of the template DNA strand forming a stable structure. Adapted from Seegene, (www.seegene.com, 2008).

During the second priming PCR reaction, the shorter priming fragment (3'end) takes part in target-specific extension during which it selectively binds to the target site, thus acting as a determiner (Figure 1.10).

The difference between the DPO and conventional priming systems is that a single priming event occurs between primer and template in the conventional system as opposed to the DPO system where two priming events take place due to two separate primer fragments (Figure 1.11).

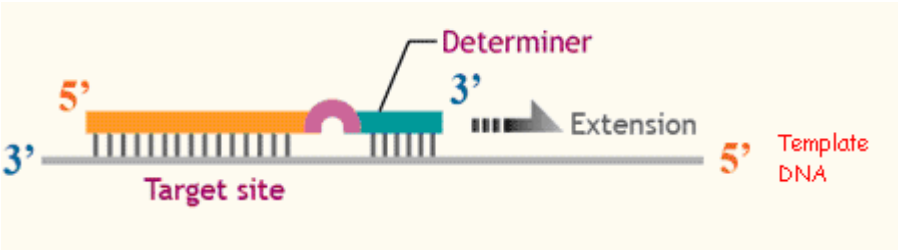

Figure 1.10: Diagrammatic illustration of the second priming PCR reaction involving DPO. The shorter 3'end region determines target-specific extension by selectively binding to the template DNA strand. It therefore acts as a determiner. Adapted from Seegene, (http://www.seegene.com).

In these two priming events, although the longer 5'-segment binds a non target site, the shorter 3'-segment resists non-specific extension. Because of this aspect, the DPO technology eliminates extension of non-specifically primed templates generating high PCR specificity even if PCR conditions are below optimum (Chun *et al.,* 2007).

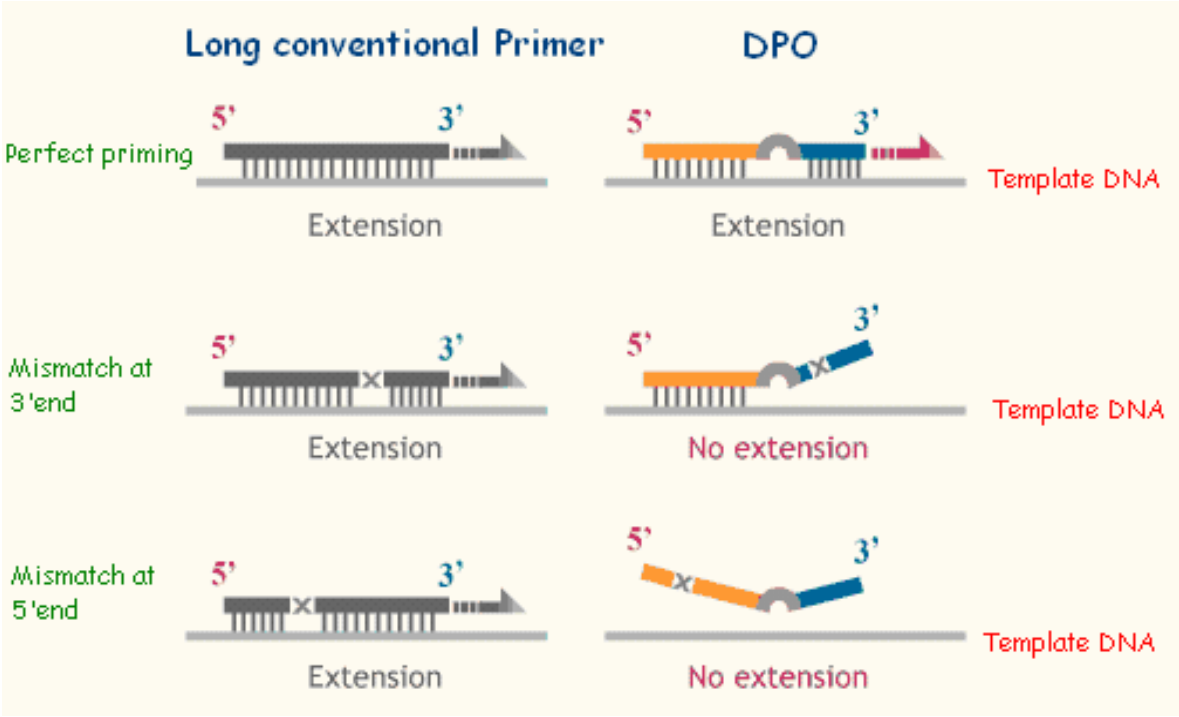

Figure 1.11: Difference in conventional and DPO priming systems. A perfect match between the primers and the target in both priming systems results in extension. Any sort of mismatch either in the 3'end or 5'end of conventional system will still result in extension in the conventional priming system but not in the DPO system. Adapted from Chun *et al* (2007).

In real-time PCR, primer extension may proceed even in the presence of mismatches between a primer and a template. In the contrary, extension in the DPO system only proceeds when there is a perfect match between the two priming fragments and the template (Figure 1.11, perfect match). Even supposing the 5'-segment which initiates stable annealing binds to the template, any mismatch in the 3'-segment will result in no extension (Figure 1.11, mismatch at 3'end). A mismatch at the 5'-segment will mean that due to the low T_m of the short 3'-segment (below 30°C), it is unable to anneal at the high reaction temperatures of 55-65°C, thus no extension will occur (Figure 1.11, mismatch at 5'end).

Multiplex PCR detection kits that apply the DPO system were used in conjunction with real-time PCR in this study to detect respiratory pathogens in patient samples.

1.8. Brief description of organisms to be investigated

Ten viruses, 4 bacteria, 1 fungus and 2 internal controls were selected to be studied in this project. In this section, various aspects of the organisms ranging from their taxonomy (classification and structure), pathogenesis, effects of the disease they cause in adults as well as the respective genes targeted in the real-time PCR reactions performed, will be briefly discussed.

1.8.1. Viruses

As electron microscopy became a more widely available tool, the morphology of the virus particle (Figure 1.12) became a key feature for virus classification (Buchen-Osmond, 2003).

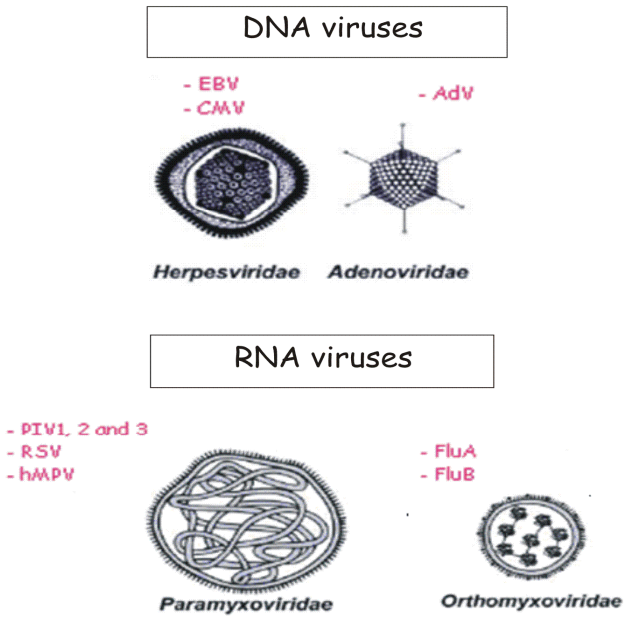

Figure 1.12: Morphology of human viral pathogens and the families they belong to. Abbreviations in pink: EBV (Epstein-Barr virus), CMV (cytomegalovirus), AdV (adenovirus), PIV (Parainfluenza virus), RSV (respiratory syncytial virus), hMPV (human metapneumovirus), FluA (Influenza A virus), FluB (Influenza B virus). Adapted from Buchen-Osmond (2003).

1.8.1.1. Influenza (Flu) A and B viruses

Classification and structure

Influenza viruses are a member of the family *Orthomyxoviridae* and contain a segmented, linear, single- stranded, negative-sense RNA genome. They are enveloped viruses with a helical symmetry and are 80-120nm in diameter. The RNA is closely associated with the nucleoprotein (NP) to form a helical structure. The Influenza genus is divided into three types, A, B and C, based on epitopes on the internal nucleoprotein and the M protein. Human influenza A virus strains are further classified in the subtypes H1N1, H3N2 and the presently not circulating H2N2 subtype, based on the antigenic differences of the hemagglutinin and the neuraminidase surface proteins shown in figure 1.13 (Claas *et al.,* 1992). There are life-threatening implications of the predicted seasonal occurrence of influenza virus infections,

thus, there is a need for rapid and accurate identification of both influenza A and B virus genotypes. This provides an opportunity for intervention with effective antiviral treatment if provided to the patient in the early stages of this viral disease (Espy *et al.,* 2006)

Pathogenesis

Respiratory droplets spread the viral infection. The viral particles attach to cells of the respiratory epithelium which are rich in viral receptors. The neuraminidase recognition probe on the virus particles initiates the infectious process by releasing virus particles bound by mucous present on the surface of the epithelial cells. Incubation period of the virus is 1-4 days (Wat, 2004).

Effect of disease in adults

Following an incubation period of 48 hours, the typical symptoms of influenza present as fever, photophobia, headache, dry cough and myalgia. The fever is continuous and lasts approximately 3 days.

Target gene for real-time PCR:

FluA - Non-structural protein gene: Non-structural protein of influenza A virus, contributes to its pathogenicity and virulence. It is a multifunctional protein that plays a major role in resisting the host antiviral response during the influenza infection (Lin *et al.,* 2007).

FluB - Nucleoprotein gene: The nucleoprotein is the major protein component of the ribonucleoprotein core of influenza virions and is a type-specific antigen defining influenza viruses as either type A or B (Rota *et al.,* 1990).

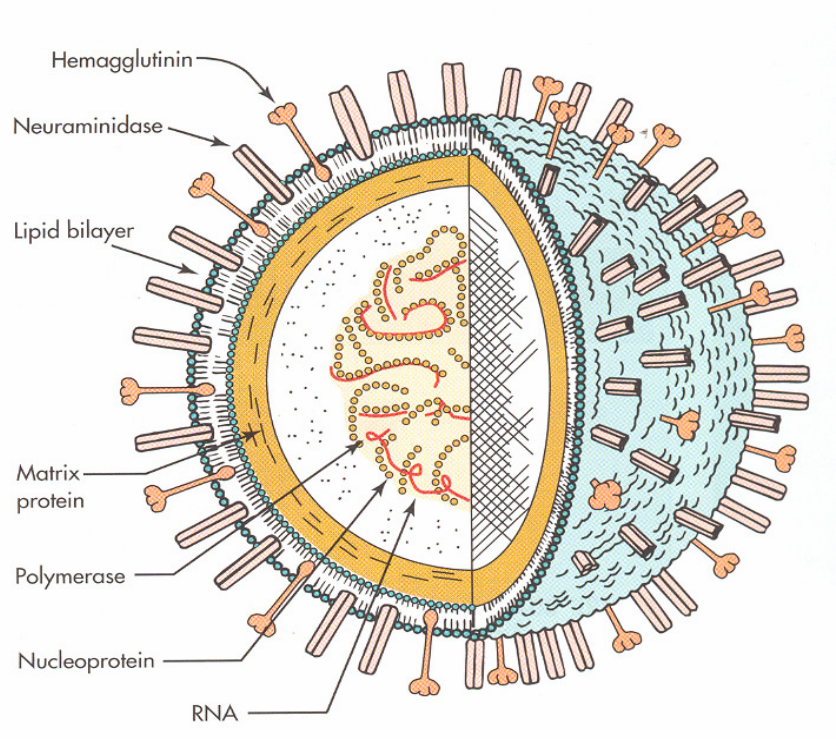

Figure 1.13: Diagrammatic representation of Influenza virus. Hemagglutinin and neuraminidase spikes are embedded in the lipid bilayer. Taken from Ackermann and Berthiaume (1995).

1.8.1.2. Human metapneumovirus (hMPV)

Classification and structure

Taxonomically, hMPV is the first human pathogen placed in the *Metapneumovirus* genus, the *Paramyxoviridae* family and the subfamily *Paramyxovirinae* (Mejias *et al.,* 2004). This classification scheme is based on the organization of the viral genome, morphologic criteria, the viral RNA genomic sequence relationships of the encoded proteins and the biologic activities of the virus-encoded proteins (Domachowske, 2003).

The hMPV has a pleomorphic, enveloped virion with an average diameter of approximately 200nm. It contains a single-stranded negative-sense, nonsegmented RNA (13.3kb) that forms a helical nucleocapsid, and has surface glycoproteins and projections (Peret *et al.,* 2002; van den

Hoogen *et al.,* 2002). It is termed human metapneumovirus because it does not have the ability to infect chickens or turkeys, making it an unlikely zoonotic source (Mejias *et al.,* 2004).

This virus differs from the human respiratory syncytial virus (hRSV), another paramyxovirus by virtue of a lack of two non-structural proteins (NS1 and NS2) and by a slightly different gene order for the other common genes, i.e., the phosphoprotein (P), nucleoprotein (NP), matrix (M), polymerase (L), fusion (F), small hydrophobic protein (SH), and attachment glycoprotein (G) (van den Hoogen *et al.,* 2002). The NP, F, L, and M genes are the most conserved and the G and SH genes being the least conserved (Biacchesi *et al.,* 2003).

Pathogenesis

Little direct experimental work has been reported on the mechanisms of pathogenesis in humans. Clinical manifestations of hMPV, ranging from mild-to-severe bronchiolitis and occasionally pneumonia, resemble those of RSV (Mejias *et al.,* 2004). Using animal models, the virus has been shown to replicate in both the upper and lower respiratory tract, but the particular cell types that are affected have not been defined (Crowe 2004, Hamelin and Boivin, 2005).

Formal transmission studies have not been reported, although the mode of transmission is almost undoubtedly large particle respiratory secretions and fomites, based on the relatedness of this virus to other pneumoviruses (Crowe, 2004). Nosocomial transmission does occur, suggesting that contact isolation and thorough hand washing by health care providers is necessary in the hospital or office setting (Esper *et al.,* 2003).

Effect of disease in adults

Several reports have linked hMPV with acute respiratory tract infections in all age groups, with more severe diseases occurring in young children, elderly individuals and immunocompromised hosts (Hamelin and Boivin, 2005). The clinical symptoms include severe cough, high fever, difficulty breathing or abnormally rapid breathing and wheezing. These symptoms are indistinguishable from those in a RSV infected individual (Boivin *et al.,* 2003); however the most commonly reported diagnosis associated with hMPV infection is bronchiolitis, with or without pneumonitis. Associations with acute wheezing and asthma exacerbation have also been reported (Hamelin and Boivin, 2005).

Naturally acquired infection does not seem to protect against re-infection (Crowe, 2004). However it is possible that infection does stimulate partial protection against severe disease, because most serious lower respiratory tract illnesses occur in the first year of life (Williams *et al.,* 2004).

Target gene for real-time PCR

Nucleoprotein (NP) gene: Protection of viral RNA

1.8.1.3. Parainfluenza viruses (PIV) 1-3

Classification and structure

Parainfluenza viruses are from the family *Paramyxoviridae* and subfamily *Paramyxovirus.* They are relatively large enveloped viruses (150-300nm) with a pleomorphic or spherical shape. They contain helical RNA that is negative-sense, unsegmented and single-stranded (Buchen-Osmond, 2003). They have an RNA-dependent polymerase complex that contains 3

non-structural proteins that are tightly associated with the RNA: Nucleoprotein, phosphoprotein and large protein.

Pathogenesis

PIV initially colonises nasopharyngeal mucosa before infecting the respiratory epithelium. Firstly, the virus attaches to the host cell sialic acid receptors via the hemagglutinin-neuraminidase glycoprotein it possesses (Figure 1.14) and spreads to the lower respiratory epithelium in 1-3 days. The incubation period is usually 3-10 days and most infections are asymptomatic (Wat, 2004). Transmission occurs via fomites and aerosols of respiratory secretions. Re-infections are clinically less severe and most commonly involve the upper respiratory tract and occur throughout life (Henrickson, 2003).

Effect of disease in adults

Air-sampling experiments have revealed that PIV1 could be recovered from only 2 of 40 infected children at a distance of 60 cm (McLean *et al.,* 1967) thus transmission is unlikely to take place by small-particle aerosol spread. Additionally, spread of PIV by direct hand contact from one individual to the next also appears to be an unlikely means of transmission because an experiment has demonstrated that PIV3 placed on fingers loses more than 90% of its infectivity in the first 10 minutes (Ansari *et al.,* 1991). PIV1, 2 and 3 have all been shown to survive for up to 10 hours on nonporous surfaces and 4 hours on porous surfaces (Brady *et al.,* 1990) thus contaminated surfaces might then result in direct self-inoculation (Hall and Douglas, 1981).

Target gene for real-time PCR:

PIV 1, 2 and 3 - Hemagglutinin-neuraminidase (HN) gene: Parainfluenza viruses display two surface glycoproteins; namely, the haemagglutinin-neuraminidase (HN) and the fusion protein (F) (Figure 1.14). HN has three functions: (i) a receptor-binding (haemagglutinin) activity; (ii) a receptor destroying (neuraminidase) activity that liberates terminal sialic acid (N-acetyl neuraminic acid, Neu5Ac) residues from glycol-conjugates; and (iii) a fusion activating activity operating via an as yet undefined mechanism believed to involve an interaction of HN with the F protein (Hall, 2001).

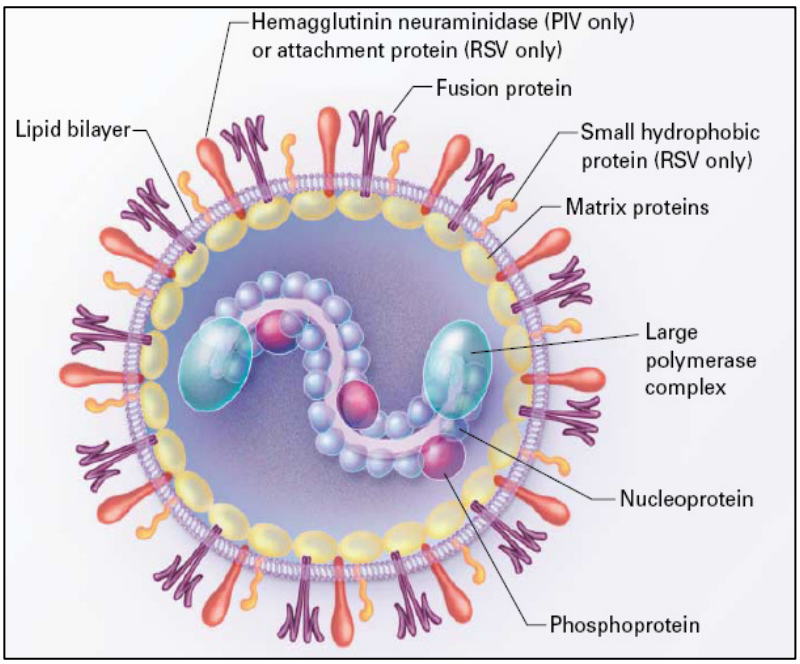

Figure 1.14: Structure of parainfluenza virus and respiratory syncytial virus. Taken from Hall (2001).

1.8.1.4. Respiratory syncytial virus (RSV)

Classification and structure

RSV is an enveloped negative-sense RNA virus that is a member of the family *Paramyxoviridae* and classified within the genus *Pneumovirus.* Its genome is nonsegmented

and single-stranded and is composed of approximately 15 222 nucleotides (Collins *et al.,* 1996). It is pleomorphic and is 150-300nm in size. The structure of RSV is shown in figure 1.14.

Pathogenesis

After a 2 to 8 day incubation period, the RSV virus replicates in the nasopharyngeal epithelium and spreads to the lower respiratory tract 1 to 3 days later. The distinctive inflammation of RSV bronchiolitis is necrosis and sloughing of the epithelium, with edema, and increased mucus secretion, which obstructs flow in the small airways (Hall, 2001).The manifestations of RSV may be difficult to distinguish from those of other respiratory viruses; however, there are symptoms which may suggest RSV. A typical RSV illness begins with nasal congestion and discharge and this helps distinguish RSV from influenza (Mathur *et al.,* 1980). Cough is common and affects 90 to 97% of patients. Fever is observed in 50% of patients as opposed to 75% with influenza virus or bacterial infections (Falsey *et al.,* 1995). Although temperatures of 39 to 40°C are frequently observed, fevers are usually lower than in influenza (Falsey and Walsh, 2000).

Transmission of RSV occurs by direct inoculation of infectious respiratory secretions from the hands or by large-particle aerosols into the eyes and nose, but rarely the mouth (Wat, 2004).

Effect of disease in adults

Excretion of RSV from infected adults averages 3 to 6 days, but may occur over 1 to 12 days. RSV is spread primarily by fomites and large droplets and can survive on nonporous surfaces, skin and gloves for several hours thus person-to-person contact or contact with contaminated

surfaces is required for transmission. The virus is not stable when aerosolized thus small particle aerosols are not considered a main mode of transmission (Falsey and Walsh, 2000).

Target gene for real-time PCR:

Non-structural protein 1: Function is to antagonise interferon-induced antiviral response (Hacking and Hull, 2002).

1.8.1.5. Adenovirus (AdV)

Classification and structure

Adenoviruses (Genus *Mastadenovirus*, Family *Adenoviridae*) are ubiquitous pathogens of both animals and humans. They are isometric in shape, 70-90nm in size and have linear double-stranded DNA. They possess a nucleocapsid that has an icosahedral symmetry (Buchen-Osmond, 2003).

To date, 51 different human adenovirus serotypes, organised into six major subgroups (subgenera or species A-F), have been identified based on their oncogenic, morphologic, hemagglutinating and DNA sequence properties as well as their responses to neutralizing antibodies (Horwitz, 2001).

Pathogenesis

They cause a variety of diseases ranging from respiratory illnesses, encephalitis, cystitis and keratoconjunctivitis to gastroenteritis and can be recovered from most parts of the body affected by the infection (Ko *et al.,* 2005). However, adenovirus infections in immunocompromised patients tend to become invasive and disseminated disease is associated with very high mortality rates (Ebner *et al.,* 2005). The incubation period is in the range of 4–7

days, but could be as long as 2 weeks and its mode of transmission is airborne or by direct contact with self-inoculation (Wat, 2004).

Effect of disease in adults

The duration of excretion of adenovirus ranges from 2 to 12 months in immunocompromised patients (throat, urine, stool, organ biopsies), 3 to 6 weeks in children with respiratory or generalized illnesses (throat , stool), 2 weeks in adults with keratoconjunctivitis (eye) and 3 to 5 days in patients with pharyngoconjunctival fever (eye, ear, nose, throat, urine, stool) or central nervous system symptoms (cerebrospinal fluid), to 1 to 3 days in adults with common colds (throat). It is therefore necessary to be able to identify adenoviruses in any clinical specimen without regard to the type of specimen or the amount of virus present (Hierholzer *et al.,* 1993).

Currently available treatment options, which include antiviral agents such as cidofovir and ribavirin, immunomodulation, and more recently, cytotoxic T cells, have been reported to work successfully at least in a proportion of patients thus emphasizing the importance of adequate diagnostic techniques permitting timely detection and monitoring of the course of infection (Ljungman, 2004). Molecular methods such as PCR and probe hybridization have been used to detect pathogenic microorganisms, including adenoviruses, because the methods are rapid, sensitive, and specific (Xu *et al.,* 2000).

Target gene for real-time PCR:

Hexon gene: This gene codes for one of the structural proteins in the viral coat and is synthesized during late infection (Pring-Akerblom *et al.,* 1995).

1.8.1.6. Cytomegalovirus (CMV)

Classification and structure

CMV is a viral genus of the Herpesviridae group. It belongs to the *Betaherpesvirinae* subfamily of *Herpesviridae.* It is spherical in shape, has an icosahedral symmetry and is 150nm in size. It has linear double-stranded DNA that is monopartite (Buchen-Osmond, 2003).

Pathogenesis

All herpesviruses share a characteristic ability to remain latent within the body over long periods. CMV infections are frequently associated with salivary glands though they may be found throughout the body. Some people infected with CMV develop an infectious glandular-like syndrome with prolonged fever and a mild hepatitis. A sore throat is common. After infection the virus remains latent in the body for the rest of the person's life and evident disease rarely occurs unless immunity is suppressed by infection, drugs or old age.

Transmission of CMV occurs from person to person through bodily fluids. Infection requires close contact with a person excreting the virus in their saliva, urine, blood, tears, semen or breast milk.

Effect of disease in adults

Initial infection with CMV typically causes no symptoms. The virus continues to live in the body silently without causing obvious damage or illness. It seldom becomes active for the first time unless the immune system weakens and is no longer able to hold the virus in check. Active infection in both children and adults causes chills, severe tiredness, prolonged high fever, headache, and an enlarged spleen. In severe cases, CMV infection can cause pneumonia, anaemia, gastrointestinal and liver infection.

Target gene for real-time PCR:

Major immediate-early region: The major immediate-early gene region of human cytomegalovirus plays a major role in affecting activation and repression of cellular and viral genes. This gene intimately associate and/or interact with viral and cellular proteins throughout this process (Stenberg, 1996).

1.8.1.7. Epstein-Barr Virus (EBV)

Classification and structure

EBV is a member of the *Herpesviridae*, the only human virus in the subfamily *Gammaherpesvirinae.* It is a ubiquitous human B-lymphotropic herpesvirus that is spherical, 150-200nm in diameter and has circular, double-stranded DNA of approximately 172kbp in size (Buchen-Osmond, 2003).

Pathogenesis

EBV infects more than 90% of the world's population and establishes a lifelong (usually asymptomatic) persistent infection in its host. It has been estimated that the number of EBV-infected B cells is controlled in healthy individuals by EBV-specific immunity (Wagner *et al.,* 1992). EBV is characterised by a primary infection that generally occurs in a sub-clinical fashion in early childhood, with subsequent lifelong latent infection. At any time following initial infection, reactivation may occur. Reactivation of EBV may be severe and even life-threatening in immunocompromised individuals such as bone marrow and solid-organ transplant recipients and in AIDS patients. Therefore, early diagnosis of EBV infections is important in the management of high-risk patients (Jebbink *et al.,* 2003). Several malignancies have been associated with EBV infections especially in immunosuppressed patients who lack

antibodies to the virus. EBV associated malignancies can occur in the central nervous system especially in HIV patients (Espy *et al.,* 2006). The virus is transmitted primarily by saliva and transmission by blood transfusion is rare.

Effect of disease in adults

When infection with EBV occurs during adolescence or early adulthood, there is a 35-50% chance that glandular fever will develop after an incubation period of 4-6 weeks. Other common symptoms are sore throat and lymphadenopathy. EBV is linked to the development of several malignant tumours including Burkitt's lymphoma, some forms of T cell lymphoma, Hodgkin's disease and undifferentiated nasopharyngeal carcinoma.

Target gene for real-time PCR:

RPMS1 protein: RPMS1 is an open reading frame that encodes a nuclear protein termed RPMS. This open reading frame is contained in one of the *Bam*HI rightward transcripts that are expressed in all EBV-associated tumors. RPMS1 acts as an antagonist of Notch signalling (Zhang *et al.,* 2001).

1.8.2. Bacteria

Chlamydia pneumoniae, *Mycoplasma pneumoniae*, *Legionella pneumophila* have emerged as an important cause of respiratory tract infections, accounting for between 15 to 50% of CAP (Sopena *et al.,* 1999).

1.8.2.1. Chlamydia pneumoniae and *Chlamydia psittaci*

Classification and structure

Chlamydia pneumoniae and *Chlamydia psittaci* belong to the family Chlamydiaceae and the genus, *Chlamydophila*. At one point, the Chlamydiaceae were thought to be viruses because they are small enough to pass through 0.45μm filters and are obligate intracellular parasites, however, they also have the following characteristics of bacteria: (1) they contain both deoxyribonucleic acid (DNA) and ribonucleic acid (RNA); (2) they possess inner and outer membranes similar to those of gram-negative bacteria; (3) they manufacture their own proteins; (4) they are susceptible to various antibiotics; and (5) they possess prokaryotic ribosomes (Murray *et al.,* 2005). Chlamydiaceae, unlike other bacteria, have a unique developmental biphasic growth cycle whereby they form elementary bodies which are the metabolically inactive infectious forms (extracellular) and reticulate bodies, which are the metabolically active non-infectious forms (intracellular) (Hahn *et al.,* 2002).

Chlamydia pneumoniae is an ubiquitous, obligate, intracellular bacterium associated with a wide variety of acute and chronic diseases. *Chlamydia*e multiply within membrane-bound vacuoles in eukaryotic host cells but are incapable of generating adenosine triphosphate (ATP) and thus are dependant on the host cell ATP deposits for all energy requirements. In addition,

they are incapable of *de novo* nucleotide biosynthesis and are thus dependent on host nucleotide pools (Cosentini *et al.,* 2001).

Pathogenesis

Chlamydia inflicts damage by causing the release of antigen onto epithelial cell surfaces that stimulate host immune (inflammatory) responses and ciliostasis (Shemer-Avni and Lieberman, 1995). The organism also infects alveolar macrophages, although it is almost certainly incapable of establishing productive infections in these cells (Hahn *et al.,* 2002).

It is transmitted from person to person via respiratory droplets and has an incubation period of 7-21 days (Grayston *et al.,* 1990).

C. psittaci is the cause of psittacosis (parrot fever) which can be transmitted to humans from parrots. The natural reservoir of *C. psittaci* is virtually any species of birds, mostly psittacine birds (e.g., parrots, parakeets, macaws) and the bacterium is usually transmitted to humans through inhalation of urine, respiratory secretions or dried bird excrement. Person-to-person transmission is rare. Illness develops after an incubation of 5 to 14 days (Murray *et al.,* 2005).

Effect of disease in adults

C. pneumoniae causes acute respiratory disease including pneumonia, bronchitis, sinusitis and pharyngitis (Gouriet *et al.,* 2006). Initial symptoms most frequently reported by patients with *C. pneumoniae* are sore throat and hoarseness and a dry persistent cough often sets in after a period of up to a week (Grayston *et al.,* 1990). Although PCR holds a promise as a rapid diagnostic test for *C. pneumoniae* infection, serological testing remains the most commonly used method (Kumar and Hammerschlag, 2007).

Infection by *C. psittaci* occurs by means of the respiratory tract, after which the bacteria spread to the reticuloendothelial cells of the liver and spleen. Symptoms range from headache, high fever, chills and malaise. Patients may also experience gastrointestinal tract symptoms such as diarrhoea, nausea and vomiting. Untreated cases may result in death (Murray *et al.,* 2005).

Target gene for real-time PCR

***C. pneumoniae* - 16S ribosomal RNA gene:** This is a highly conserved region in the Chlamydiaceae family. This gene contains conserved and variable regions according to their taxonomic genetic stability. Organisms can be classified into different taxonomy levels based on variations of DNA sequences in these regions. Organisms within a domain frequently share the same DNA sequence in the most conserved region, while species of the same genus may be distinguished using the DNA sequence in the variable regions (Woese *et al.,* 1990).

***C. psittaci* - Outer membrane protein (OmpA) gene:** OmpA genes encode the cysteine-rich major outer membrane protein (MOMP). MOMP has a function in immunogenicity and potential function as a cellular adhesion (Millman *et al.,* 2001).

1.8.2.2. Mycoplasma pneumoniae

Classification and structure

Mycoplasma pneumoniae is the smallest of all free-living organisms (10 x 200nm), stains Gram negative, appears filamentous, does not possess a peptidoglycan wall, and is bounded instead by a sterol triple-layered plasmic membrane (Gleason, 2002). It displays a neuraminic acid receptor site for attachment to host cell membranes (Cosentini *et al.,* 2001).

The lack of a cell wall has been linked to atypical biochemical, cultural and serological behaviour, distinct pleiomorphism, and from a clinical perspective, resistance to antibiotics that hinder cell wall synthesis. It is taxonomically separate from bacteria and belongs to the class Mollicutes. It is a slow growing, pleiomorphic, nonmotile, aerobe that ferments glucose (Cosentini *et al.,* 2001).

Pathogenesis

M. pneumoniae is a frequent causative agent of CAP and lower respiratory tract infections (LRTI) in children and young adults (Templeton *et al.,* 2003) ranging from mild to life-threatening infections. *M. pneumoniae* attaches to the respiratory epithelium, acquiring essential exogenous nutrients for growth. It may become intracellular (Baseman and Tully, 1997). Additionally, it produces hydrogen peroxide and superoxide, causing injury to epithelial cells and associated cilia. This damage to the epithelial layer likely facilitates co-infection with other pathogens.

M. pneumoniae can be transmitted through aerosol droplets or nasal secretions from person to person after exposure to an acutely ill coughing individual. The incubation period ranges from 2 to 4 weeks (Gouriet *et al.,* 2006). After attaching to epithelial cells by means of its neuraminic differentiated terminal unit, *M. pneumoniae* disrupts cell RNA and protein synthesis, resulting in inflammatory cell recruitment, ciliostasis, denaturation of cilia and extensive epithelial cell injury (Cosentini *et al.,* 2001).

Effect of disease in adults

Infection caused by *M. pneumoniae* usually mimics viral respiratory syndrome. The most common manifestations include sore throat, hoarseness, fever, a non-productive cough, headache, chills, coryza, myalgias and general malaise. Since this organism is not sensitive to β-lactam antibiotics which are often used for the empirical treatment of LRTI, a rapid diagnostic method is required for the prescription of effective antibiotics (Hardegger *et al.,* 2000).

Target gene for real-time PCR

Cytadhesin P1 protein: The protein is the major adhesin mediating the attachment of this mycoplasma to respiratory epithelium (Yang *et al.,* 2002).

1.8.2.3. Legionella pneumophila

Classification and structure

The genus *Legionella* includes about 40 different species of thin, nonspore-forming, pleiomorphic, uncapsulated, aerobic, gram-negative bacilli, with more than 60 described serogroups. *Legionella* is rich in ramified fatty acids and thrives in water reservoirs (Cosentini *et al.,* 2001). Within the species *L. pneumophila* there are 15 serogroups, with serogroups 1 being commonly found clinically and the only serogroup identified by the commercially available urine antigen test for *Legionella* (Gleason, 2002). They are fastidious organisms and only grow on specialised media (Gouriet *et al.,* 2006).

Pathogenesis

Legionella can replicate intracellularly within respiratory monocytic cells and invoke their damage by inhibiting phagocyte-liposome fusion. Risk factors for infection with *Legionella* include advanced age, alcoholism, cigarette smoking, chronic disease, immunosuppression and organ transplantation (Marston *et al.,* 1994).

Effect of disease in adults

Available data indicate that the most likely mode of transmission is direct inhalation from *Legionella*-contaminated water supply systems. Patient isolation is not required as no person-person transmission has been reported. The incubation period ranges from 2 to 10 days. Most patients report high fever (>40°C) and dry cough (Cosentini *et al.,* 2001). In immunocompromised patients, pneumonia produced by *Legionella* can result in a fatal outcome in up to 50% of cases (Yu, 2000). The vast majority of such cases (up to 85%) are caused by *L. pneumophila*, the most common pathogenic species of the *Legionella* genus (Cosentini *et al.,* 2001).

Target gene for real-time PCR:

Macrophage infectivity potentiator (*mip*) gene: The *mip* gene sequences of *Legionella* species code for an immunophilin of the FK506 binding protein (FKBP) class and belongs to the enzyme family of peptidylprolyl *cis*/*trans* isomerases (Hacker and Fischer, 1993). This protein, which ranges in size from 232 to 251 amino acids, depending on the *Legionella* species (Ratcliff *et al.,* 1997), is an outer membrane protein essential in the intracellular cycle of *Legionella*. The reason for targeting the *mip* gene of *L. pneumophila* is because the gene encodes a macrophage infectivity potentiator and is identified only in *L. pneumophila* (Morozumi *et al.,* 2006).

1.8.3. Fungi

1.8.3.1. Pneumocystis jirovecii

Classification and structure

Pneumocystis jirovecii is an ascomycetous fungus that causes opportunistic infections, predominantly pneumonia, in patients with weakened immunity due to HIV, transplantation, malignancy and connective tissue disease (Miller and Huang, 2004). This organism was first called *P. carinii* after it had been identified in rat lungs by Antonio Carinii in 1910 (Thomas and Limper, 2007). Based on the histological characteristics of its trophozoite and cyst life forms, it was classified as a protozoan. However, in 1988, *P. carinii* was placed into the fungal kingdom after sequencing of the small ribosomal RNA subunit (Edman *et al.,* 1988). Since its discovery, every mammal has been shown to possess a unique form of *Pneumocystis* with different genetics and strong host specificity. The form that infects humans has been named *P. jirovecii* after Jirovec, the pathologist who first reported it in humans (Stringer *et al.,* 2002). Study of the organism has been severely hindered by the fact that it cannot be cultured *in vitro* (Thomas and Limper, 2004).

Pathogenesis

The route by which human *Pneumocystis* is transmitted is unclear. It's DNA has been identified in air spores from both rural and hospital environments, and it is possible that transmission between humans occurs via the airborne route (Miller *et al.,* 2001). Studies have shown a decline in the number of AIDS-related opportunistic infections attributed to the use of highly active antiretroviral therapy (HAART), increasing use of HIV prophylaxis, and improved awareness of this infection (Pulvirenti *et al.,* 2003).

Serologic studies have resulted in the detection of specific antibodies to the pathogen in most children early in life (Medrano *et al.,* 2003) and based on this finding, disease in immunocompromised patients has been thought to result from reactivation of latent infection acquired in childhood. This "latency" hypothesis has been disputed by studies showing a lack of *Pneumocystis* in the lungs of healthy humans (Wakefield *et al.,* 1990) and by studies which showed that *Pneumocystis* organisms are frequently acquired and cleared by the immune system of immune competent individuals (Miller *et al.,* 2001).

In the last 10 years, PCR has considerably increased the sensitivity of detection of *Pneumocystis*, to 86-100% in BAL, aspirates, and induced sputum specimens (Flori *et al.,* 2004). However, one problem with the technique is that it is frequently positive (2-21%) in patients with asymptomatic carriage (Maskell *et al.,* 2003). Real-time PCR could have a role in distinguishing between colonization and clinical disease with the application of threshold cutoff values as described by Larsen *et al*., (2002). *P. jirovecii* patients would have a higher organism's burden than colonised patients indicated by the threshold values obtained form the real-time PCR fluorescence curves generated.

Effect of disease in adults

Typical symptoms of pneumocystis pneumonia include the subtle onset of progressive dyspnea, nonproductive cough or cough productive of clear sputum, malaise, and low-grade fever (Thomas and Limper, 2004). These symptoms are amplified in HIV-infected patients with them often presenting with a higher arterial oxygen tension and a lower alveolar-arterial oxygen gradient (Krajicek *et al.,* 2008).

Target gene for real-time PCR

Mitochondrial large subunit rRNA (mtLSU rRNA) gene: The mtLSU rRNA gene is implicated in basic metabolic functions and this is the locus used most extensively for PCR-based detection of *P. jirovecii*, as it is present in a large number of copies (Esteves *et al.,* 2008).

1.8.4. Glyceraldehyde-3-phosphate dehydrogenase (GAPDH)

GAPDH is a tetramer composed of four identical 37 kDa monomers (Sirover, 1996). It can be used as an endogenous control i.e. a template that occurs naturally within the specimen being examined which in this case is human. GAPDH has vital functions in mammalian cells as shown in Table 1.1 and therefore will always be present in human tissue. Housekeeping genes have been used successfully to quantitate gene expression by real-time PCR and monitor the integrity of a template for quantification and other purposes (Chehab *et al.,* 1987).

Table 1.1: Functions performed by GAPDH in mammalian cells. Adapted from Sirover, (1996).

CELL FUNCTION	INTRACELLULAR LOCALIZATION	ACTIVITY
Macromolecular transport	Cytoplasm	Endocytosis
Energy generation	Cytoplasm	Glycolysis
Control of gene expression	Cytoplasm, Nucleus	Regulation of translation
Prevention of genomic instability	Nucleus	Repair of DNA molecules
Transfer of genetic information	Nucleus	Replication of DNA

1.9. Statement of the problem

The diagnostic capacity of the classical microbiology laboratory in the routine identification of the causative organisms in patients with CAP has limitations. Culture of samples typically requires several days and an isolated pathogen is documented in less than 50% of patients with CAP (Stralin *et al.,* 2006). Since CAP is a serious infection, antimicrobial treatment cannot be delayed while awaiting microbiological identification of the etiological agents. Empiric antimicrobial therapy must be initiated based on clinical symptoms, radiographic and other laboratory findings.

Recent studies (Templeton *et al.,* 2005; Morozumi *et al.,* 2006) have shown that real-time PCR assays are more sensitive for the detection of the major viral, typical and atypical bacterial causative agents of CAP than standard microbiological methods. Since the spectrum of organisms in an area will define which diagnostic tests and treatment should be offered, it is essential to establish the most common causative agents of CAP in the selected population. Routine investigation of sputum specimens for diagnosis of CAP is not currently regarded as a rational approach, but the periodic surveillance of etiological organisms in an area should result in more informed treatment decisions being made.

`

1.10. Justification of the study

There remains much that is still unknown regarding the etiology of CAP in South Africa. Data from prospective studies are restricted to a few European countries, with most performed in the UK and Spain and few on the African continent (Woodhead, 2002). Since early intervention with appropriate antibiotics has been shown to decrease mortality and transmission of infection, knowledge of the most likely agents to cause CAP at the Charlotte

Maxeke Johannesburg Hospital should improve the care of patients with CAP at this facility. (Moine *et al.,* 1994; Leroy *et al.,* 1995). There is therefore a need to establishment sensitive and rapid pathogen detection methods to reduce the potential of nosocomial transmission to high-risk patients such as neonates and direct appropriate therapy following specific pathogen detection.

Real-time PCR in conjunction with multiplex PCR kits employing the DPO technology were the molecular methods used in this study to detect a panel of respiratory viruses that literature has suggested as common causative organisms of CAP. These methods have been proved in other studies to have increased sensitivity, throughput and quantitative potential.

Real-time PCR has been described for a variety of clinical applications, namely genotyping, mRNA quantification and pathogen detection just to mention a few. For pathogen detection, this technique has been found to be reproducible (Loeb *et al.,* 2000) and accurate when using TaqMan probes (Desjardin *et al.,* 1998). TaqMan assays have proved to be much more sensitive than culture methods (Schweiger *et al.,* 2000) and ELISA-based assays (Guiver *et al.,* 2000).

The multiplex PCR kits that employ DPO technology have also been validated for the detection of respiratory pathogens (Chun *et al.,* 2007). The DPO technology does not suffer from any limitations of annealing temperature. Because the long DPO primer is divided into two target specific priming regions by the linker, the segments have distinct priming functions and non-target amplification is eliminated.

1.11. Objectives

1.11.1. Overall Objective

The primary objective of this study was to establish molecular methods for the detection of atypical bacterial, fungal and viral etiological agents that could be used to study their prevalence locally.

The specific objectives of this study were to:

1.11.2. Specific Objectives

- To establish a nucleic acid extraction method for isolation of both DNA and RNA from patient sputa and nasopharyngeal swabs, that permits downstream PCR analysis.
- To establish methods for the rapid, qualitative detection of: *Mycoplasma pneumoniae*, *Chlamydia pneumoniae, Chlamydia psittaci, Pneumocystis jirovecii, Legionella pneumophila,* parainfluenza virus (PIV) 1, 2 and 3, adenovirus (AdV), respiratory syncytial virus (RSV), influenza virus (Flu) A and B, cytomegalovirus (CMV), human metapneumovirus (hMPV), and Epstein-Barr virus (EBV) using the BioRad Chromo4 real-time detection system.
- To compare results of real-time PCR with those of respiratory pathogen detection kits using patient samples and simulations.

CHAPTER 2: MATERIALS AND METHODS

All reagents were of analytical or molecular grade. For a complete list of the composition of all media and buffers/solutions used, see Appendix A.

2.1. Bacterial, fungal and viral controls

Positive controls in the form of viral culture supernatants, direct culture and in some cases, nucleic acid, of bacteria, fungi and viruses were obtained from the following sources:

- National Institute for Communicable Diseases (NICD)
- University of Cape Town (Craig Corcoran)

These laboratories could not provide information on bacterial, fungal or viral loads of the positive controls.

DNA and RNA used for the human internal controls were obtained from buccal swabs.

2.2. Sample collection

Ethics clearance to allow patient sample collection for this research was obtained from the Human Ethics Committee (Medical) with the ethics clearance number M070345 (Appendix F). This project is part of a larger CAP etiology study (see ethics clearance certificate), involving collection of samples by clinicians at the Charlotte Maxeke Johannesburg Hospital. However, due to factors beyond our control, sample collection was sporadic and only 3 samples were submitted during 2008. Therefore, for the purpose of method validation, patient samples were simulated. Because nasopharyngeal swabs are standard specimens for respiratory viral diagnosis, Copan ESwabs (Copan Italia, Brescia, Italy) were used to collect samples from the nasopharynx of 3 CAP patients and also used to simulate the collection of a further 2 swabs on which detection

of viruses could be performed. Copan ESwabs enable collection and safe transportation of swab samples. The Copan ESwab has a nylon flocked applicator intended for the collection of samples from the nasopharynx. The swab incorporates a modified Liquid Amies transporting medium comprising calcium, inorganic phosphate buffer, and magnesium salts. This medium sustains the viability of a number of organisms that are of clinical importance and is free of enzymes and inhibitors that may interfere with molecular amplification assays. In addition, it stabilizes bacterial and viral antigens and nucleic acids during transit to the testing laboratory. For bacterial and fungal detection, sputum samples were collected from the same CAP patients from whom nasopharyngeal swabs were collected.

To simulate the conditions of a nasopharyngeal swab, Copan ESwabs were immersed in a mixture of 50 µl each FluA, RSV, CMV, PIV1 and PIV2 viral culture (viral load not quantified) for a few seconds before the swab was transferred into the liquid Amies medium that was supplied with the swabs. Nasopharyngeal swab simulations were done in duplicate.

For sample simulation, sputum samples from cystic fibrosis patients were obtained from Charlotte Maxeke Johannesburg Hospital (formally Johannesburg General Hospital). Samples from these patients were used since they are collected routinely and not due to clinical suspicion of CAP. They were judged to be less likely than clinical specimens to contain the organisms under investigation.

2.3.DNA/RNA extraction

Both RNA (FluA, FluB, RSV, hMPV, PIV1, PIV2, and PIV3) and DNA (EBV, CMV, AdV, *P. jirovecii, M. pneumoniae*, *C. pneumoniae*, *L. pneumophila* and *C. psittaci*) organisms were

investigated in this study. Both RNA and DNA reactions were internally controlled using GAPDH (DNA) for DNA organisms and GAPDH (RNA) for RNA organisms. The purpose of including GAPDH internal controls was to monitor extraction and reaction steps involving both DNA and RNA organisms to enable the detection of inhibition. Nucleic acids were extracted from the culture supernatants or colonies and patient samples and simulations.

2.3.1. Positive control extraction

DNA and RNA were extracted from 200 µl of the bacterial, fungal and viral cultures and from buccal swabs (GAPDH) using a commercial extraction kit (RTP® DNA/RNAVirus Mini Kit; Invitek, Berlin, Germany) according to the instructions of the manufacturer. Briefly, 200 µl of cell culture supernatant was mixed with 200 µl of nuclease free H_2O and transferred to an extraction tube. The mixture was vortexed and incubated in a thermomixer for 15 min at 65°C and then for 10 min at 95°C with continuous shaking. Binding solution (400 µl) was added to the mixture in the extraction tube and after vortexing, the sample was transferred into a spin filter set. The spin filter set was centrifuged for 1 min at 10 600 x *g* after which 500 µl of wash buffer R1 was added and centrifuged for 30 sec at 10 600 x *g*. The filtrate was discarded and the spin filter washed with wash buffer R2 (800 µl), and centrifuged at 10 600 x *g* for 30 sec. Residual ethanol was removed by centrifuging the spin filter for 4 min at 14 000 x *g*. The nucleic acids were eluted into a 1.5ml tube by adding 40-50 µl of prewarmed (80°C) elution buffer directly onto the spin filter surface, incubating for 3 min at room temperature and centrifuging for 1 min at 10 600 x *g*.

2.3.2. Specimen extraction

A pre-extraction procedure provided by BioMe´rieux (St. Laurent, Quebec, Canada), specifically to make sputum samples more fluid, was applied to all sputum samples. Briefly, equal volumes of whole sputum and proteinase K buffer (250 µl each) were added and vortexed. Handling of all sputum samples was done under a Biosafety II hood. The mixture was incubated at 55°C for 60 min, making sure to vortex every 15 min. The complete 500 µl was used for the downstream extraction procedure.

The NucliSens miniMAG System (BioMe´rieux, St. Laurent, Quebec, Canada), which uses silica extraction technology, was used for the nucleic acid extraction from the all sputum and nasopharyngeal swabs following manufacturer's recommendations. Briefly, lysis buffer was centrifuged for 10 sec at 1500 x *g* before the sample (10-1000 µl) was added to the buffer in the lysis buffer tube. Lysis Buffer contains a chaotropic salt for efficient lysis and inactivation of nucleases. The mixture was briefly vortexed, incubated at room temperature for 10 min, then centrifuged for 10 min at 1500 x *g*. The silica slurry was vortexed briefly before transferring 50 µl of it to the mixture in the lysis buffer tube to allow DNA binding. The contents of the lysis buffer tube were mixed gently and incubated at room temperature without further mixing. After 2 min, the lysis buffer tube was centrifuged at 1500 x *g* for 2 min. Next, the supernatant was transferred to a screw cap 1.5 ml tube and the silica particles were washed twice with 400 µl of Wash Buffer 1 (guanidine thiocyanate, Tris/HCl, TritonX 100, EDTA) for 30 sec per wash, once with 500 µl of Wash Buffer 2 (morpholine-4-ethanesulfonic acid (MES) hydrate) for 30 sec, and once with 500 µl of Wash Buffer 3 (component: disodium tetraborate) for 15 sec using the NucliSens® miniMAG™ instrument to remove any contaminants from the specimen. The removal of wash buffer between each wash step was done by vacuum aspiration. The magnet was

activated during the wash steps and when removing the wash buffer. Finally, DNA was recovered from the particles by adding elution buffer (25 µl) to the silica and incubating in a thermoshaker for 5 min at 60°C shaking at 1400 rpm. The tubes were placed on a magnetic rack and the extracted DNA and RNA (25 µl) was transferred by pipetting to a clean storage tube and used for real-time PCR amplification.

2.4.Reverse Transcription

Reverse transcription of RNA was performed using the High Capacity cDNA Reverse transcription Kit (Applied Biosystems, Foster City, CA) according to manufacturer's recommendations. Briefly, reverse transcription master mix (10µl) was prepared: 10X RT Buffer (2 µl); 25X dNTP Mix (0.8 µl); 10X RT random primers (2 µl); MultiScribe ™ Reverse Transcriptase (1 µl); RNase Inhibitor (1 µl); nuclease-free H_2O (3.2 µl). An equal volume of RNA sample was added to the master mix in 0.2 ml white PCR tubes (Abgene, Surrey, UK) and mixed by pipetting up and down. The mixture was briefly centrifuged to settle the contents. The tubes were placed into the Chromo4 Thermal cycler system (Bio-Rad, Hercules, USA) and incubated at 25°C for 10 min, followed by 37°C for 120 min and 85°C for 5 sec to inactivate the enzyme.

2.5.Real-time PCR

All reactions were initially performed in singleplex using SYBR® Green I (Bio-Rad, Hercules, USA) to determine whether the primers and reaction conditions worked. On establishing this, singleplex reactions using TaqMan probes (Inqaba Biotech, Pretoria, South Africa and TIB MolBiol, Berlin, Germany) were then performed to test the probes and establish appropriate primer and probe concentrations.

Multiplex reactions were performed thereafter using TaqMan probes to reduce the number of total reactions performed. Different master mixes were used for singleplex and multiplex reactions. Total volumes of master mixes used were 12.5µl in total reaction volumes of 25µl and 25µl in total reaction volumes of 50µl. Most reactions were performed in total volumes of 25 µl in thin-walled 0.2 ml white PCR tube strips (Abgene, Surrey, UK).

Some of the primers and probes used for the real-time PCR reactions described in this study were adapted from literature (Table 2.1 and Table 2.2). GAPDH (RNA) primers were adopted from Barber *et a*l., 2005 which were designed such that the majority of primer nucleotides were within the exon region of the genome so that only RNA would be amplified and not DNA. Some primers and probes were designed using the Beacon Designer Software Program (Biosoft International, Strategene, La Jolla, CA, USA) since suitable primers and probes could not be found in the literature (Tables 2.1 and 2.2). GAPDH (DNA) primers were designed such that the majority of primer nucleotides were within the intron region of the genome so that only DNA would be amplified and not RNA.

The factors taken into consideration when designing probes were the length (15 to 35 nucleotides), G+C content (40 to 60% with more Cs than Gs) and melting temperature (T_m) (5-10°C higher than that of the primers). In addition, it was ascertained that no self-complementarity was present, no G nucleotides were present at the 5' end to quench the fluorescent signal after hydrolysis and no runs of the same nucleotides were present. Primers were designed to amplify fragments of sufficiently different sizes to allow them to be distinguished by gel electrophoresis. A BLAST search (http://www.ncbi.nlm.nih.gov/blast) was performed to check specificity of the sequences of the primers and probes.

2.5.1. Primer sequences

Table 2.1: Primer sequences and final concentrations used for real-time PCR assays and product sizes.

Primer[a]	Primer Sequence	Polarity	Final concentration	Origin	Amplicon Size
FluA F[b]	5' AAAGCGAATTTCAGTGTGAT 3'	+	750 nM	Templeton *et al*., 2004	104bp
FluA R[c]	5' GAAGGCAATGGTGAGATTT 3'	-	750 nM		
FluB F	5' GTCCATCAAGCTCCAGTTTT 3'	+	1000 nM	Gunson *et al*., 2005	145bp
FluB R	5' TCTTCTTACAGCTTGCTTGC 3'	-	1000 nM		
MPV F	5' AACCGTGTACTAAGTGATGCACTC 3'	+	1500 nM	Gunson *et al*., 2005	213bp
MPV R	5' CATTGTTTGACCGGCCCCATAA 3'	-	1500 nM		
PIV1 F	5' ACCTACAAGGCAACAACATC 3'	+	500 nM	Templeton *et al*., 2004	129bp
PIV1 R	5' CTTCCTGCTGGTGTGTTAAT 3'	-	500 nM		
PIV2 F	5' GCATTTCCAATCTTCAGGACTATGA 3'	+	500 nM	Brittain-Long *et al*., 2008	90bp
PIV2 R	5' ACCTCCTGGTATAGCAGTGACTGAAC 3'	-	500 nM		
PIV3 F	5' CCAGGGATATACTACAAAGGCAAAA 3'	+	500 nM	Gunson *et al*., 2005	101bp
PIV3 R	5' CCGGGACACCCAGTTGTG 3'	-	500 nM		
EBV F	5' CGGAAGCCCTCTGGACTTC 3'	+	500 nM	Wada *et al*., 2007	90bp
EBV R	5' CCCTGTTTATCCGATGGAATG 3'	-	500 nM		
CMV F	5' GACTAGTGTGATGCTGGCCAAG 3'	+	500 nM	Wada *et al*., 2007	201bp
CMV R	5' GCTACAATAGCCTCTTCCTCATCTG 3'	-	500 nM		
RSV F	5' GCAAATATGGAAACATACGTGAACA 3'	+	500 nM	Brittain-Long *et al*., 2008	115bp
RSV R	5' GCACCCATATTGTWAGTGATGCA 3'	-	500 nM		
AdV F	5' GCCGCAGTGGTCTTACATGCACATC 3'	+	500 nM	Brittain-Long *et al*., 2008	132bp
AdV R	5' GCCCCAGTGGTCTTACATGCACATC 3'	-	500 nM		
MpneumoF	5' AAAACAAGGTCCCCGTCGAG 3'	+	500 nM	This study	102bp
MpneumoR	5' GCTGCAACTGCTCATAGTACAC 3'	-	500 nM		
LpneumoF	5' AGAGTTAGCGGTCGCATTCAG 3'	+	500 nM	This study	107bp
LpneumoR	5' ATGTGATCTGCAAGTCGAAAAGTC 3'	-	500 nM		
CpneumoF	5' CGGAGCTAACGTGTTAAGTATGC 3'	+	500 nM	This study	127bp
CpneumoR	5' TAAGGTCCTTCGCGTTGCATC 3'	-	500 nM		
GAPDH (DNA) F	5' GAGAAGTATGACAACAGCCTCAAG 3'	+	500 nM	This study	112bp
GAPDH (DNA) R	5' TGAGTCCTTCCACGATACCAAAG 3'	-	500 nM		
GAPDH (RNA) F	5' GAAGGTGAAGGTCGGAGTCAAC 3'	+	200 nM	Barber *et al*., 2005	71bp
GAPDH (RNA) R	5' CAGAGTTAAAAGCAGCCCTGGT 3'	-	200 nM		
Cpsi F	5' TGCAAGACACTCCTCAAAGCC 3'	+	500 nM	This study	102bp
Cpsi R	5' TGTGCTCGCTATTCTAATTTGCTC 3'	-	500 nM		
PjiroF	5' CTTAAAATAAATAATCAGACTATGTGCGATAAG 3'	+	1000 nM	Meliani *et al*., 2003	79bp
Pjiro R	5' GGAGCTTTAATTACTGTTCTGGGC 3'	-	1000 nM		

[a] **FluA** (Influenza A virus); **FluB** (Influenza B virus); **MPV** (human metapnemovirus); **PIV1** (Parainfluenza virus 1); **PIV2** (Parainfluenza virus 2); (**PIV3** (Parainfluenza virus 3); **EBV** (Epstein-Barr virus); **CMV** (Cytomegalovirus); **RSV** (Respiratory syncytial virus); **AdV** (adenovirus); **Mpneumo** (*M. pneumoniae*); **Lpneumo** (*L. pneumophila*), **Cpneumo** (*C. pneumoniae*); **GAPDH** (Glyceraldehyde-3-phosphate dehydrogenase); **Cpsi** (*C. psittaci*); **Pjiro** (*P. jirovecii*).
[b]F (Forward), [c]R (Reverse)

2.5.2. Probe sequences

Table 2.2: TaqMan probe sequences and final concentrations used for real-time PCR assays.

Probe	Probe Sequence [d]	Final concentration	Origin
FluA Probe	5' **FAM**-AGGGCTTTCACCGAAGAGGG-**BHQ1** 3'	200 nM	Templeton *et al.*, 2004
FluB Probe	5' **HEX**-AACGAAGTAGGTGGAGACGGAGG-**BBQ** 3'	200 nM	Gunson *et al.*, 2005
MPV Probe	5' **Cy5**- CTTTGCCATACTCAATGAACAAAC -**BHQ3** 3'	300 nM	Gunson *et al.*, 2005
PIV1 Probe	5' **FAM**-CAAACGATGGCTGAAAAAGGGA-**BHQ1** 3'	300 nM	Templeton *et al.*, 2004
PIV3 Probe	5' **Cy5.5**-TGGATGTTCAAGACCTCCATACCCGAGAAA-**BBQ** 3'	300 nM	Gunson *et al.*, 2005
EBV Probe	5' **FAM**-TGTACACGCACGAGAAATGCGCC-**BHQ1** 3'	300 nM	Wada *et al.*, 2007
CMV Probe	5' **HEX**-AGCCTGAGGTTATCAGTGTAATGAAGCGCC-**BHQ1** 3'	300 nM	Wada *et al*., 2007
RSV Probe	5' **FAM**-CTTCACGAAGGCTCCACATACACAGCWG-**BHQ1** 3'	300 nM	Brittain-Long *et al*., 2008
AdV Probe	5' **HEX**-TGCACCAGACCCGGGCTCAGGTACTCCGA-**BHQ1** 3'	300 nM	Brittain-Long *et al*., 2008
Mpneumo Probe	5' **FAM**-TGGCCCAAGACCCCTCCAATCCTT-**BHQ1** 3'	300 nM	This study
Lpneumo Probe	5' **HEX**-CTCGCGTCACAATGCCACGGTGT- **BHQ1** 3'	300 nM	This study
Cpneumo Probe	5' **HEX**-ACATGCTCCACTGCTTGTGCGGGC-**BHQ1** 3'	300 nM	This study
GAPDH (DNA) Probe	5' **FAM**- TCAGCAATGCCTCCTGCACCACCA-**BHQ1** 3'	300 nM	This study

[d]**FAM**: 6-carboxyfluorescein; **HEX**: hexachloro-6-carboxyfluoroscein; **Cy5.5/Cy5**: tetramethyl-indodicarbocyanine, **BHQ1**- Black hole quencher 1; **BHQ3**- Black hole quencher 3; **BBQ**- BlackBerry quencher**.**

2.5.3. Singleplex reactions

Singleplex real-time PCR reactions were initially performed using SYBR Green I to establish the appropriate reaction conditions and to ascertain whether the primers were functional. TaqMan probes were subsequently individually tested to establish whether the probe was functioning correctly and that the reaction conditions were suitable.

2.5.3.1. SYBR® Green I

The SYBR Green I based real-time PCR assay does not require probes and is economical and easily adapted from conventional PCR. iQ™ SYBR Green Supermix (Bio-Rad, Hercules, USA) was used for SYBR Green I reactions. Melting curves were generated at the end of reactions involving SYBR Green I using the Chromo4 Opticon Monitor™ version 3.1 software to confirm the identity of the organism. However, melting temperatures may vary slightly as the SYBR

Green I concentration changes. Thermocycling conditions of organisms investigated are shown in the tables below. Some organisms shared the same cycling conditions and these were later grouped and multiplexed, as will be shown in the next section of this chapter.

Table 2.3: Real-time PCR thermocycling conditions for FluA, FluB and hMPV. These reactions were initially done as separate single real-time PCR reactions using SYBR Green I, then using TaqMan probes and finally multiplexed.

Step	Temperature	Time	Number of Cycles
Initial denaturation	95°C	3 minutes	1
Denaturation	95°C	30 seconds	49
Annealing	55°C	30 seconds	
Extension	72°C	30 seconds	
Plate Read			
Melting Curve	55°C to 90°C	1 second	1

Three-step real-time PCR reactions were performed for all bacteria and viruses investigated and thermocycling conditions using SYBR Green I were the same as those shown in Table 2.3 for all except for the annealing temperatures: PIV1 and PIV3 (49°C), EBV, CMV and GAPDH (RNA) (56°C), RSV, AdV and GAPDH (DNA) (58°C) and PIV2 (57°C). A two-step real-time PCR reaction was performed for *P. jirovecii* and thermocycling conditions are shown in Table 2.4.

Table 2.4: Real-time PCR thermocycling conditions for *P. jirovecii*.

Step	Temperature	Time	Number of Cycles
Initial denaturation	95°C	3 minutes	1
Denaturation	95°C	1 minute	39
Annealing + Extension	60°C	1 minute	
Plate Read			
Melting Curve	55°C to 90°C	1 second	1

2.5.3.2. TaqMan probes

After succeeding with the SYBR Green I real-time PCR reactions, reactions incorporating TaqMan probes were performed. Thermocycling conditions used were the same as those used in the SYBR Green I reactions but excluded the melting curve generation step. SYBR Green I only was used for PIV2, *C. psittaci* and *P. jirovecii*. These organisms were detected only with SYBR Green I since they could not be multiplexed and SYBR Green I is more economical than probes.

All primers and probes were manufactured by Inqaba Biotech (Pretoria, South Africa) except for FluB, hMPV, PIV1 and PIV3 which were manufactured by TIB MolBiol (Berlin, Germany). Probes were labeled with the dyes FAM, HEX, CY5 and CY5.5 as they are distinguishable from each other due to their different wavelength maxima. Primers and probes were added to each PCR reaction at the concentrations shown (Tables 2.1 and 2.2). iQ™ Supermix (Bio-Rad, Hercules, USA) was the master mix used for TaqMan singleplex reactions and iQ™ Multiplex PowerMix (Bio-Rad, Hercules, USA) for TaqMan multiplex reactions.

2.5.4. Multiplex reactions

Multiplex real-time PCR allows for the exponential amplification of nucleic acid with the use of more than one primer and probe set, thereby permitting the detection of several DNA, cDNA or plasmid targets in the same reaction vessel. All multiplex real-time PCR reactions were performed in total volumes of 50 µl in thin-walled 0.2 ml white PCR tube strips (Abgene, Surrey, UK) unless otherwise stated. Negative controls (no template) for each organism were included in each experiment. Primers and probes of the organisms multiplexed correspond to those described above (Tables 2.1 and 2.2). It was ensured that organisms to be multiplexed had probes labeled with different dyes to prevent overlap. Organisms were grouped to be multiplexed in the manner shown below from reaction 1 to reaction 6. Although many of the primers and probes have been published, in this study, they have been multiplexed in novel ways (Reaction 1, 2 and 4). In reaction 1, primer and probe sequences of Influenza virus A were adopted from Templeton *et al*., 2004 and those of Influenza virus B and hMPV were from Gunson *et al*., 2005. In reaction 2, primer and probe sequences of PIV1 were adopted from Templeton *et al*., 2004 and those for PIV3 from Gunson *et al*., 2005. In reaction 4, both primer and probe sequences were adopted from Brittain-Long *et al*., 2008, but were not multiplexed as was done in this article.

- **Reaction 1: Influenza virus A, Influenza virus B and human Metapneumovirus**

  The multiplex reaction was performed at final forward and reverse primer concentrations of 1500nM (FluA), 500nM (FluB) and 750nM (hMPV). Probes were added to the reaction at the concentrations shown (Table 2.2).

- **Reaction 2: Parainfluenza virus 1 and parainfluenza virus 3**

  The multiplex reaction was performed using final forward and reverse primer concentrations of 1000nM (PIV1) and 500nM (PIV3). Probes were added to the reaction at the concentrations shown (Table 2.2).

- **Reaction 3: Epstein-Barr virus and cytomegalovirus**

  The reaction was performed in a total volume of 25 µl. Primers and probes were added at the concentrations shown (Tables 2.1 and 2.2).

- **Reaction 4: Respiratory syncytial virus and adenovirus**

  This multiplex reaction was performed at final primer concentrations of 1000nM (RSV) and 500nM (AdV). Probes were added at the concentrations shown (Table 2.2).

- **Reaction 5: *Mycoplasma pneumoniae* and *Legionella pneumophila***

  The reaction was performed in a total volume of 25 µl. Primers and probes were added at the concentrations shown (Tables 2.1 and 2.2).

- **Reaction 6: *Chlamydia pneumoniae* and Glyceraldehyde-3-phosphate dehydrogenase (DNA)**

  The reaction was performed in a total volume of 25 µl. Primers and probes were added to at the concentrations shown (Tables 2.1 and 2.2).

2.6.Interpretation of real-time PCR data

A positive real-time PCR result was determined by identifying the threshold cycle number (C_t) at which standardized reporter dye emission raised above background noise (equivalent to the mean baseline emission plus 10X the standard deviation of the mean baseline fluorescence calculated for PCR cycles 3 – 15) (Mackay 2004) which was calculated by the Chromo4 Opticon Monitor 3.1 software. Manual adjustment of the baseline was done in instances where fluorescence was low, or background noise was high.

2.7.Agarose gel electrophoresis

After real-time PCR on the Chromo4 thermocycler (Bio-Rad, Hercules, USA), amplification products were analysed by electrophoresis in 2% (w/v) (singleplex reactions) or 3% (w/v) (multiplex reactions) electroendosmotic (EEO) agarose in 1X Tris acetate EDTA (TAE) buffer. Six microliters of 50bp O'GeneRuler™ (Fermentas GMBH, Germany) was used as the marker. DNA was resolved at a constant voltage of 100 V. DNA bands were visualised and its image captured under UV light in the Gel doc 1000 image system (Bio-Rad, Hercules, USA).

2.8.Seeplex detection kits

The Seeplex® RV5 auto-capillary electrophoresis (ACE) Screening kit (Seegene, Seoul, Korea) was used to screen for viruses in nasopharyngeal swabs. Fifteen viral pathogens (FluA, FluB, hMPV, PIV1, PIV2, PIV3, rhinovirus A, rhinovirus B, coronavirus 229E, coronavirus NL63, coronavirus OC43, coronavirus HKU1 and bocavirus) can be detected by this kit, 6 of which can be detected by the real-time PCR assays used in this study. For bacterial detection, the Seeplex® Pneumobacter ACE detection kit (Seegene, Seoul, Korea) was used. The kit detects 6 pathogens (*M. pneumoniae*, *L. pneumophila*, *S. pneumoniae*, *Haemophilus influenzae*, *Bordetella pertussis*

and *C. pneumoniae*), 3 of which can be detected by the real-time PCR reactions developed in this study. Briefly, PCR was conducted in a final volume of 20 µl containing 4 µl of 5X RV5 ACE primer mix in the case of viral detection from nasopharyngeal swabs or 5X PB ACE primer mix in the case of bacterial detection from sputum samples, 3 µl of 8-MOP solution and 10 µl 2X Multiplex Master Mix and 3 µl of the sample nucleic acid. A positive and negative control supplied with the kits was included for all reactions performed. PCR was performed in an iCycler iQ™ (Bio-Rad, Hercules, USA) with the following thermal profile: An initial hot start step at 94°C for 15min, 40 cycles at 94°C for 30 sec, 60°C for 1.5 min, 72°C for 1.5 min and 1 cycle for 10 min at 72°C. Detection was performed on a 2% agarose gel stained with ethidium bromide (0.5µg/ml). DNA marker (5 µl) (PB ACE Marker or RV5 ACE Marker) supplied with the individual kits and 5µl of PCR product was loaded on the agarose gel. Six microlitres of a 50bp DNA ladder (Fermantas, O'GeneRuler™ #SM1138, Fermentas GMBH, Germany) was also loaded next to the kit DNA marker to compare band sizes. Gels images were captured using a Gel Doc 1000 image system (Bio-Rad, Hercules, USA).

2.9.Cloning

The viral culture supernatants, bacterial and fungal cultures that were used as positive controls (except *L. pneumophila* and hMPV) could not be quantitated so, as a result, plasmids containing target sequences were constructed. The targets of all studied organisms were cloned except for *L. pneumophila* which was available as a viable culture, and human metapneumovirus, which was available commercially as a plasmid (TIB MolBiol, Berlin, Germany). Bands in the gel were rapidly excised under UV illumination and purified using the QIAquick Gel Extraction Kit (Qiagen, Hilden, Germany) according to the manufacturer's protocol. The product was ligated to pGEM®-T Easy Vector System (Promega, Madison, WI) according to manufacturer's

recommendations using T4 DNA ligase (Amersham Pharmacia Biotech, Little Chalfont, UK). This was transformed into Library Efficiency® DH5α Competent Cells (Invitrogen, Carlsbad, USA) with the genotype F- φ80*lac*ZΔM15 Δ(*lac*ZYA-*arg*F)U169 *rec*A1 *end*A1 *hsd*R17(r_k^-, m_k^+) *pho*A supE44 *thi*-1 *gyr*A96 *rel*A1 λ^-. Transformed cells were plated onto Luria-Bertani (LB)-agar supplemented with ampicillin (100μg/ml), 5-bromo-4-chloro-3-indole-β-D-galactopyranoside (X-gal), and Isopropyl-β–D-thiogalactopyranoside (IPTG) overnight at 37°C.

To confirm the presence of the insert in white colonies, a crude nucleic acid extraction was performed on 3 colonies of each ligation. Briefly, sterile toothpicks were used to pick the colonies and transfer them to 200 μl sterile water in 1.5 ml tubes. The tubes were centrifuged at 14 000 x *g* for 2 min before being placed in a boiling water bath for 5 min. The lysates were then centrifuged at 6 800 x *g* for 2 min to settle the debris and the supernatant containing the nucleic acid was then transferred to a new tube. A real-time PCR using specific primers was performed to ensure the presence of the insert. Minipreps of recombinant pGEM-T plasmids were prepared from viral, fungal and bacterial cultures using Qiagen-tip 20 columns (Qiagen, Hilden, Germany) following the QIAGEN plasmid Mini Kit protocol. Briefly, a freshly streaked transformed colony was picked from LB-agar supplemented with ampicillin (100μg/ml) and inoculated into 5 ml LB broth containing 5 μl ampicillin (100μg/ml) for 8 hrs at 37°C shaking at 300 rpm. This starter culture was then diluted by transferring 6μl into 3 ml of LB broth supplemented with 3 μl ampicillin (100μg/ml). The culture was left to shake at 37°C for 12-16 hrs at approximately 300 rpm. The cell cultures were harvested by centrifugation at 6000 x *g* for 15 min and the pellet resuspended in 0.3 ml of Buffer P1 with RNase A and LyseBlue reagent added to it. Buffer P2 (0.3 ml) was added to the mixture and the tube inverted 4-6 times. The mixture immediately turned blue upon adding Buffer 2 and this was incubated at room temperature for 5 min. Chilled

Buffer P3 (0.3 ml) was added to the blue solution and mixed thoroughly by vigorously inverting the tube 4-6 times before incubating on ice for 5 min. A fluffy white material immediately formed in the tube on addition of Buffer P3. All traces of blue disappeared on mixing and a homogenous colorless suspension was formed indicating effective precipitation of SDS. Centrifugation was performed at 14 000 x *g* and the clear supernatant was promptly transferred to the QIAGEN-tip 20 column which had been calibrated with 1ml of Buffer QBT and allowed to enter the resin by gravity flow. The column was then washed twice with 2 ml Buffer QC before eluting plasmid with 0.8 ml Buffer QF into a clean 1.5 ml tube. Isopropanol (0.56 ml) was added to the eluted DNA, mixed and centrifuged at 14 000 x *g* for 30 min to precipitate it. The supernatant was decanted carefully making sure not to disturb the pellet. One milliliter of ethanol (70%) was used to wash the pellet by centrifuging at 14 000 x *g* for 10 min. The supernatant was decanted and the pellet was air-dried for 5-10 min before redissolving the plasmid in TE buffer (pH 8.0).

The presence of the correct insert was confirmed by sequencing using the plasmid M13 forward primer (5'-GTAAAACGACGGCCAGT-3') manufactured by Inqaba Biotech (South Africa). The sequencing reactions were cycled for 25 cycles using the following conditions: 95°C for 30 sec, 50°C for 30 sec and 60°C for 4 min on the iCycler iQ^{TM} (Bio-Rad, Hercules, USA). Separation of the labeled fragments was done by Inqaba Biotech and results were analysed using Ridom Trace Edit and Ridom Q Align software (Ridom, Würzburg, Germany). Presence of the conserved regions within the plasmids was identified using the BLAST program on PubMed (www.ncbi.nlm.nih.gov/blast).

2.10. Glycerol stock preparation

One of the colonies of each organism containing the insert was plated out on LB-agar supplemented with ampicillin (100µg/ml) and incubated at 37°C overnight. A single colony of the clone was picked off of the plate and inoculated in a McCartney bottle containing 3 ml LB broth with 3 µl ampicillin (100µg/ml). The bottles were incubated in an incubator-shaker (New Brunswick Scientific, Series 25, New Brunswick, NJ) at 37°C shaking at 225 rpm for 8 hrs. The culture was transferred to 1.5 ml tubes and centrifuged at maximum speed for 2 min (Eppendorf centrifuge 5417C, Eppendorf, UK). The supernatant was removed and the pellet resuspended in a 1:1 ratio of 30% sterile glycerol (SMM Chemicals, Booysens, South Africa) and water by vortexing. The glycerol stocks were stored at -70°C.

2.11. Sensitivity assays

The plasmid concentration of each of the organisms cloned was measured using the NanoDrop ND-100 spectrophotometer (NanoDrop Technologies, Wilmington, DE) at 260 nm. Serial dilutions using sterile water were thereafter performed (1 to 100 000 copies/µl). The sensitivity of the real-time PCR assays was tested on the 3 lowest dilutions (1 to 100 copies/µl) of the target gene plasmid construct as the template. Multiplex assays were tested for their ability to co-amplify multiple gene targets present at the lowest concentrations detectable by the singleplex assays.

CHAPTER 3A: REAL-TIME PCR ASSAYS (POSITIVE CONTROLS)

Real-time PCR assays were initially optimized in singleplex using SYBR ® Green I (Figures 3.1-3.17) and then TaqMan probes (Figures 3.18-3.30) before multiplex reactions (Figures 3.31a-3.36c) were performed. Appropriate primer combinations that could allow multiplexing of *M. pneumoniae*, *C. pneumoniae*, *C. psittaci*, *L. pneumophila* and GAPDH could not be obtained from the literature and as a result, they were designed using the Beacon Designer Software Program (Biosoft International). In instances where no suitable multiplex partner was found, or where limitations on the synthesis of appropriately labelled probes were encountered, the reactions were performed using SYBR Green I in singleplex.

3.1. Singleplex reactions

3.1.1. SYBR® Green I

Initially performing the reactions with SYBR Green I helped to establish the appropriate reaction conditions and to ascertain that the primers were working correctly. For the majority of reactions performed (FluA, FluB, hMPV, RSV, PIV1, PIV2, PIV3, *L. pneumophila*, *M. pneumoniae* and GAPDH (DNA)), two or more different sets of primers had to be tested before a positive real-time PCR result was obtained and the reactions multiplexed successfully. All SYBR Green I PCR end products were separated on 2% agarose gels (see appendix B).

a. Influenza A virus

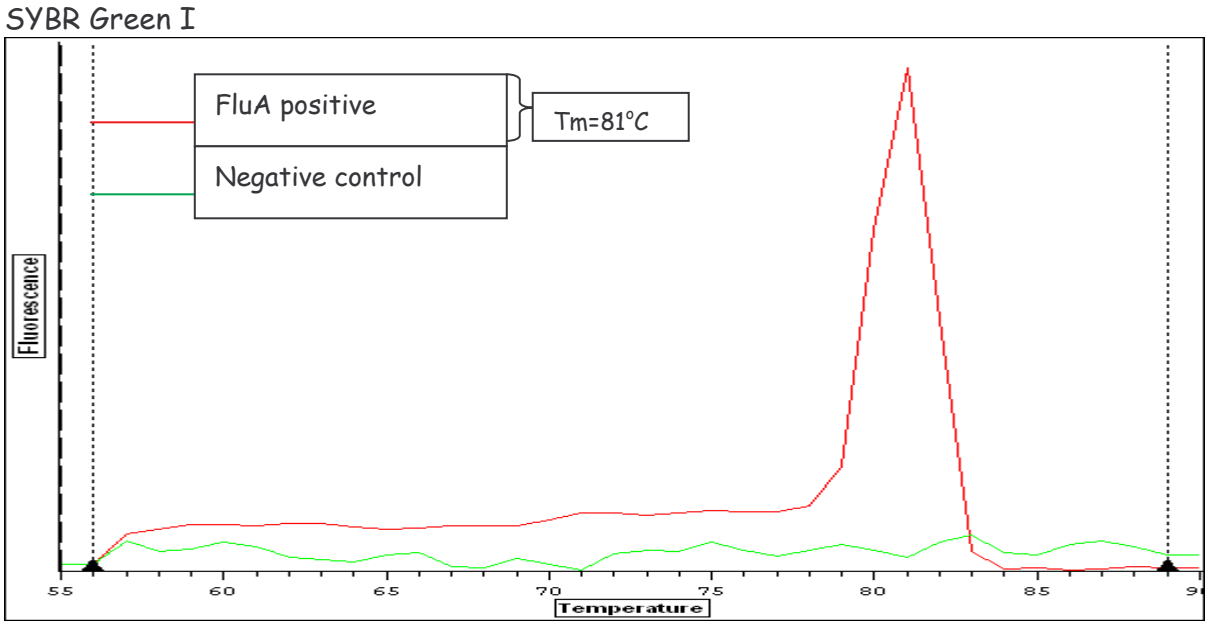

Figure 3.1: Melting curve analysis of FluA generated when using SYBR Green I. The signature melting temperature of FluA (81°C) is indicated by the sharp red peak corresponding to the positive control. Temperature is plotted versus fluorescence signal.

b. Influenza B virus

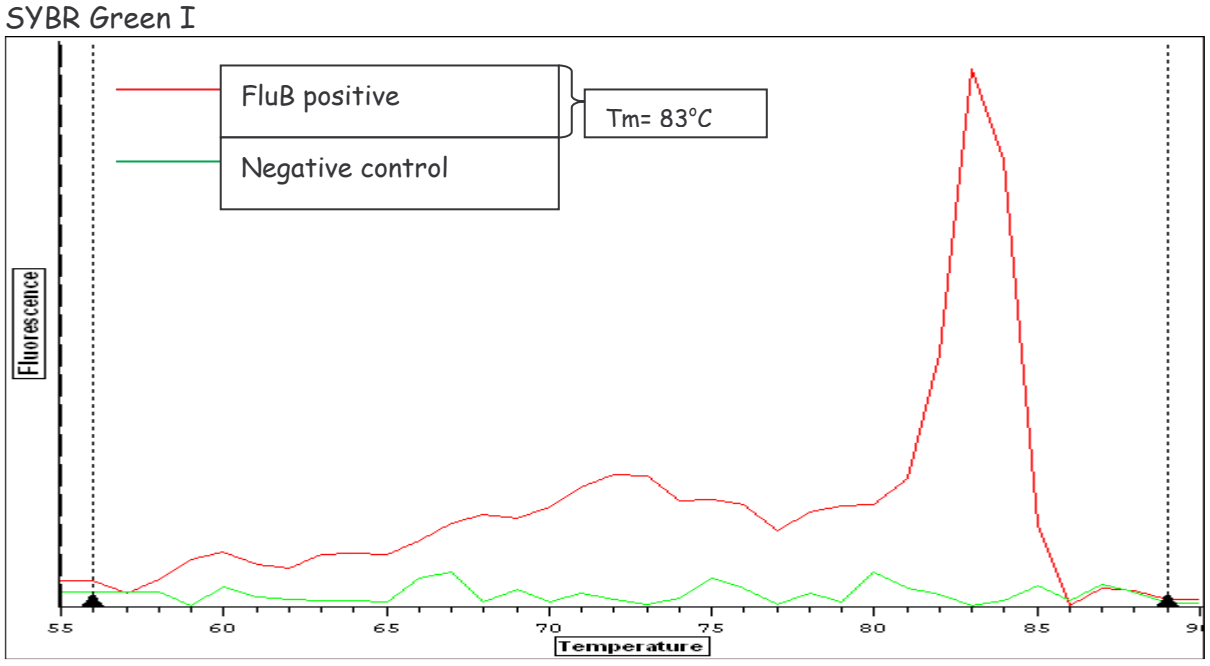

Figure 3.2: Melting curve analysis of FluB generated when using SYBR Green I. The signature melting temperature of FluB (83°C) is indicated by the sharp red peak corresponding to the positive control. Temperature is plotted versus fluorescence signal.

c. Human metapneumovirus

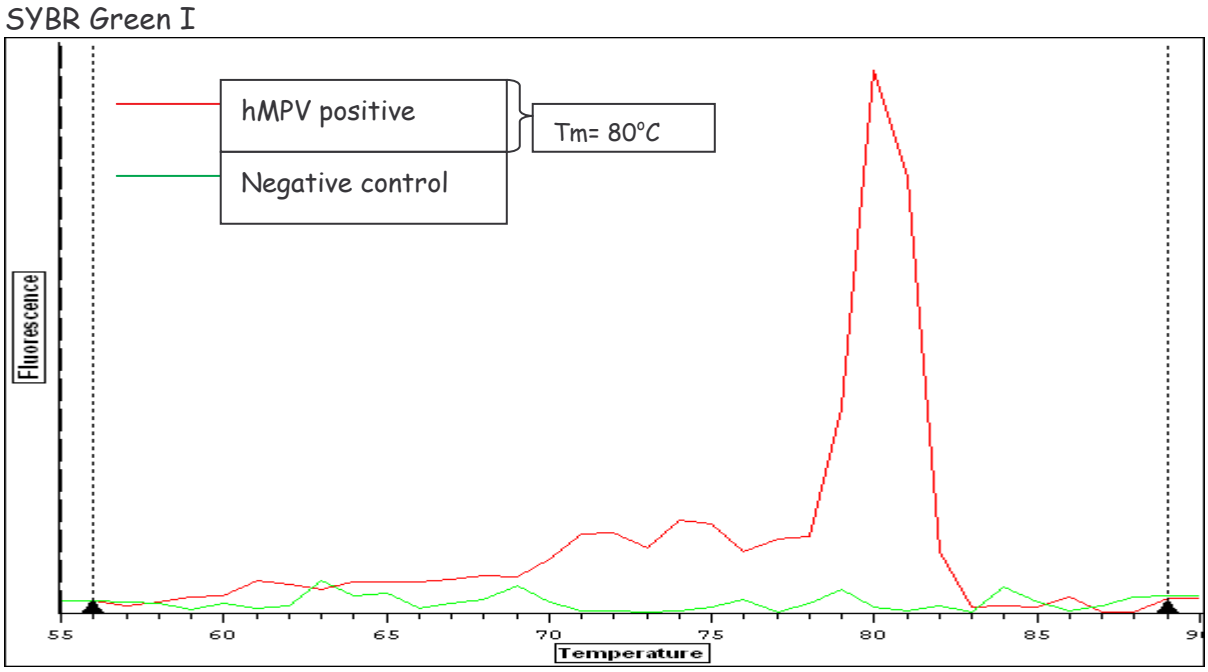

Figure 3.3: Melting curve analysis of hMPV generated when using SYBR Green I. The signature melting temperature of hMPV (80°C) is indicated by the sharp red peak corresponding to the positive control. Temperature is plotted versus fluorescence signal.

d. Parainfluenza virus 1

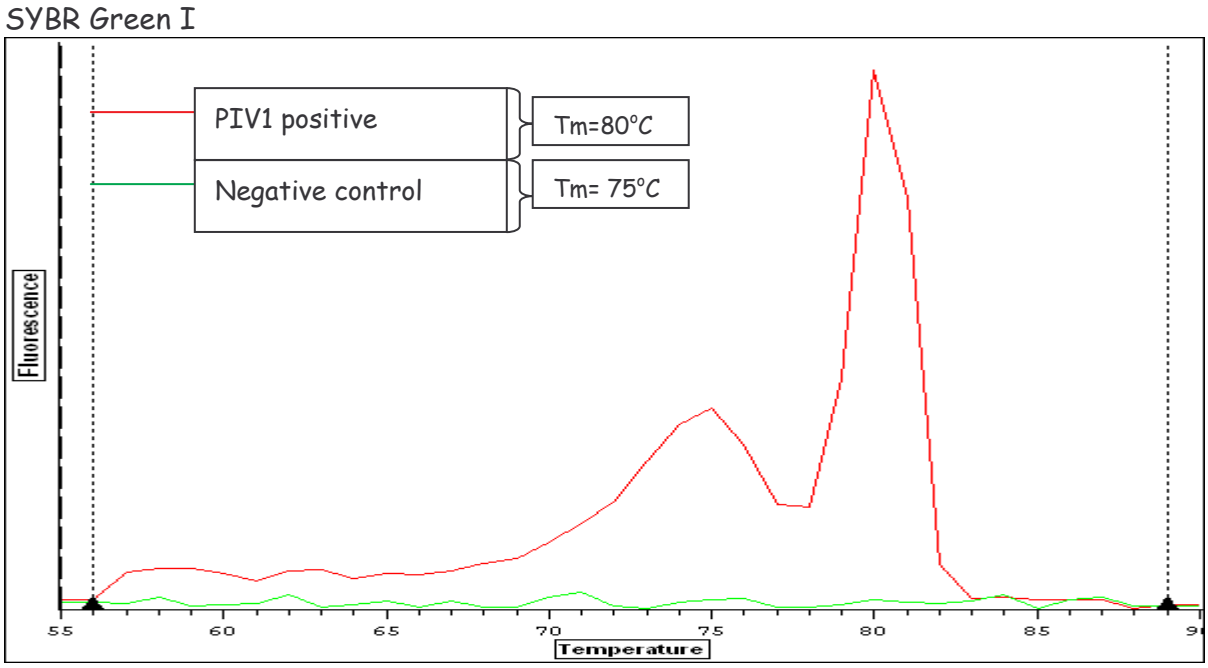

Figure 3.4: Melting curve analysis of PIV1 generated when using SYBR Green I. The signature melting temperature of PIV1 (80°C) is indicated by the sharp tall red peak corresponding to the positive control. The smaller red peak indicates a primer-dimer (75°C) as judged by gel electrophoresis (Figure B3A). Temperature is plotted versus fluorescence signal.

e. Parainfluenza virus 2

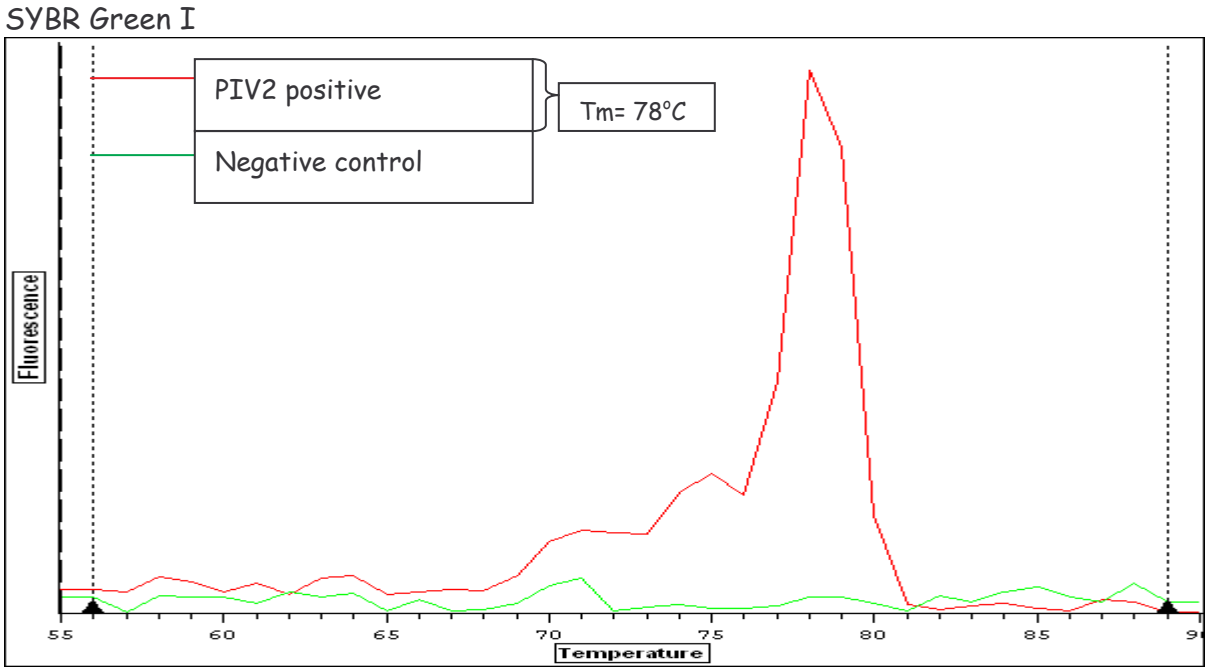

Figure 3.5: Melting curve analysis of PIV2 generated when using SYBR Green I. The signature melting temperature of PIV2 (78°C) is indicated by the sharp red peak corresponding to the positive control. Temperature is plotted versus fluorescence signal.

f. Parainfluenza virus 3

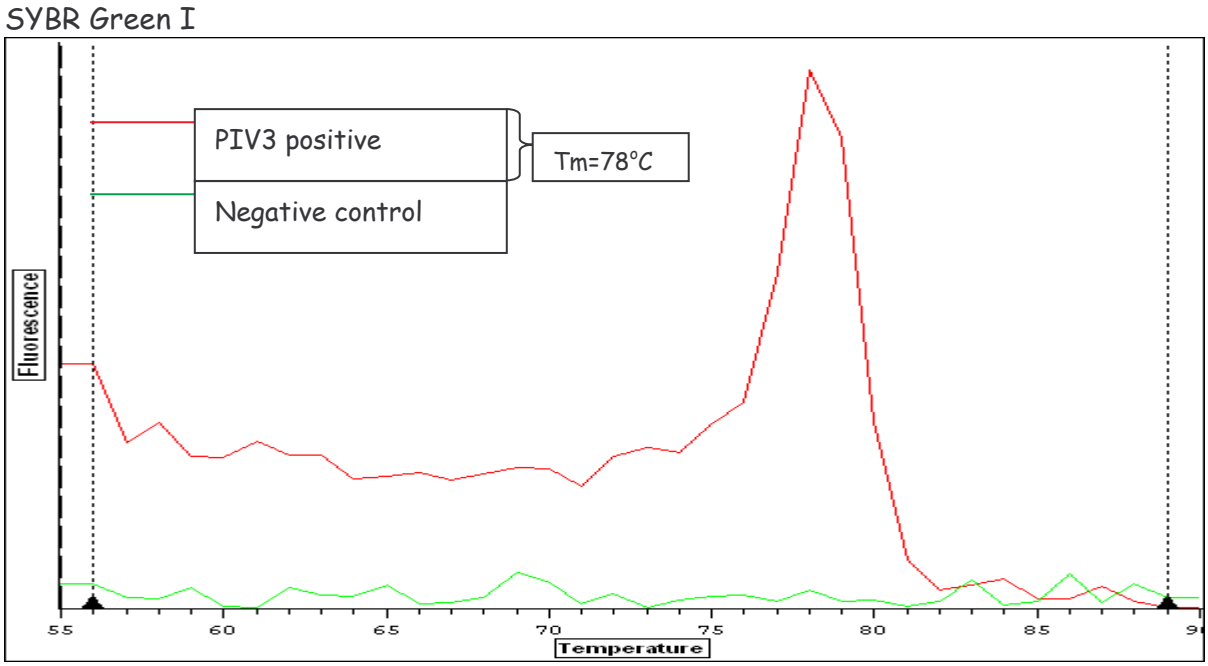

Figure 3.6: Melting curve analysis of PIV3 generated when using SYBR Green I. The signature melting temperature of PIV3 (78°C) is indicated by the sharp red peak corresponding to the positive control. Temperature is plotted versus fluorescence signal.

g. Adenovirus

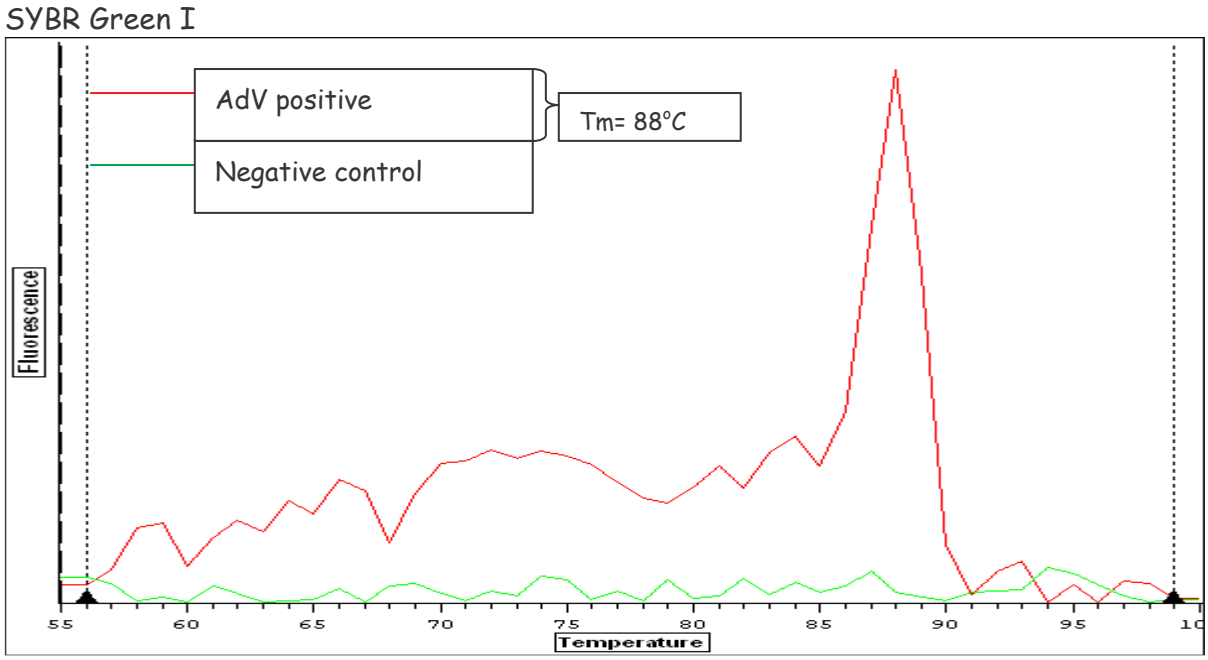

Figure 3.7: Melting curve analysis of AdV generated when using SYBR Green I. The signature melting temperature of AdV (88°C) is indicated by the sharp red peak corresponding to the positive control. Temperature is plotted versus fluorescence signal.

h. Respiratory syncytial virus

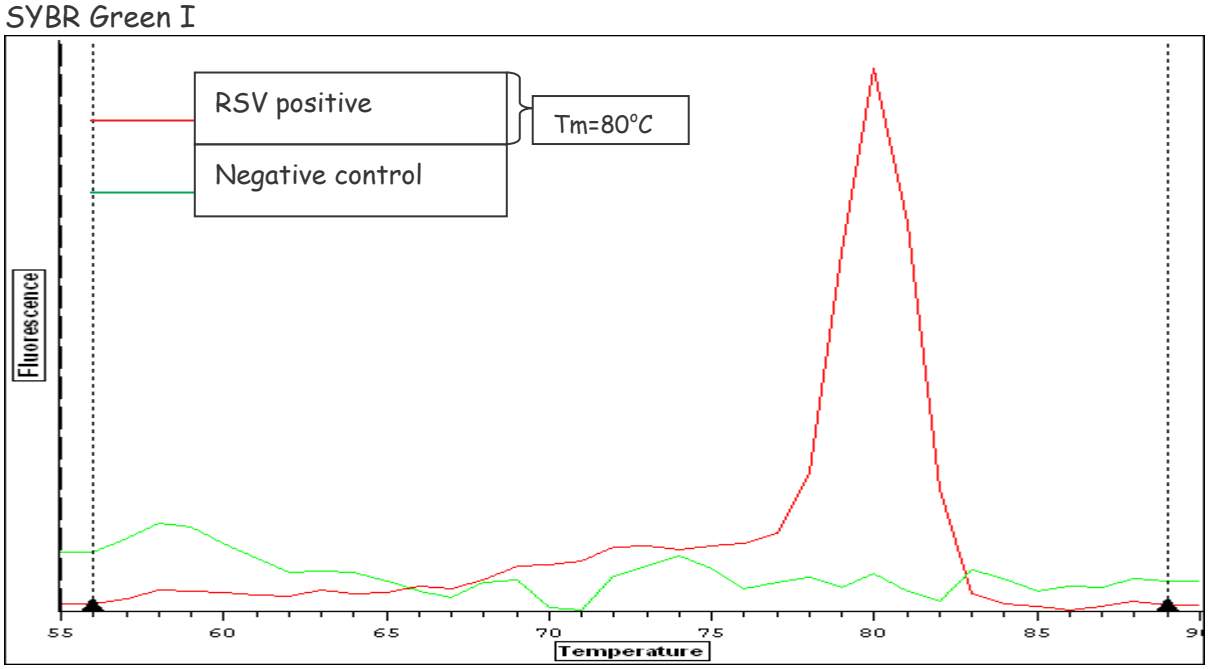

Figure 3.8: Melting curve analysis of RSV generated when using SYBR Green I. The signature melting temperature of RSV (80°C) is indicated by the sharp red peak corresponding to the positive control. Temperature is plotted versus fluorescence signal.

i. Cytomegalovirus

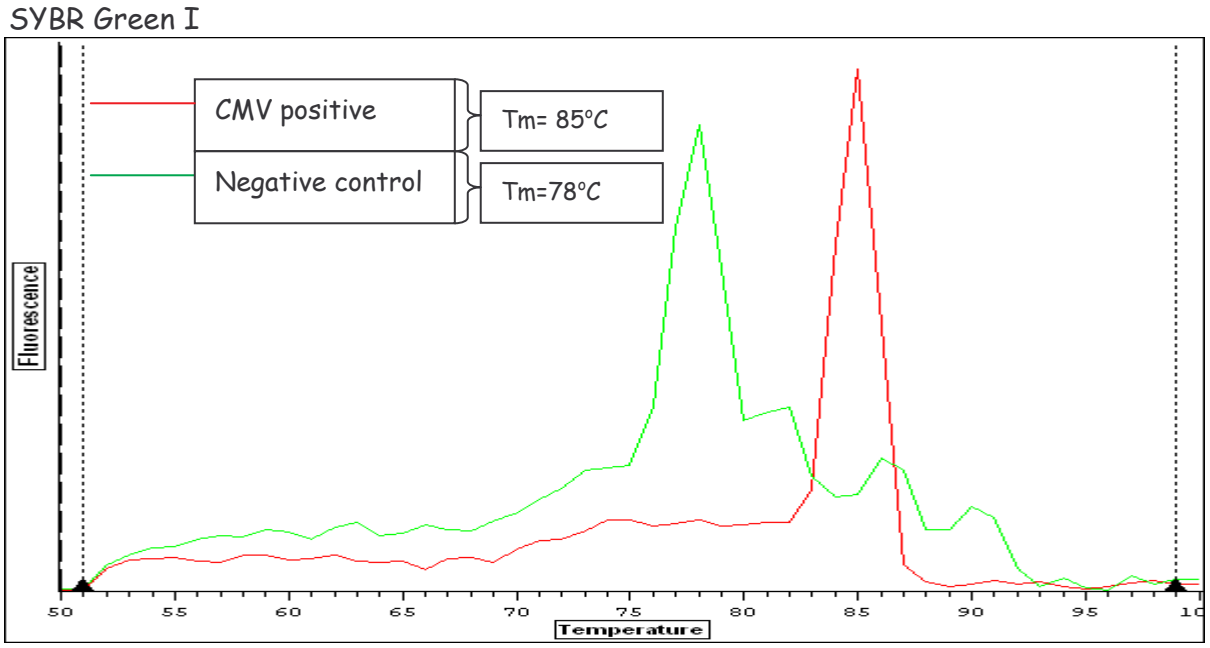

Figure 3.9: Melting curve analysis of CMV generated when using SYBR Green I. The signature melting temperature of CMV (85°C) is indicated by the sharp red peak corresponding to the positive control. The green peak indicated a primer-dimer (78°C) as judged by gel electrophoresis (Figure B1A). Temperature is plotted versus fluorescence signal.

j. Epstein-Barr virus

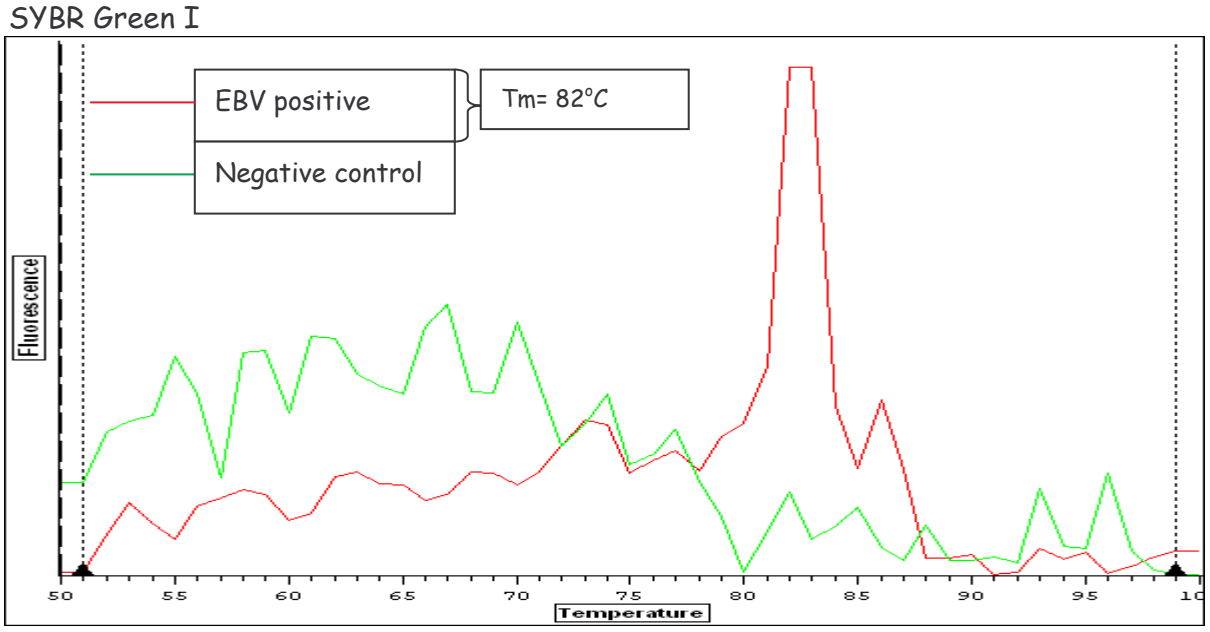

Figure 3.10: Melting curve analysis of EBV generated when using SYBR Green I. The signature melting temperature of EBV (82°C) is indicated by the sharp red peak corresponding to the positive control. Temperature is plotted versus fluorescence signal.

k. *M. pneumoniae*

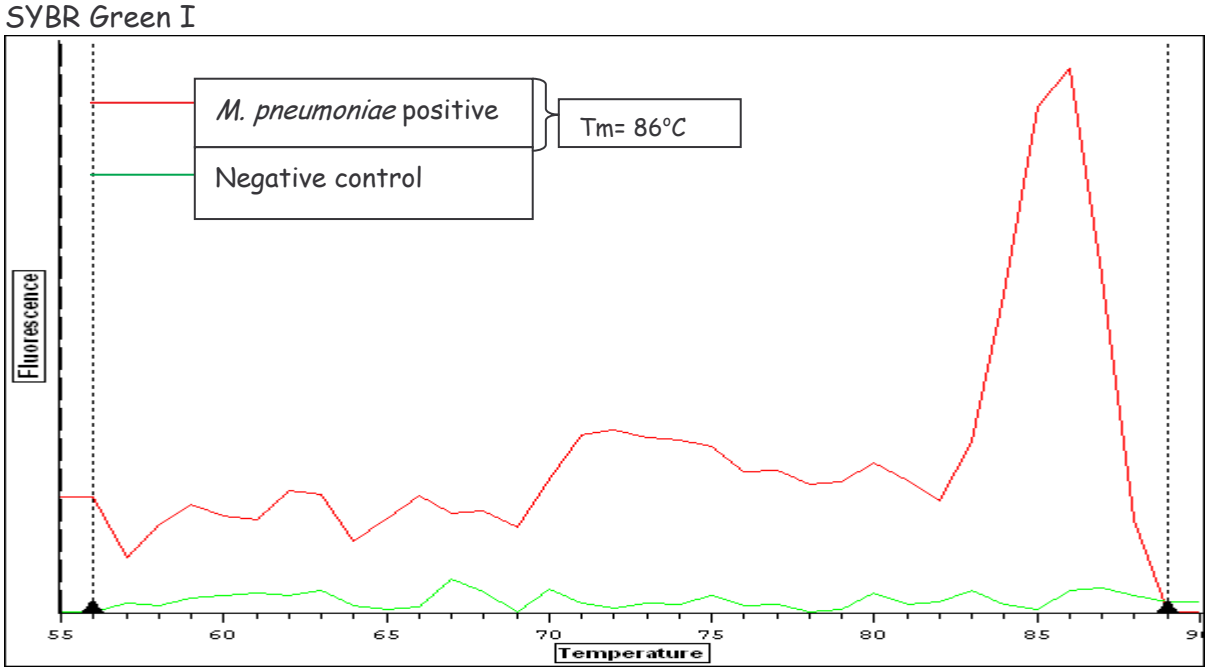

Figure 3.11: Melting curve analysis of *M. pneumoniae* generated when using SYBR Green I. The signature melting temperature of *M. pneumoniae* (86°C) is indicated by the sharp red peak corresponding to the positive control. Temperature is plotted versus fluorescence signal.

l. *L. pneumophila*

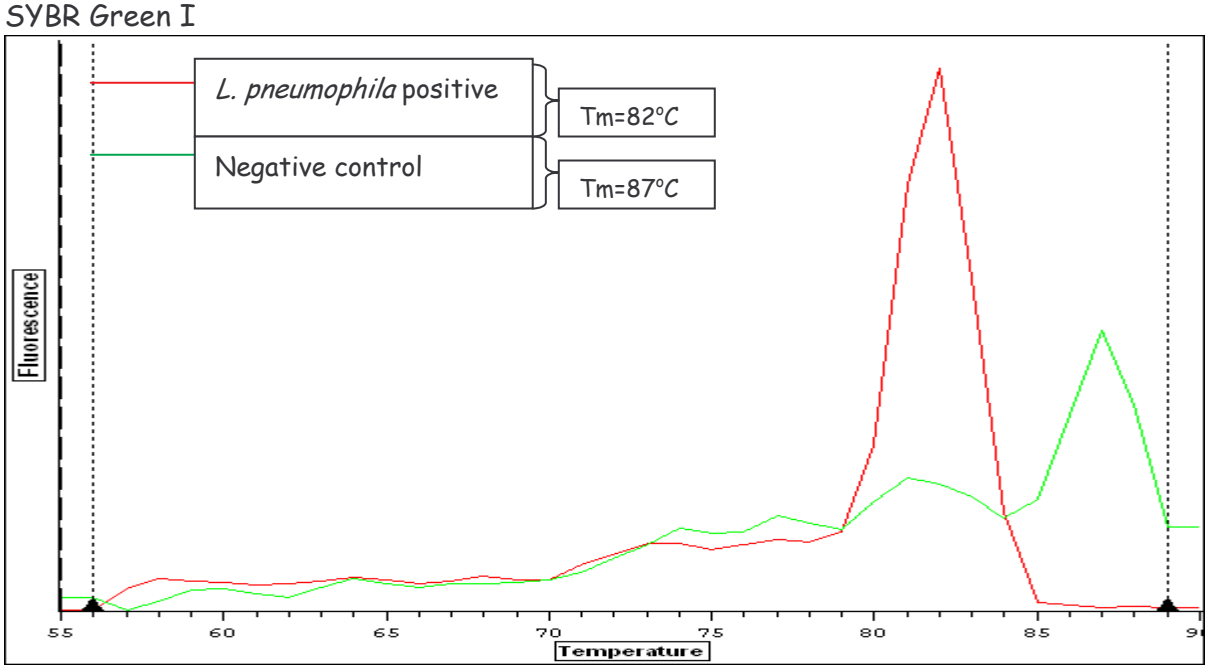

Figure 3.12: Melting curve analysis of *L. pneumophila* generated when using SYBR Green I. The signature melting temperature of *L. pneumophila* (82°C) is indicated by the sharp red peak corresponding to the positive control. The green peak indicates the formation of non-specific PCR product (87°C) as judged by gel electrophoresis (Figure B9A). Temperature is plotted versus fluorescence signal.

m. *C. pneumoniae*

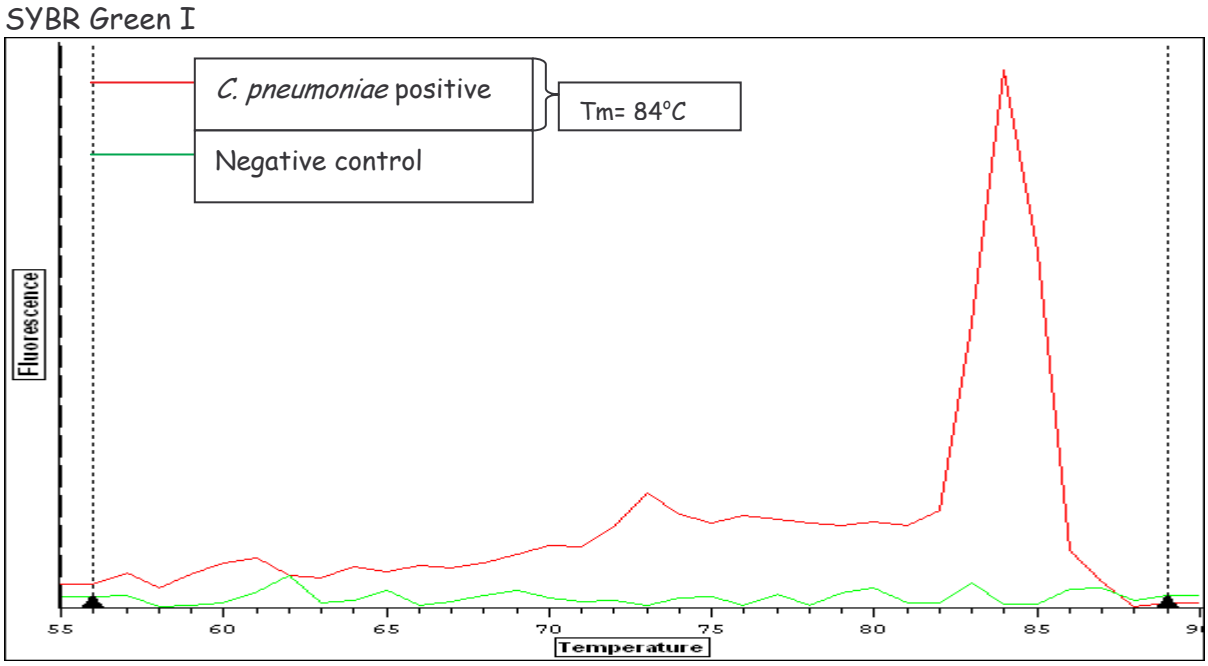

Figure 3.13: Melting curve analysis of *C. pneumoniae* generated when using SYBR Green I. The signature melting temperature of *C. pneumoniae* (84°C) is indicated by the sharp red peak corresponding to the positive control. Temperature is plotted versus fluorescence signal.

n. GAPDH (DNA)

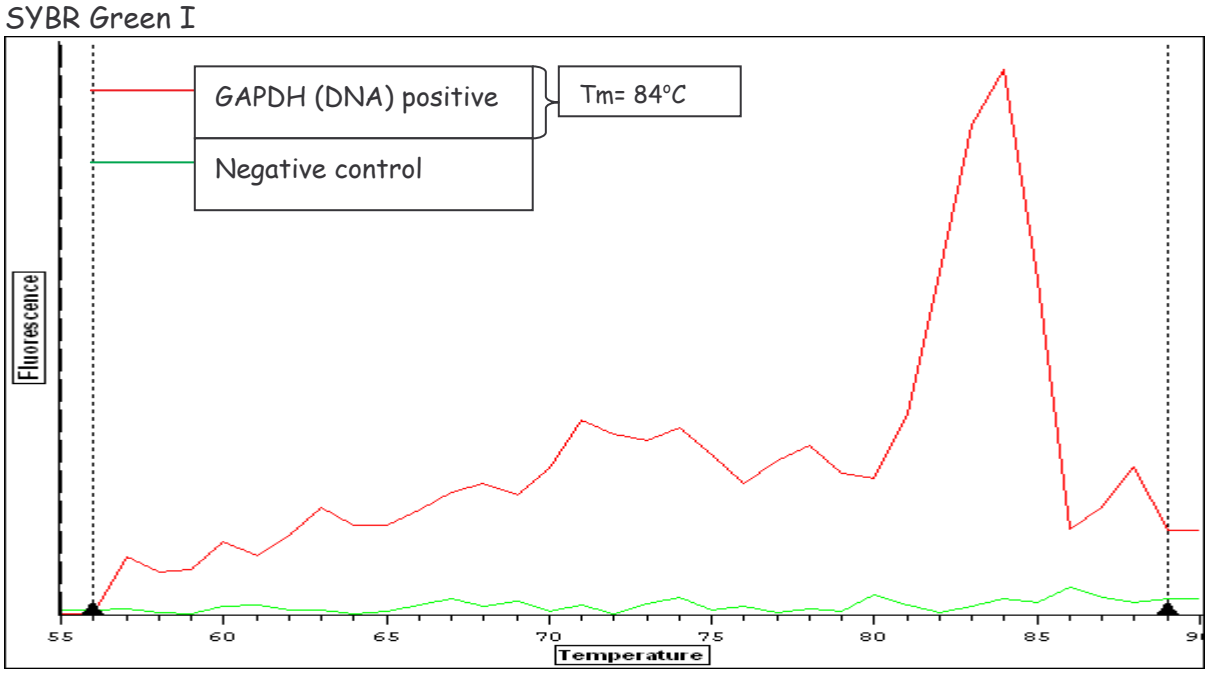

Figure 3.14: Melting curve analysis of GAPDH (DNA) generated when using SYBR Green I. The signature melting temperature of GAPDH (DNA) (84°C) is indicated by the sharp red peak corresponding to the positive control. Temperature is plotted versus fluorescence signal.

o. GAPDH (RNA)

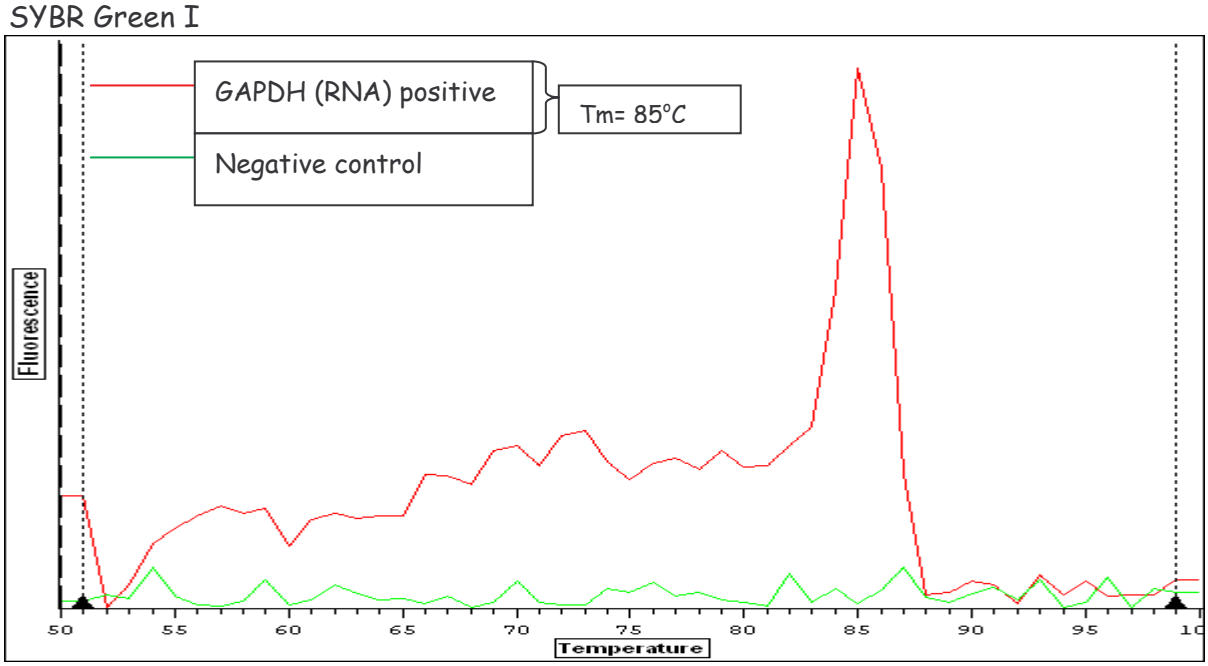

Figure 3.15: Melting curve analysis of GAPDH (RNA) generated when using SYBR Green I. The signature melting temperature of GAPDH (RNA) (85°C) is indicated by the sharp red peak corresponding to the positive control. Temperature is plotted versus fluorescence signal.

p. *P. jirovecii*

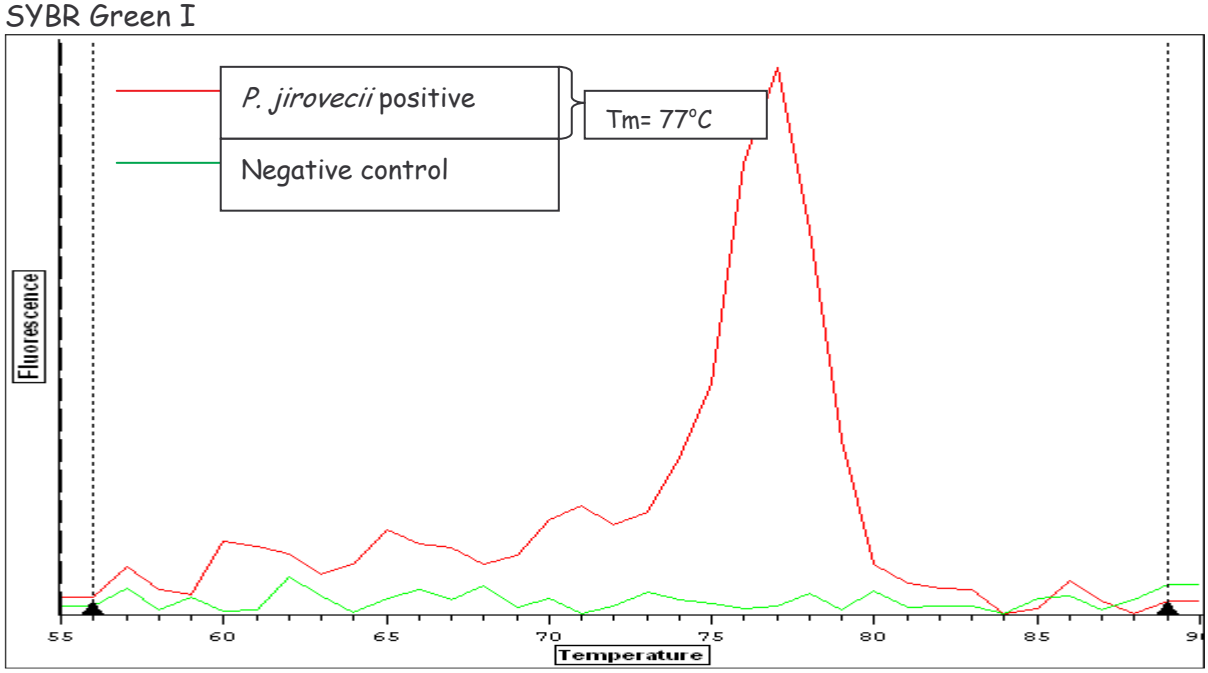

Figure 3.16: Melting curve analysis of *P. jirovecii* generated when using SYBR Green I. The signature melting temperature of *P. jirovecii* (77°C) is indicated by the sharp red peak corresponding to the positive control. Temperature is plotted versus fluorescence signal.

q. *C. psittaci*

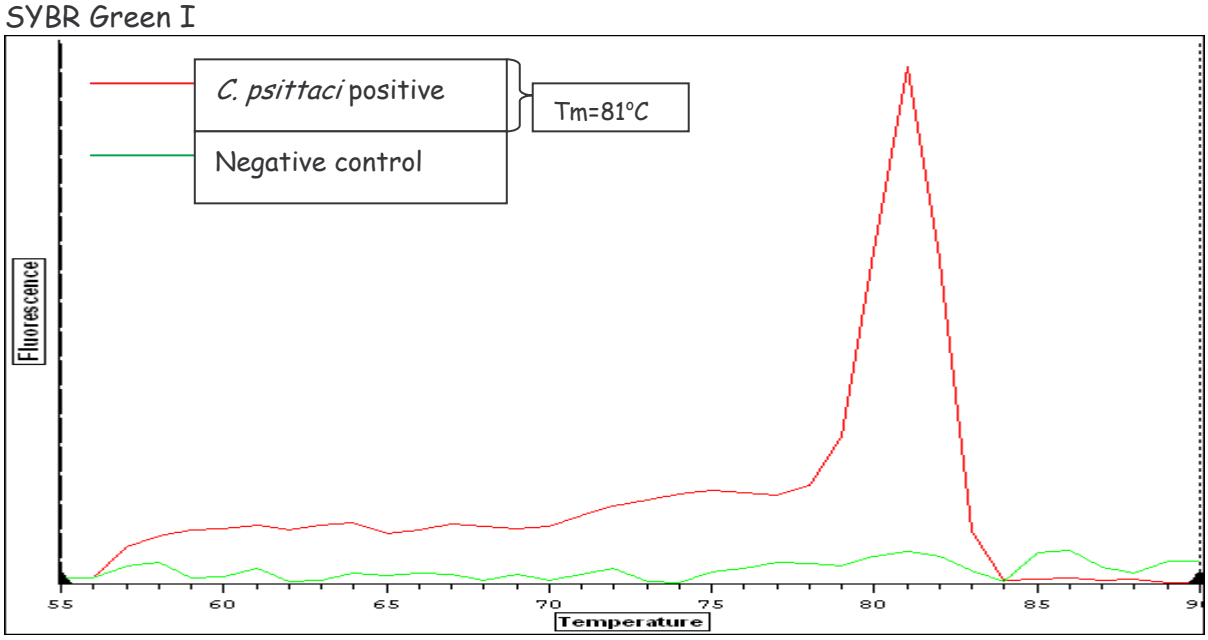

Figure 3.17: Melting curve analysis of *C. psittaci* generated when using SYBR Green I. The signature melting temperature of *C. psittaci* (81°C) is indicated by the sharp red peak corresponding to the positive control. Temperature is plotted versus fluorescence signal.

3.1.2 TaqMan probes

Once primers and reactions conditions were found to work with SYBR Green I, TaqMan probes were used. In all real-time PCR reactions performed, the variation in fluorescence levels of the TaqMan probes was considerable and dye-dependent. Reactions involving probes possessing the FAM, CY5 and CY5.5 dyes displayed a higher maximum fluorescence level in the order of 0.11 to 0.62 than those possessing the HEX dye which were in the order of 0.006 to 0.55. Some of the graphs generated using TaqMan probes (hMPV, PIV1, PIV3 and CMV) did not display a typical exponential real-time PCR fluorescence curves and this is believed to be due to the degradation of the probes after storage. All real-time PCR end products of TaqMan probe reactions were separated on 2% agarose gels (see appendix B).

a. Influenza A virus

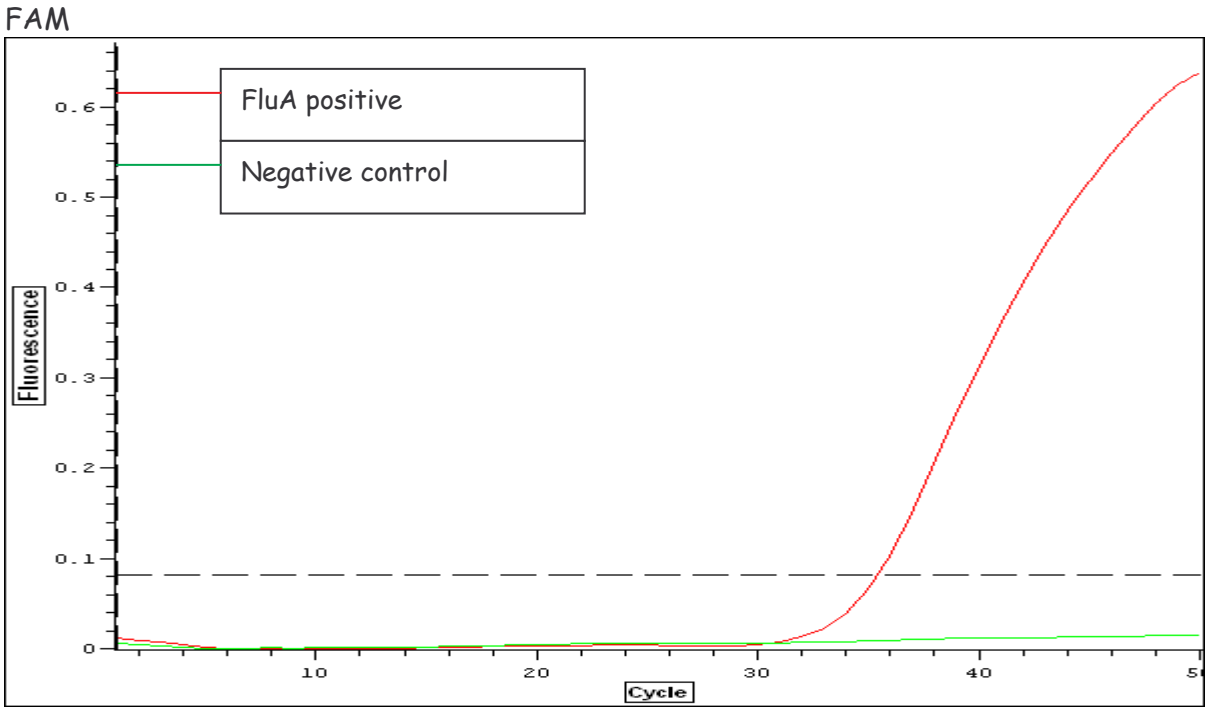

Figure 3.18: Real-time PCR singleplex analysis of FluA using a TaqMan probe. Plot of change in fluorescence signal versus cycle number is shown.

b. Influenza B virus

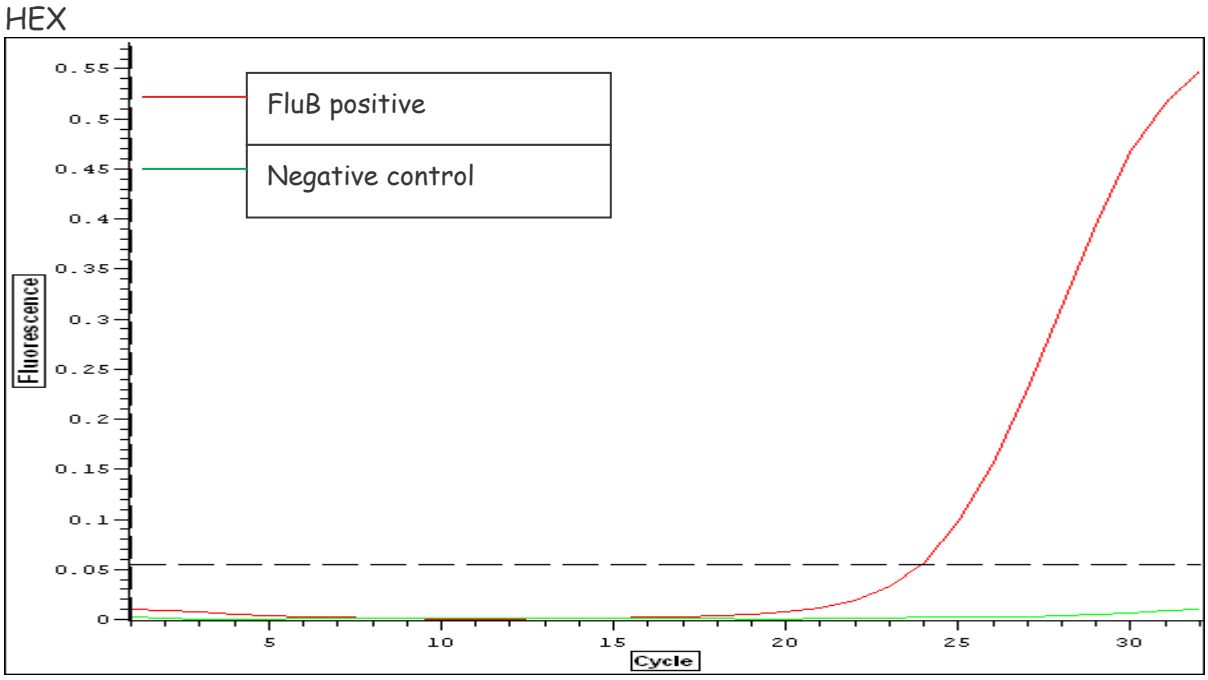

Figure 3.19: Real-time PCR singleplex analysis of FluB using a TaqMan probe. Plot of change in fluorescence signal versus cycle number is shown.

c. Human metapneumovirus

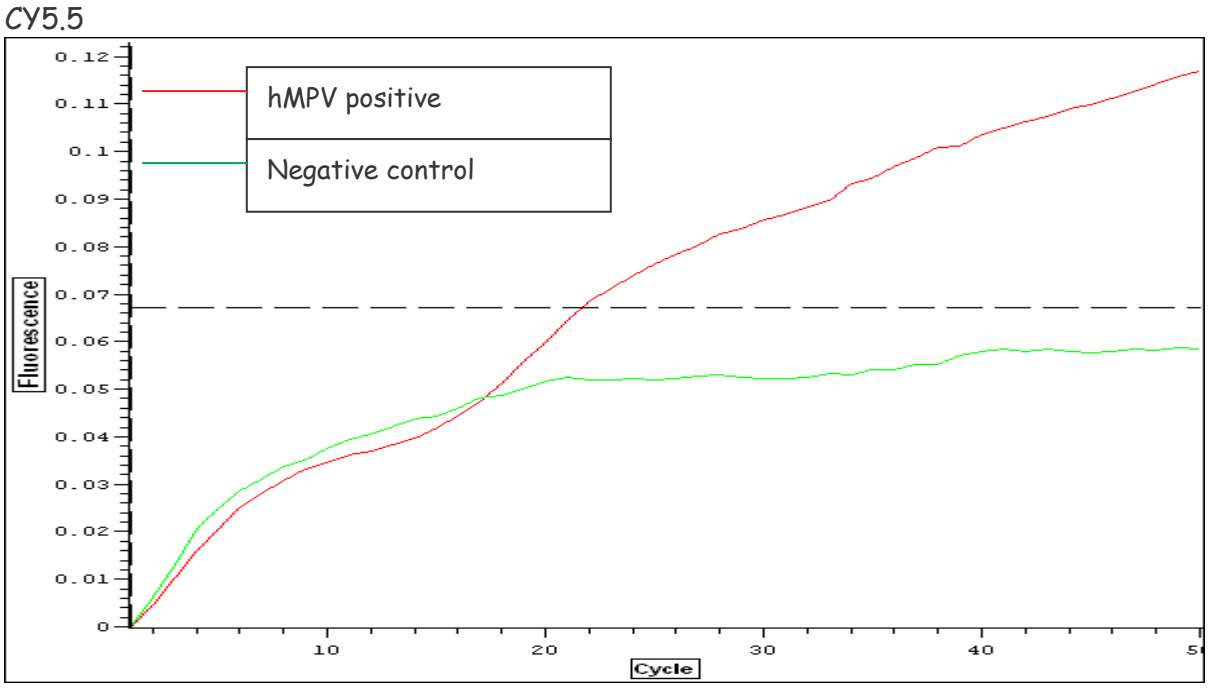

Figure 3.20: Real-time PCR singleplex analysis of hMPV using a TaqMan probe. Plot of change in fluorescence signal versus cycle number is shown.

d. Parainfluenza virus 1

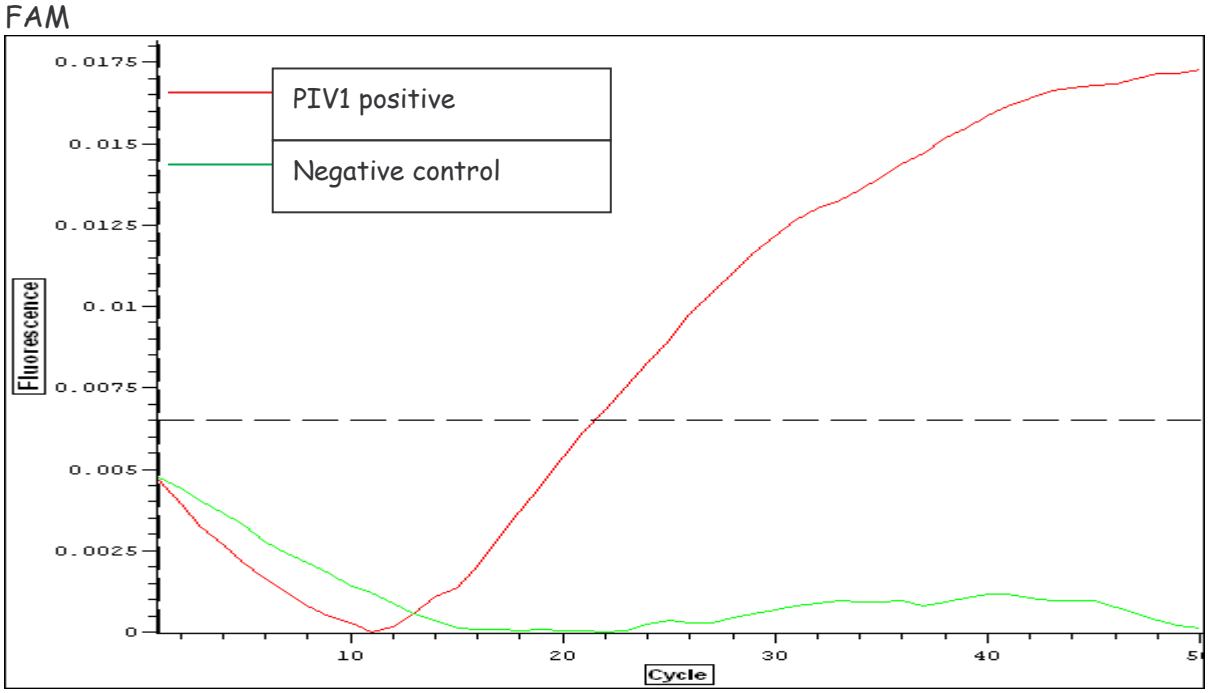

Figure 3.21: Real-time PCR singleplex analysis of PIV1 using a TaqMan probe. Plot of change in fluorescence signal versus cycle number is shown.

e. Parainfluenza virus 3

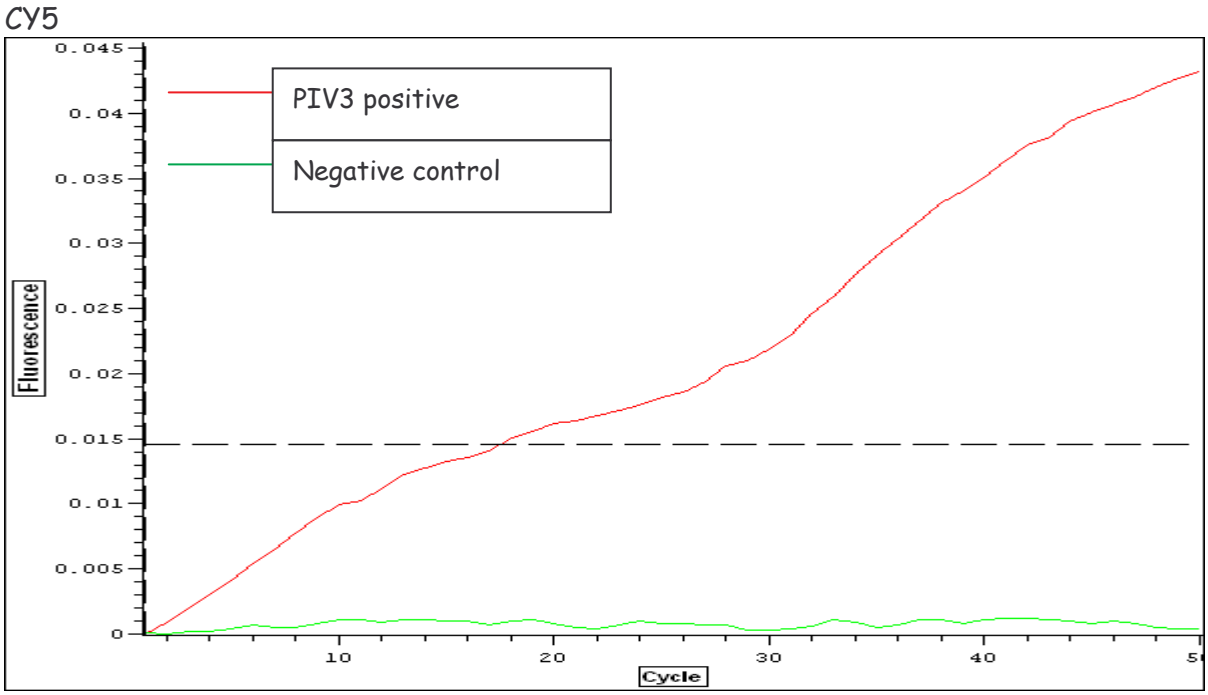

Figure 3.22: Real-time PCR singleplex analysis of PIV3 using a TaqMan probe. Plot of change in fluorescence signal versus cycle number is shown.

Adenovirus

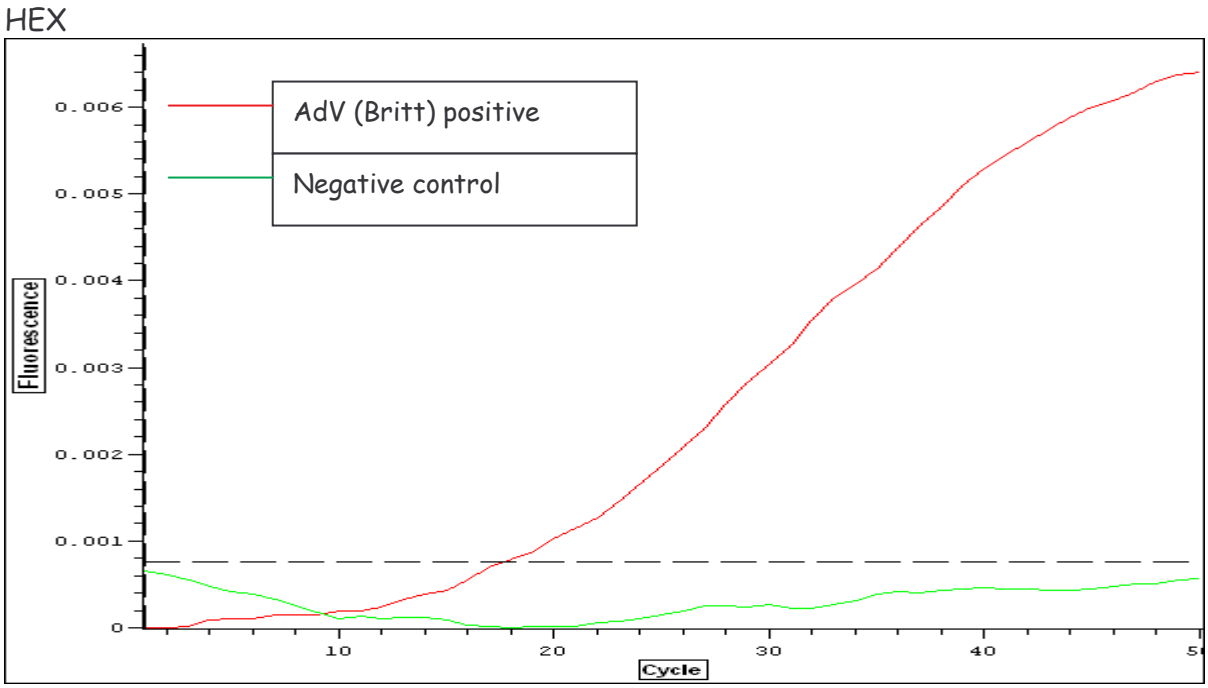

Figure 3.23: Real-time PCR singleplex analysis of AdV using a TaqMan probe. Plot of change in fluorescence signal versus cycle number is shown.

Respiratory syncytial virus

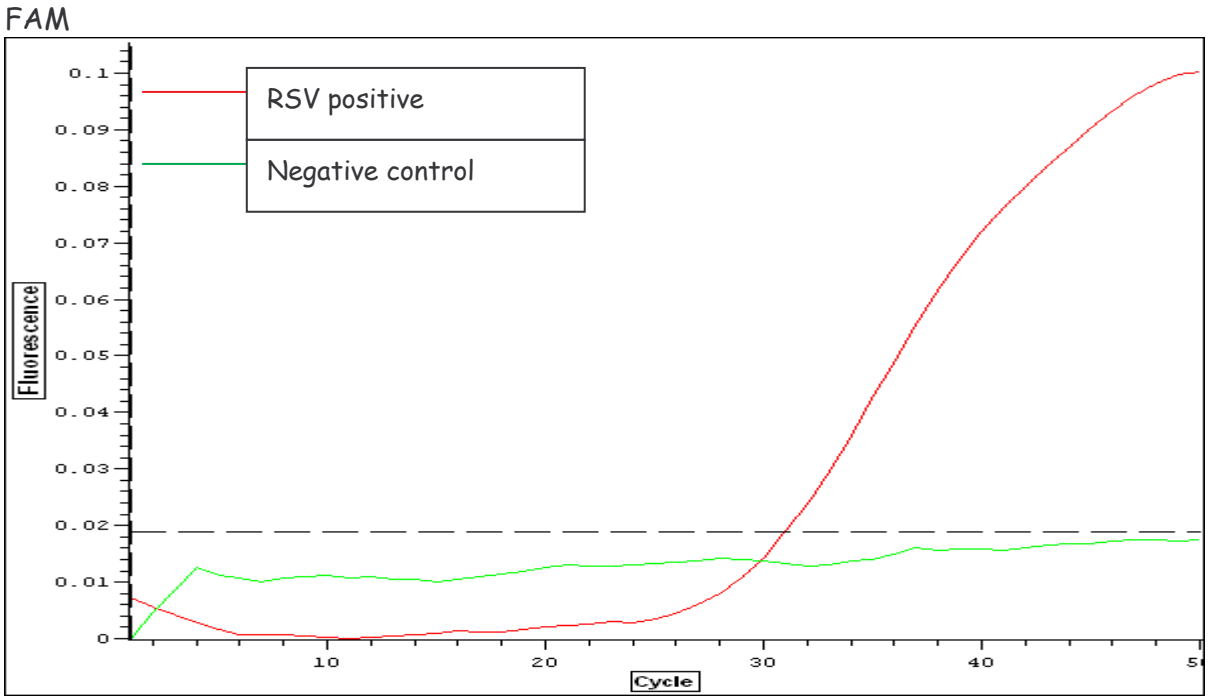

Figure 3.24: Real-time PCR singleplex analysis of RSV using a TaqMan probe. Plot of change in fluorescence signal versus cycle number is shown.

f. Cytomegalovirus

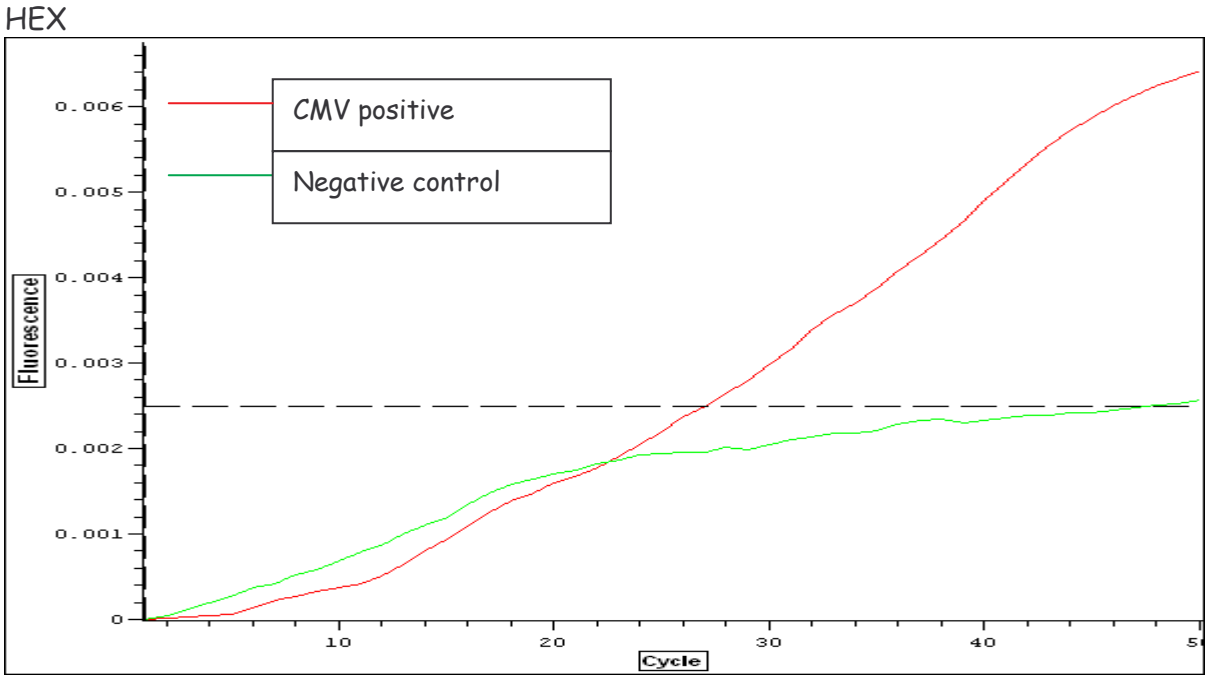

Figure 3.25: Real-time PCR singleplex analysis of CMV using a TaqMan probe. Plot of change in fluorescence signal versus cycle number is shown.

Epstein-Barr virus

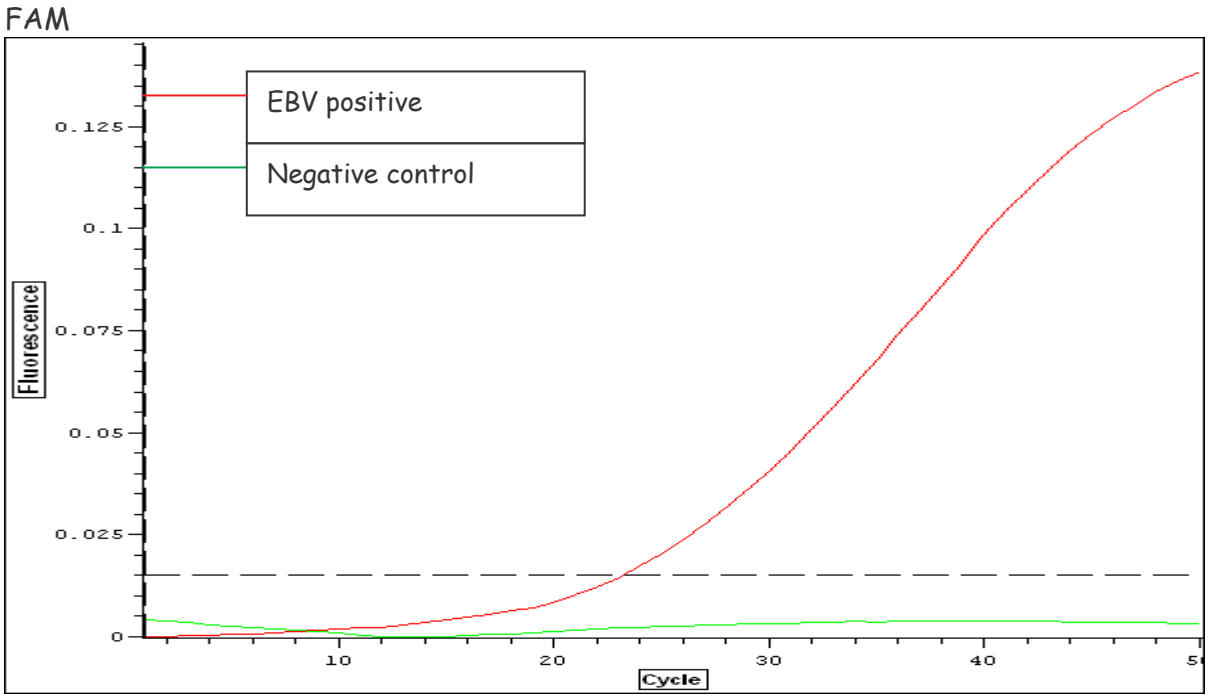

Figure 3.26 Real-time PCR singleplex analysis of EBV using a TaqMan probe. Plot of change in fluorescence signal versus cycle number is shown.

g. *M. pneumoniae*

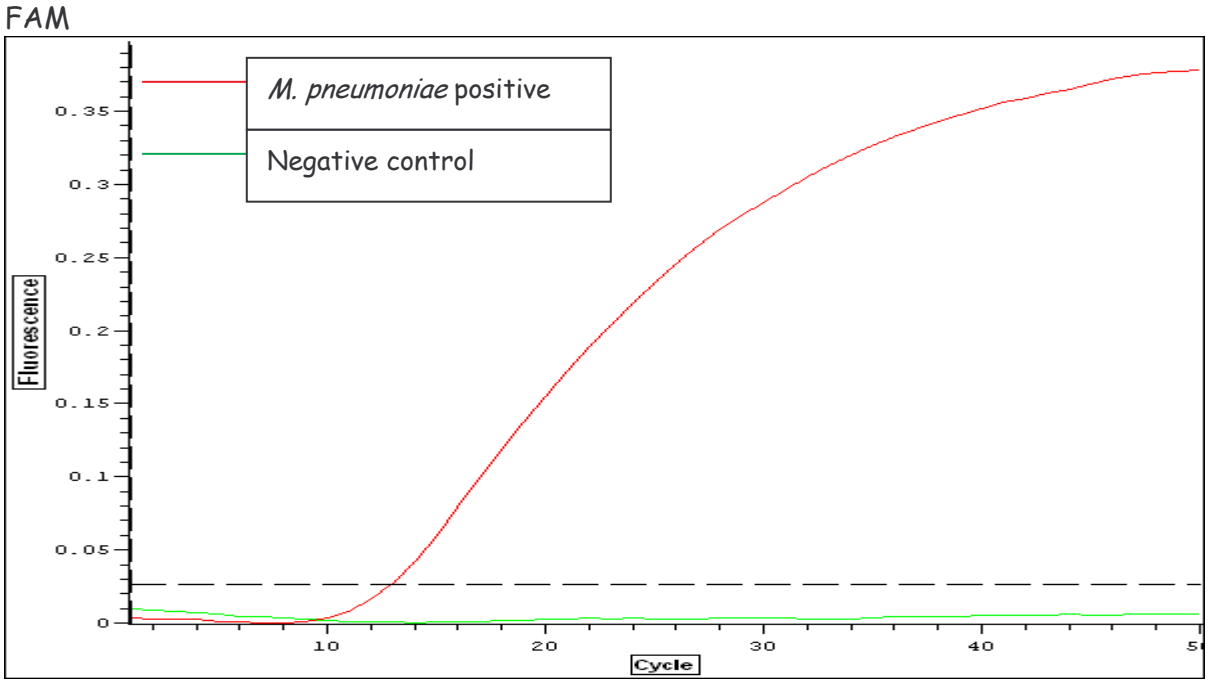

Figure 3.27: Real-time PCR singleplex analysis of *M. pneumoniae* using a TaqMan probe. Plot of change in fluorescence signal versus cycle number is shown.

h. *L. pneumophila*

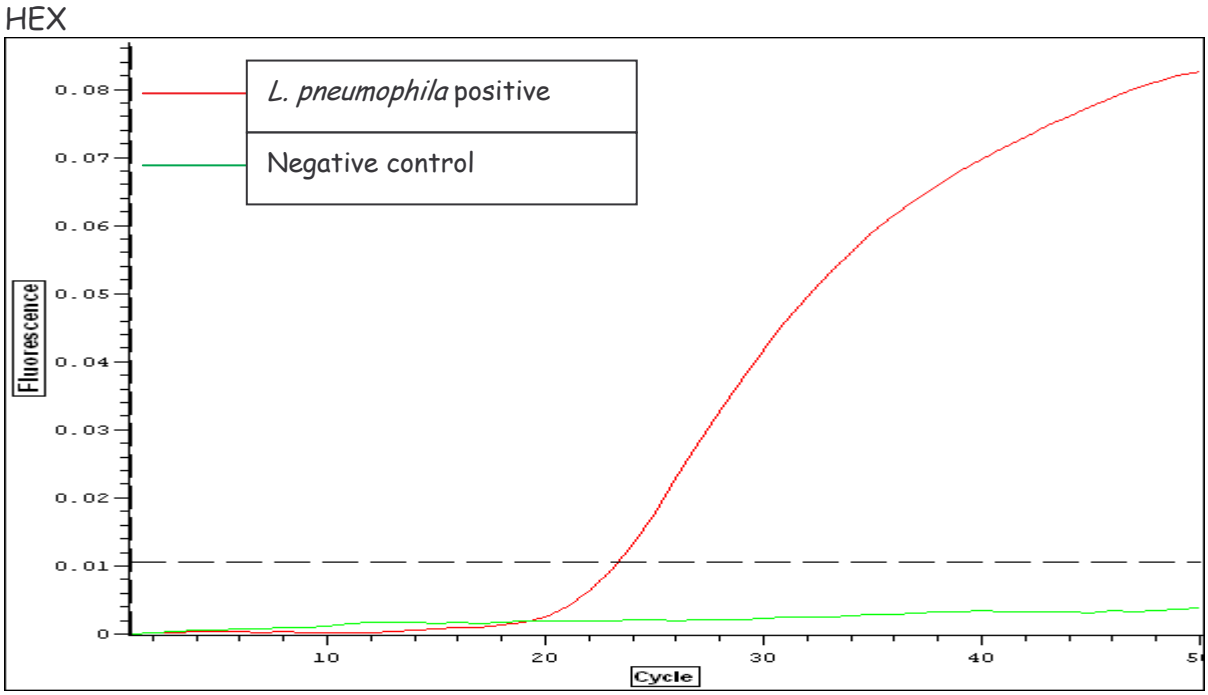

Figure 3.28: Real-time PCR singleplex analysis of *L. pneumophila* using a TaqMan probe. Plot of change in fluorescence signal versus cycle number is shown.

i. *C. pneumoniae*

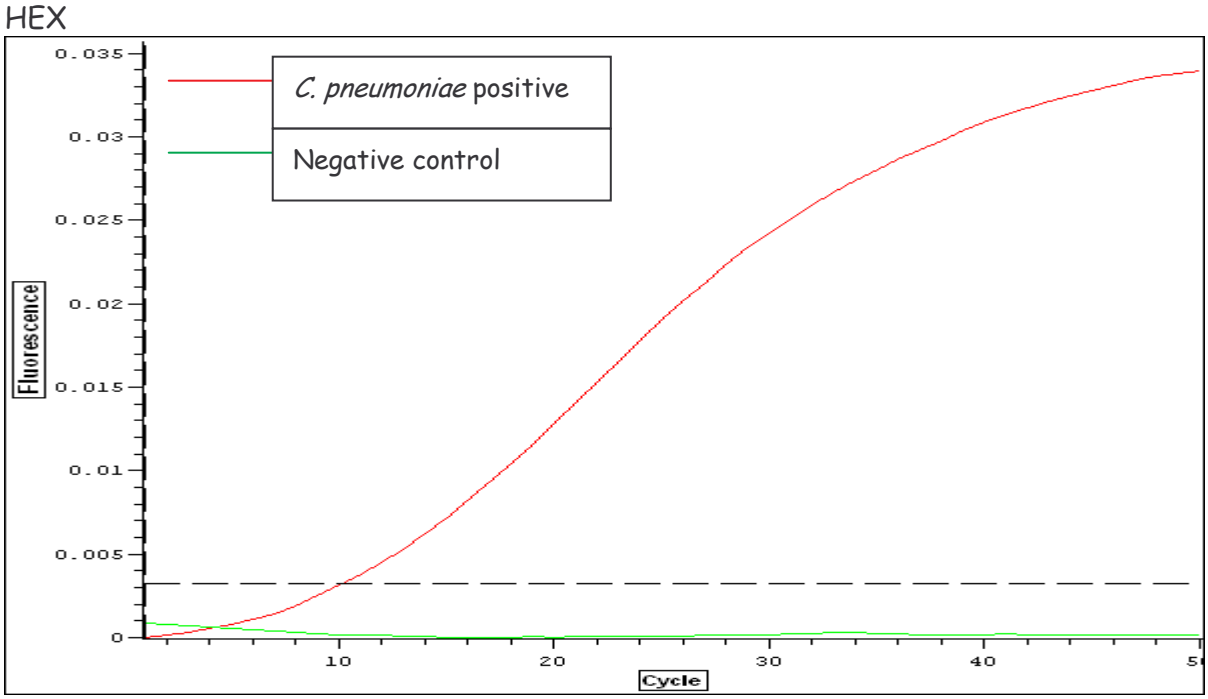

Figure 3.29: Real-time PCR singleplex analysis of *C. pneumoniae* using a TaqMan probe. Plot of change in fluorescence signal versus cycle number is shown.

j. GAPDH (DNA)

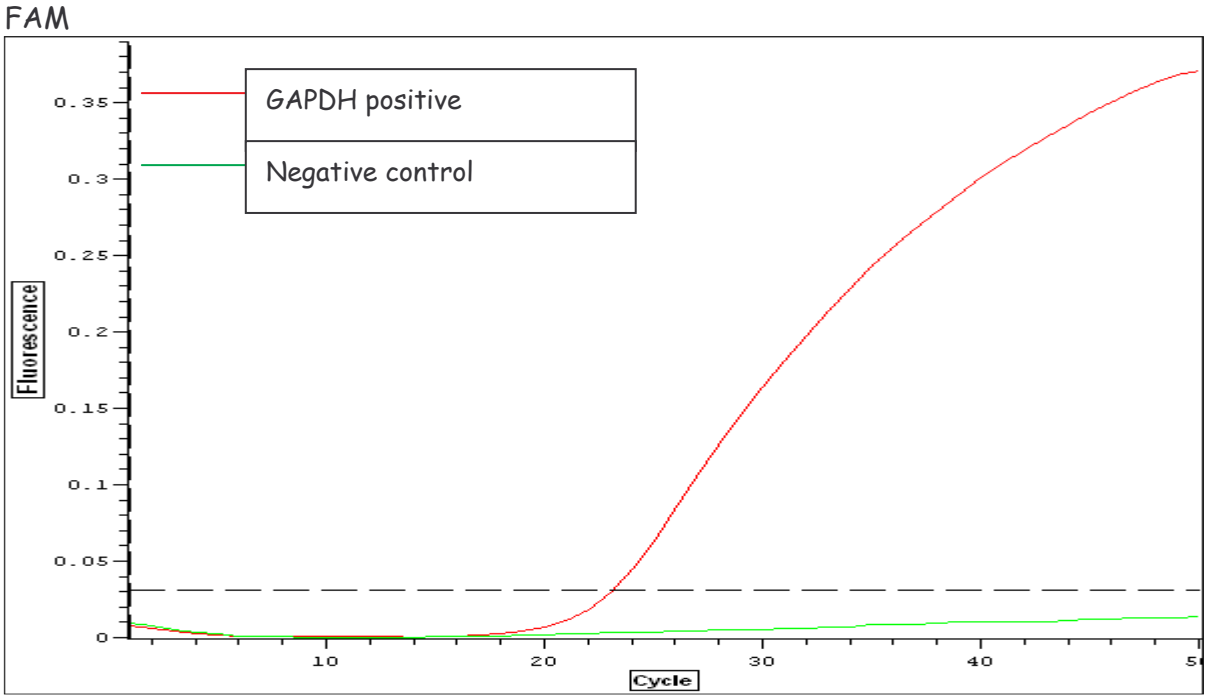

Figure 3.30: Real-time PCR singleplex analysis of GAPDH (DNA) using a TaqMan probe. Plot of change in fluorescence signal versus cycle number is shown.

3.2. Multiplex reactions

To reduce the number of total reactions performed using TaqMan probes, the reactions were multiplexed. Below is shown individual traces of fluorescence graphs of each organism as multiplexed. The multiplex reactions were grouped as follows: PIV1 and PIV3; RSV and AdV; EBV and CMV, *M. pneumoniae* and *L. pneumophila*; GAPDH and *C. pneumoniae*; and lastly, FluA, FluB and hMPV. The multiplex real-time PCR end products were separated on a 3% agarose gel to confirm that products of the expected sizes were produced (see Appendix C). The presence of several pairs of primers and probes in a single reaction tube increases the probabilities of obtaining non-specific amplification products, and in particular, the formation of primer-dimers was observed in the agarose gels (Appendix C). We noted that *M. pneumoniae* and *L. pneumophila* amplicons were too similar in size to be distinguished accurately on an agarose

gel (102 and 107bp respectively) (Figure C5A). However, it was evident from the real-time PCR fluorescence graphs, that product had been formed (Figures 3.34a and b).

a. Parainfluenza virus 1 and Parainfluenza virus 3

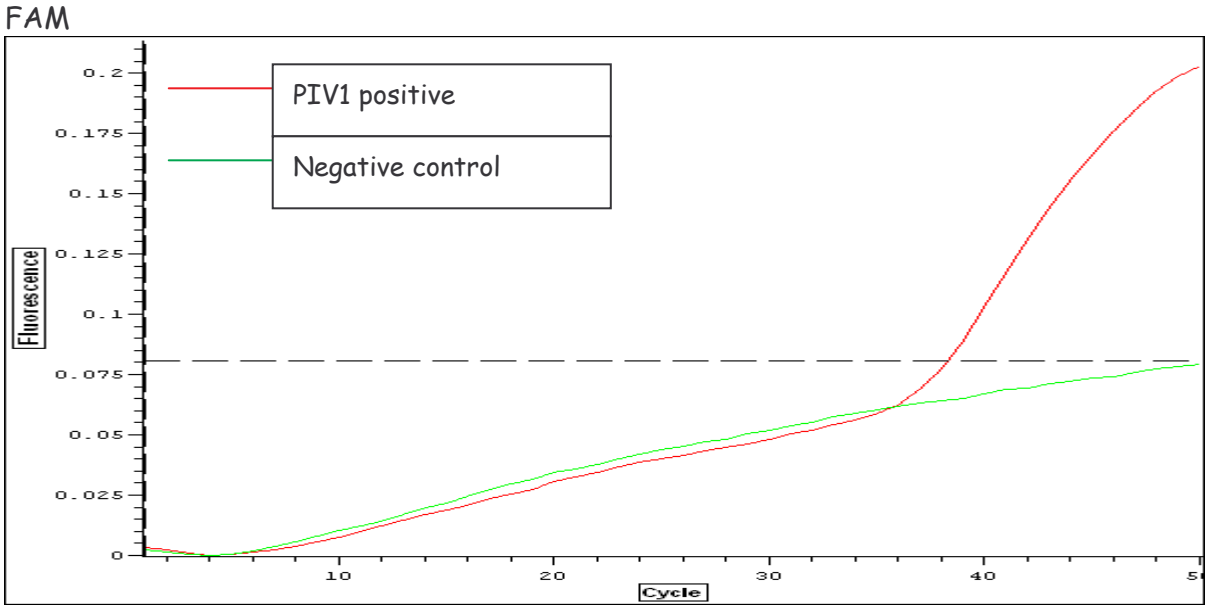

Figure 3.31a: Real-time PCR analysis of PIV1 in a multiplex reaction using a TaqMan probe. Plot of change in fluorescence signal versus cycle number is shown.

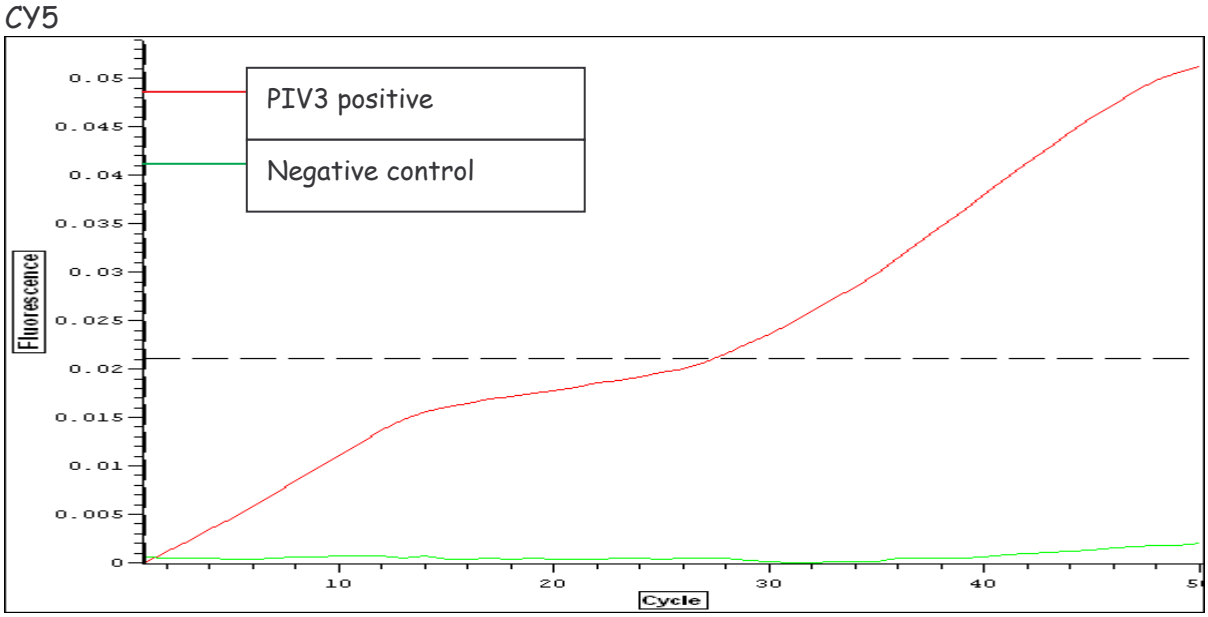

Figure 3.31b: Real-time PCR analysis of PIV3 in a multiplex reaction using a TaqMan probe. Plot of change in fluorescence signal versus cycle number is shown.

b. Respiratory syncytial virus and Adenovirus

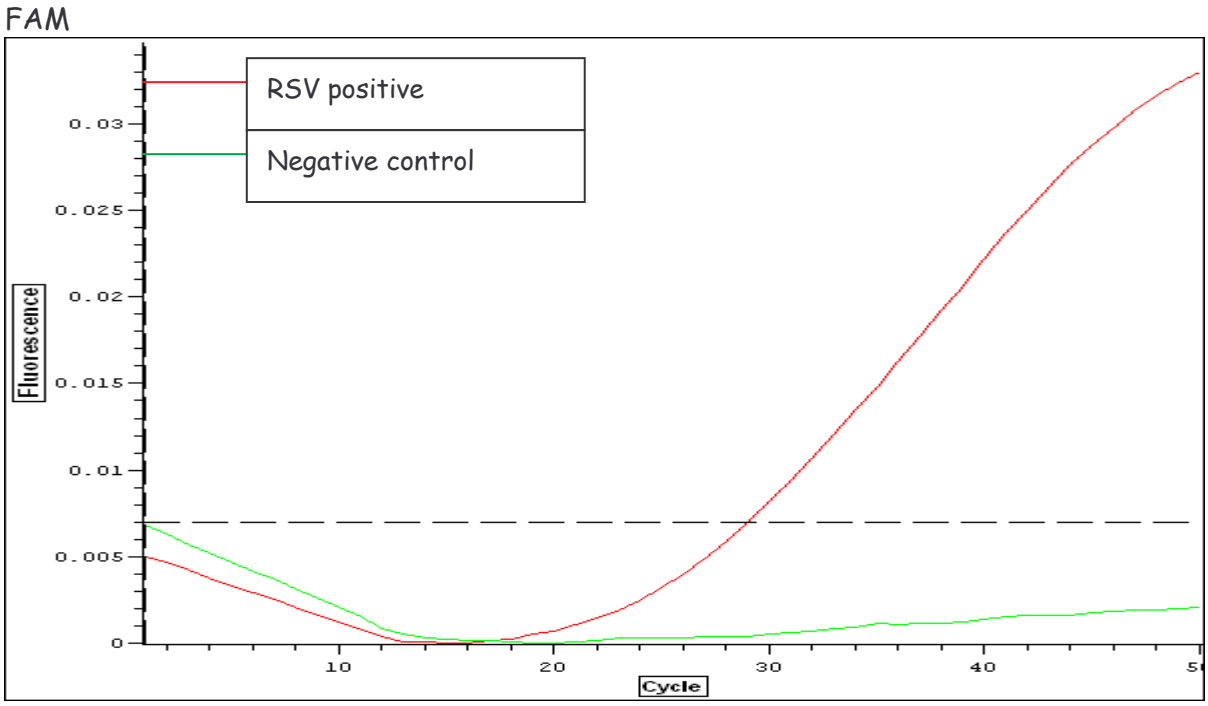

Figure 3.32a: Real-time PCR analysis of RSV in a multiplex reaction using a TaqMan probe. Plot of change in fluorescence signal versus cycle number is shown.

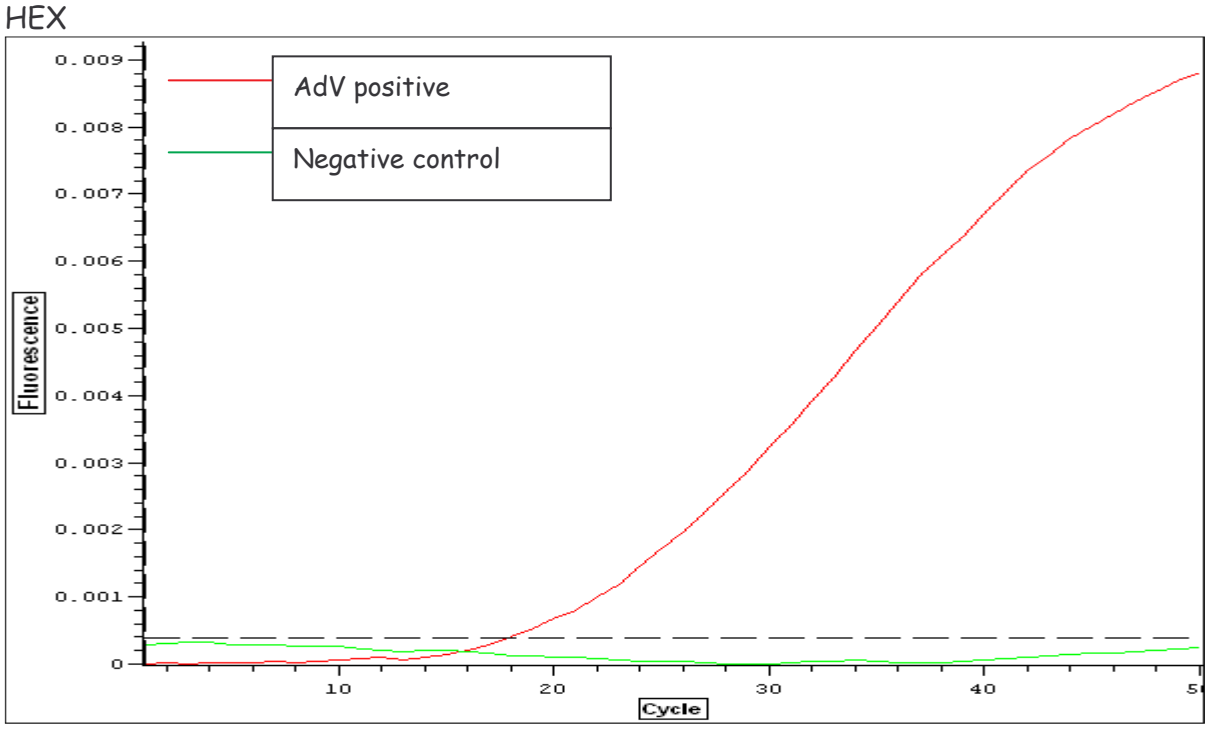

Figure 3.32b: Real-time PCR analysis of AdV in a multiplex reaction using a TaqMan probe. Plot of change in fluorescence signal versus cycle number is shown.

c. Cytomegalovirus and Epstein-Barr virus

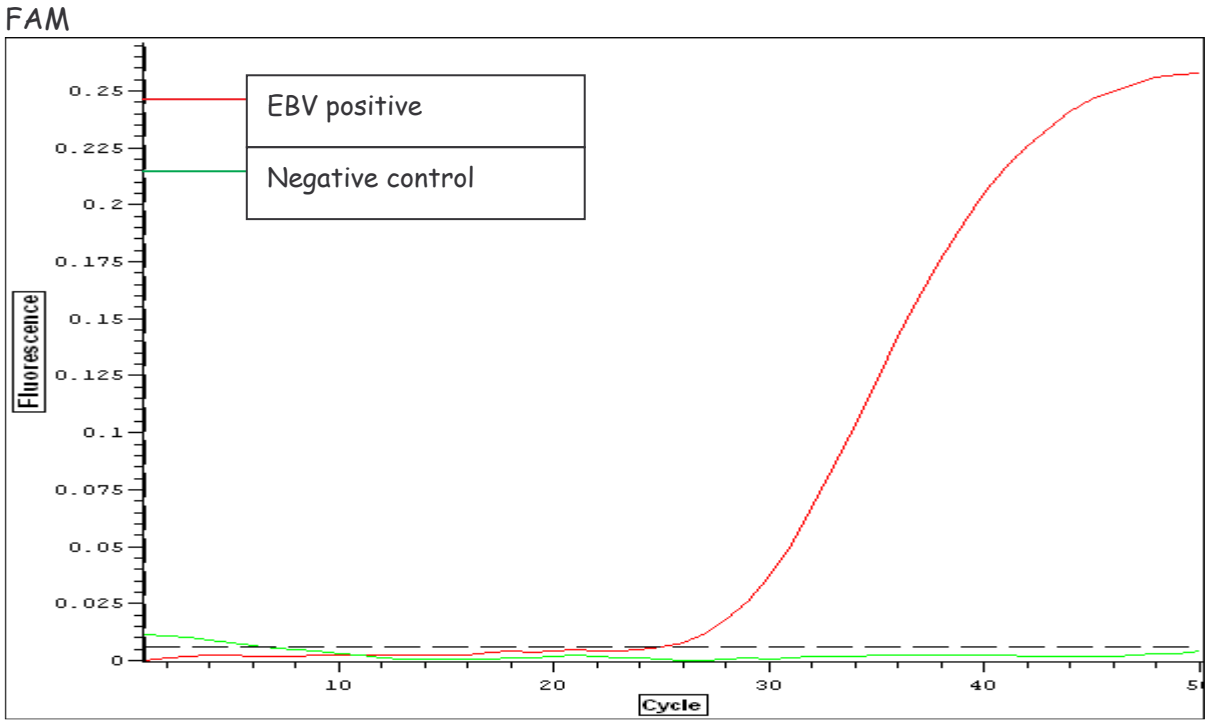

Figure 3.33a: Real-time PCR analysis of EBV in a multiplex reaction using a TaqMan probe. Plot of change in fluorescence signal versus cycle number is shown.

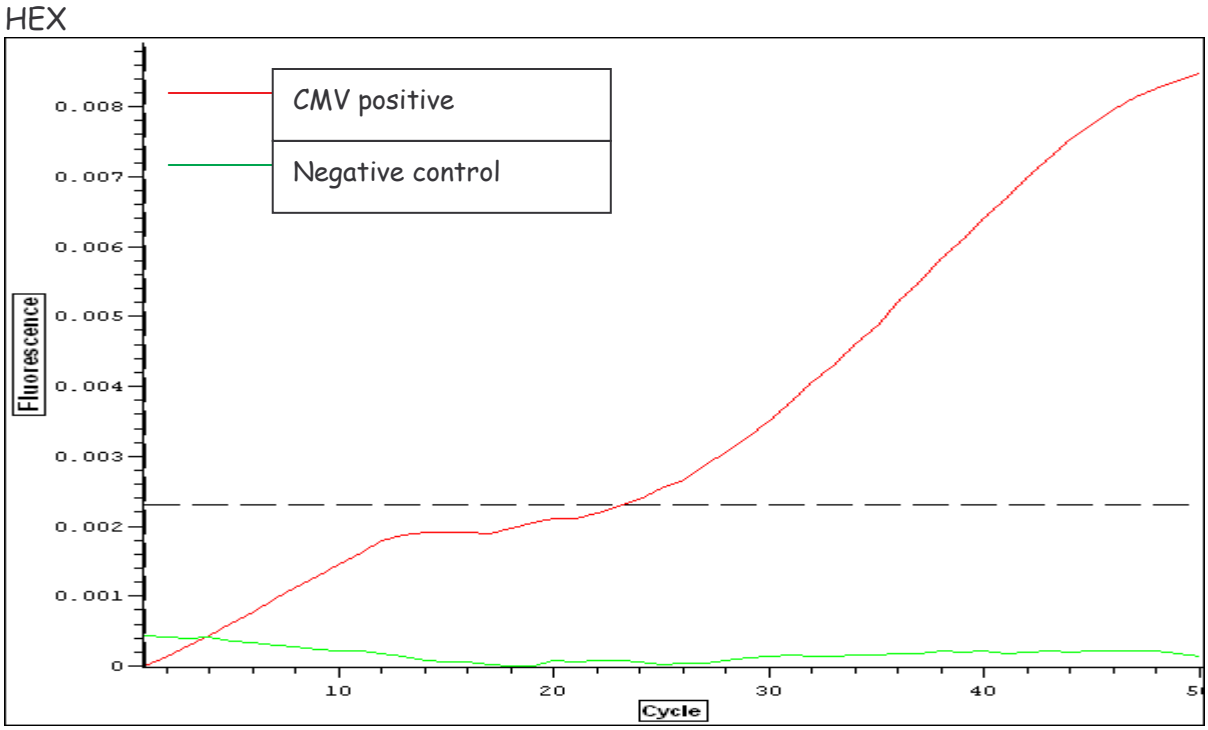

Figure 3.33b: Real-time PCR analysis of CMV in a multiplex reaction using a TaqMan probe. Plot of change in fluorescence signal versus cycle number is shown.

d. *M. pneumoniae* and *L. pneumophila*

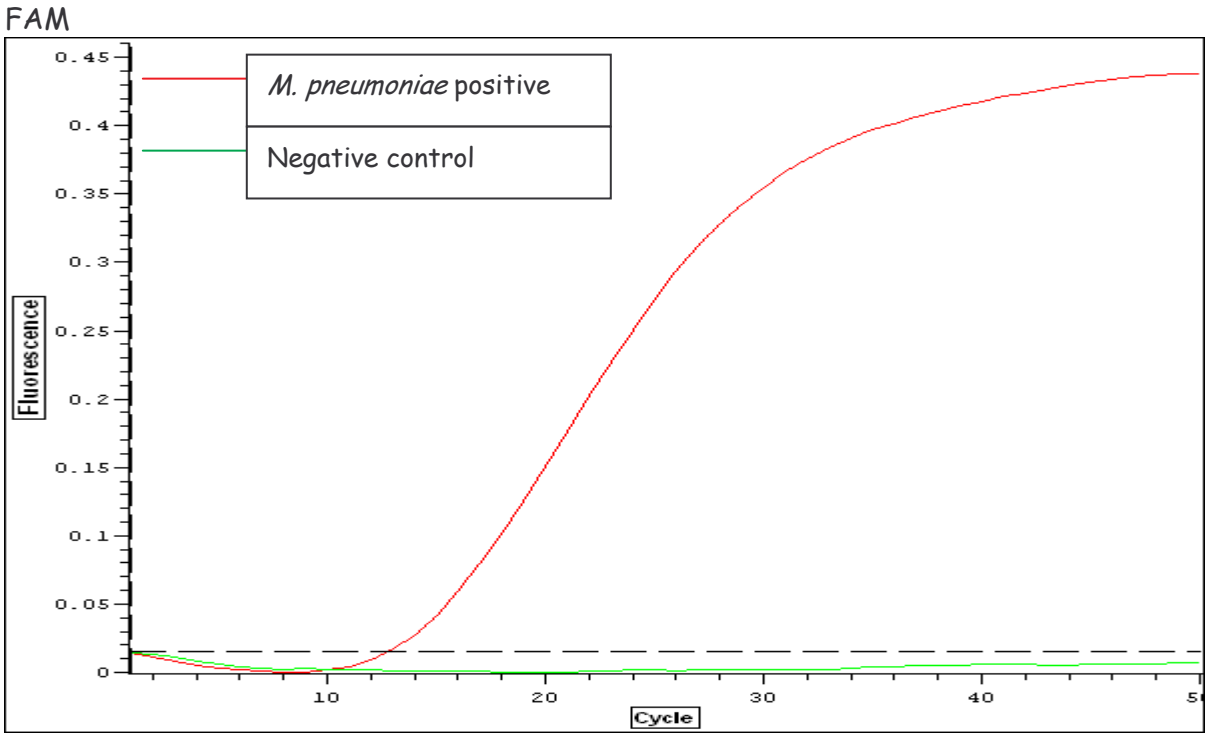

Figure 3.34a: Real-time PCR analysis of *M. pneumoniae* in a multiplex reaction using a TaqMan probe. Plot of change in fluorescence signal versus cycle number is shown.

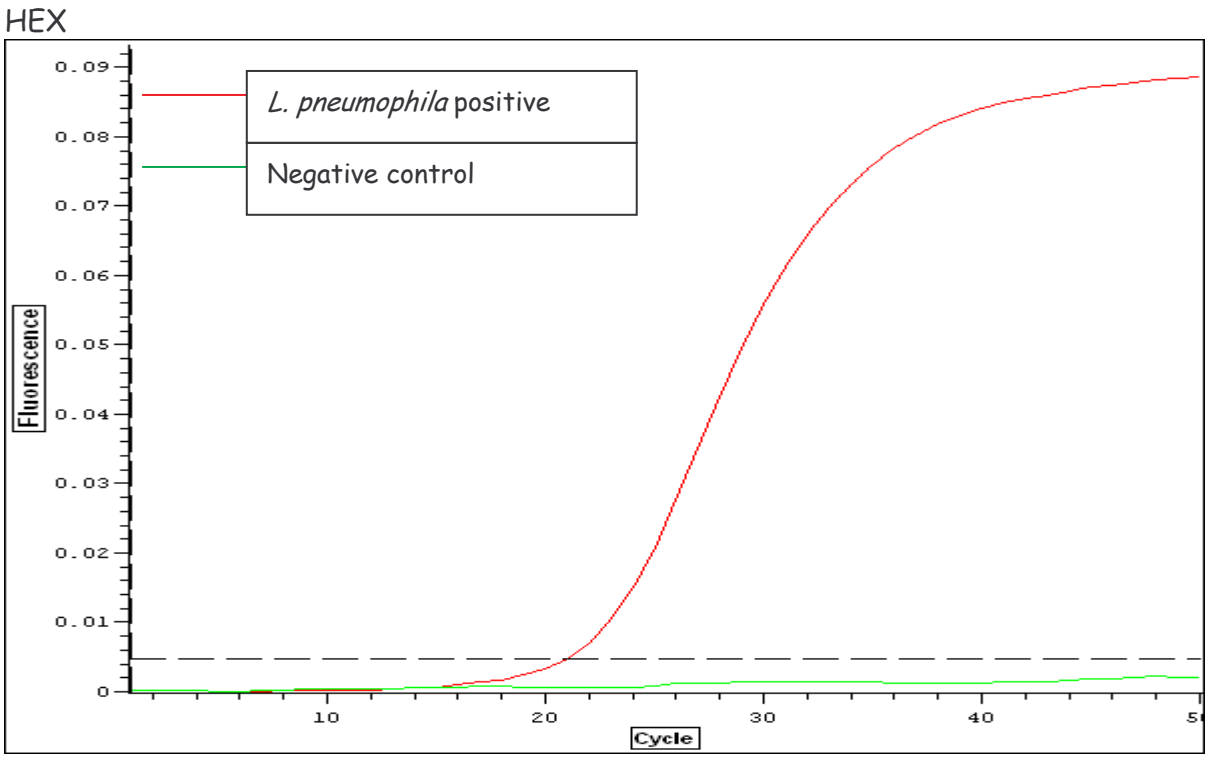

Figure 3.34b: Real-time PCR analysis of *L. pneumophila* in a multiplex reaction using a TaqMan probe. Plot of change in fluorescence signal versus cycle number is shown.

e. GAPDH (DNA) and *C. pneumoniae*

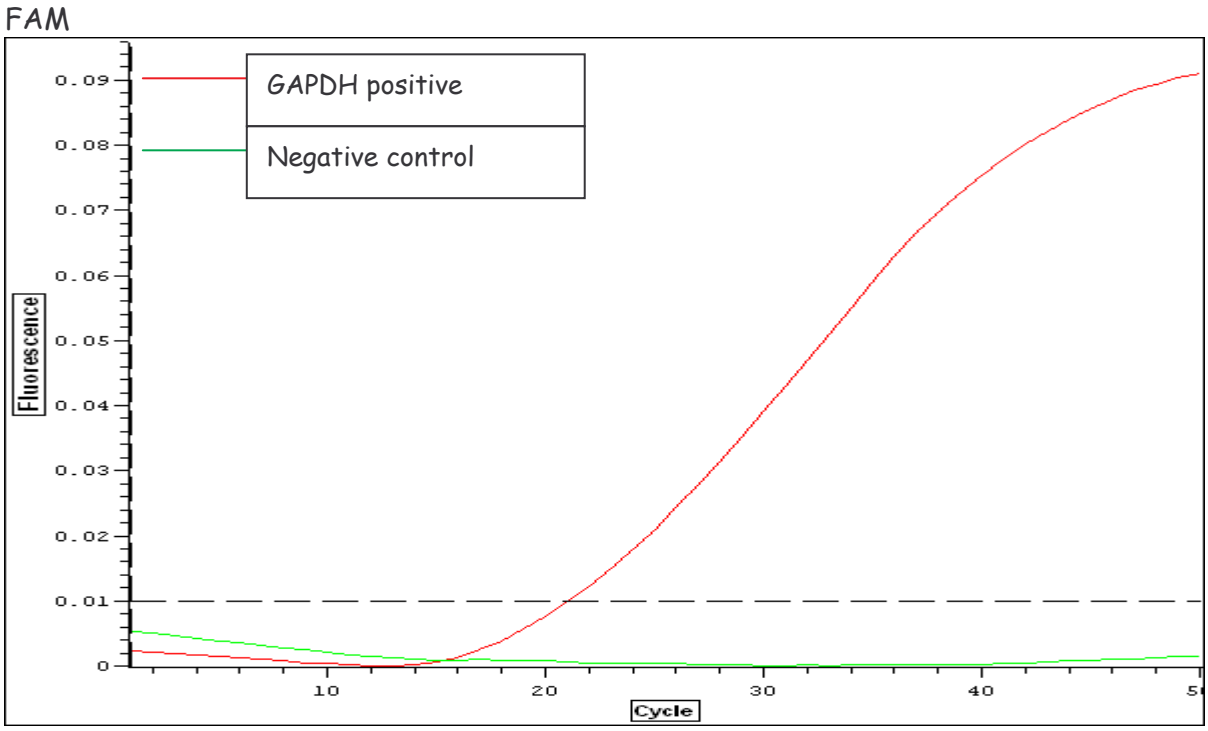

Figure 3.35a Real-time PCR analysis of GAPDH (DNA) in a multiplex reaction using a TaqMan probe. Plot of change in fluorescence signal versus cycle number is shown.

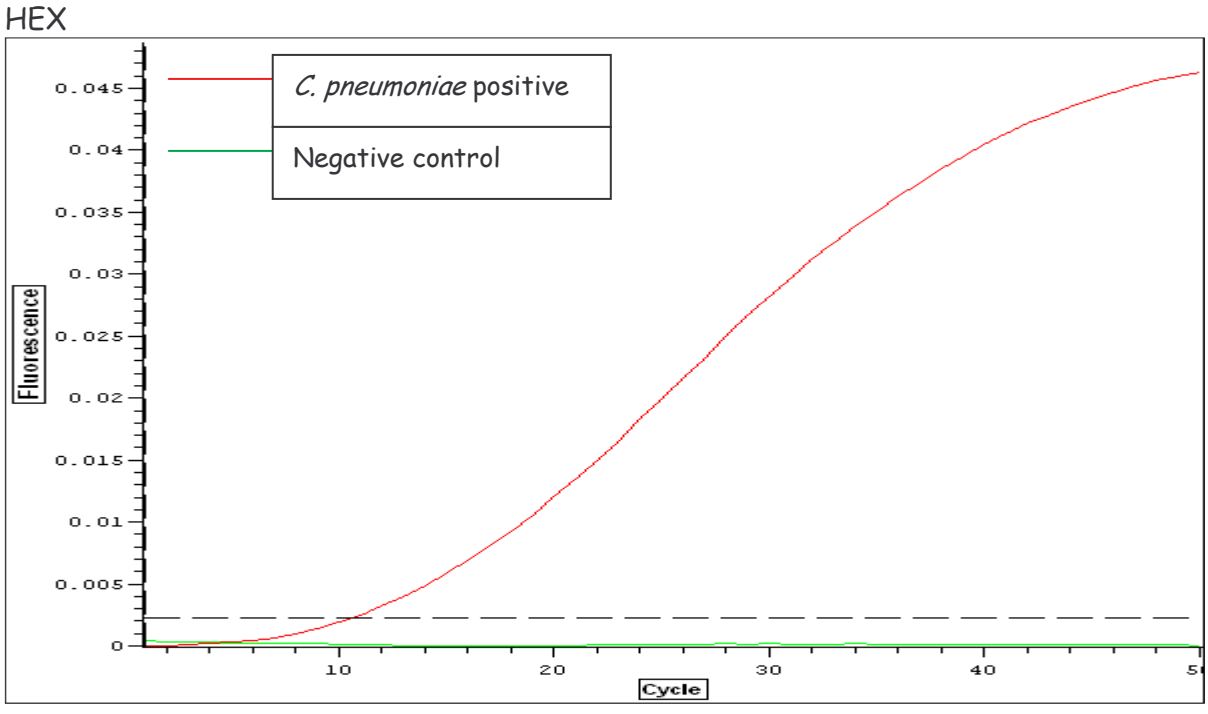

Figure 3.35b: Real-time PCR analysis of *C. pneumoniae* in a multiplex reaction using a TaqMan probe. Plot of change in fluorescence signal versus cycle number is shown.

f. Influenza A virus Influenza B virus and human metapneumovirus

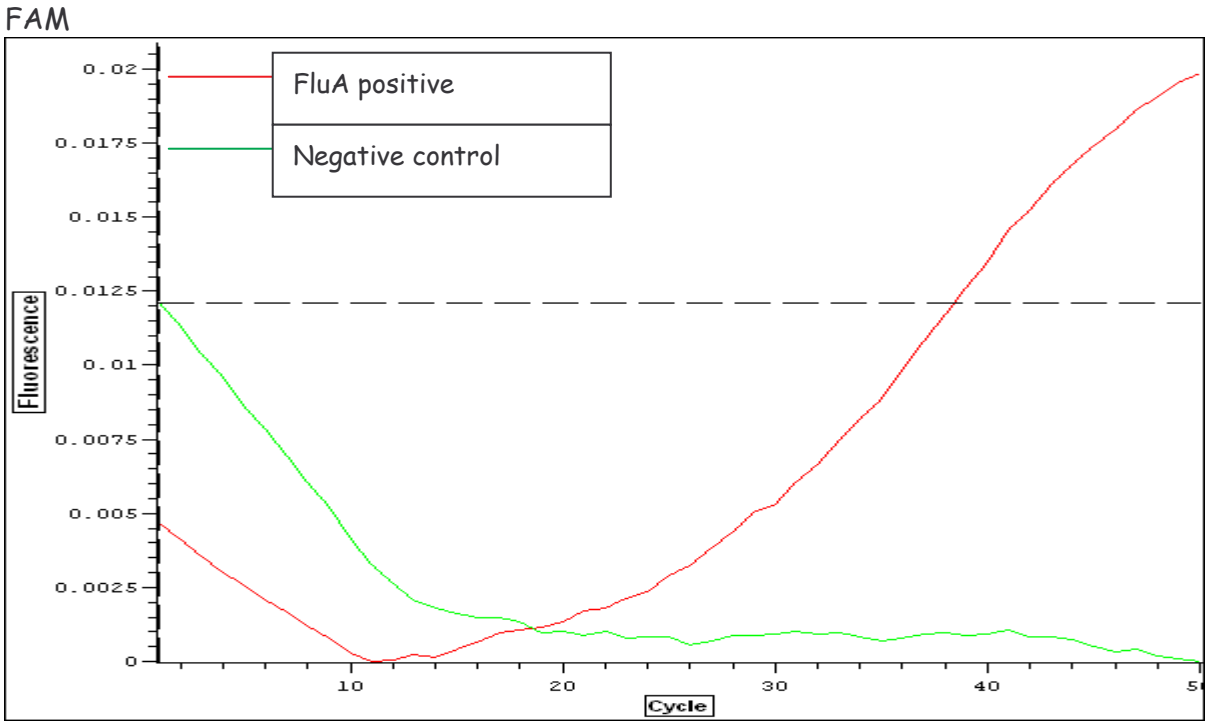

Figure 3.36a: Real-time PCR analysis of FluA in a multiplex reaction using a TaqMan probe. Plot of change in fluorescence signal versus cycle number is shown.

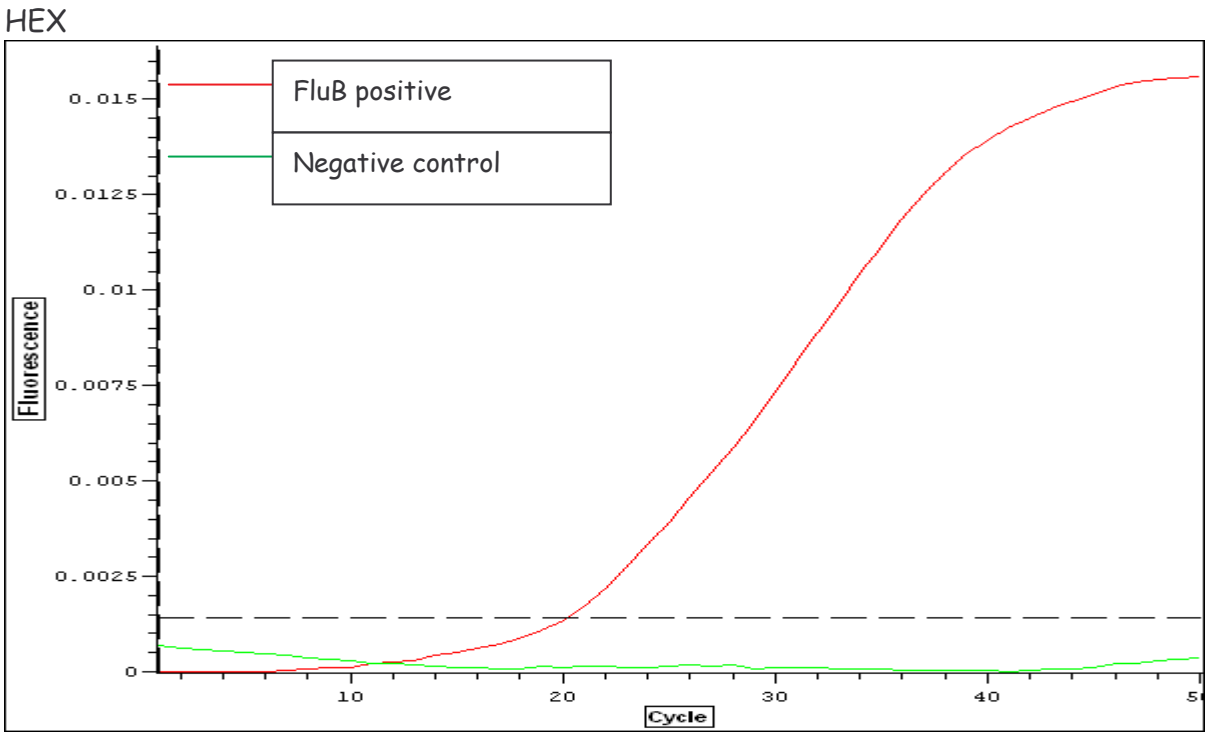

Figure 3.36b: Real-time PCR analysis of FluB in a multiplex reaction using a TaqMan probe. Plot of change in fluorescence signal versus cycle number is shown.

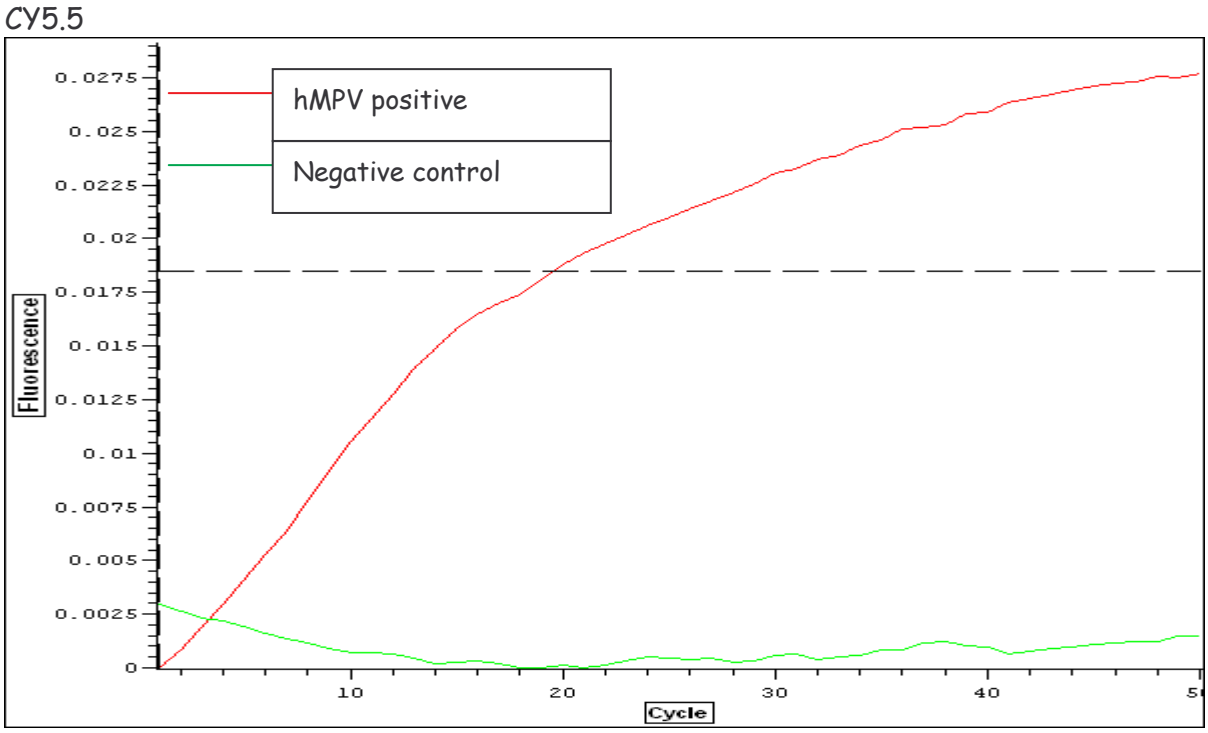

Figure 3.36c: Real-time PCR analysis of hMPV in a multiplex reaction using a TaqMan probe. Plot of change in fluorescence signal versus cycle number is shown.

3.3. Efficiency of reactions

Generally, the efficiency of a real-time reaction can be calculated using data from the fluorescence curve using the following formula: Efficiency = $10^{(-1/slope)}$ (Wong and Medrano, 2005). A steep slope (value = 2) indicates doubling of amplicons thus optimal PCR efficiency. In this project, it was observed that, according to calculations performed by the Opticon Monitor™ version 3.1 software of the Chromo4 system, real-time PCR reaction efficiencies of the SYBR Green I reactions were higher than those of TaqMan singleplex probe assays (Figure 3.37). This can be attributed to the use of different reaction mastermixes, the non-specificity of SYBR Green I which results in the formation of primer-dimer artifacts and non-specific products contributing to the increase in double-stranded molecules detected and more generally, the different chemistries involved.

The majority of probe reactions had a PCR efficiency of less than 1.4 and this is believed to be due to probe degradation over time as the TaqMan probes were used later in the project.

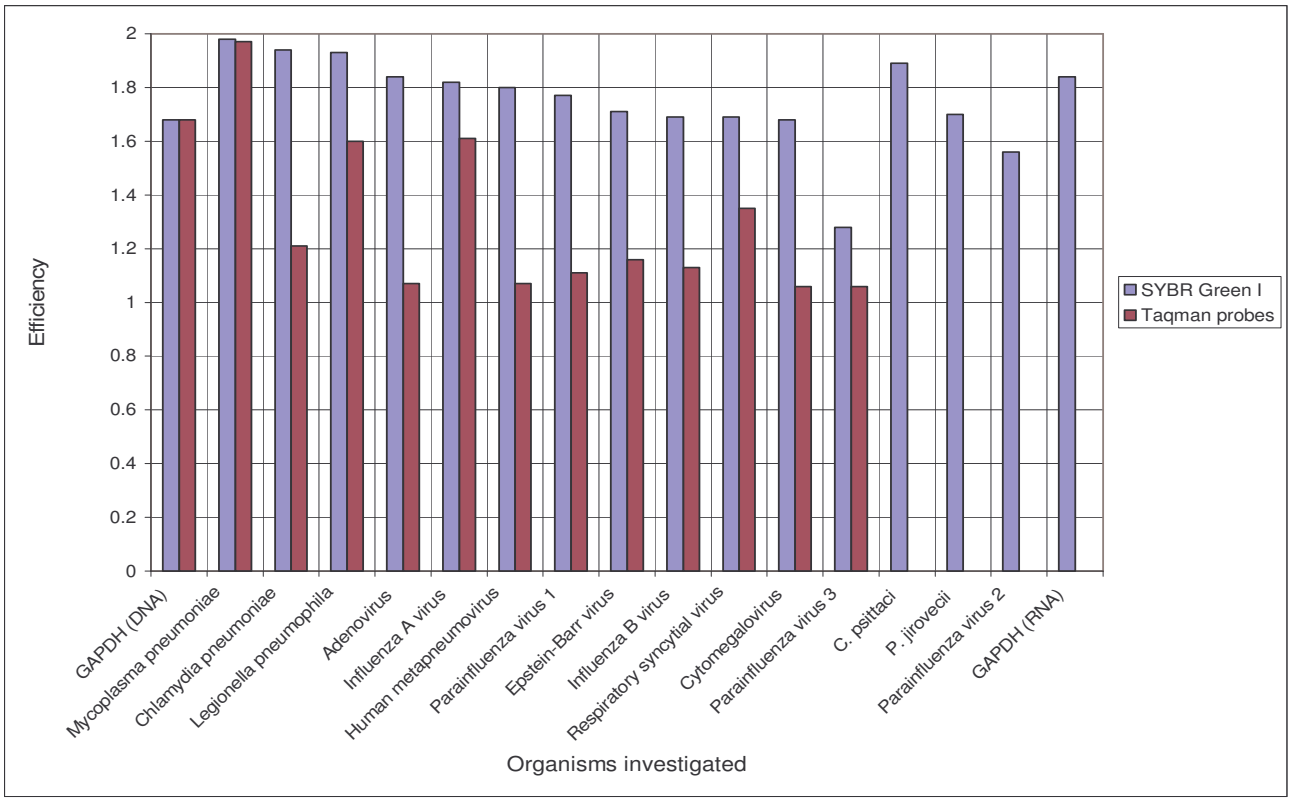

Figure 3.37: Bar chart illustrating the difference in amplification efficiencies between TaqMan probes and SYBR Green I for each organism. The Opticon Monitor™ version 3.1 software of the Chromo4 real-time PCR machine was used to calculate the values.

CHAPTER 3B: RESULTS - CLONING

3.4. Cloning

With the exception of *L. pneumophila* and hMPV, the positive controls obtained contained an unknown copy number. It was therefore necessary to generate positive control plasmids to use for sensitivity assays. After obtaining positive results for the real-time PCR assays performed on the controls, the product was cloned. After transformation, real-time PCR was performed on the white colonies (Figure 3.38) to confirm the presence of the insert. Confirmed clones were purified and the plasmid separated on a 2% agarose gel. All colonies picked presumptively contained inserts as judged by agarose gel electrophoresis. This was confirmed by organism specific PCR and sequencing of the plasmid inserts for all relevant organisms.

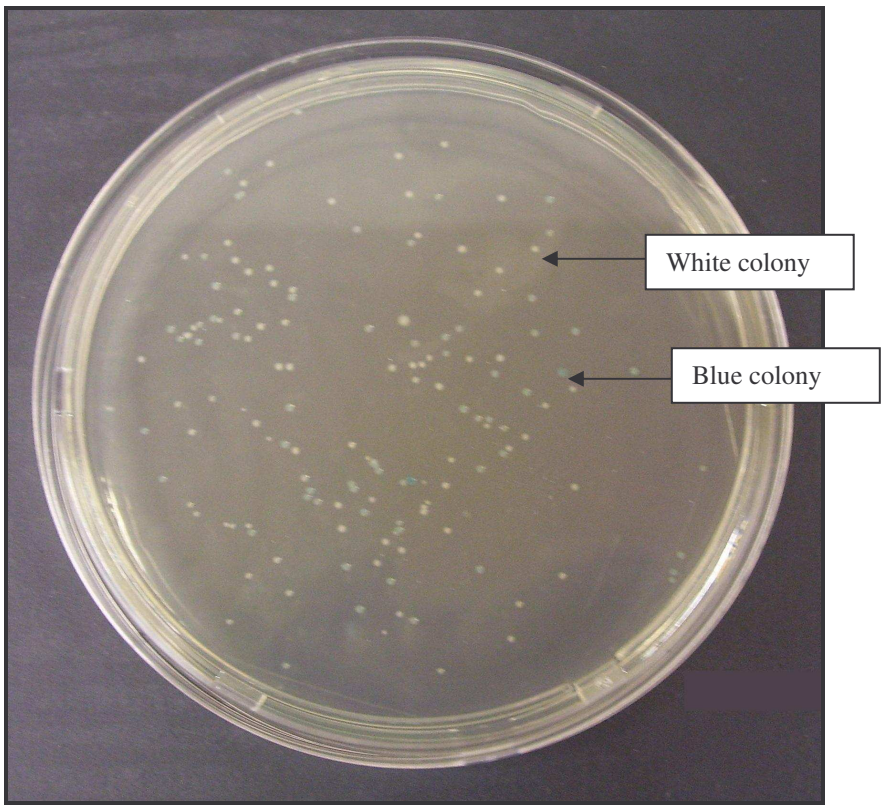

Figure 3.38: Blue-white screening of transformed cells plated out on LB agar supplemented with ampicillin, X-gal and IPTG. The white colonies contain the insert and the majority of the blue colonies do not.

CHAPTER 3C: RESULTS - SENSITIVITY ASSAYS

Despite the fact that the assays used in this study were qualitative, it is of value to know the detection limits of the reactions used to enable their application in a clinical setting. Serial dilutions of recombinant plasmids were performed (10000 copies/µl to 1 copy/µl) using milliQ water. Real-time PCR reactions were performed in both singleplex and multiplex, on the 3 lowest copy numbers (1, 10 and 100 copies/µl) to determine the detection limit of the assays.

3.5. Singleplex reactions

Detection limits of the real-time PCR assays were determined using TaqMan probes for all reactions that could be multiplexed (Figures 3.39-3.51) and SYBR Green I for those that were not (PIV2, *C. psittaci* and *P. jirovecii*) (Figures 3.52-3.54). All real-time PCR end products of singleplex sensitivity assays were run on 2% agarose gels (see appendix B). Amplification products were visible on the agarose gel indicating decreasing band intensity with increasing dilutions. No amplicons were detected for the negative controls. The lower limits of detection for the majority of the assays were 1 copy/µl of plasmid with CMV and *L. pneumophila* assays detected at 10 copies/µl and 10 CFUs/µl respectively.

3.5.1. TaqMan Probes

a. Influenza A virus

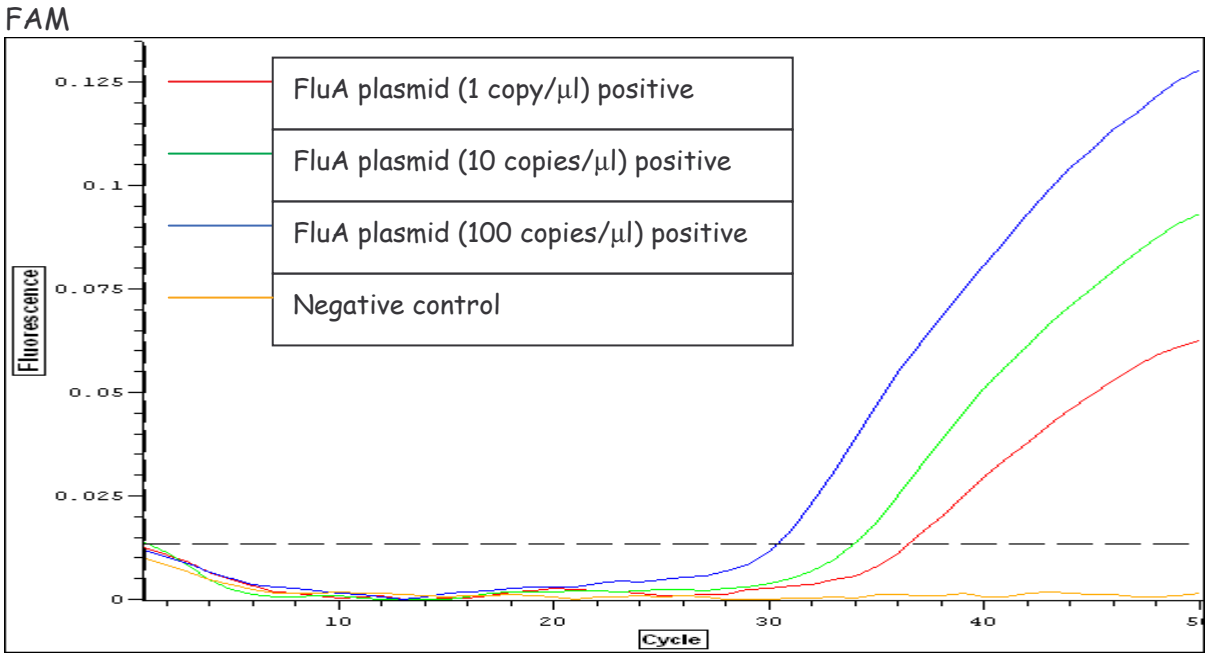

Figure 3.39: Fluorescence graph of FluA plasmid serial dilutions demonstrating the sensitivity of the TaqMan assay. Change in fluorescence signal is plotted versus cycle number.

b. Influenza B virus

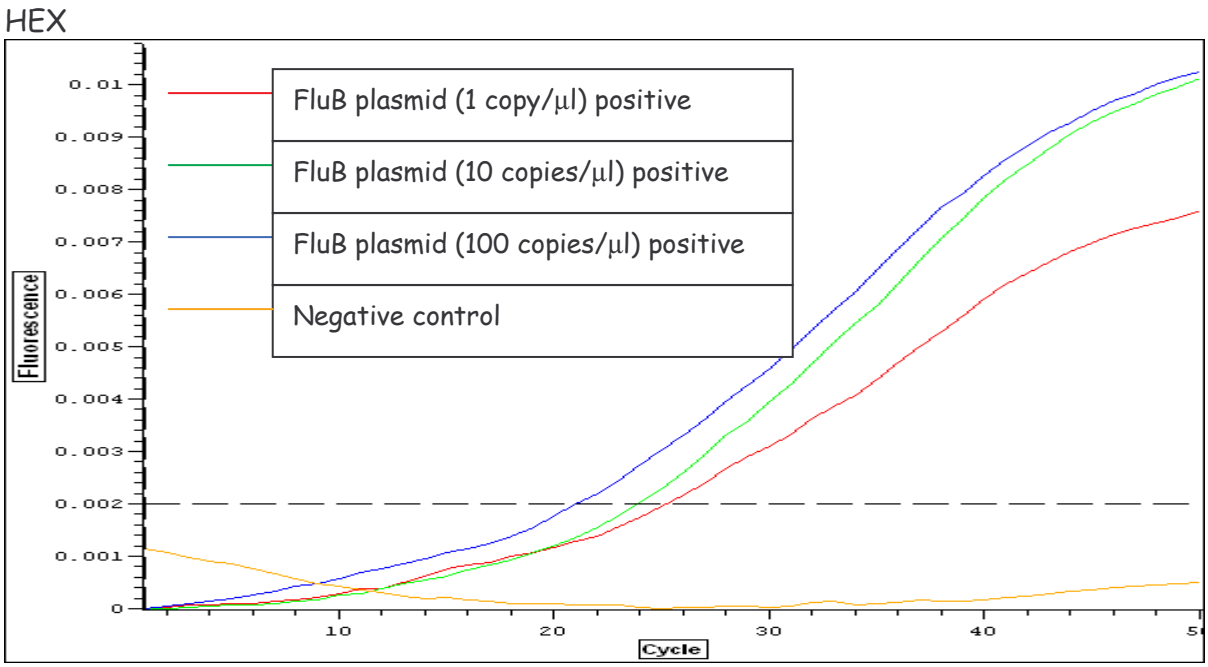

Figure 3.40: Fluorescence graph of FluB plasmid serial dilutions demonstrating the sensitivity of the TaqMan assay. Change in fluorescence signal is plotted versus cycle number.

c. Human metapneumovirus

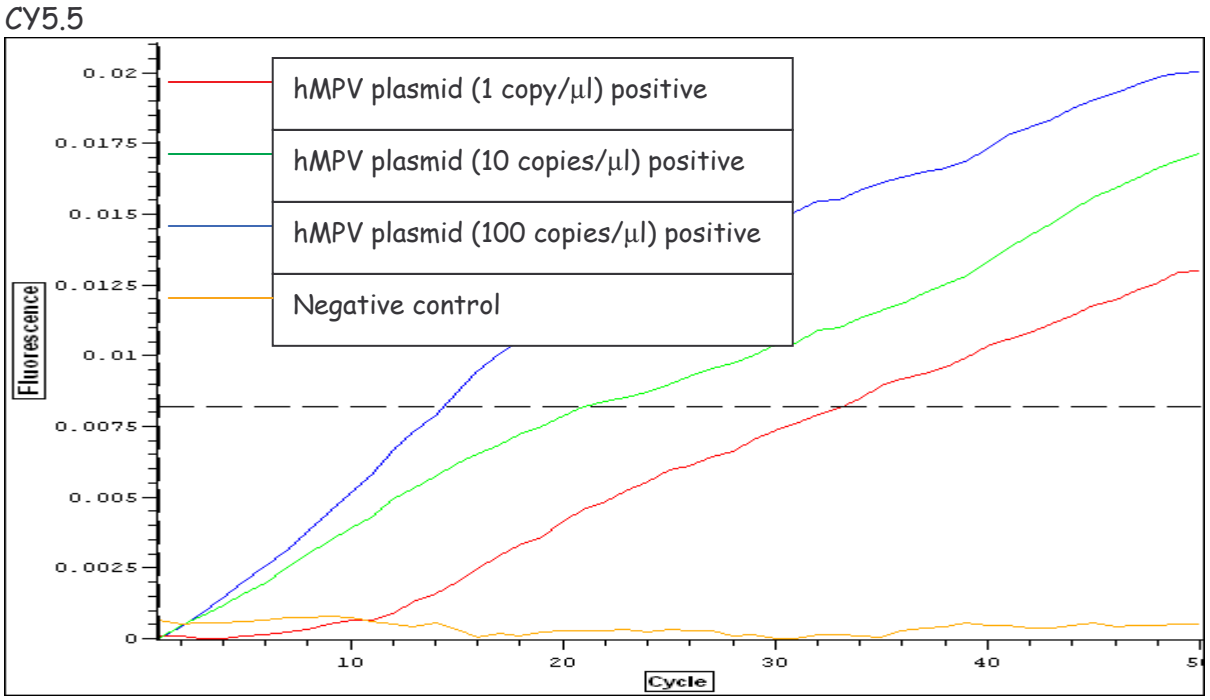

Figure 3.41: Fluorescence graph of hMPV plasmid serial dilutions demonstrating the sensitivity of the TaqMan assay. Change in fluorescence signal is plotted versus cycle number.

d. Parainfluenza virus 1

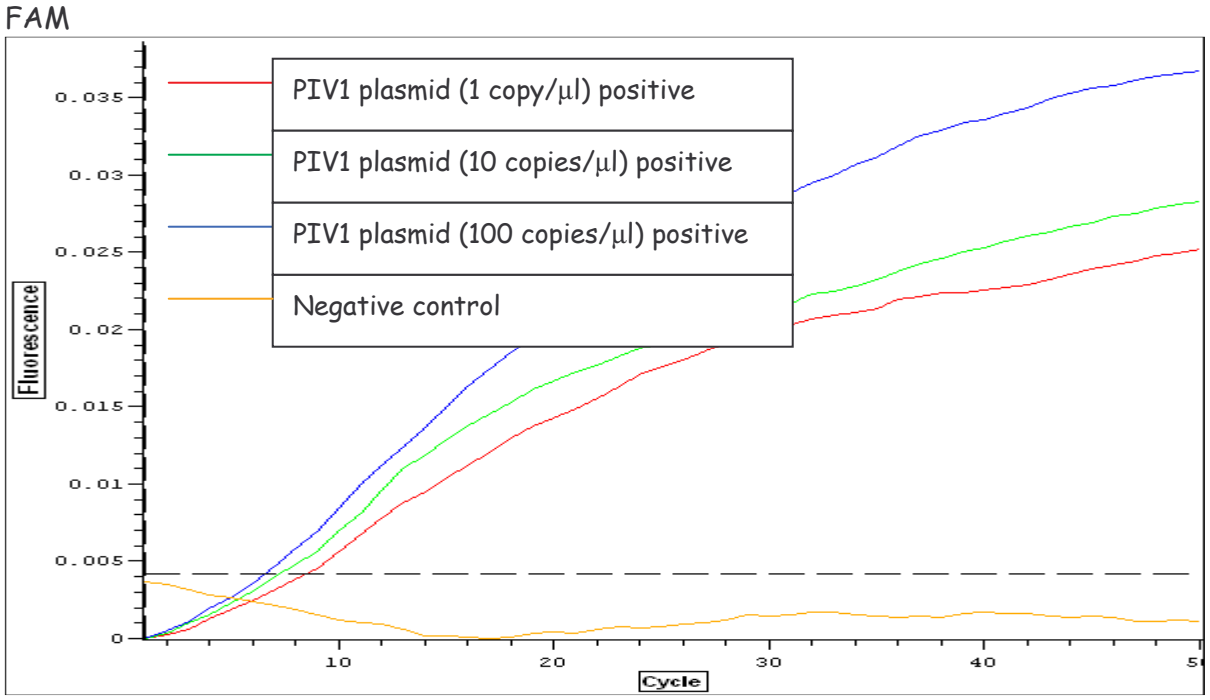

Figure 3.42: Fluorescence graph of PIV1 plasmid serial dilutions demonstrating the sensitivity of the TaqMan assay. Change in fluorescence signal is plotted versus cycle number.

e. Parainfluenza virus 3

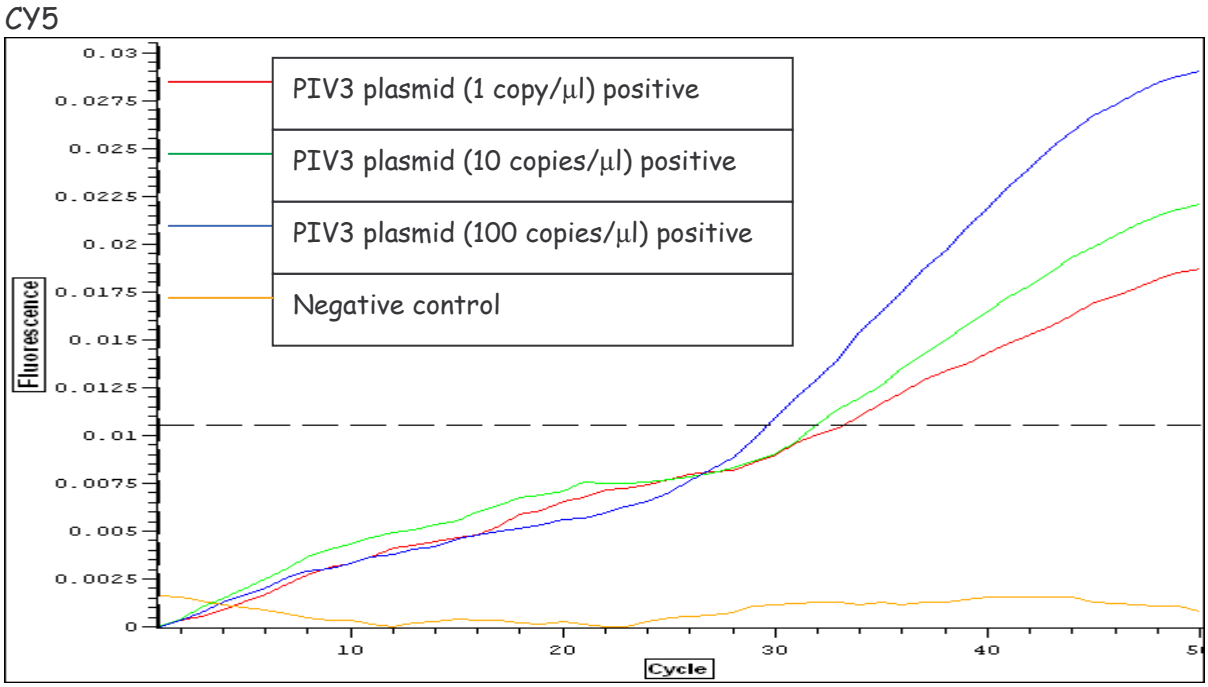

Figure 3.43: Fluorescence graph of PIV3 plasmid serial dilutions demonstrating the sensitivity of the TaqMan assay. Change in fluorescence signal is plotted versus cycle number.

f. Adenovirus

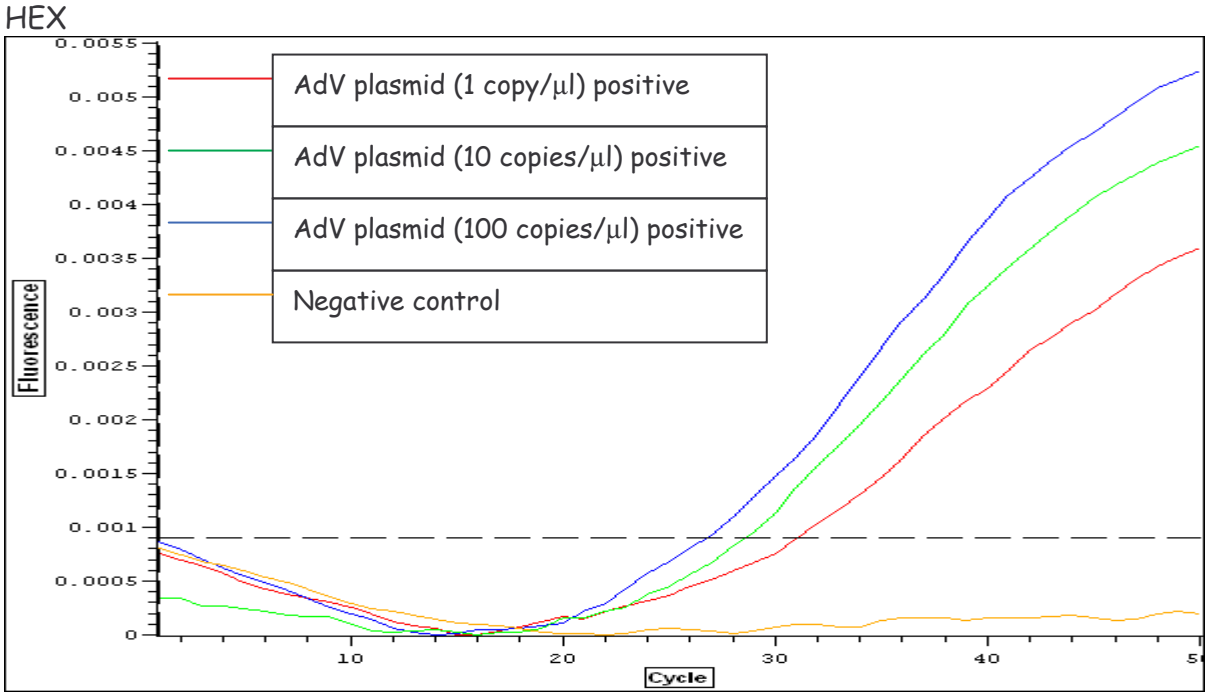

Figure 3.44: Fluorescence graph of AdV plasmid serial dilutions demonstrating the sensitivity of the TaqMan assay. Change in fluorescence signal is plotted versus cycle number.

g. Respiratory syncytial virus

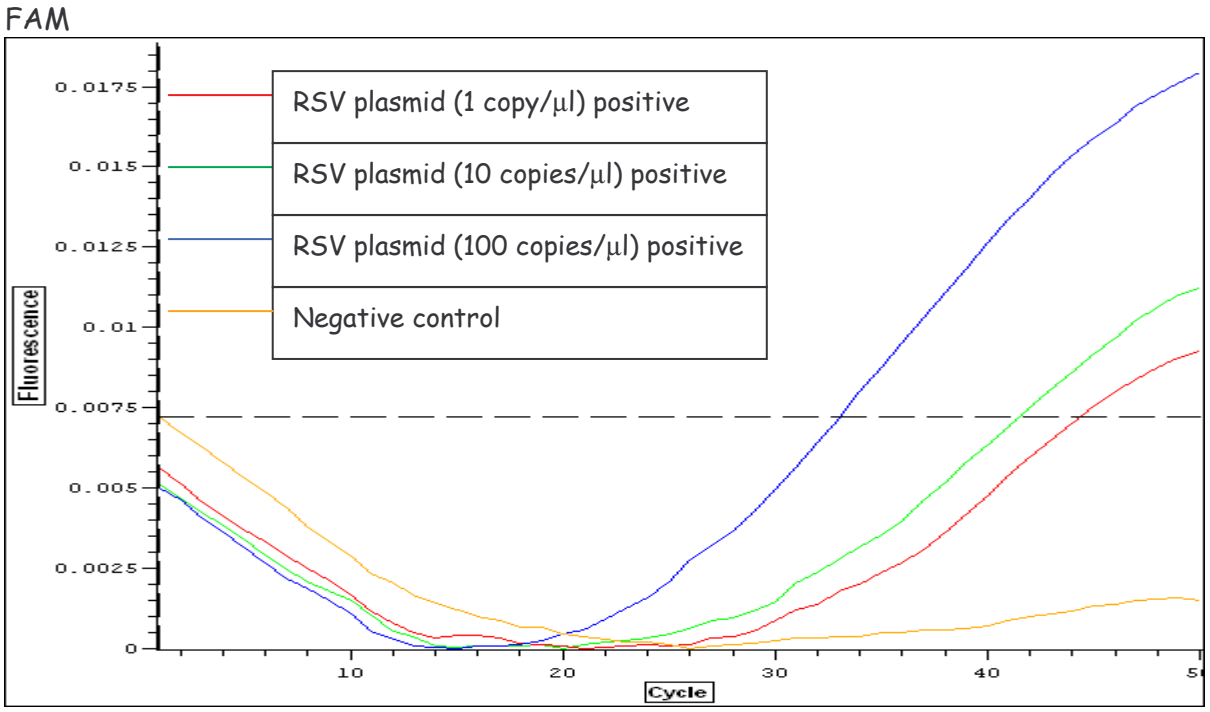

Figure 3.45: Fluorescence graph of RSV plasmid serial dilutions demonstrating the sensitivity of the TaqMan assay. Change in fluorescence signal is plotted versus cycle number.

h. Cytomegalovirus

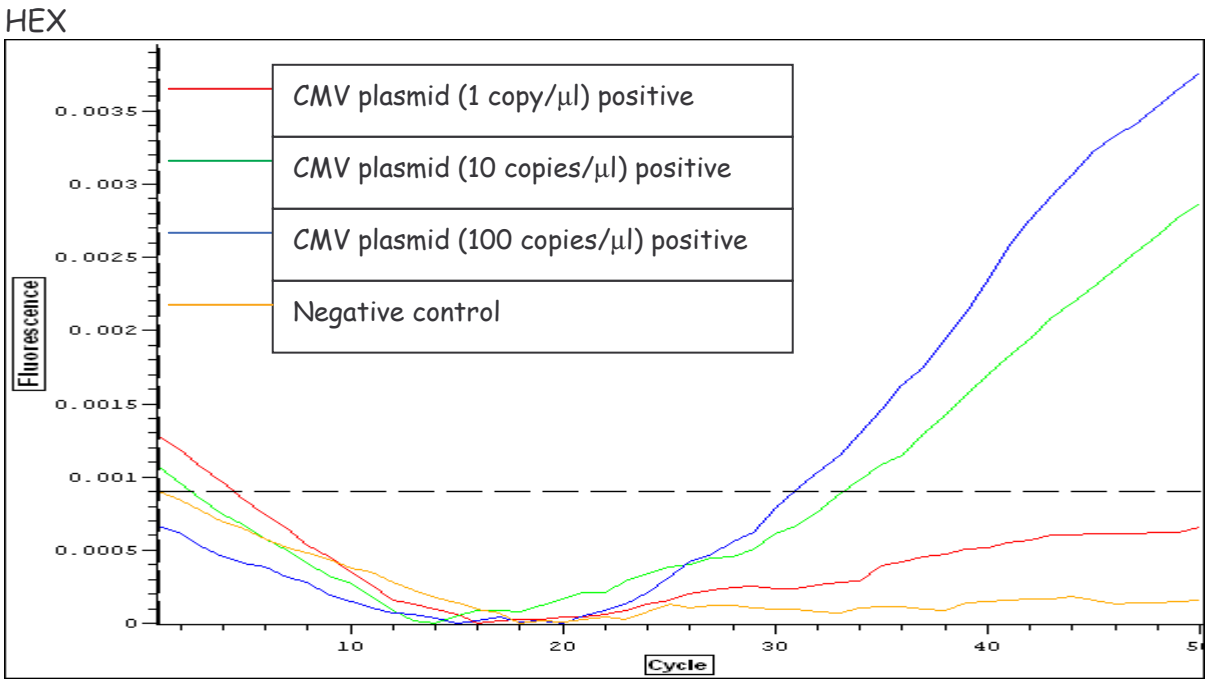

Figure 3.46: Fluorescence graph of CMV plasmid serial dilutions demonstrating the sensitivity of the TaqMan assay. Change in fluorescence signal is plotted versus cycle number.

i. Epstein-Barr virus

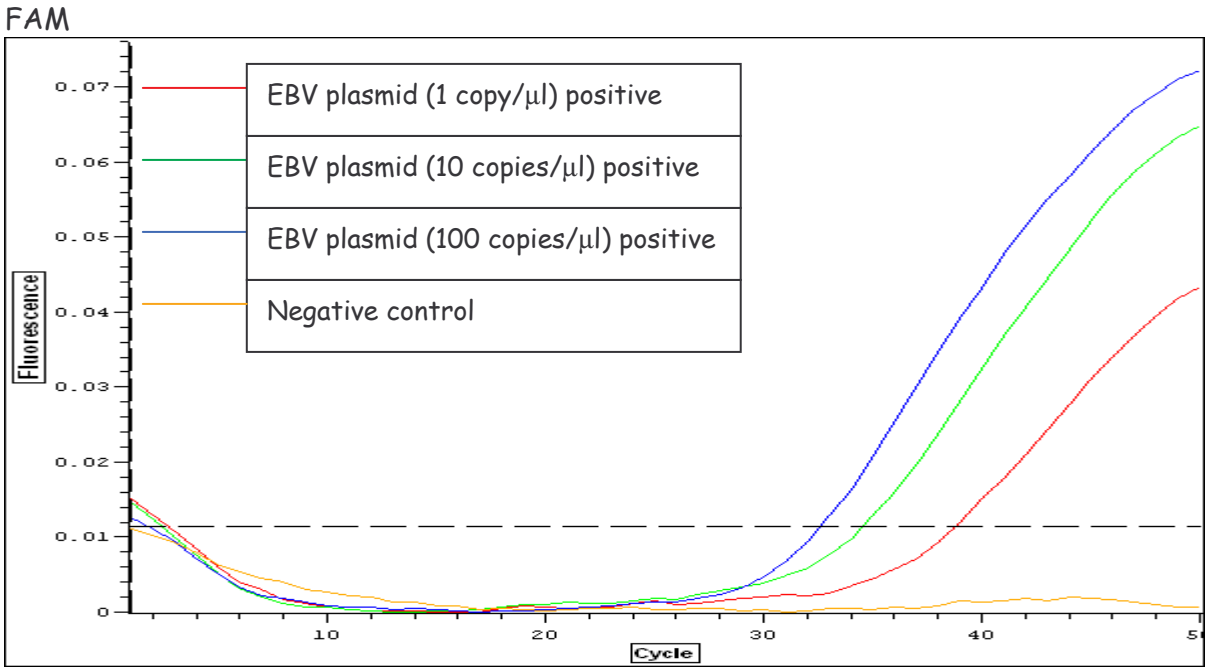

Figure 3.47: Fluorescence graph of EBV plasmid serial dilutions demonstrating the sensitivity of the TaqMan assay. Change in fluorescence signal is plotted versus cycle number.

j. *M. pneumoniae*

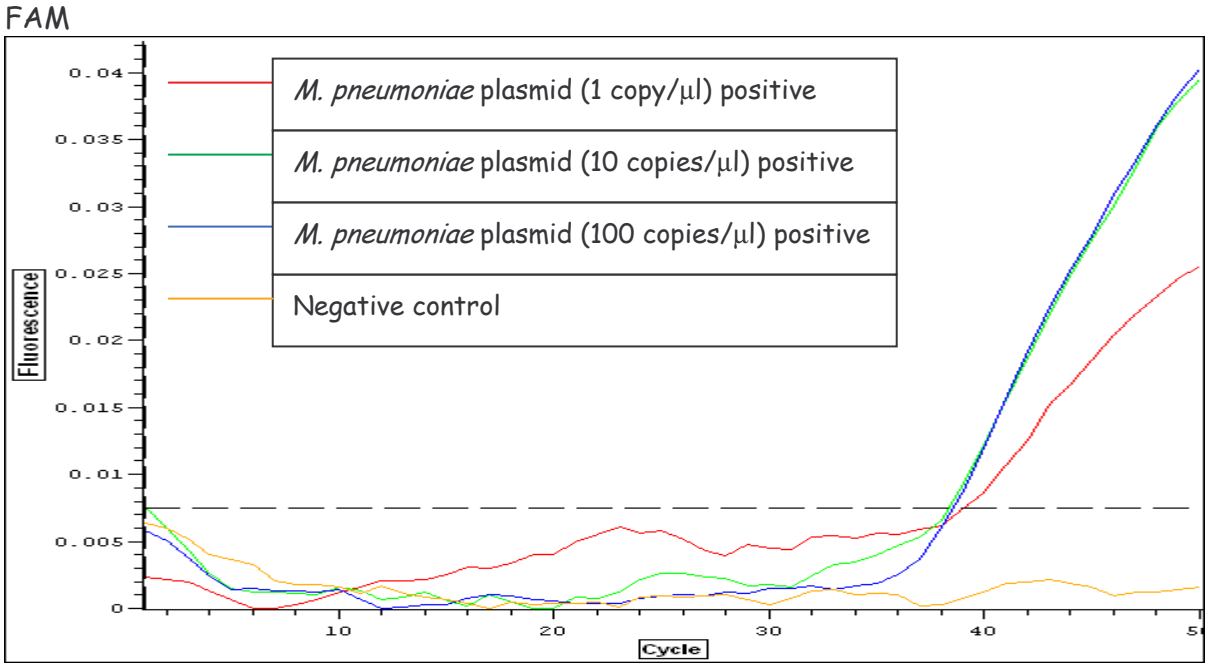

Figure 3.48: Fluorescence graph of *M. pneumoniae* plasmid serial dilutions demonstrating the sensitivity of the TaqMan assay. Change in fluorescence signal is plotted versus cycle number.

k. *L. pneumophila*

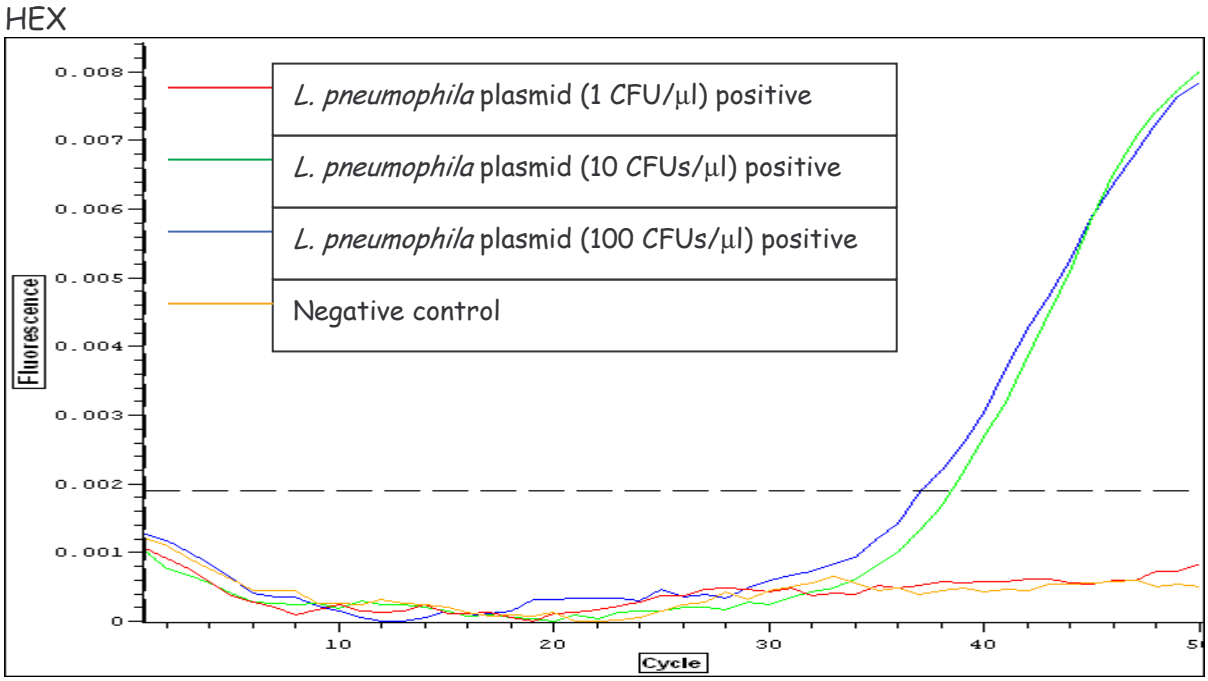

Figure 3.49: Fluorescence graph of *L. pneumophila* plasmid serial dilutions demonstrating the sensitivity of the TaqMan assay. Change in fluorescence signal is plotted versus cycle number.

l. *C. pneumoniae*

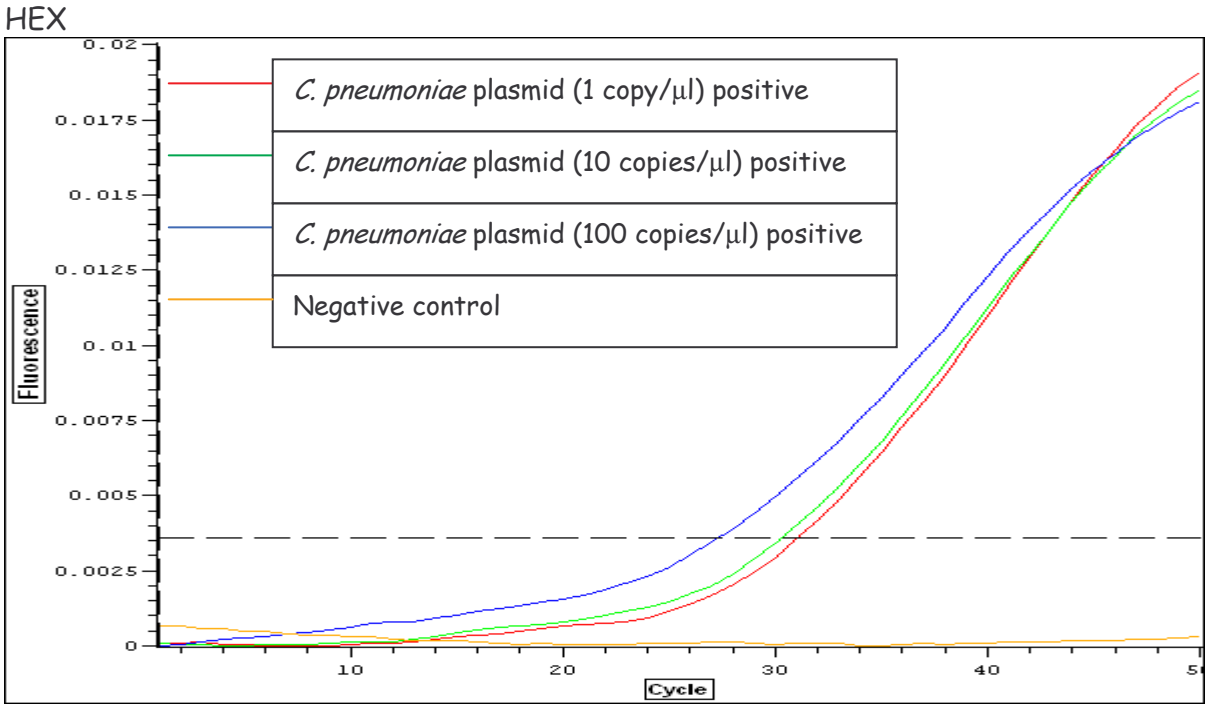

Figure 3.50: Fluorescence graph of *C. pneumoniae* plasmid serial dilutions demonstrating the sensitivity of the TaqMan assay. Change in fluorescence signal is plotted versus cycle number.

m. GAPDH (DNA)

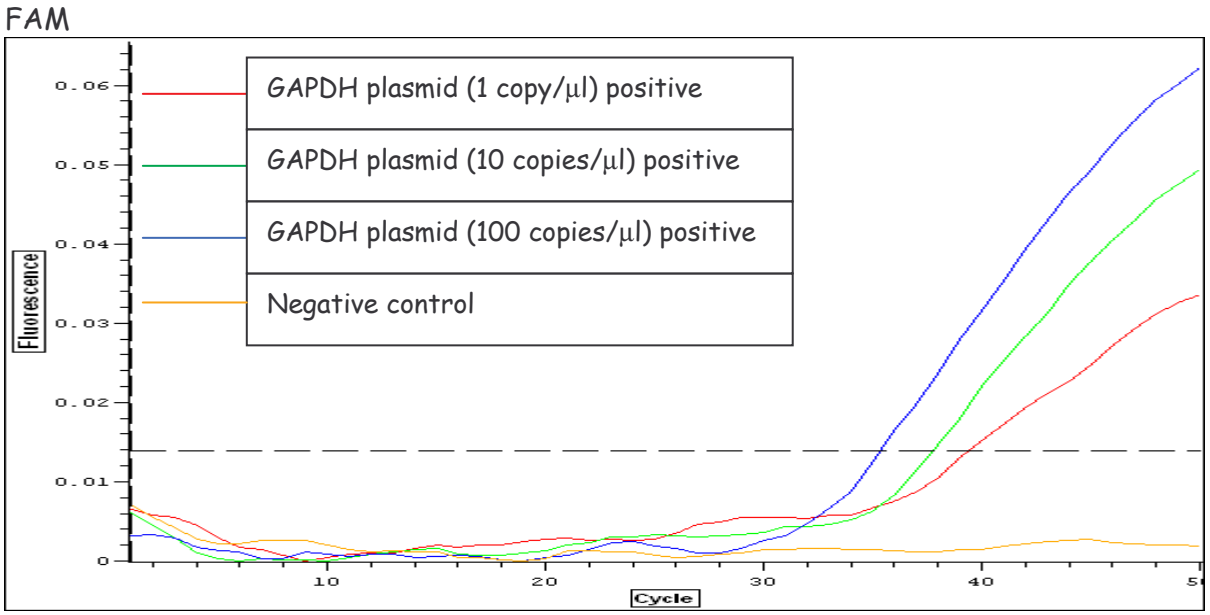

Figure 3.51: Fluorescence graph of GAPDH (DNA) plasmid serial dilutions demonstrating the sensitivity of the TaqMan assay. Change in fluorescence signal is plotted versus cycle number.

3.5.2 SYBR® Green I

a. *P. jirovecii*

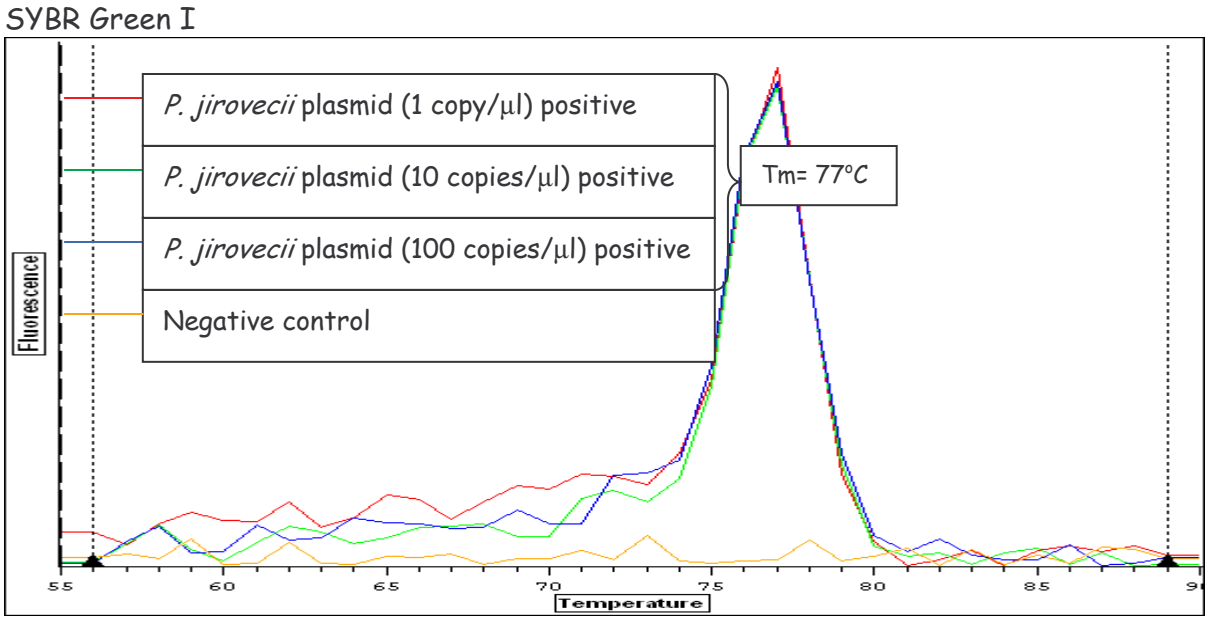

Figure 3.52: Melting curve analysis of *P. jirovecii* plasmid serial dilutions demonstrating the sensitivity of the SYBR Green I assay. The signature melting temperature of *P. jirovecii* (77°C) is indicated by the sharp red, green and blue peaks. Temperature is plotted versus fluorescence signal.

b. *C. psittaci*

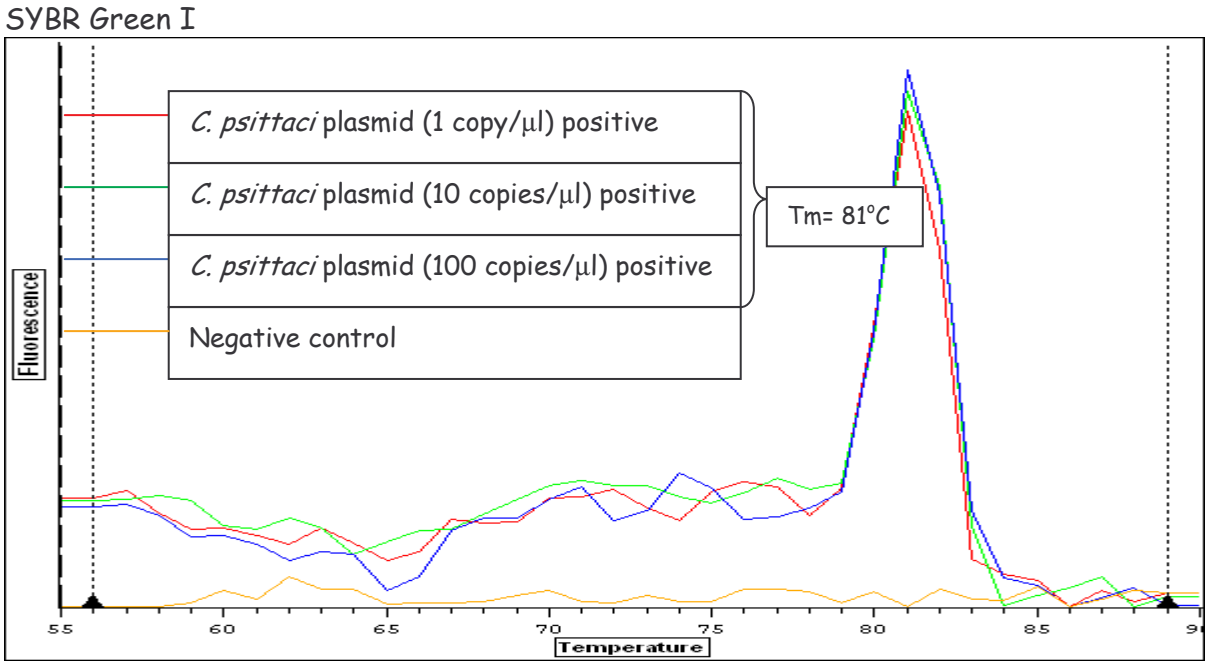

Figure 3.53: Melting curve analysis of *C. psittaci* plasmid serial dilutions demonstrating the sensitivity of the SYBR Green I assay. The signature melting temperature of *C. psittaci* (81°C) is indicated by the sharp red, green and blue peaks. Temperature is plotted versus fluorescence signal.

c. Parainfluenza virus 2

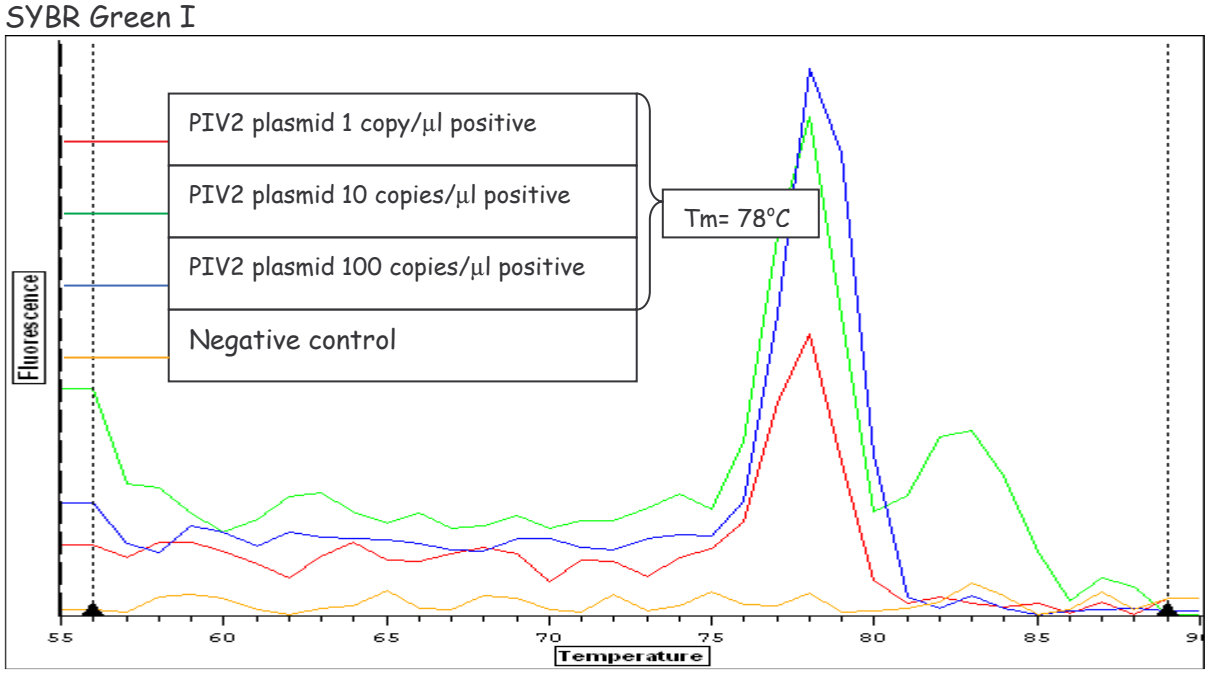

Figure 3.54: Melting curve analysis of PIV2 plasmid serial dilutions demonstrating the sensitivity of the SYBR Green I assay. The signature melting temperature of PIV2 (78°C) is indicated by the sharp red, green and blue peaks. Temperature is plotted versus fluorescence signal.

3.6.Multiplex reactions

To determine whether the presence of multiple organisms or targets could potentially reduce multiplex sensitivity, lowest dilutions of each target were tested. For *L. pneumophila* and CMV, the lowest concentration detected in their singleplex sensitivity reactions was 10 CFU/µl and 10 copies/µl respectively and these were the dilutions used for the multiplex reactions. Below is shown individual traces of fluorescence graphs of each organism multiplexed (Figures 3.55a-3.60c). The real-time PCR end products for multiplex reactions were separated on a 3% agarose gel to confirm that products of the expected sizes were produced (see Appendix C). Despite the anomalous fluorescence curve produced for PIV1 in the multiplex reaction (Figure 3.59a), amplicon separation on 3% agarose gel (Figure C4B) indicated that the desired amplicon was produced.

a. Respiratory syncytial virus and Adenovirus

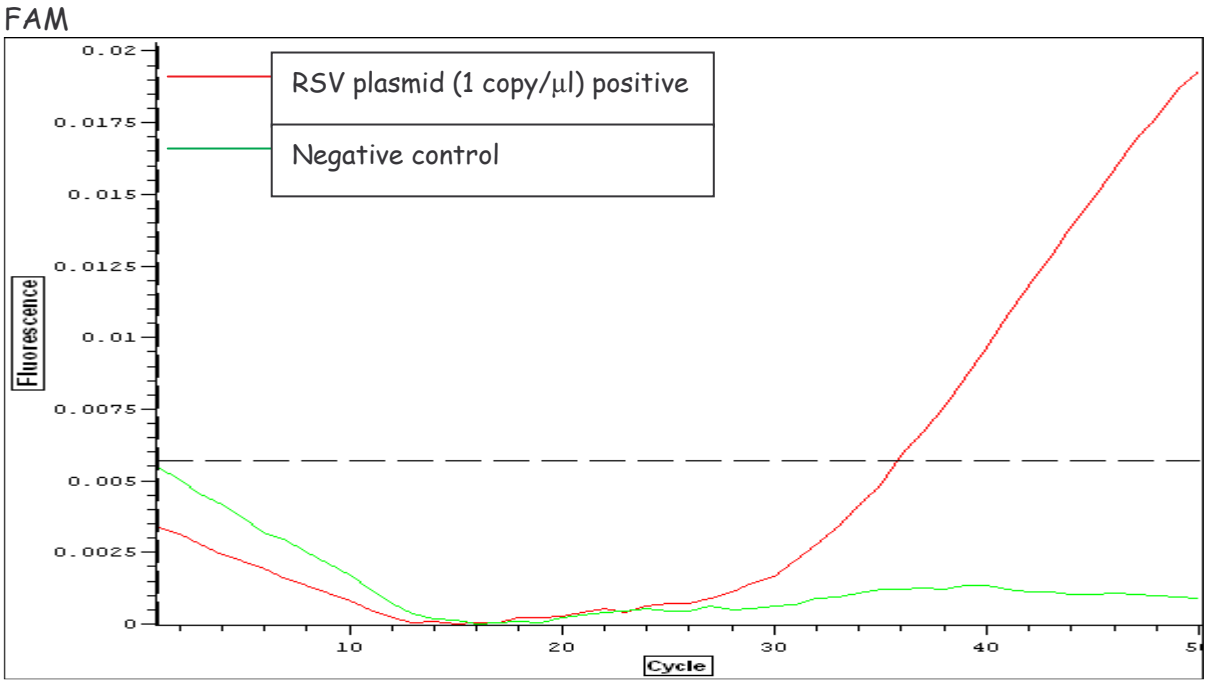

Figure 3.55a: Fluorescence graph of RSV multiplex reaction indicating sensitivity of the TaqMan assay. Change in fluorescence signal is plotted versus cycle number.

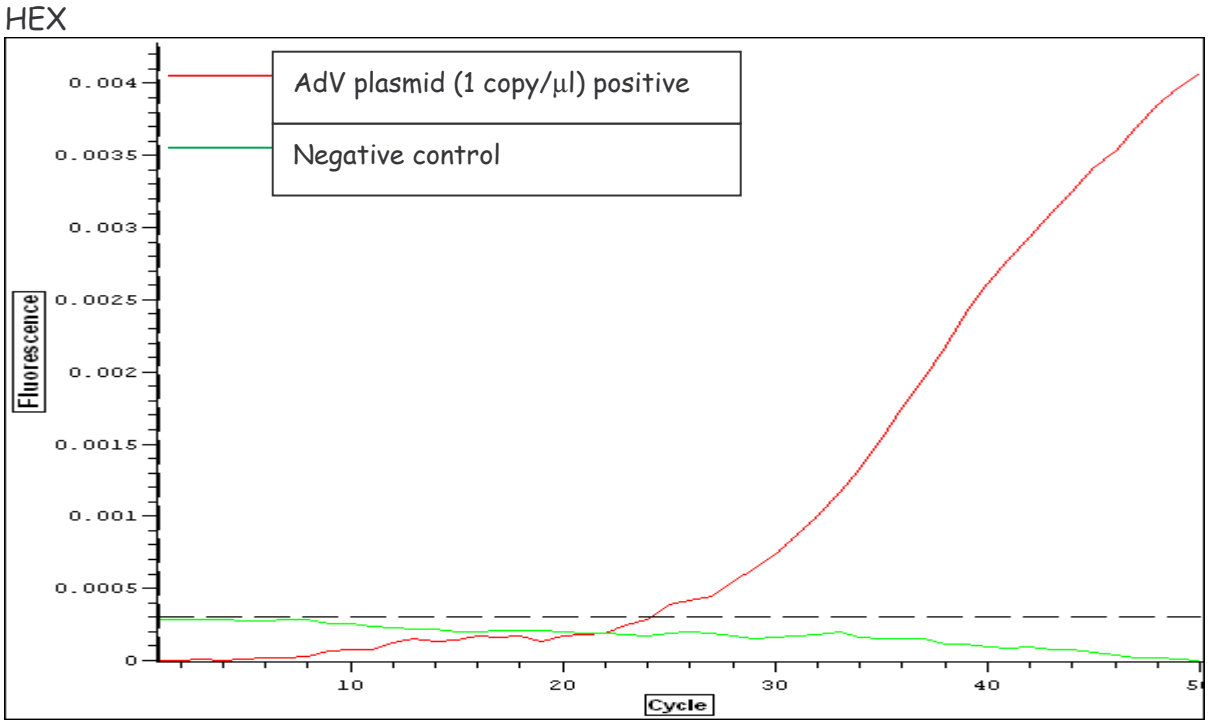

Figure 3.55b: Fluorescence graph of AdV multiplex reaction indicating sensitivity of the TaqMan assay. Change in fluorescence signal is plotted versus cycle number.

b. Epstein-Barr virus and Cytomegalovirus

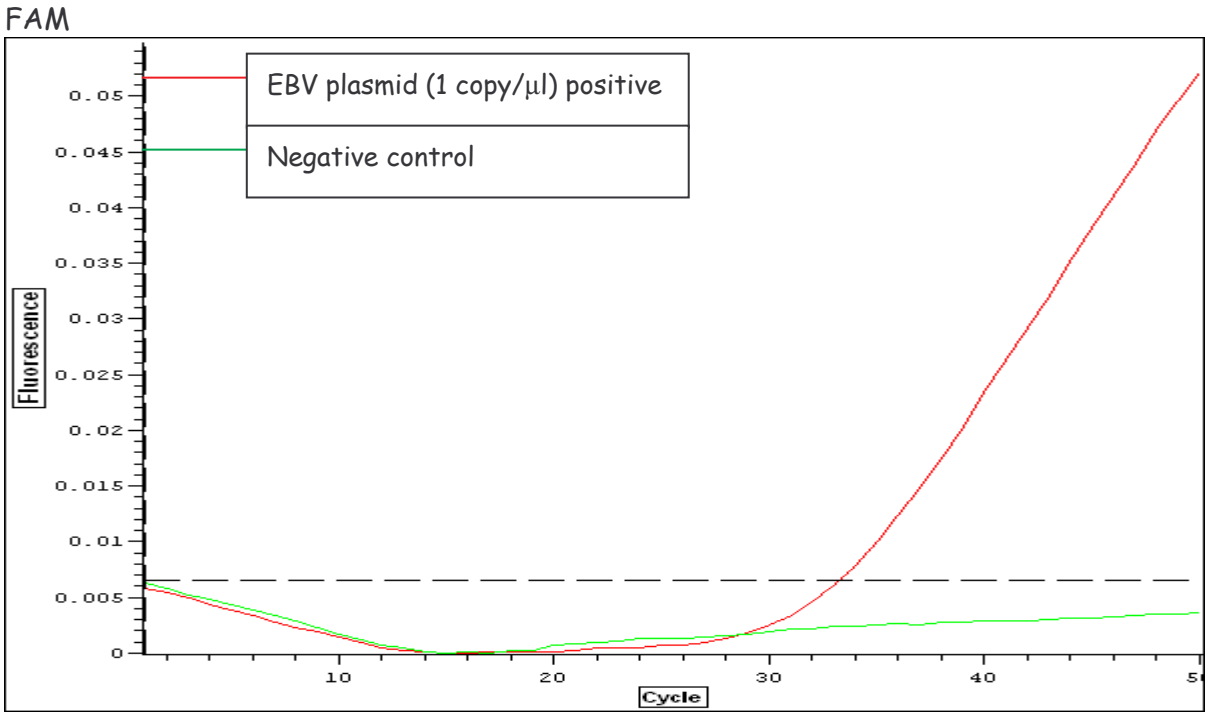

Figure 3.56a: Fluorescence graph of EBV multiplex reaction indicating sensitivity of the TaqMan assay. Change in fluorescence signal is plotted versus cycle number.

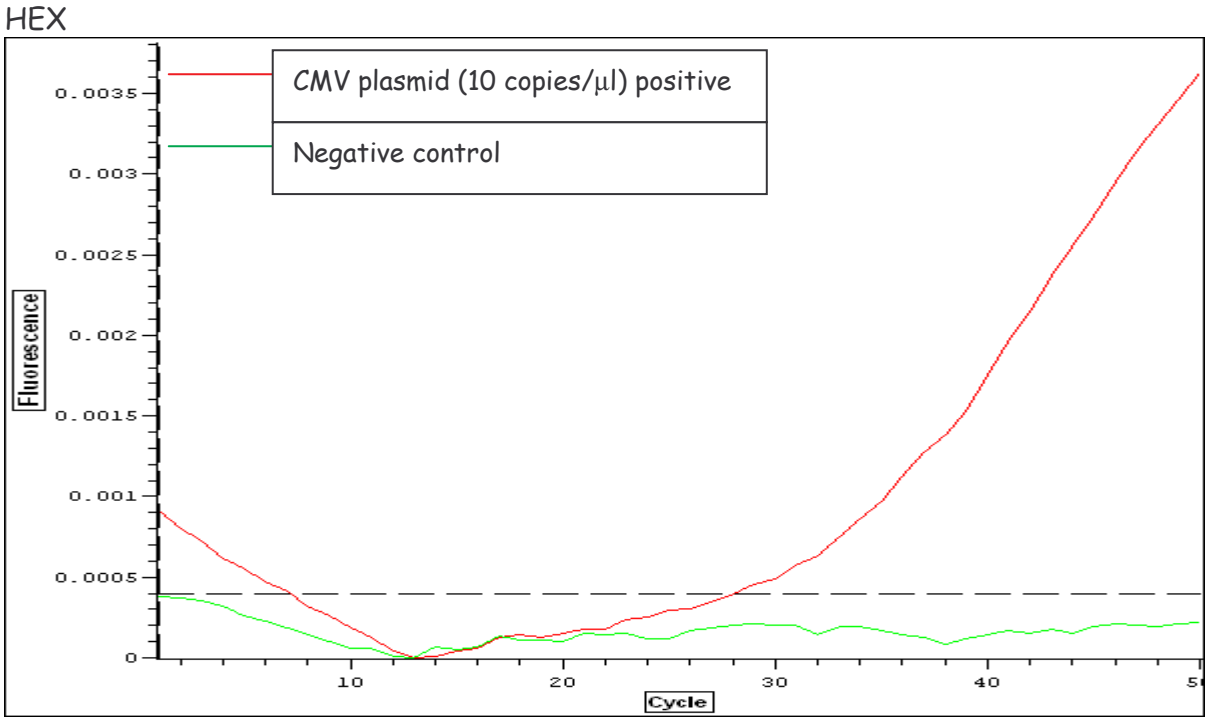

Figure 3.56b: Fluorescence graph of CMV multiplex reaction indicating sensitivity of the TaqMan assay. Change in fluorescence signal is plotted versus cycle number.

c. GAPDH (DNA) and *C. pneumoniae*

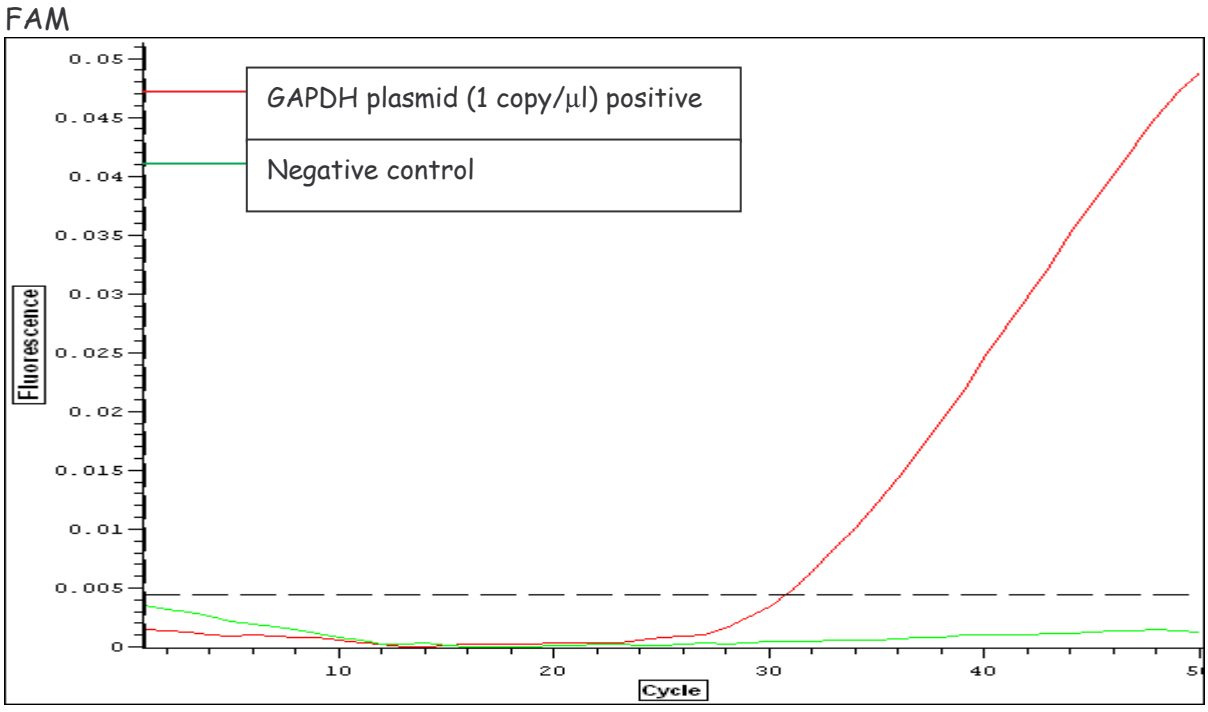

Figure 3.57a: Fluorescence graph of GAPDH (DNA) multiplex reaction indicating sensitivity of the TaqMan assay. Change in fluorescence signal is plotted versus cycle number.

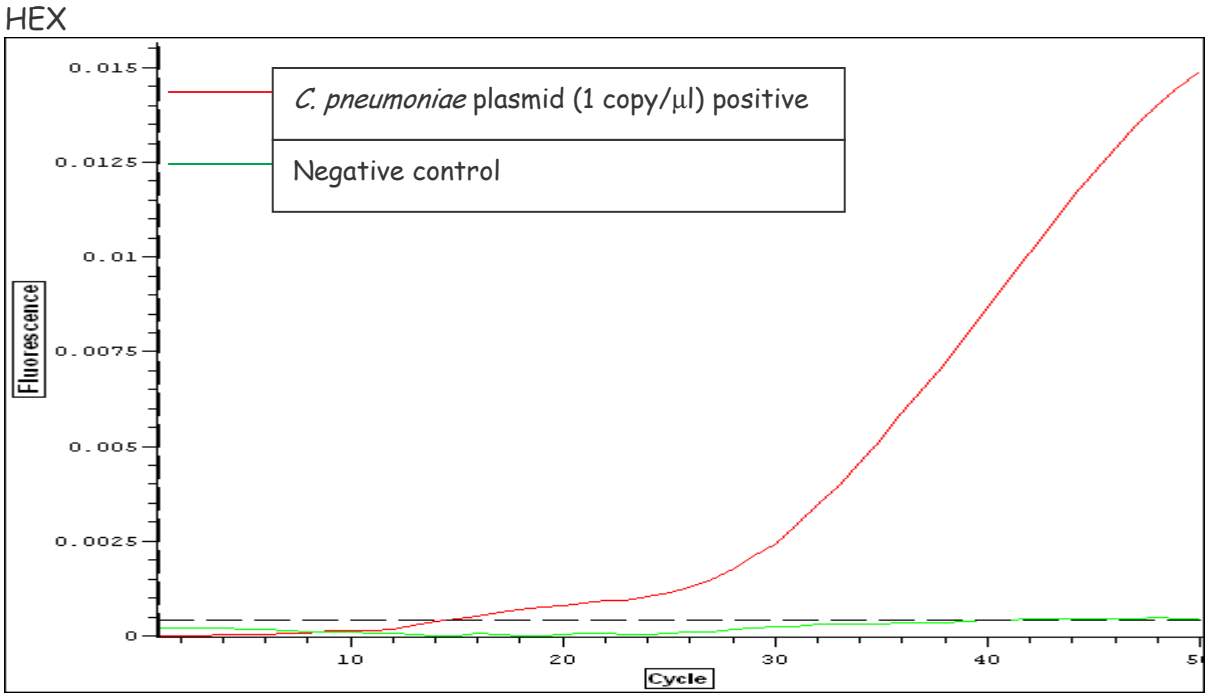

Figure 3.57b: Fluorescence graph of *C. pneumoniae* multiplex reaction indicating sensitivity of the TaqMan assay. Change in fluorescence signal is plotted versus cycle number.

d. *M. pneumoniae* and *L. pneumophila*

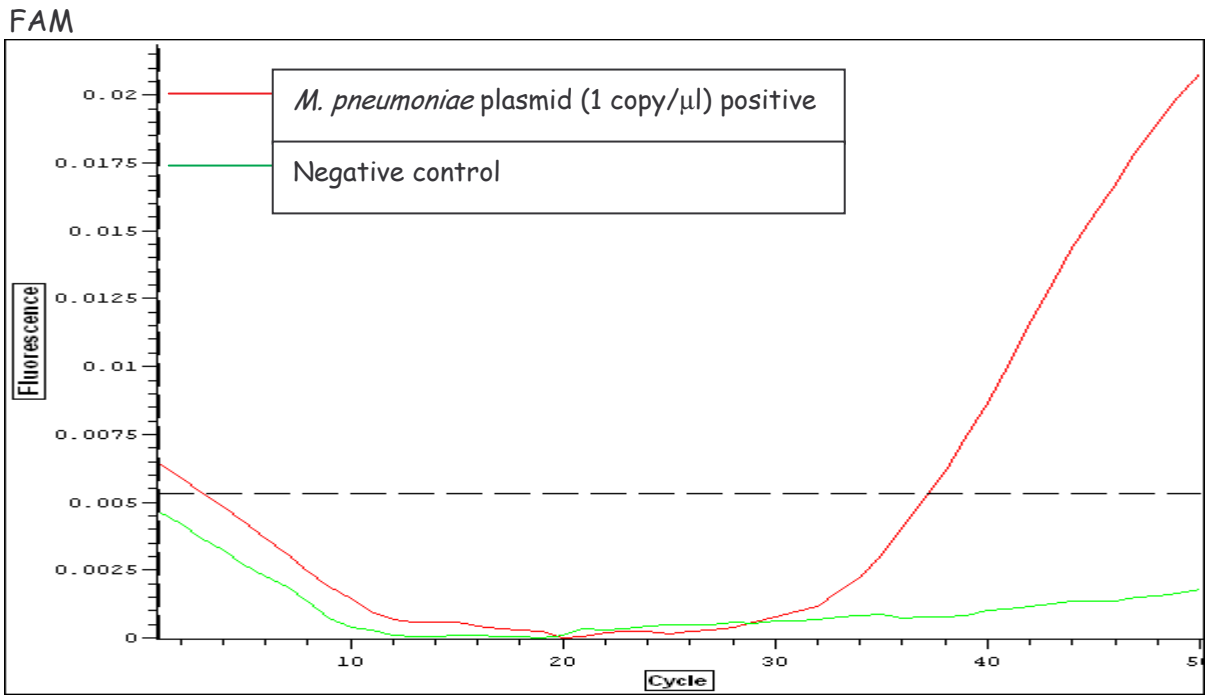

Figure 3.58a: Fluorescence graph of *M. pneumoniae* multiplex reaction indicating sensitivity of the TaqMan assay. Change in fluorescence signal is plotted versus cycle number.

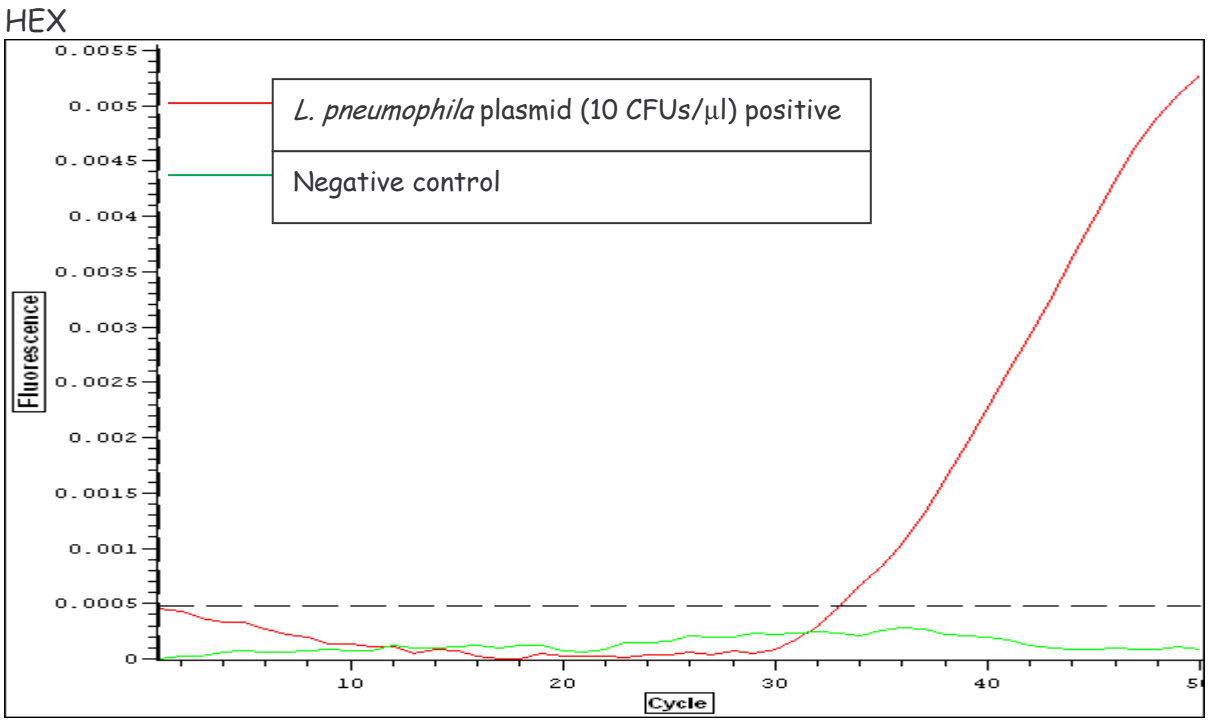

Figure 3.58b: Fluorescence graph of *L. pneumophila* multiplex reaction indicating sensitivity of the TaqMan assay. Change in fluorescence signal is plotted versus cycle number.

e. Parainfluenza virus 1 and Parainfluenza virus 3

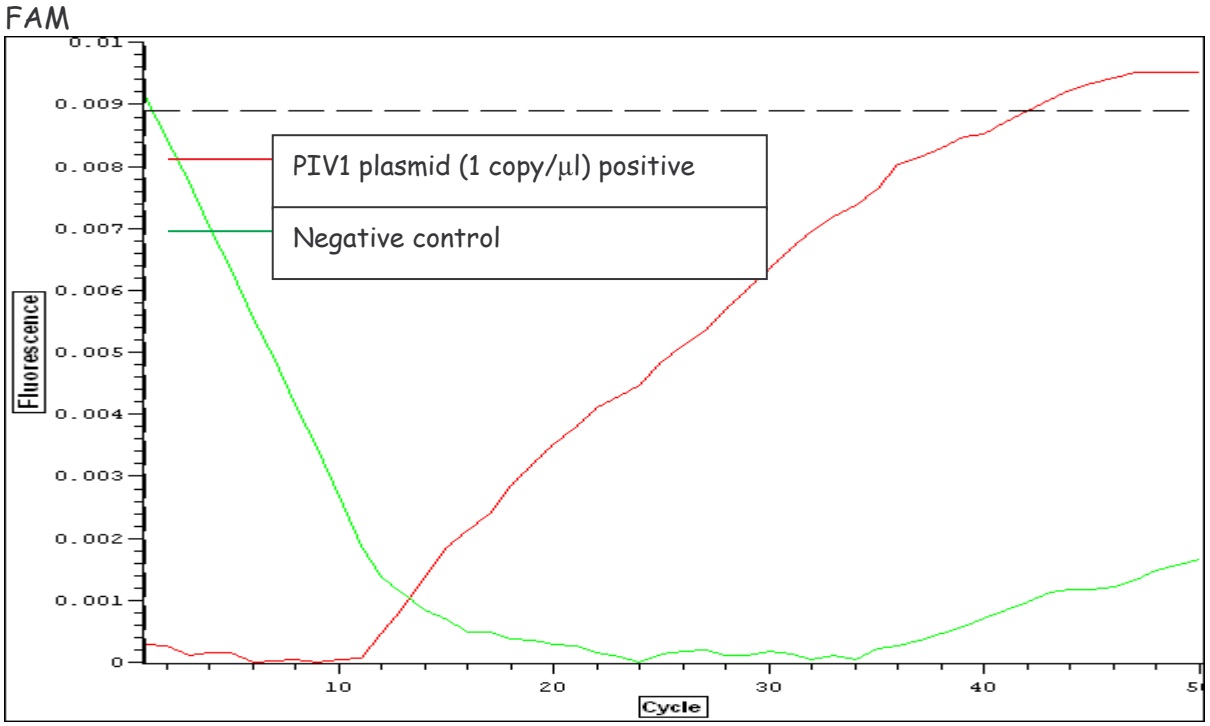

Figure 3.59a: Fluorescence graph of PIV1 multiplex reaction indicating sensitivity of the TaqMan assay. Change in fluorescence signal is plotted versus cycle number.

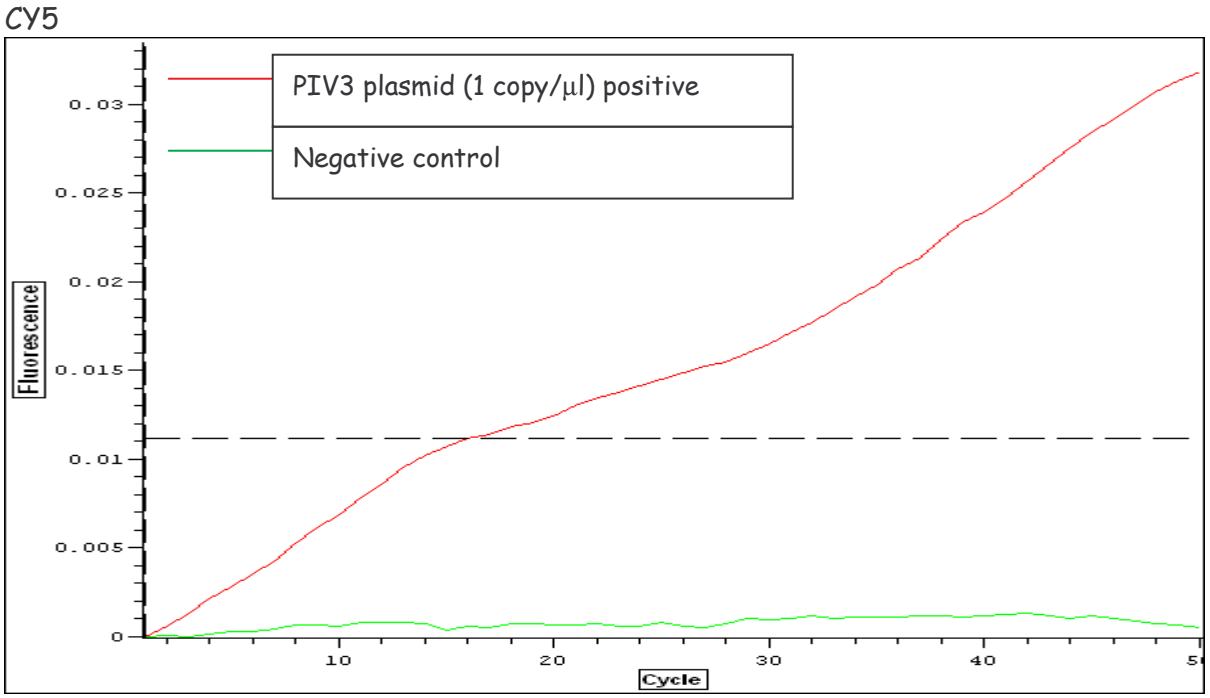

Figure 3.59b: Fluorescence graph of PIV3 multiplex reaction indicating sensitivity of the TaqMan assay. Change in fluorescence signal is plotted versus cycle number.

f. Influenza virus A Influenza virus B and human metapneumovirus

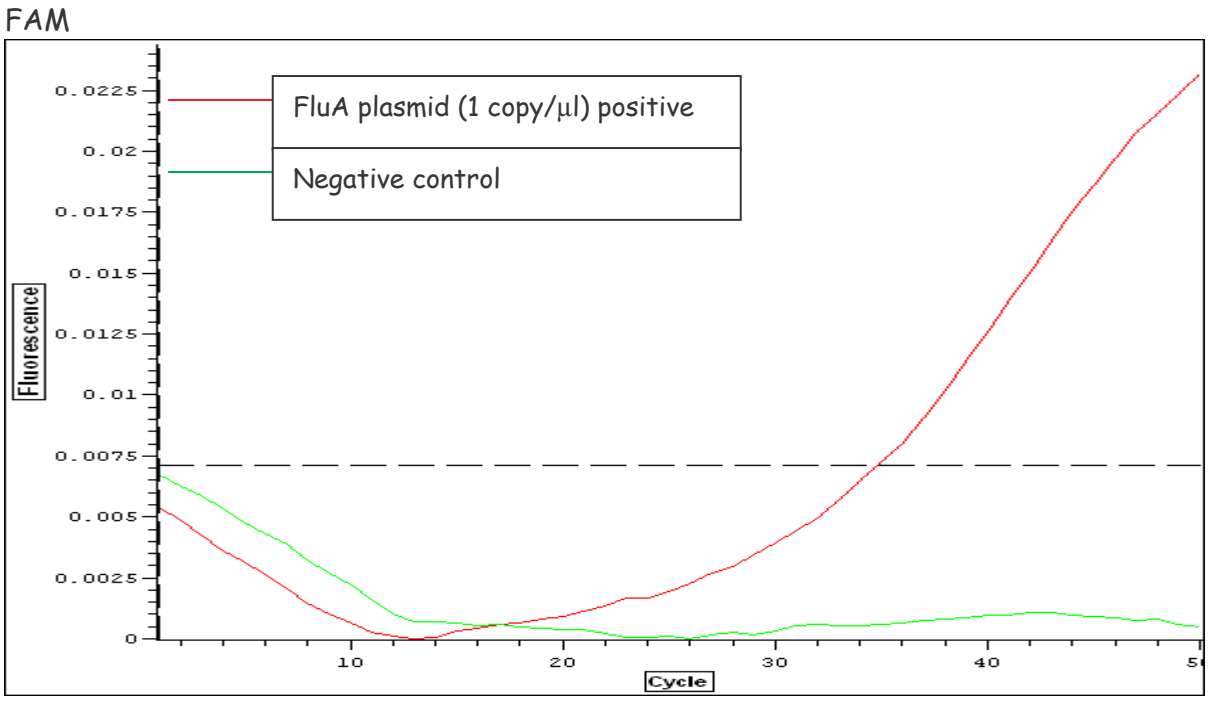

Figure 3.60a: Fluorescence graph of FluA multiplex reaction indicating sensitivity of the TaqMan assay. Change in fluorescence signal is plotted versus cycle number.

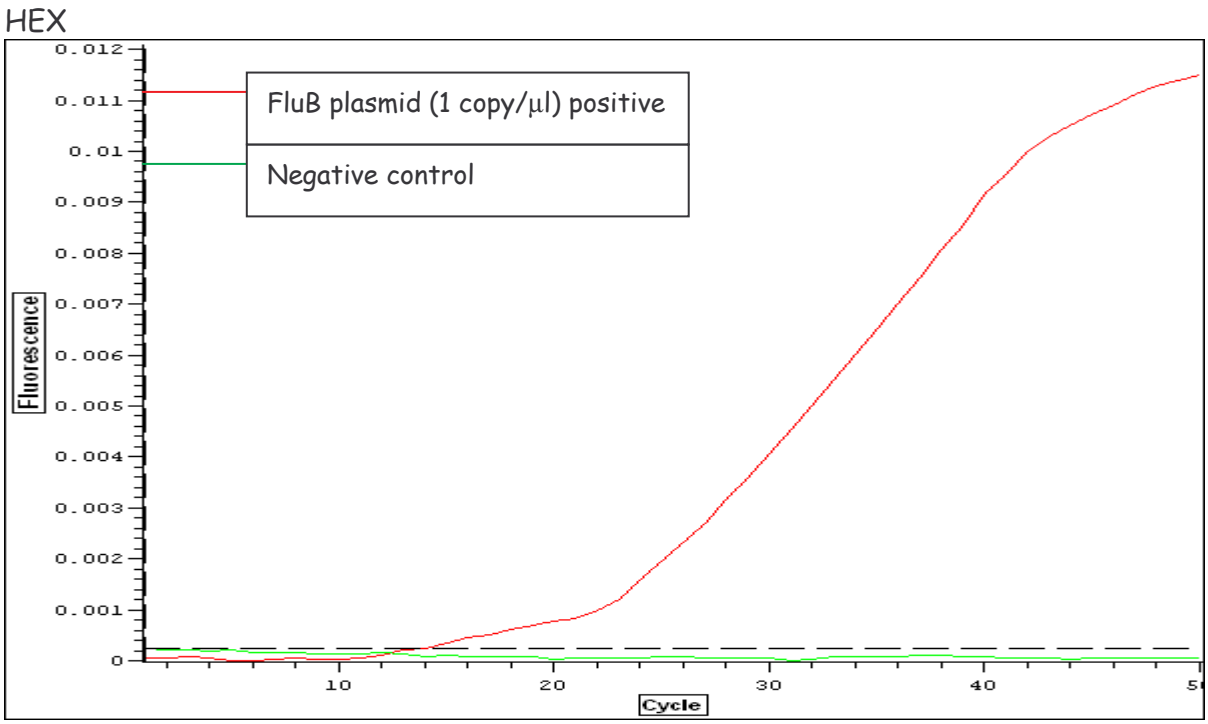

Figure 3.60b: Fluorescence graph of FluB multiplex reaction indicating sensitivity of the TaqMan assay. Change in fluorescence signal is plotted versus cycle number.

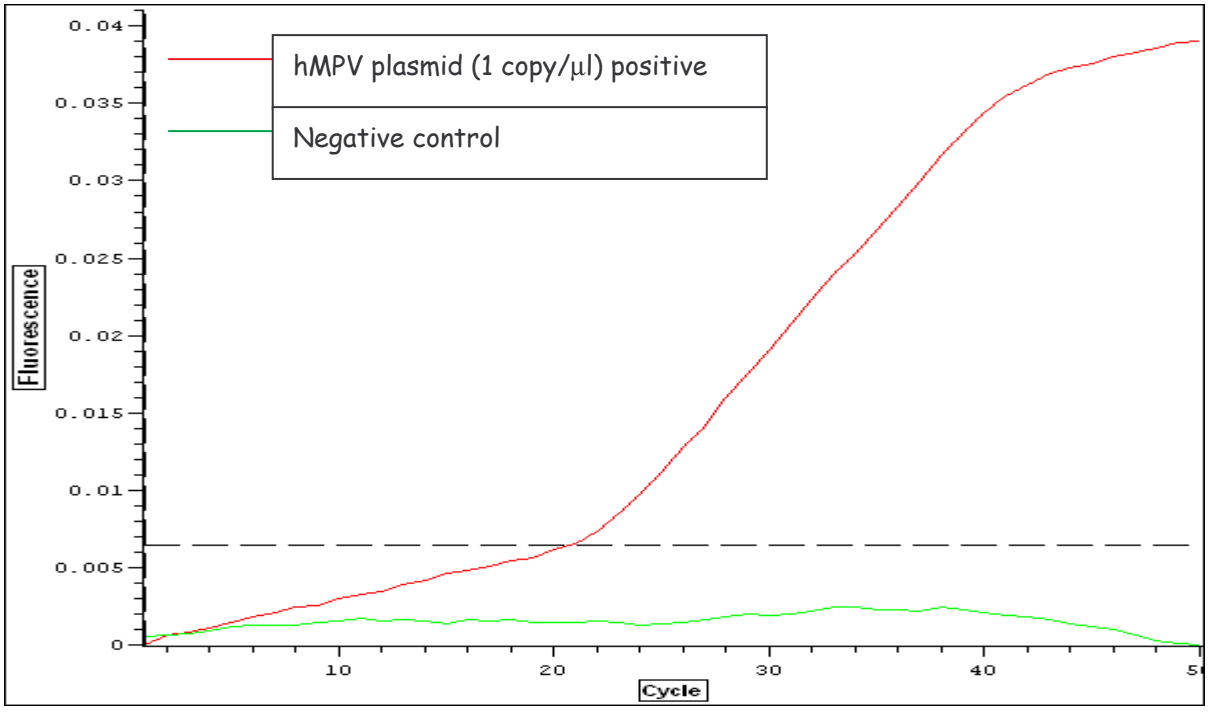

Figure 3.60c: Fluorescence graph of hMPV multiplex reaction indicating sensitivity of the TaqMan assay. Change in fluorescence signal is plotted versus cycle number.

3.7. Summary of sensitivities of real-time PCR assays

All the assays except those of CMV and *L. pneumophila* were able to detect the lowest copy number of 1 copy/µl.

CHAPTER 3D: RESULTS - PATIENT SAMPLES AND SIMULATIONS

The 3 patients enrolled in this study were too few to be a representative of the incidence of CAP locally. However, we still proceeded to use these samples to test both real-time PCR assays as well as the Seeplex detection kits. The detection limits of Seeplex kits are reported by the manufacturer as 10 copies/3µl (3.3 copies/µl). The specificity of the Seeplex® RV5 ACE Screening kit and the Seeplex® Pneumobacter ACE Detection kit was validated with 26 and 23 different respiratory viruses and bacteria respectively by the manufacturer.

Nasopharyngeal swabs and sputum samples were collected from each of the CAP patients enrolled. The simulation of sample collection was performed in duplicate for nasopharyngeal swabs and on 2 different cystic fibrosis patient sputum samples. The duplicates were named simulation 1 and 2. Each of the nasopharyngeal simulation swabs was dipped into a viral culture mixture containing an equal volume of FluA, PIV1, PIV2, RSV and CMV. Other viruses were not included in sample simulation because they were either supplied in the form of RNA or cDNA or no viral culture remained.

Each Seeplex detection kit was supplied with a size marker which displays all the bands corresponding to the amplicons that the kit can detect, including the internal control band. If a specimen showed the same sized fragment as any of the bands displayed by the marker bands, it was considered positive for that organism.

3.8.Pathogen detection using Seeplex kits

3.8.1. Seeplex® Pneumobacter ACE detection kit

The Pneumobacter ACE detection kit is designed to detect the internal control (900bp), *M. pneumoniae* (583bp), *L. pneumophila* (472bp), *S. pneumoniae* (350bp), *H. influenzae* (257bp), *B. pertussis* (200bp), and *C. pneumoniae* (146bp). This kit was used to test sputum samples for respiratory pathogens. An internal control in the form of a DNA plasmid is included in the Pneumobacter ACE Detection kit to identify specimens that contain substances that may interfere with the PCR reaction and to guarantee equivalent amplification of this internal control and the target DNA organisms. The internal control was co-amplified with target DNA from each sample tested. The internal control band was however absent for patient 3 in lane 7 of the gel shown in figure 3.61. Possible reasons for this may have been the presence of high pathogen load and depletion of reagents for the control reaction. A positive and negative control was included in the reaction performed and the 50bp DNA Ladder (Fermentas GMBH, Germany) was used alongside the PB ACE Marker supplied with the kit to ascertain band sizes produced.

All the pathogens used to spike the simulated patient samples that were in the detection panel of the kits were detected. The simulated samples 1 and 2 were spiked with *C. pneumoniae*, *C. psittaci* and a single colony of *L. pneumophila*. These were the only samples that tested positive for *L. pneumophila* (lanes 3 and 4). All CAP patient samples as well as simulated sputum samples from cystic fibrosis patients tested positive for *S. pneumoniae* and *H. influenzae*. The simulated sputum samples were not spiked with either of these bacteria suggesting that the cystic fibrosis patients from whom the sputa were obtained were colonised with them. CAP patient 2 (lane 6) appears not to be infected with *C. pneumoniae* whilst the other 2 CAP patients are.

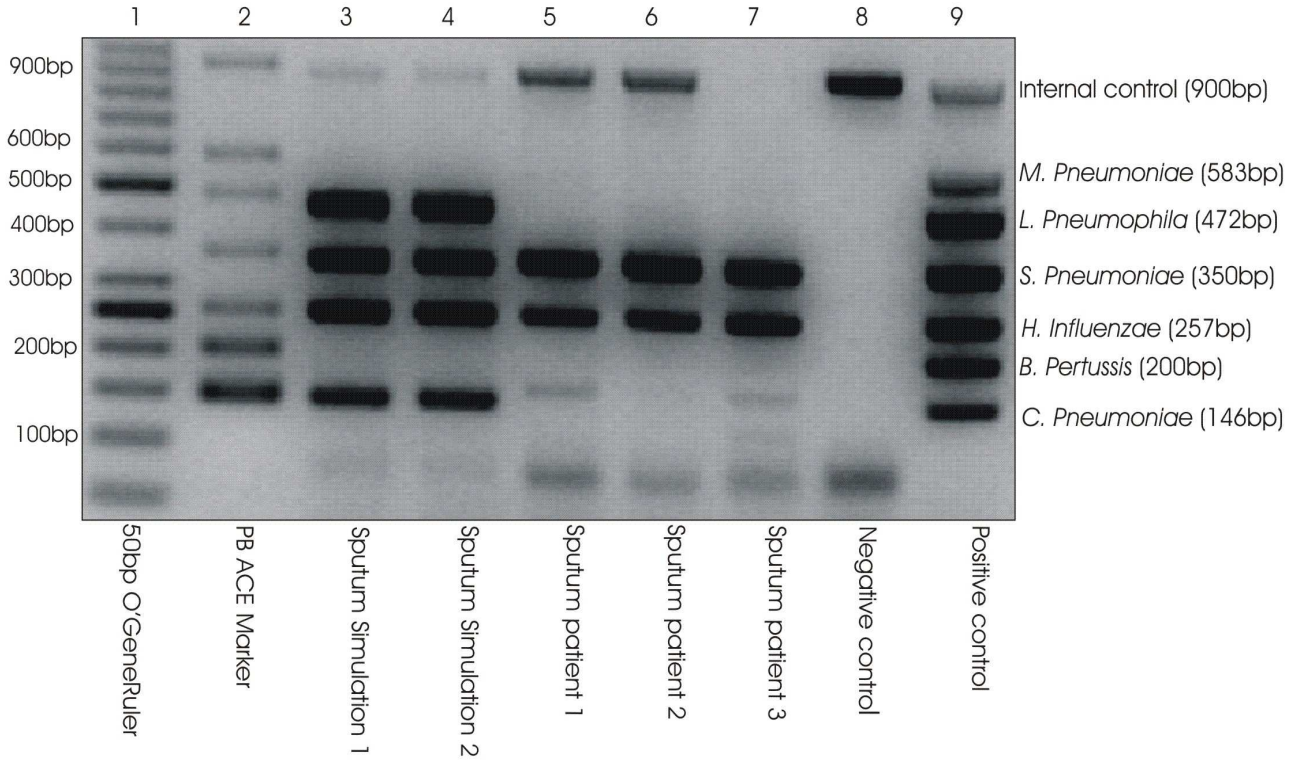

Sputum Samples	Spiked organisms	Detected organisms
Simulation 1	*L. pneumophila*, *C. pneumoniae*, *C. psittaci*	*L. pneumophila*, *C. pneumoniae*, *S. pneumoniae*, *H. influenzae*
Simulation 2	*L. pneumophila*, *C. pneumoniae*, *C. psittaci*	*L. pneumophila*, *C. pneumoniae*, *S. pneumoniae*, *H. influenzae*
Patient 1	N/A	*C. pneumoniae*, *S. pneumoniae*, *H. influenzae*
Patient 2	N/A	*S. pneumoniae*, *H. influenzae*
Patient 3	N/A	*C. pneumoniae*, *S. pneumoniae*, *H. influenzae*

Figure 3.61: PCR results obtained using the Seeplex® Pneumobacter ACE detection kit. Amplicons of sputum samples from CAP patients (lanes 5-7) and simulated sputum samples obtained from cystic fibrosis patients (lane 3 and 4) and spiked with CAP causing pathogens were separated on a 2% agarose gel stained with ethidium bromide.

3.8.2. Seeplex® RV5 ACE detection kit

The RV5 ACE detection kit is specifically designed to detect the internal control (1000bp), Influenza A virus (FluA) (206bp), Influenza B virus (FluB) (709bp), human respiratory syncytial virus (RSV) A or B (273bp), Others 1 (Human adenovirus (AdV), human parainfluenza virus (PIV) 1, 2, and 3, human bocavirus (BoV)) (534bp), Others 2 (human metapneumovirus (hMPV),

human coronavirus (CoV) 229E, NL63, OC43 and HKU1, human rhinovirus (hRV) A and B) (394bp). This kit was used to test nasopharyngeal swabs. The 50bp O'GeneRuler (Fermentas GMBH, Germany) was used in addition to the RV5 ACE Marker that was supplied with the kit to confirm the sizes of the bands produced. The internal control included in the kit was in the form of a DNA plasmid and was used to identify any contaminating substances interfering with the PCR reaction.

All the pathogens used to spike the simulated patient samples that were in the detection panel of the kit were identified. Simulated swabs 1 and 2 (lanes 3 and 4) were spiked with viral culture supernatants of RSV, FluA, PIV1, PIV2 and CMV and tested positive for RSV A or B, FluA and "Others 1" which was either AdV, PIV 1, 2, 3 or BoV (Figure 3.62). The band corresponding to "Others 1" (534bp) in simulation 2 (lane 4) was however very faint. CMV detection is not within the scope of the kit thus its presence could not be confirmed using the kit. Patient 1 (lane 5) tested positive for "Others 2" which was hMPV, hRV or CoV. Patients 2 and 3 tested negative for all viruses within the detection panel of the kit. The internal control was co-amplified with target DNA from each sample tested.

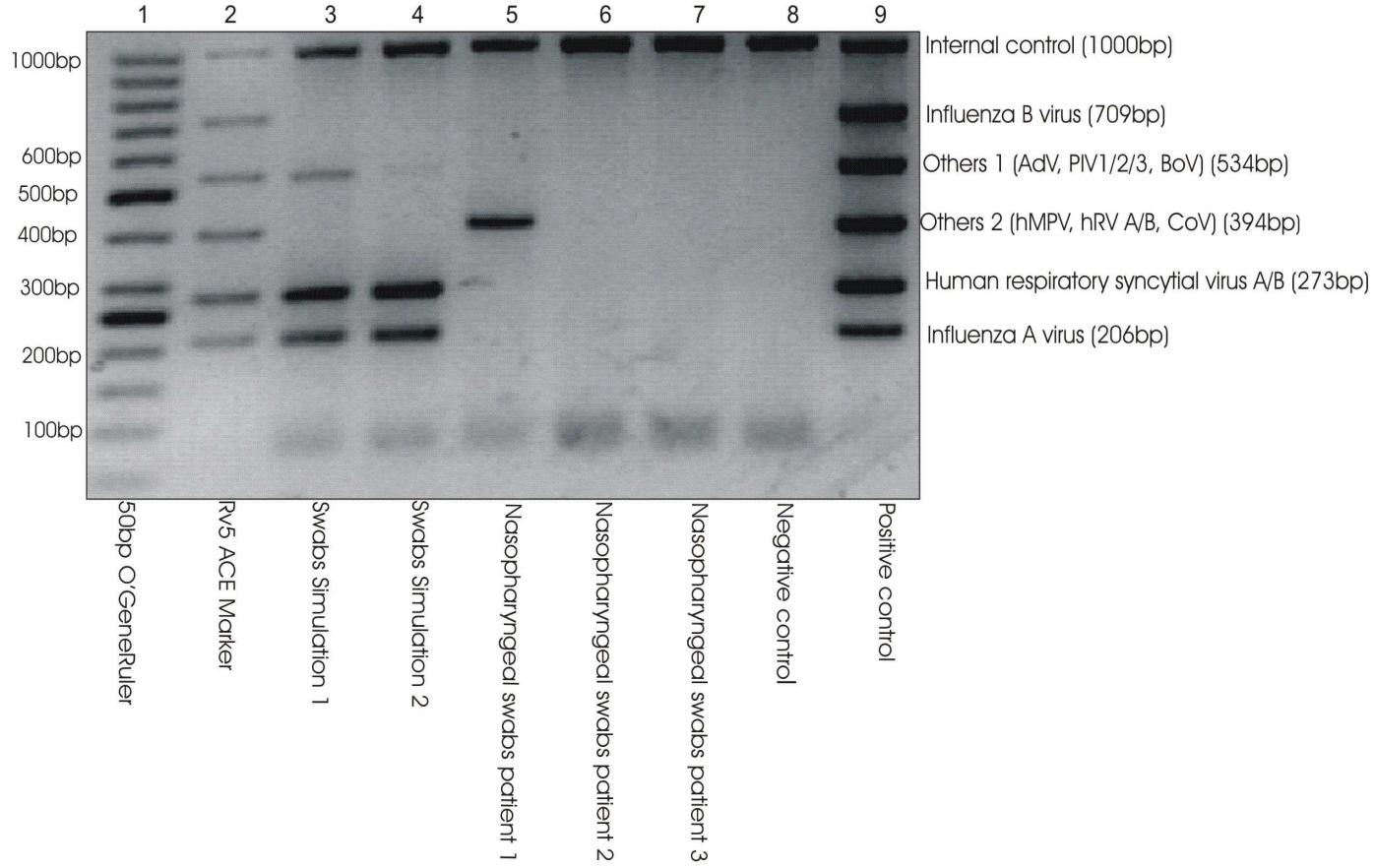

Swab Samples	Spiked organisms	Detected organisms
Simulation 1	FluA, PIV1, PIV2, CMV, RSV	FluA, RSV, Others 1
Simulation 2	FluA, PIV1, PIV2, CMV, RSV	FluA, RSV, Others 1
Patient 1	N/A	Others 2
Patient 2	N/A	[a]--------
Patient 3	N/A	--------

[a]-----: No organism detected

Figure 3.62: PCR results obtained using the Seeplex® RV5 ACE detection kit. Amplicons from nasopharyngeal swabs obtained from CAP patients (lanes 5-7) and simulated nasopharyngeal swabs spiked with CAP causing pathogens (lanes 3 and 4) were separated on a 2% agarose gel stained with ethidium bromide.

3.9. Pathogen detection using real-time PCR assays

Real-time PCR was used to confirm the presence of spiked organisms, to compare the results with the Seeplex® Pneumobacter and RV5 detection kits, as well as to detect other organisms which were not within the detection panel of the Seeplex kits.

3.9.1. Pathogen detection in simulated samples

Only real-time PCR reactions to detect organisms used to spike the sputum samples and nasopharyngeal swabs were performed. All organisms used to spike the sputa and swabs were detected in the real-time PCR assays (see appendix E). Real-time PCR reactions were performed in duplicate on nasopharyngeal swabs and on two different sputum samples collected from cystic fibrosis patients. No large difference in C_t values was observed between any two duplicate samples for each organism tested, showing the reproducibility of the assays (Figures 3.63 and 3.64).

3.9.1.1. Singleplex reactions

Singleplex reactions were performed using SYBR Green I for *C. psittaci* and PIV2 and TaqMan probes were used for *L. pneumophila*, *C. pneumoniae*, GAPDH (DNA), RSV, PIV1, FluA and CMV. Viruses were tested for in simulated nasopharyngeal swabs and bacteria in simulated sputum samples. GAPDH (RNA) was not tested for in simulated nasopharyngeal swabs because these swabs were not obtained from human subjects thus did not contain human cells. GAPDH (DNA) was co-extracted and co-amplified with the spiked bacteria to detect any inhibition present. All real-time PCR end products of singleplex assays were run on 2% agarose gels (see appendix D). No amplicons were detected for the negative controls.

All the viruses used to spike the swabs were detected by real time PCR and the ΔC_t values obtained for the duplicates were in the range of 0.41 (1.53%) and 4.66 (19%) C_t. (Figure 3.63)

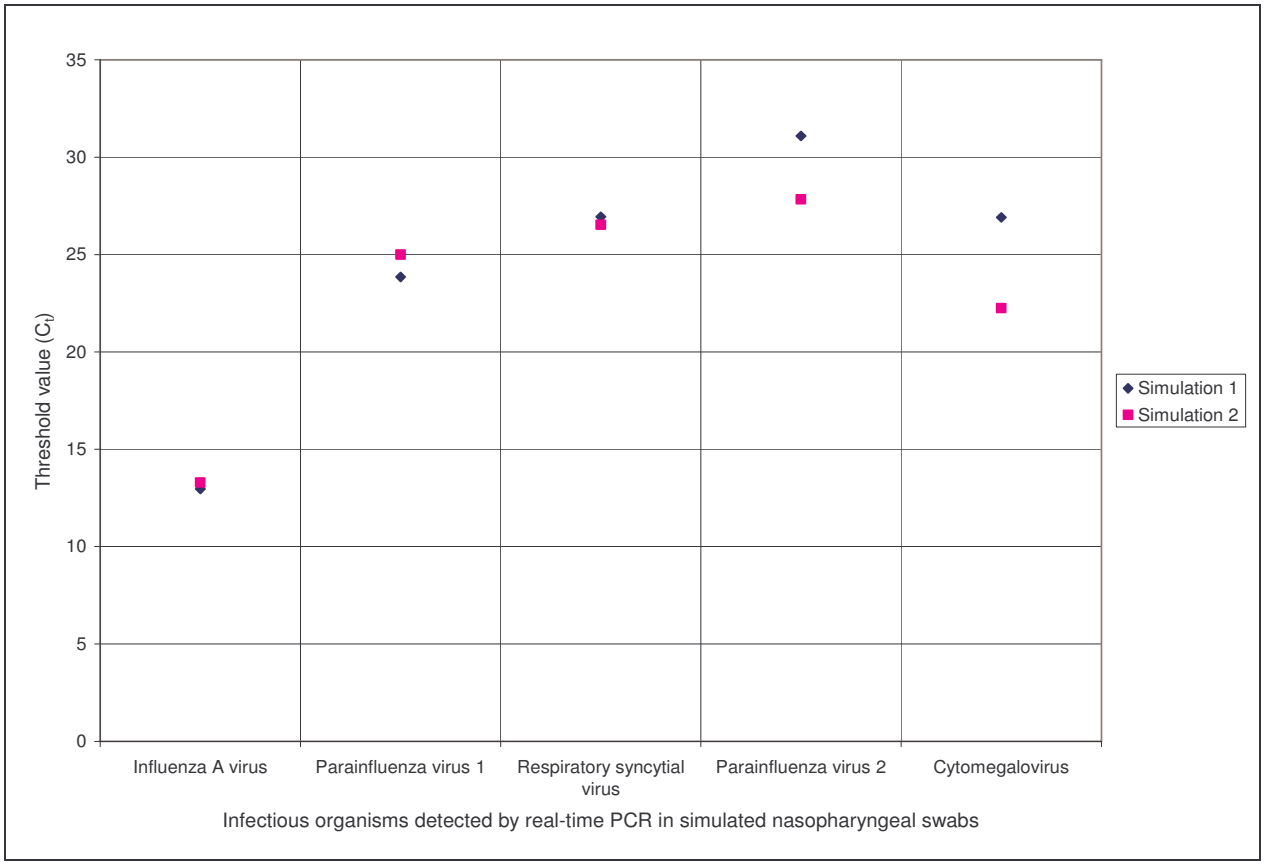

Figure 3.63: Analysis of real-time PCR results obtained from nasopharyngeal swabs spiked with different viral cultures simulating multiple viral infections in a patient

Larger differences in ΔC_t were observed with PIV2 and CMV (11% and 19% respectively) as calculated using the equation: $\frac{C_{t1} - C_{t2}}{(C_{t1} + C_{t2})/2} x100$. The C_t values in simulation 1 for both these organisms were higher. This may have been due to pipetting errors.

All the bacteria used to spike the sputum samples as well as the GAPDH (DNA) internal control were detected by real-time PCR. The range in ΔC_t values of the bacteria in the spiked sputum duplicate samples was from 0.11 (0.004%) to 1.48 (5.7%) C_t (Figure 3.64). This was an

indication of the good reproducibility of the assays performed as no large differences were observed.

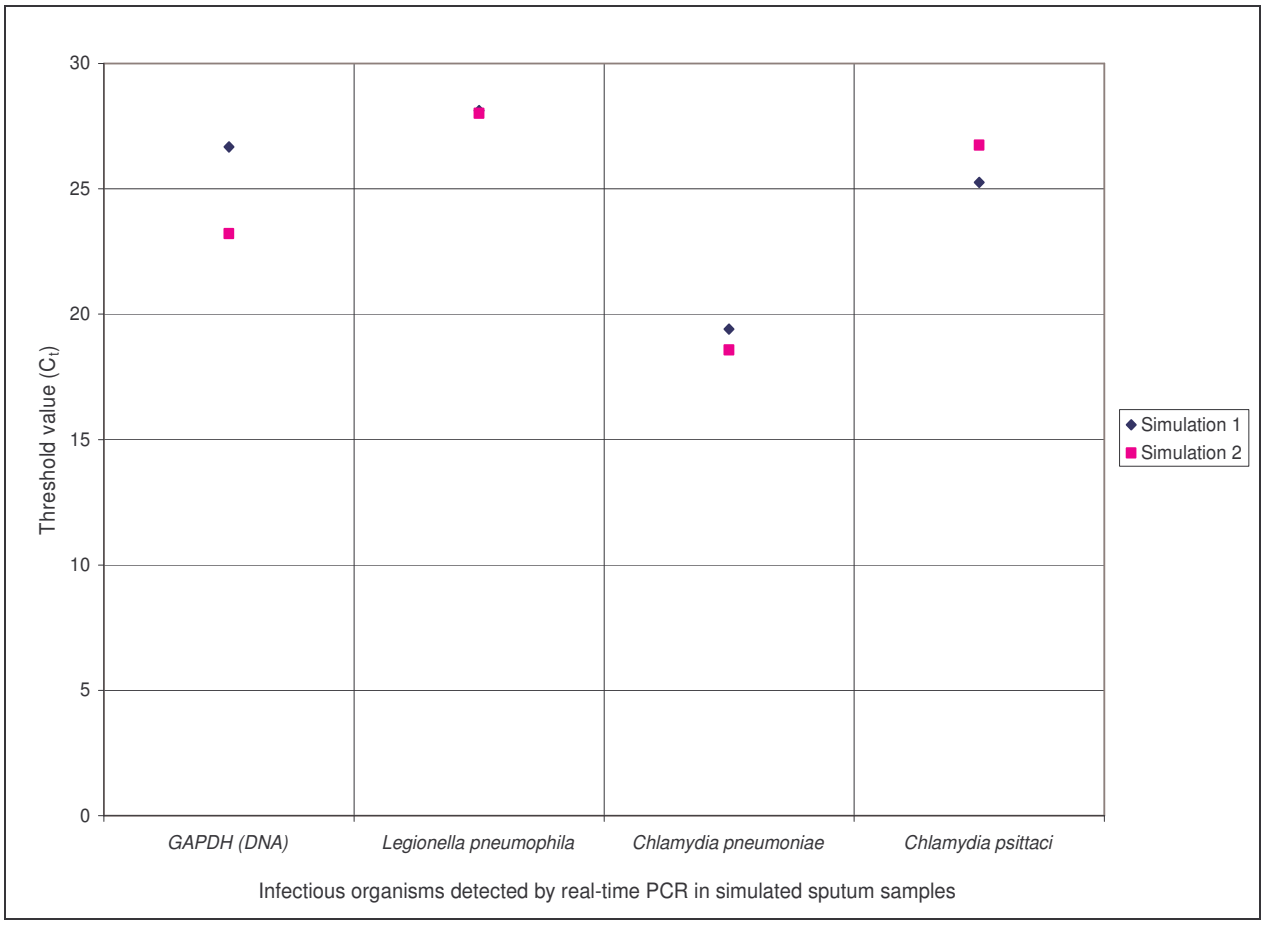

Figure 3.64: Analysis of real-time PCR results obtained from cystic fibrosis patient sputum samples spiked with bacterial cultures of *C. pneumoniae* and *C. psittaci* and a colony of *L. pneumophila* simulating multiple bacterial infections in a patient

The internal control was successfully co-extracted and co-amplified in the reaction resulting in a fixed cycle threshold value. This indicated that DNA extraction was performed adequately without any major interference from inhibitory substances. The difference in GAPDH (DNA) C_t values between simulation 1 and 2 (3.46 C_t) was however higher than the ΔC_t values observed for the bacteria investigated (Figure 3.64). This was to be expected, as the sputum samples would have contained different amounts of epithelial cells.

3.9.1.2. Multiplex reactions

Of all the organisms available to spike sputum and nasopharyngeal swabs for the simulation of patient samples, the only multiplex reaction that could be performed was that of GAPDH (DNA) and *C. pneumoniae*. Real-time PCR end products of the multiplex assay were run on a 3% agarose gel (see appendix D). No amplicons were detected for the negative controls.

3.9.2. Pathogen detection in CAP patient samples

Real-time PCR was used to confirm the presence of organisms detected by the Seeplex Pneumobacter and RV5 detection kits as well as to detect other organisms which were not within the detection panel of the Seeplex detection kits. GAPDH (DNA) and GAPDH (RNA) were used as internal controls for real-time PCR reactions involving DNA and RNA organisms respectively. Real-time PCR reactions were performed in singleplex using SYBR Green I for those organisms that could not be multiplexed and an allowance of $1^{o}C$ was given on the melting temperature of real-time PCR product produced to conclude that it was the desired amplicon since melting temperature can be affected by SYBR Green I concentrations (Giglio *et al.*, 2003). This would allow for any pipetting errors. GAPDH (DNA) was first performed in singleplex using TaqMan probes to ensure the extraction process and real-time PCR reactions were not inhibited before multiplexing it with *C. pneumoniae*. No amplicon was detected in any negative controls. All amplicons of singleplex reactions were separated in 2% agarose gels stained with ethidium bromide (see appendix D) and those from multiplex reactions on 3% agarose gels.

A large amount of non-specific product was produced as evidenced by agarose gel electrophoresis (Figures D13-D19). Both internal controls were amplified for all three patient samples as seen by real-time PCR results. Tables 3.1 and 3.2 give a summary of the comparison between results obtained from Seeplex® Pneumobacter and Seeplex RV5 ACE detection kits

(Figure 3.61 and 3.62 respectively) and real-time PCR assays (appendix E). Results obtained are in agreement for all three detection methods for *L. pneumophila*, *C. pneumoniae*, FluB, hMPV, PIV1, PIV3, AdV and RSV. hMPV was excluded as an organism infecting patient 1 in lane 5 (Figure 3.62) because it was not detected by real-time PCR, leaving human rhinovirus or coronavirus as possible infecting organisms.

C. psittaci, *P. jirovecii*, EBV and CMV cannot be detected by the Seeplex kits thus results were based only on real-time PCR. Fluorescence observed for real-time PCR corresponded with product bands present on the agarose gels: *P. jirovecii* was detected in patients 1 and 2; *C. psittaci* in patients 1 and 3; EBV in all 3 patients and CMV only in patient 3.

Table 3.1: Comparison of results obtained from real-time PCR assays and the Seeplex® Pneumobacter ACE detection kit.

Target organism	Sample source	Real-time PCR result	Seeplex kit result
Mycoplasma pneumoniae	Patient 1	absent	absent
	Patient 2	PRESENT	absent
	Patient 3	PRESENT	absent
Legionella pneumophila	Patient 1	absent	absent
	Patient 2	absent	absent
	Patient 3	absent	absent
Chlamydia pneumoniae	Patient 1	PRESENT	PRESENT
	Patient 2	PRESENT	PRESENT
	Patient 3	PRESENT	PRESENT
Pneumocystis jirovecii	Patient 1	PRESENT	[a]CND
	Patient 2	PRESENT	CND
	Patient 3	absent	CND
Chlamydia psittaci	Patient 1	PRESENT	CND
	Patient 2	absent	CND
	Patient 3	PRESENT	CND
GAPDH (DNA)	Patient 1	PRESENT	PRESENT
	Patient 2	PRESENT	PRESENT
	Patient 3	PRESENT	PRESENT

[a]CND: organism cannot be detected using the Seeplex kit

In some cases such as the detection of PIV2, FluA and *M. pneumoniae*, results did not correspond in both detection methods. Real-time PCR detected PIV2 in patient 2, *M. pneumoniae* in patients 2 and 3 and FluA in patient 3 but Seeplex detection kits were not able to identify them. This may have been due to the greater sensitivity of the real-time PCR assays (1 copy/µl) compared to the Seeplex detection kits (3.3 copies/µl).

Table 3.2: Comparison of results obtained from real-time PCR assays and the Seeplex® RV5 ACE detection kit.

Target organism	Sample source	Real-time PCR result	Seeplex kit result
Influenza A virus	Patient 1	absent	absent
	Patient 2	absent	absent
	Patient 3	PRESENT	absent
Influenza B virus	Patient 1	absent	absent
	Patient 2	absent	absent
	Patient 3	absent	absent
Human metapneumovirus	Patient 1	absent	absent
	Patient 2	absent	absent
	Patient 3	absent	absent
Parainfluenza virus 1	Patient 1	absent	absent
	Patient 2	absent	absent
	Patient 3	absent	absent
Parainfluenza virus 3	Patient 1	absent	absent
	Patient 2	absent	absent
	Patient 3	absent	absent
Adenovirus	Patient 1	absent	absent
	Patient 2	absent	absent
	Patient 3	absent	absent
Respiratory syncytial virus	Patient 1	absent	absent
	Patient 2	absent	absent
	Patient 3	absent	absent
Cytomegalovirus	Patient 1	absent	[b]CND
	Patient 2	absent	CND
	Patient 3	PRESENT	CND
Epstein-Barr virus	Patient 1	PRESENT	CND
	Patient 2	PRESENT	CND
	Patient 3	PRESENT	CND
Parainfluenza virus 2	Patient 1	absent	absent
	Patient 2	PRESENT	absent
	Patient 3	absent	absent
GAPDH (RNA)	Patient 1	PRESENT	PRESENT
	Patient 2	PRESENT	PRESENT
	Patient 3	PRESENT	PRESENT

[b]CND: organism cannot be detected using the Seeplex kit

3.10. Pathogen detection using microbiological methods

Microbiological methods were used to detect organisms present in sputum samples of the 3 CAP patients and were performed by the microbiological laboratory at Charlotte Maxeke Johannesburg Hospital. Patients 2 and 3 were blood culture negative and their sputum samples tested positive for *S. pneumoniae* and negative for *H. influenzae*. *H. influenzae* may not have been detected in these patients due to the low quality of sputum collected indicated by the negative Bartlett score obtained (-1). Patient 1 tested positive for *S. pneumoniae* in blood and patient 3 for *Staphylococcus aureus*.

In summary, all three CAP patients investigated in this study had viral and bacterial co-infections and these are outlined in table 3.3. In addition, patients 2 and 3 were infected with *P. jirovecii.* The ability of real-time PCR assays used in this study to detect all these organisms demonstrates that it could be used for surveillance and prevalence studies.

Table 3.3: Diagnosis of patients 1, 2 and 3. Real-time PCR and Seeplex® Pneumobacter and RV5 ACE detection kits were used in parallel to detect organisms infecting these patients.

Subject	**Infecting organisms**
Patient 1	EBV, *M. pneumoniae*, *C. pneumoniae*, *P. jirovecii*, *C. psittaci*, *S. pneumoniae*, *H. influenzae*, Others 2 (RV or CoV)
Patient 2	EBV, PIV2, *M. pneumoniae*, *C. pneumoniae*, *P. jirovecii*, *S. pneumoniae*, *H. influenzae*
Patient 3	FluA, CMV, EBV, *C. pneumoniae*, *C. psittaci*, *S. pneumoniae*, *S. aureus*, *H. influenzae*

CHAPTER 4: DISCUSSION

A wide range of organisms are responsible for causing community-acquired pneumonia. At present, many of these remain unidentified, which may be due to infrequent test requests, the lack of sensitivity of the detection methods employed, agents as yet undescribed, presence of viral inhibitors, low copy number in the clinical sample, and poor specimen collection and handling (Henrickson, 2004). Before implementing a molecular technique for diagnostic or surveillance purposes, several issues must be addressed to ascertain that the method is suitable: which clinical specimens are to be tested; what are the target organisms; will this technique be sensitive and specific enough; is it fast enough, simple enough and is it of clinical relevance.

The first aim of this study was to establish a DNA extraction method for isolation of both DNA and RNA from patient sputa and nasopharyngeal swabs that permits downstream PCR analysis. Sputum samples and nasopharyngeal swabs were to be obtained from TB negative CAP patients. Sputum samples were to be tested for non-viral agents of CAP (*M. pneumoniae*, *C. pneumoniae, C. psittaci, P. jirovecii* and *L. pneumophila*) and nasopharyngeal swabs for viral agents of CAP (PIV1, 2 and 3, AdV, RSV, FluA and B, CMV, hMPV and EBV).

4.1. NucliSens miniMAG System (miniMag) for nucleic acid extraction

Three patient samples were collected, which were too few to be representative of CAP locally. Therefore, in addition to these patient samples, simulations of 2 nasopharyngeal swabs and 2 sputum samples was performed to evaluate the test methods. The miniMag was used to extract nucleic acid from all samples. The main concern was to effectively extract nucleic acid from the

samples and to eliminate polymerase enzyme inhibitors, especially in sputum samples, as they have a direct influence on the result of amplification.

The miniMag procedure is based on the use of magnetic particles, consisting mainly of iron oxide particles (Fe_3O_4) (Saiyed *et al.*, 2003) in combination with silica. It represents a universal, highly flexible extraction instrument in which (a) different sample input and volumes within the same run are possible, (b) up to 12 samples can be processed in parallel, (c) DNA and RNA extraction can be performed within the same run and in the same tube, (d) the nucleic acid extract can be used for both DNA and cDNA amplification. The silica specifically binds to the nucleic acids while contaminating substances or PCR inhibitors that may be present in the sample are effectively removed. This makes this method ideal for use with human specimens, especially sputum samples, which usually contain a large amount of inhibitors and contaminants that may inhibit downstream applications.

Tang and colleagues (Tang *et al.*, 2005) performed a comparative validation on three nucleic acid extraction systems on urine specimens. Two of them were manual while the other one was the semi-automated miniMag used in this study. They observed that the miniMag produced the highest quality of nucleic acids and had the best precision amongst the three extraction systems despite it requiring significantly more hands-on time (45 min).

In our study, GAPDH (DNA) and GAPDH (RNA) were amplified by real-time PCR in all patient samples suggesting that minimal inhibition was experienced. All organisms used to spike the sample simulations were detected by both real-time PCR and Seeplex detection kits.

The results suggest that nucleic acid extraction using the miniMag was successful. The miniMag was user-friendly and had a hands-on-time of approximately 50 min.

The second aim of the study was to establish molecular methods for the rapid, qualitative detection of all the organisms investigated.

4.2.Molecular methods

4.2.1. Real-time PCR assays

Six multiplex reactions were successfully developed to simultaneously detect 12 organisms and the internal control GAPDH (DNA) using TaqMan probes. These multiplex reactions were grouped as follows: (i) Influenza A, Influenza B and hMPV; (ii) PIV1 and PIV3; (iii) EBV and CMV; (iv) AdV and RSV; (v) *M. pneumoniae* and *L. pneumophila*; and (vi) *C. pneumoniae* and GAPDH (DNA). *C. psittaci, P. jirovecii*, PIV2 and GAPDH (RNA) were detected in singleplex using SYBR Green I as they could not be included into the multiplex reactions and SYBR Green I was the more cost-effective option. All the organisms incorporated into the multiplex reactions were at first detected in singleplex using SYBR Green I to ensure the primers and reaction conditions worked adequately, and then with TaqMan probes individually before being multiplexed

4.2.2. Seeplex detection kits

Two Seeplex detection kits were also evaluated for the detection of respiratory pathogens using patient samples and simulations. The Seeplex® Pneumobacter ACE detection kit was used for the detection of *M. pneumoniae*, *L. pneumophila*, *S. pneumoniae, H. influenzae*, and *C. pneumoniae*, while the Seeplex® RV5 ACE detection kit was used to detect Influenza A virus,

Influenza B virus, human respiratory syncytial virus A or B, Others 1 (human adenovirus, human parainfluenza virus 1, 2, and 3, human bocavirus), Others 2 (human metapneumovirus, human coronavirus 229E, NL63, OC43 and HKU1, human rhinovirus A and B and an internal control. The Seeplex kits successfully detected all organisms used to spike sputum samples and nasopharyngeal swabs. Co-infections in all patients were observed.

4.3.Sensitivity of real-time PCR assays using TaqMan probes

Plasmids containing target DNA were constructed and used in assays to enable detection limit analysis. Results obtained showed that the assays were sufficiently sensitive, with the majority detecting 1 copy/µl. The CMV and *L. pneumophila* assays were the only ones with a detection limit of 10 copies. Multiplex reactions reflected the same sensitivities as the singleplex reactions, indicating that two or more organisms at low concentrations in the same sample could be detected in the multiplex assays. This suggests that these assays are sensitive enough to be applied in a clinical setting for the detection of CAP and maybe of use diagnostically.

Using plasmids coding for the target sequence has the advantage that once constructed, they can be prepared in large amounts and can be stored without significant degradation for long periods at -20°C. Long-term storage of transformed *E. coli* also permits continuity and consistency of the positive control DNA for future assays.

4.4.Fluorescence intensity is dependent on the fluorescence dye attached to the probe

Fluorescence intensity was observed to be higher in the majority of reactions involving probes with the FAM, CY5 and CY5.5 dyes compared to those coupled to HEX. FAM is a popular choice for use in singleplex reactions as a fluorophore since it has a very strong fluorescence

signal. Some researchers believe that this makes FAM unsuitable for multiplexing (Cirino *et al.*, 2007). However, in our experience, FAM was shown to have strong fluorescence, but did not mask the fluorescence emitted by other dyes during multiplexing. Mackay (2007) states that fluorescence is generally lower in multiplex reactions than it is in singleplex reactions due to limiting primer and probe concentrations when multiplexing. This effect was not observed in this study with the majority of multiplex reactions exhibiting higher fluorescence than singleplex reactions. This observation may be due to the different master mixes used in singleplex and multiplex reactions. The iQ^{TM} Multiplex Powermix (Bio-Rad) used for multiplex reactions has been optimized to deliver maximum PCR efficiency, sensitivity and precision in multiplex reactions as compared to singleplex probe assays.

4.5. TaqMan probes for real-time PCR assays

When the TaqMan probes were first reconstituted, C_t values observed were lower than those generated when using SYBR Green I. After approximately 6 months, fluorescence levels of the TaqMan probes were observed to have decreased drastically. The most marked instance was FluB which initially had a maximum fluorescence level of 0.55 and 6 months later, had a fluorescence of 0.01 even though the same reagents and reaction conditions were used. This is believed to be a result of probe degradation over time. Probes were supplied in the lyophilized form and reconstituted in Tris-EDTA (TE) buffer. Probe stock solutions were stored at -20°C and only thawed once to make up fresh working solution when fluorescence was observed to decrease. The probe working solutions were stored in the fridge (4°C) and in the dark (wrapped in foil and in a black bag) as recommended by TIB MolBiol. The same batch of probes, manufactured at the same time and stored by the manufacturer, was requested from TIB MolBiol. These too produced a similarly low level of fluorescence (results not shown).

Although TaqMan probes have been reported to have a longer shelf-life at -20°C, and it may have been preferable to aliquot the working solution and store it at that temperature, the observed decrease in fluorescence using the same batch of probes stored by TIB MolBiol suggests that probe degradation occurs primarily due to time related decay. Primer degradation was ruled out as a cause of reduced fluorescence levels since they were evaluated with SYBR Green I and fluorescence was observed to be high. Probe degradation was furthermore reflected in some of the real-time PCR amplification curves (PIV1, PIV3, CMV and hMPV) that did not display a typical exponential curve. This is also reported to have been observed in other laboratories (personal communication Jasmin Dehnhard, TIB Molbiol).

The process of probe degradation over time is a problem, as evidenced by the lower fluorescence of the TaqMan assays. Two degradation scenarios can be envisioned - cleavage of the oligonucleotide, or photobleaching of the fluorescent dye. In the former, the fluorophore is separated from the quencher resulting in an increase in fluorescence because the fluorophore is no longer quenched. This fluorescence is however not evident from the amplification curves generated by the Chromo4 since the baseline fluorescence is subtracted automatically in each well before increases in fluorescence are measured. In the latter, the fluorophore is bleached over time resulting in lower fluorescence. The outcome in both cases would be similar – a lowered maximum fluorescence.

Efficiency of PCR amplification can be influenced by several parameters: magnesium and salt concentrations, reaction conditions (i.e. time and temperature), PCR target size and composition, primer and probe sequences, and sample purity (Heid *et al.*, 1996). In the case of real-time PCR, the binding of fluorescent dyes and labelled probes to the DNA results in a

signal that is used as a surrogate indicator of PCR efficiency. The low PCR efficiencies generated for reactions involving TaqMan probes were unexpected and are not believed to be a true reflection of the actual amplification efficiencies. This is qualitatively supported by the strong positive signals obtained by standard gel electrophoresis of PCR products in cases where low fluorescence and efficiencies were observed. It is unclear what effect the suspected probe degradation would have on the efficiency, since the kinetics of probe binding and hydrolysis should be unchanged, although the fluorescence intensity observed would be lower.

4.6.Multiplex real-time PCR reactions

Although the majority of primers and probes used in 4 out of 6 multiplex reactions were adopted from literature, the format in which the organisms were grouped to be multiplexed in 3 out of the 4 reactions was novel. The primer and probe sequences of the multiplex groups (i) *M. pneumoniae* and *L. pneumophila*, and (ii) *C. pneumoniae* and GAPDH (DNA), were designed in this study using the Beacon Designer software program (Biosoft International). The multiplex reactions of (i) FluA, FluB and hMPV, (ii) PIV1 and PIV3 and (iii) AdV and RSV were performed using primers and probes adopted from literature, but grouped in a different manner from the publications from which they were taken. Even with these multiplex reactions not being performed as per the original publication, the desired amplicons were still produced and the multiplex reactions were sensitive. Up to 3 probe and primer combinations per organism were evaluated for the following multiplex groups: FluA, FluB and hMPV and PIV1 and PIV3, and 2 combinations for *L. pneumophila* and *M. pneumoniae* and *C. pneumoniae* and GAPDH (DNA) before a grouping that functioned well and could be multiplexed was obtained. The most complex multiplex combination was the FluA, FluB and hMPV multiplex reaction, which despite having a range of primers, probes and targets in the same reaction tube, still successfully

amplified all 3 targets at a detection limit of 1 copy/µl. Regardless of the decrease in fluorescence that was observed over time in the TaqMan based reactions, our assays proved to be capable of detecting diverse organisms without a dramatic reduction in sensitivity.

4.7.Bacterial and viral detection on patient samples and simulations

Since kit based methods for the CAP study were found to be prohibitively expensive, in-house real-time PCR assays were developed. The more reasonably priced conventional PCR kits from Seegene were only launched in the second-half of 2008.

For the detection of respiratory agents infecting patients 1, 2 and 3, real-time PCR was used in parallel with the Seeplex® Pneumobacter ACE detection kit and the Seeplex® RV5 ACE detection kit. These detection methods were also used to confirm the presence of organisms used to spike the simulated patient samples as well as to identify any other organisms that may have been present. The reagent cost for singleplex real-time PCR is R197.14 whilst multiplex reactions cost approximately R95.61 per organism per reaction for both 2 target and 3 target specific reactions. Multiplex reactions are cheaper, have reduced handling time and occupy less space in the thermocycler as compared to singleplex reactions, and therefore were the option of choice. Seeplex® Pneumobacter (6 organisms) and the Seeplex® RV5 (3 organisms and "Others 1" and "Others 2") ACE detection kits cost R170 and R240 respectively per reaction. More organisms can be detected per reaction by the kits than by real-time PCR; however, comparison of overall affordability of the two detection methods depends on the organisms one is interested in. Seeplex® RV/PB18 auto-sequencer electrophoresis (ASE) detection kit which covers a larger panel of respiratory pathogens (Influenza A virus, Influenza B virus, human respiratory syncytial virus A and B, human parainfluenza virus 1, 2, and 3, human bocavirus,

human adenovirus, human coronavirus OC43/HKU1, human coronavirus 229E/NL63, human rhinovirus, human enterovirus, *M. pneumoniae*, *L. pneumophila*, *S. pneumoniae, H. influenzae* and *C. pneumoniae*) could have also been used instead of the Seeplex® Pneumobacter and the Seeplex® RV5 ACE detection kits, but due to the cost (R481 per reaction) and the requirement of a genetic analyzer for product detection, this kit was not selected.

Although Seeplex detection kits are marginally less sensitive compared to real-time PCR, reactions involving these kits are easier to perform and do not require complex equipment. Consequently, the Seeplex® Pneumobacter ACE detection kit and the Seeplex® RV5 ACE detection kit were used to complement real-time PCR.

Results obtained in this study indicate minimal non-specific amplification when using Seeplex detection kits. Multiplex real-time PCR reactions on the contrary amplified non-specific products in clinical samples as evidenced by agarose gel electrophoresis. This indicates that due to the presence of a range of organisms and other substances in the patient samples and failure to further optimize real-time PCR reactions used due to time limitations, these reactions were not as specific as they were hoped to be. The Seeplex ACE detection kits were validated and tested for cross reactivity and sensitivity by the manufacturer and are reported to have a low rate of false positives. Seeplex kits were reported to have a sensitivity of 10 copies/3µl while the real-time PCR singleplex and multiplex assays of our study were mostly found to have a sensitivity of 1 copy/µl.

Real-time PCR assays detected FluA in the nasopharyngeal swabs of patient 3, *M. pneumoniae* in the sputum samples of patients 2 and 3 and PIV2 in the nasopharyngeal swab of patient 2. Seeplex kits failed to detect these organisms suggesting that they were present in concentrations below the detection limit of the kits. Viral pneumonias caused by influenza viruses can be life threatening in adults and immunocompromised patients due to direct involvement of lung tissue or by secondary bacterial infections due to *S. pneumoniae, S. aureus*, *H. influenzae* and other gram-negative organisms as is the case in patient 3 who is co-infected by all these organisms (Oosterheert *et al.*, 2003).

The multiplex real-time PCR reaction of CMV and EBV detected co-infection with both these organisms in patient 3. This indicates that multiplex real-time PCR can detect all organisms targeted, even in clinical samples.

The Seeplex® Pneumobacter ACE detection kit detected *H. influenzae* in all patient sputum samples and simulations. Murphy (2003) states that non-typeable (non-encapsulated) *H. influenzae* is a common cause of pneumonia and lower respiratory tract infections in adults. It is also the most frequent cause of infections in patients with cystic fibrosis hence the detection of this bacterium in simulated sputum samples used in this study.

Results obtained in this study support evidence obtained by Lee *et al*., (2002) that atypical pathogens cause CAP more frequently than was previously thought. Marston *et al*., (1997) (Marston *et al.*, 1997) showed that atypical pathogens cause up to 60% of etiology-proven CAP cases.

4.8. Limitations of study

This study has several limitations. Firstly, the low number of patient samples prevented adequate validation of our real-time assays as well as the Seeplex detection kits. The initial aim of the study was to enroll 100 patients presenting with CAP symptoms from whom sputa and nasopharyngeal swabs would be obtained. However, due to factors beyond our control, only 3 patients were enrolled. Secondly, although real-time PCR produced rapid results and amplicons could be detected based on real-time PCR alone, in some cases fluorescence and efficiency were low. It therefore became necessary to analyze the amplicons by gel electrophoresis to confirm results. Also, due to the limited number of organisms that could be detected by both real-time PCR and the Seeplex detection kits, it could not be confirmed whether the other organism infecting patient 1 was RV or CoV, therefore stressing the need to implement additional means to detect a wider range of organisms. Thirdly, due to complications experienced with probe design, *C. psittaci* and PIV2 could not be incorporated into any multiplex real-time PCR combination. Lastly, time was a limiting factor in this study and as a result, real-time PCR assays could not be fully optimized to reduce the formation of primer-dimer artifacts and non-specific amplification.

CHAPTER 5: CONCLUSION

More often than not, empiric treatment of CAP is based upon available epidemiological data and clinical experience. It is therefore important to have data on which pathogens are prevalent locally. Such a prevalence study requires the establishment of detection methods to efficiently identify the most common causative agents of CAP.

The goal of this study was to establish a nucleic acid extraction method for isolation of both DNA and RNA from patient sputa and nasopharyngeal swabs and thereafter, to establish molecular methods for the rapid, qualitative detection of all the organisms investigated.

We have successfully used the miniMag to extract nucleic acids from patient samples and simulated samples. Multiplex and singleplex real-time PCR assays with high sensitivity were successfully established for all organisms to detect 15 CAP-associated agents. Six of these assays were performed in multiplex to simultaneously detect 12 organisms and a GAPDH (DNA) internal control, and 4 were performed in singleplex. In this pilot study, the assays were performed on simulated samples as well as 3 patient samples in parallel with Seeplex commercial PCR kits. The results obtained were promising in terms of establishing reliable, rapid methods of organism detection for potential causative agents of CAP.

On early reception of the patient sample, analysis using the Seeplex® Pneumobacter detection kit can be completed within the same day to detect 6 organisms and one and a half days when using the Seeplex® RV5 detection kit to detect 3 organisms and confirm the identity of

organisms in the "Others" group using real-time PCR. When using the real-time PCR assays, with a single real-time PCR cycler, analysis of 15 organisms can be completed within 2 days. It would be advisable to use these methods to complement each other since some respiratory pathogens such as hRV, BoV, CoV, *H. influenzae*, *S. pneumoniae* and *B. pertussis* that are included in the detection panel of the Seeplex kits were not included in the design of the real-time PCR assays whilst organisms such as CMV, EBV, *C. psittaci* and *P. jirovecii*, which are detected by the real-time PCR assays in this study cannot be detected by the kits and require further testing. The real-time PCR assays could therefore be used as a follow-on system to identify organisms that the Seeplex® RV5 ACE detection kit cannot differentiate between, namely, Others 1 (AdV, PIV1, 2, 3 or BoV) and Others 2 (hMPV, hRV or CoV). However, using real-time PCR with TaqMan probes for the diagnosis of CAP would mean purchasing fresh probes every 6 months due to reduction in fluorescence and PCR efficiency, making the real-time option best for periodic surveillance and prevalence purposes which can be completed in less than 6 months. Using this detection option for diagnostic purposes would require a redesign of probes, such as the use of Molecular Beacon aptamers which have a longer shelf-life (Drake and Tan *et al*., 2004) and increased hybridisation specificity as a result, reduce non-specific amplification.

Preliminary comparison of Seeplex kits and real-time PCR suggests that the two can be used to complement each other for prevalence studies and potentially for selected diagnostic applications.

CHAPTER 6: REFERENCES

Ackermann, H.W. and L. Berthiaume (1995). Atlas of Virus Diagrams, CRC Press.

Ansari, S. A., V. S. Springthorpe, S. A. Sattar, S. Rivard and M. Rahman (1991). Potential role of hands in the spread of respiratory viral infections: studies with human parainfluenza virus 3 and rhinovirus 14. J Clin Microbiol **29**: 2115-9.

Barber, R. D., D. W. Harmer, R. A. Coleman and B. J. Clark (2005). GAPDH as a housekeeping gene: analysis of GAPDH mRNA expression in a panel of 72 human tissues. Physiol Genomics **21**: 389-95.

Baseman, J. B. and J. G. Tully (1997). Mycoplasmas: sophisticated, reemerging, and burdened by their notoriety. Emerg Infect Dis **3**: 21-32.

Biacchesi, S., M. H. Skiadopoulos, G. Boivin, C. T. Hanson, B. R. Murphy, P. L. Collins and U. J. Buchholz (2003). Genetic diversity between human metapneumovirus subgroups. Virology **315**: 1-9.

Bio-Rad. (2008). Chromo4 Real-Time PCR Detection System. Bulletin 5215 2008.

Bio-Rad (2007). Experimental Design Considerations for qPCR. Real-time PCR Applications Guide

Boivin, G., G. De Serres, S. Cote, R. Gilca, Y. Abed, L. Rochette, M. G. Bergeron and P. Dery (2003). Human metapneumovirus infections in hospitalized children. Emerg Infect Dis 9: 634-40.

Brady, M. T., J. Evans and J. Cuartas (1990). Survival and disinfection of parainfluenza viruses on environmental surfaces. Am J Infect Control **18**: 18-23.

Brittain-Long, R., S. Nord, S. Olofsson, J. Westin, L. M. Anderson and M. Lindh (2008). Multiplex real-time PCR for detection of respiratory tract infections. J Clin Virol **41**: 53-6.

Buchen-osmond, C. (2003). Taxonomy and classification of viruses. Manual of Clinical Microbiology. A. Press. Washington D.C. **76** 1217-1225.

Bustin, S. A. (2000). Absolute quantification of mRNA using real-time reverse transcription polymerase chain reaction assays. J Mol Endocrinol **25**: 169-93.

Bustin, S. A. (2005). Real-Time PCR. Encyclopedia of Diagnostic Genomics and Proteomics. New York, Marcel Dekker, Inc.**:** 1117-1125.

Bustin, S. A. and T. Nolan (2004). Pitfalls of quantitative real-time reverse-transcription polymerase chain reaction. J Biomol Tech **15**: 155-66.

Chan, Y. R. and A. Morris (2007). Molecular diagnostic methods in pneumonia. Curr Opin Infect Dis **20**: 157-64.

Chehab, F. F., M. Doherty, S. P. Cai, Y. W. Kan, S. Cooper and E. M. Rubin (1987). Detection of sickle cell anaemia and thalassaemias. Nature **329**: 293-4.

Chun, J. Y., K. J. Kim, I. T. Hwang, Y. J. Kim, D. H. Lee, I. K. Lee and J. K. Kim (2007). Dual priming oligonucleotide system for the multiplex detection of respiratory viruses and SNP genotyping of CYP2C19 gene. Nucleic Acids Res **35**: e40.

Cirino, N. M., N. P. Tavakoli, S. M. Madison-Antenucci and C. Egan (2007). Multiplex rtPCR in Microbiology. Real-time PCR in Microbiology from diagnosis to characterization, Caister Academic Press 6**:** 183-229.

Claas, E. C., M. J. Sprenger, G. E. Kleter, R. van Beek, W. G. Quint and N. Masurel (1992). Type-specific identification of influenza viruses A, B and C by the polymerase chain reaction. J Virol Methods **39**: 1-13.

Collins, P. L., M. G. Hill, J. Cristina and H. Grosfeld (1996). Transcription elongation factor of respiratory syncytial virus, a nonsegmented negative-strand RNA virus. Proc Natl Acad Sci U S A **93**: 81-5.

Cosentini, R., P. Tarsia, F. Blasi, E. Roma and L. Allegra (2001). Community-acquired pneumonia: role of atypical organisms. Monaldi Arch Chest Dis **56**: 527-34.

Crowe, J. E., Jr. (2004). Human metapneumovirus as a major cause of human respiratory tract disease. Pediatr Infect Dis J **23**: S215-21.

Desjardin, L. E., Y. Chen, M. D. Perkins, L. Teixeira, M. D. Cave and K. D. Eisenach (1998). Comparison of the ABI 7700 system (TaqMan) and competitive PCR for quantification of IS6110 DNA in sputum during treatment of tuberculosis. J Clin Microbiol **36**: 1964-8.

Domachowske, J. B. (2003). Human Metapneumovirus: a Newly Described Respiratory Pathogen of Humans. Clinical Microbiology Newsletter. **25:** 17 - 20.

Drake, T. J. and W. Tan (2004). Molecular beacon DNA probes and their bioanalytical applications. Appl Spectrosc **58**: 269A-280A.

Ebner, K., M. Suda, F. Watzinger and T. Lion (2005). Molecular detection and quantitative analysis of the entire spectrum of human adenoviruses by a two-reaction real-time PCR assay. J Clin Microbiol **43**: 3049-53.

Edman, J. C., J. A. Kovacs, H. Masur, D. V. Santi, H. J. Elwood and M. L. Sogin (1988). Ribosomal RNA sequence shows Pneumocystis carinii to be a member of the fungi. Nature **334**: 519-22.

Esper, F., D. Boucher, C. Weibel, R. A. Martinello and J. S. Kahn (2003). Human metapneumovirus infection in the United States: clinical manifestations associated with a newly emerging respiratory infection in children. Pediatrics **111**: 1407-10.

Espy, M. J., J. R. Uhl, L. M. Sloan, S. P. Buckwalter, M. F. Jones, E. A. Vetter, J. D. Yao, N. L. Wengenack, J. E. Rosenblatt, F. R. Cockerill, 3rd and T. F. Smith (2006). Real-time PCR in clinical microbiology: applications for routine laboratory testing. Clin Microbiol Rev **19**: 165-256.

Esteves, F., M. A. Montes-Cano, C. de la Horra, M. C. Costa, E. J. Calderon, F. Antunes and O. Matos (2008). Pneumocystis jirovecii multilocus genotyping profiles in patients from Portugal and Spain. Clin Microbiol Infect **14**: 356-62.

Exner, M. M. and M. A. Lewinski (2002). Sensitivity of multiplex real-time PCR reactions, using the LightCycler and the ABI PRISM 7700 Sequence Detection System, is dependent on the concentration of the DNA polymerase. Mol Cell Probes **16**: 351-7.

Falsey, A. R., C. K. Cunningham, W. H. Barker, R. W. Kouides, J. B. Yuen, M. Menegus, L. B. Weiner, C. A. Bonville and R. F. Betts (1995). Respiratory syncytial virus and influenza A infections in the hospitalized elderly. J Infect Dis **172**: 389-94.

Falsey, A. R. and E. E. Walsh (2000). Respiratory syncytial virus infection in adults. Clin Microbiol Rev **13**: 371-84.

Flori, P., B. Bellete, F. Durand, H. Raberin, C. Cazorla, J. Hafid, F. Lucht and R. T. Sung (2004). Comparison between real-time PCR, conventional PCR and different staining techniques for diagnosing Pneumocystis jiroveci pneumonia from bronchoalveolar lavage specimens. J Med Microbiol **53**: 603-7.

Garcia-Sastre, A., A. Egorov, D. Matassov, S. Brandt, D. E. Levy, J. E. Durbin, P. Palese and T. Muster (1998). Influenza A virus lacking the NS1 gene replicates in interferon-deficient systems. Virology **252**: 324-30.

Giglio, S., P. T. Monis and C. P. Saint (2003). Demonstration of preferential binding of SYBR Green I to specific DNA fragments in real-time multiplex PCR. Nucleic Acids Res **31**: e136.

Gleason, P. P. (2002). The emerging role of atypical pathogens in community-acquired pneumonia. Pharmacotherapy **22**: 2S-11S; discussion 30S-32S.

Gouriet, F., M. Drancourt and D. Raoult (2006). Multiplexed serology in atypical bacterial pneumonia. Ann N Y Acad Sci **1078**: 530-40.

Grayston, J. T., L. A. Campbell, C. C. Kuo, C. H. Mordhorst, P. Saikku, D. H. Thom and S. P. Wang (1990). A new respiratory tract pathogen: Chlamydia pneumoniae strain TWAR. J Infect Dis **161**: 618-25.

Gudnason, H., M. Dufva, D. D. Bang and A. Wolff (2007). Comparison of multiple DNA dyes for real-time PCR: effects of dye concentration and sequence composition on DNA amplification and melting temperature. Nucleic Acids Res **35**: e127.

Guiver, M., R. Borrow, J. Marsh, S. J. Gray, E. B. Kaczmarski, D. Howells, P. Boseley and A. J. Fox (2000). Evaluation of the Applied Biosystems automated Taqman polymerase chain reaction system for the detection of meningococcal DNA. FEMS Immunol Med Microbiol **28**: 173-9.

Gunson, R. N., T. C. Collins and W. F. Carman (2005). Real-time RT-PCR detection of 12 respiratory viral infections in four triplex reactions. J Clin Virol **33**: 341-4.

Gunson, R. N., T. C. Collins and W. F. Carman (2006). Practical experience of high throughput real time PCR in the routine diagnostic virology setting. J Clin Virol **35**: 355-67.

Hacker, J. and G. Fischer (1993). Immunophilins: structure-function relationship and possible role in microbial pathogenicity. Mol Microbiol **10**: 445-56.

Hacking, D. and J. Hull (2002). Respiratory syncytial virus--viral biology and the host response. J Infect **45**: 18-24.

Hahn, D. L., A. A. Azenabor, W. L. Beatty and G. I. Byrne (2002). Chlamydia pneumoniae as a respiratory pathogen. Front Biosci **7**: e66-76.

Hall, C. B. (2001). Respiratory syncytial virus and parainfluenza virus. N Engl J Med **344**: 1917-28.

Hall, C. B. and R. G. Douglas, Jr. (1981). Modes of transmission of respiratory syncytial virus. J Pediatr **99**: 100-3.

Hamelin, M. E. and G. Boivin (2005). Human metapneumovirus: a ubiquitous and long-standing respiratory pathogen. Pediatr Infect Dis J **24**: S203-7.

Hardegger, D., D. Nadal, W. Bossart, M. Altwegg and F. Dutly (2000). Rapid detection of Mycoplasma pneumoniae in clinical samples by real-time PCR. J Microbiol Methods **41**: 45-51.

Heid, C. A., J. Stevens, K. J. Livak and P. M. Williams (1996). Real time quantitative PCR. Genome Res **6**: 986-94.

Henrickson, K. J. (2003). Parainfluenza viruses. Clin Microbiol Rev **16**: 242-64.

Henrickson, K. J. (2004). Advances in the laboratory diagnosis of viral respiratory disease. Pediatr Infect Dis J **23**: S6-10.

Hierholzer, J. C., P. E. Halonen, P. O. Dahlen, P. G. Bingham and M. M. McDonough (1993). Detection of adenovirus in clinical specimens by polymerase chain reaction and liquid-phase hybridization quantitated by time-resolved fluorometry. J Clin Microbiol **31**: 1886-91.

Holland, P. M., R. D. Abramson, R. Watson and D. H. Gelfand (1991). Detection of specific polymerase chain reaction product by utilizing the 5'----3' exonuclease activity of Thermus aquaticus DNA polymerase. Proc Natl Acad Sci U S A **88**: 7276-80.

Horwitz, M. S. (2001). Adenoviruses. Fields Virology. D. M. Knipe, Howley, P.M. Philadelphia, Lippincott Williams & Wilkins. **2** 148-153.

Jebbink, J., X. Bai, B. B. Rogers, D. B. Dawson, R. H. Scheuermann and R. Domiati-Saad (2003). Development of real-time PCR assays for the quantitative detection of Epstein-Barr virus and cytomegalovirus, comparison of TaqMan probes, and molecular beacons. J Mol Diagn **5**: 15-20.

Ko, G., N. Jothikumar, V. R. Hill and M. D. Sobsey (2005). Rapid detection of infectious adenoviruses by mRNA real-time RT-PCR. J Virol Methods **127**: 148-53.

Kok, T. and G. Higgins (1997). Prevalence of respiratory viruses and Mycoplasma pneumoniae in sputum samples from unselected adult patients. Pathology **29**: 300-2.

Kontanis, E. J. and F. A. Reed (2006). Evaluation of real-time PCR amplification efficiencies to detect PCR inhibitors. J Forensic Sci **51**: 795-804.

Krajicek, B. J., A. H. Limper and C. F. Thomas, Jr. (2008). Advances in the biology, pathogenesis and identification of Pneumocystis pneumonia. Curr Opin Pulm Med **14**: 228-34.

Kumar, S. and M. R. Hammerschlag (2007). Acute respiratory infection due to Chlamydia pneumoniae: current status of diagnostic methods. Clin Infect Dis **44**: 568-76.

Larsen, H. H., H. Masur, J. A. Kovacs, V. J. Gill, V. A. Silcott, P. Kogulan, J. Maenza, M. Smith, D. R. Lucey and S. H. Fischer (2002). Development and evaluation of a quantitative, touch-down, real-time PCR assay for diagnosing Pneumocystis carinii pneumonia. J Clin Microbiol **40**: 490-4.

Lee, S. J., M. G. Lee, M. J. Jeon, K. S. Jung, H. K. Lee and T. Kishimoto (2002). Atypical pathogens in adult patients admitted with community-acquired pneumonia in Korea. Jpn J Infect Dis **55**: 157-9.

Leroy, O., C. Santre, C. Beuscart, H. Georges, B. Guery, J. M. Jacquier and G. Beaucaire (1995). A five-year study of severe community-acquired pneumonia with emphasis on prognosis in patients admitted to an intensive care unit. Intensive Care Med **21**: 24-31.

Lie, Y. S. and C. J. Petropoulos (1998). Advances in quantitative PCR technology: 5' nuclease assays. Curr Opin Biotechnol **9**: 43-8.

Lin, D., J. Lan and Z. Zhang (2007). Structure and function of the NS1 protein of influenza A virus. Acta Biochim Biophys Sin (Shanghai) **39**: 155-62.

Liu, W. and D. A. Saint (2002). A new quantitative method of real time reverse transcription polymerase chain reaction assay based on simulation of polymerase chain reaction kinetics. Anal Biochem **302**: 52-9.

Ljungman, P. (2004). Treatment of adenovirus infections in the immunocompromised host. Eur J Clin Microbiol Infect Dis **23**: 583-8.

Loeb, K. R., K. R. Jerome, J. Goddard, M. Huang, A. Cent and L. Corey (2000). High-throughput quantitative analysis of hepatitis B virus DNA in serum using the TaqMan fluorogenic detection system. Hepatology **32**: 626-9.

Lutfiyya, M. N., E. Henley, L. F. Chang and S. W. Reyburn (2006). Diagnosis and treatment of community-acquired pneumonia. Am Fam Physician **73**: 442-50.

Mackay, I. M. (2004). Real-time PCR in the microbiology laboratory. Clin Microbiol Infect **10**: 190-212.

Mackay, I. M. (2007). Real-time PCR: History and Flourogenic chemistries. Real-time PCR in Microbiology From diagnosis to characterization. United Kingdom, Caister Academic Press 1**:** 1-40.

Mackay, I. M., K. E. Arden and A. Nitsche (2002). Real-time PCR in virology. Nucleic Acids Res **30**: 1292-305.

Mackay, I. M., S. A. Bustin, J. M. Andrade, M. Kubista and T. P. Sloots (2007). Quantification of microorganisms: not human, not simple, not quick. Real-time PCR in Microbiology: from diagnosis to characterization. Norfolk, Caister Academic Press 5**:** 133-182.

Markoulatos, P., N. Siafakas and M. Moncany (2002). Multiplex polymerase chain reaction: a practical approach. J Clin Lab Anal **16**: 47-51.

Marston, B. J., H. B. Lipman and R. F. Breiman (1994). Surveillance for Legionnaires' disease. Risk factors for morbidity and mortality. Arch Intern Med **154**: 2417-22.

Marston, B. J., J. F. Plouffe, T. M. File, Jr., B. A. Hackman, S. J. Salstrom, H. B. Lipman, M. S. Kolczak and R. F. Breiman (1997). Incidence of community-acquired pneumonia requiring hospitalization. Results of a population-based active surveillance Study in Ohio. The Community-Based Pneumonia Incidence Study Group. Arch Intern Med **157**: 1709-18.

Maskell, N. A., D. J. Waine, A. Lindley, J. C. Pepperell, A. E. Wakefield, R. F. Miller and R. J. Davies (2003). Asymptomatic carriage of Pneumocystis jiroveci in subjects undergoing bronchoscopy: a prospective study. Thorax **58**: 594-7.

Mathur, U., D. W. Bentley and C. B. Hall (1980). Concurrent respiratory syncytial virus and influenza A infections in the institutionalized elderly and chronically ill. Ann Intern Med **93**: 49-52.

McLean, D. M., R. M. Bannatyne and K. F. Givan (1967). Myxovirus dissemination by air. Can Med Assoc J **96**: 1449-53.

Medrano, F. J., N. Respaldiza, A. Medrano, J. M. Varela, M. Montes-Cano, C. de la Horra, I. Wichmann, S. Ferrer and E. Calderon (2003). Seroprevalence of Pneumocystis human infection in southern Spain. J Eukaryot Microbiol **50 Suppl**: 649-50.

Mejias, A., S. Chavez-Bueno and O. Ramilo (2004). Human metapneumovirus: a not so new virus. Pediatr Infect Dis J **23**: 1-7; quiz 8-10.

Meliani, L., M. Develoux, M. Marteau-Miltgen, D. Magne, V. Barbu, J. L. Poirot and P. Roux (2003). Real time quantitative PCR assay for Pneumocystis jirovecii detection. J Eukaryot Microbiol **50 Suppl**: 651.

Metlay, J. P. and M. J. Fine (2003). Testing strategies in the initial management of patients with community-acquired pneumonia. Ann Intern Med **138**: 109-18.

Miller, R. and L. Huang (2004). Pneumocystis jirovecii infection. Thorax **59**: 731-3.

Miller, R. F., H. E. Ambrose and A. E. Wakefield (2001). Pneumocystis carinii f. sp. hominis DNA in immunocompetent health care workers in contact with patients with P. carinii pneumonia. J Clin Microbiol **39**: 3877-82.

Millman, K. L., S. Tavara and D. Dean (2001). Recombination in the ompA Gene but Not the omcB Gene of Chlamydia Contributes to Serovar-Specific Differences in Tissue Tropism, Immune Surveillance, and Persistence of the Organism. J Bacteriol. **183**: 5997 - 6008.

Moine, P., J. B. Vercken, S. Chevret, C. Chastang and P. Gajdos (1994). Severe community-acquired pneumonia. Etiology, epidemiology, and prognosis factors. French Study Group for Community-Acquired Pneumonia in the Intensive Care Unit. Chest **105**: 1487-95.

Morozumi, M., E. Nakayama, S. Iwata, Y. Aoki, K. Hasegawa, R. Kobayashi, N. Chiba, T. Tajima and K. Ubukata (2006). Simultaneous detection of pathogens in clinical samples from patients with community-acquired pneumonia by real-time PCR with pathogen-specific molecular beacon probes. J Clin Microbiol **44**: 1440-6.

Mulhardt, C. and E. W. Beese (2006). The polymerase chain reaction. Molecular Biology and Genomics Academic Press 4**:** 65-94.

Mullis, K. B. (1990). The unusual origin of the polymerase chain reaction. Sci Am **262**: 56-61, 64-5.

Murphy, T. F. (2003). Respiratory infections caused by non-typeable Haemophilus influenzae. Curr Opin Infect Dis **16**: 129-34.

Murray, P. R., K. S. Rosenthal and M. A. Pfaller (2005). Medical Microbiology. Philadelphia, pennsylvania, elsevier mosby.

Oosterheert, J. J., M. J. Bonten, E. Hak, M. M. Schneider and A. I. Hoepelman (2003). Severe community-acquired pneumonia: what's in a name? Curr Opin Infect Dis **16**: 153-9.

Parashar, D., D. S. Chauhan, V. D. Sharma and V. M. Katoch (2006). Applications of real-time PCR technology to mycobacterial research. Indian J Med Res **124**: 385-98.

Peret, T. C., G. Boivin, Y. Li, M. Couillard, C. Humphrey, A. D. Osterhaus, D. D. Erdman and L. J. Anderson (2002). Characterization of human metapneumoviruses isolated from patients in North America. J Infect Dis **185**: 1660-3.

Pring-Akerblom, P., F. E. Trijssenaar and T. Adrian (1995). Sequence characterization and comparison of human adenovirus subgenus B and E hexons. Virology **212**: 232-6.

Pubmed <http://www.ncbi.nlm.nih.gov/PubMed/ > (1966). Bethesda (MD): National Center for Biotechnology and Information - Updated daily. (Retrieved 8 September 2007)

Pulvirenti, J., P. Herrera, P. Venkataraman and N. Ahmed (2003). Pneumocystis carinii pneumonia in HIV-infected patients in the HAART era. AIDS Patient Care STDS **17**: 261-5.

Ratcliff, R. M., S. C. Donnellan, J. A. Lanser, P. A. Manning and M. W. Heuzenroeder (1997). Interspecies sequence differences in the Mip protein from the genus Legionella: implications for function and evolutionary relatedness. Mol Microbiol **25**: 1149-58.

Ririe, K. M., R. P. Rasmussen and C. T. Wittwer (1997). Product differentiation by analysis of DNA melting curves during the polymerase chain reaction. Anal Biochem **245**: 154-60.

Rota, P. A., R. A. Black, B. K. De, M. W. Harmon and A. P. Kendal (1990). Expression of influenza A and B virus nucleoprotein antigens in baculovirus. J Gen Virol **71 (Pt 7)**: 1545-54.

Saiyed, Z., S. Telang and C. Ramchand (2003). Application of magnetic techniques in the field of drug discovery and biomedicine. Biomagn Res Technol **1**: 2.

Schweiger, B., I. Zadow, R. Heckler, H. Timm and G. Pauli (2000). Application of a fluorogenic PCR assay for typing and subtyping of influenza viruses in respiratory samples. J Clin Microbiol **38**: 1552-8.

Seegene <http://www.seegene.com > (2007). Novel Oligo Platform for PCR: DPO. Retrieved 17 December, 2008.

Shemer-Avni, Y. and D. Lieberman (1995). Chlamydia pneumoniae-induced ciliostasis in ciliated bronchial epithelial cells. J Infect Dis **171**: 1274-8.

Singh, A., R. V. Goering, S. Simjee, S. L. Foley and M. J. Zervos (2006). Application of molecular techniques to the study of hospital infection. Clin Microbiol Rev **19**: 512-30.

Sirover, M. A. (1996). Minireview. Emerging new functions of the glycolytic protein, glyceraldehyde-3-phosphate dehydrogenase, in mammalian cells. Life Sci **58**: 2271-7.

Soheili, Z. and S. Samiei (2005). Real Time PCR: Principles and Application. Hepatitis Monthly. **5:** 83-87.

Sopena, N., M. Sabria, M. L. Pedro-Botet, J. M. Manterola, L. Matas, J. Dominguez, J. M. Modol, P. Tudela, V. Ausina and M. Foz (1999). Prospective study of community-acquired pneumonia of bacterial etiology in adults. Eur J Clin Microbiol Infect Dis **18**: 852-8.

Stenberg, R. M. (1996). The human cytomegalovirus major immediate-early gene. Intervirology **39**: 343-9.

Stralin, K., E. Tornqvist, M. S. Kaltoft, P. Olcen and H. Holmberg (2006). Etiologic diagnosis of adult bacterial pneumonia by culture and PCR applied to respiratory tract samples. J Clin Microbiol **44**: 643-5.

Stringer, J. R., C. B. Beard, R. F. Miller and A. E. Wakefield (2002). A new name (Pneumocystis jiroveci) for Pneumocystis from humans. Emerg Infect Dis **8**: 891-6.

Tang, Y. W., S. E. Sefers, H. Li, D. J. Kohn and G. W. Procop (2005). Comparative evaluation of three commercial systems for nucleic acid extraction from urine specimens. J Clin Microbiol **43**: 4830-3.

Templeton, K. E., S. A. Scheltinga, A. W. Graffelman, J. M. Van Schie, J. W. Crielaard, P. Sillekens, P. J. Van Den Broek, H. Goossens, M. F. Beersma and E. C. Claas (2003). Comparison and evaluation of real-time PCR, real-time nucleic acid sequence-based amplification, conventional PCR, and serology for diagnosis of Mycoplasma pneumoniae. J Clin Microbiol **41**: 4366-71.

Templeton, K. E., S. A. Scheltinga, M. F. Beersma, A. C. Kroes and E. C. Claas (2004). Rapid and sensitive method using multiplex real-time PCR for diagnosis of infections by influenza a and influenza B viruses, respiratory syncytial virus, and parainfluenza viruses 1, 2, 3, and 4. J Clin Microbiol **42**: 1564-9.

Templeton, K. E., S. A. Scheltinga, W. C. van den Eeden, A. W. Graffelman, P. J. van den Broek and E. C. Claas (2005). Improved diagnosis of the etiology of community-acquired pneumonia with real-time polymerase chain reaction. Clin Infect Dis **41**: 345-51.

Thomas, C. F., Jr. and A. H. Limper (2004). Pneumocystis pneumonia. N Engl J Med **350**: 2487-98.

Thomas, C. F., Jr. and A. H. Limper (2007). Current insights into the biology and pathogenesis of Pneumocystis pneumonia. Nat Rev Microbiol **5**: 298-308.

Tichopad, A., M. Dilger, G. Schwarz and M. W. Pfaffl (2003). Standardized determination of real-time PCR efficiency from a single reaction set-up. Nucleic Acids Res **31**: e122.

Valasek, M. A. and J. J. Repa (2005). The power of real-time PCR. Adv Physiol Educ **29**: 151-9.

van de Pol, A. C., T. F. Wolfs, N. J. Jansen, A. M. van Loon and J. W. Rossen (2006). Diagnostic value of real-time polymerase chain reaction to detect viruses in young children admitted

to the paediatric intensive care unit with lower respiratory tract infection. Crit Care **10**: R61.

van den Hoogen, B. G., T. M. Bestebroer, A. D. Osterhaus and R. A. Fouchier (2002). Analysis of the genomic sequence of a human metapneumovirus. Virology **295**: 119-32.

Wagner, H. J., G. Bein, A. Bitsch and H. Kirchner (1992). Detection and quantification of latently infected B lymphocytes in Epstein-Barr virus-seropositive, healthy individuals by polymerase chain reaction. J Clin Microbiol **30**: 2826-9.

Wakefield, A. E., F. J. Pixley, S. Banerji, K. Sinclair, R. F. Miller, E. R. Moxon and J. M. Hopkin (1990). Detection of Pneumocystis carinii with DNA amplification. Lancet **336**: 451-3.

Wat, D. (2004). The common cold: a review of the literature. Eur J Intern Med **15**: 79-88.

Wilhelm, J. and A. Pingoud (2003). Real-time polymerase chain reaction. Chembiochem **4**: 1120-8.

Williams, J. V., P. A. Harris, S. J. Tollefson, L. L. Halburnt-Rush, J. M. Pingsterhaus, K. M. Edwards, P. F. Wright and J. E. Crowe, Jr. (2004). Human metapneumovirus and lower respiratory tract disease in otherwise healthy infants and children. N Engl J Med **350**: 443-50.

Wittwer, C., K. Ririe and R. Rasmussen (1998). Fluorescence monitoring of rapid cycle PCR for quantification. Gene Quantification. F. F. Birkhauser, New York 129-144.

Wittwer, C. T., M. G. Herrmann, C. N. Gundry and K. S. Elenitoba-Johnson (2001). Real-time multiplex PCR assays. Methods **25**: 430-42.

Woese, C. R., O. Kandler and M. L. Wheelis (1990). Towards a natural system of organisms: proposal for the domains Archaea, Bacteria, and Eucarya. Proc Natl Acad Sci U S A **87**: 4576-9.

Wong, M. L. and J. F. Medrano (2005). Real-time PCR for mRNA quantitation. Biotechniques **39**: 75-85.

Woodhead, M. (2002). Community-acquired pneumonia in Europe: causative pathogens and resistance patterns. Eur Respir J Suppl **36**: 20s-27s.

Xu, H. X., Y. Kawamura, N. Li, L. Zhao, T. M. Li, Z. Y. Li, S. Shu and T. Ezaki (2000). A rapid method for determining the G+C content of bacterial chromosomes by monitoring fluorescence intensity during DNA denaturation in a capillary tube. Int J Syst Evol Microbiol **50 Pt 4**: 1463-9.

Xu, W., M. C. McDonough and D. D. Erdman (2000). Species-specific identification of human adenoviruses by a multiplex PCR assay. J Clin Microbiol **38**: 4114-20.

Yang, J., W. C. Hooper, D. J. Phillips and D. F. Talkington (2002). Regulation of proinflammatory cytokines in human lung epithelial cells infected with Mycoplasma pneumoniae. Infect Immun **70**: 3649-55.

Yang, S. and R. E. Rothman (2004). PCR-based diagnostics for infectious diseases: uses, limitations, and future applications in acute-care settings. Lancet Infect Dis **4**: 337-48.

Yu, V. L. (2000). Legionella pneumophila. Principles and practice of infectious diseases. G. L. Mandell, Bennet, J.E, Dolin, R. Philadelphia, Churchill Livingstone. **2** 2424-2435.

Zhang, J., H. Chen, G. Weinmaster and S. D. Hayward (2001). Epstein-Barr virus BamHi-a rightward transcript-encoded RPMS protein interacts with the CBF1-associated corepressor CIR to negatively regulate the activity of EBNA2 and NotchIC. J Virol **75**: 2946-56.

CHAPTER 7: APPENDIX A

7.1.Buffers, Media and Stains

1. 2% Agarose (30ml)
   0.6g Agarose
   30ml 1x TAE buffer
   1.5µl Ethidium bromide (10µg/ml)

2. 3% Agarose (30ml)
   0.9g Agarose
   30ml 1x TAE buffer
   1.5µl Ethidium bromide (10µg/ml)

3. 30% sterile glycerol (100ml)
   30ml glycerol (neat)
   d.H_2O
Make up to 100ml with dH_2O and autoclave.

Buffers

Otherwise stated, all buffers were autoclaved.

1. TE Buffer
   10mM Tris-HCl, pH 8.0
   1mM EDTA
   d.H_2O

2. 1M Tris-HCl pH 8.3 (200ml)
   24.2g Tris base
   d.H_2O
Dissolve powder in 150ml d.H_2O. Add approximately 8.4 ml concentrated HCl for a solution with a pH of 8.3, and check with a pH meter.

3. Protenaise K buffer (250µl)
   12.5µl 20mg/ml proteinase k
   12.5µl 10% SDS
   5µl 1M Tris-HCl (pH 8.3)
Make up to 250µl with water. Buffer was not autoclaved

4. 10% SDS (100ml)
    10g SDS
    d.H_2O

Add SDS powder to d.H_2O, and make up to 100mL. Heat at 68°C to dissolve the powder. Adjust pH to 7.2 with 1M HCl. Buffer was not autoclaved.

5. 50x TAE buffer (100ml)
    24.2g Tris base
    5.7ml glacial acetic acid
    10ml 0.5M EDTA (pH 8)
    d.H_2O

Dissolve Tris and EDTA.2H_2O in d.H_2O. Add the acetic acid and make up to 100ml with d.H_2O.

6. 0.5M EDTA (1L)
    186.1g Na_2EDTA.2H_2O
    d.H_2O

Dissolve the Na_2EDTA.2H_2O powder in d.H_2O, and adjust pH to 8.0 with 10M NaOH (~50mL). Make up to 1L with d.H_2O.

7. 1M HCl (1L)
    86.2mL concentrated HCl
    d.H_2O

Add 86.2ml concentrated HCl to 913.8ml d.H_2O. Buffer was not autoclave.

Media

1. Luria Bertani broth
    5.0g Tryptone
    10.0g Yeast extract
    5.0g Sodium chloride

Dissolve in 1L d.H_2O.

Stains

1. Ethidium Bromide (10mg/ml) (10ml)
    100mg Ethidium bromide
    d.H_2O

Make up to 10ml with d.H_2O. Do not autoclave. Store in the dark

CHAPTER 7: APPENDIX B

7.2.Agarose gels of singleplex real-time PCR reactions: positive controls and sensitivity assays

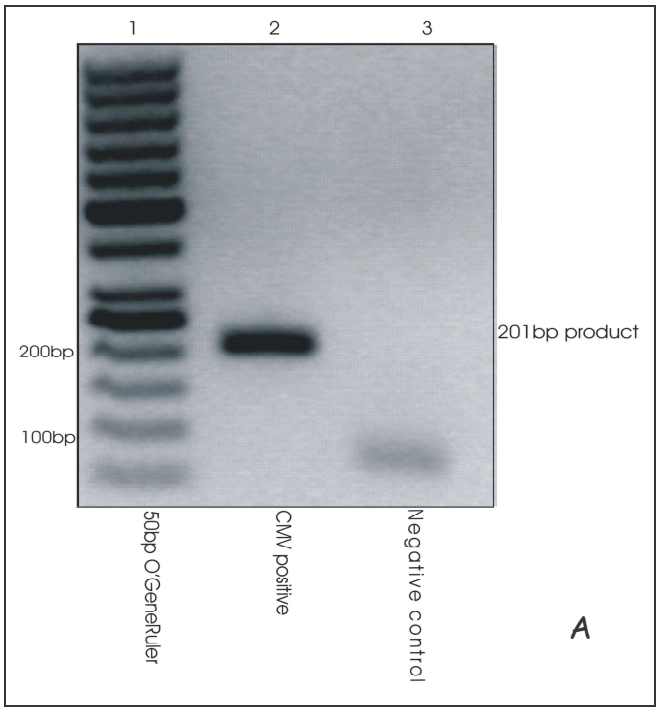

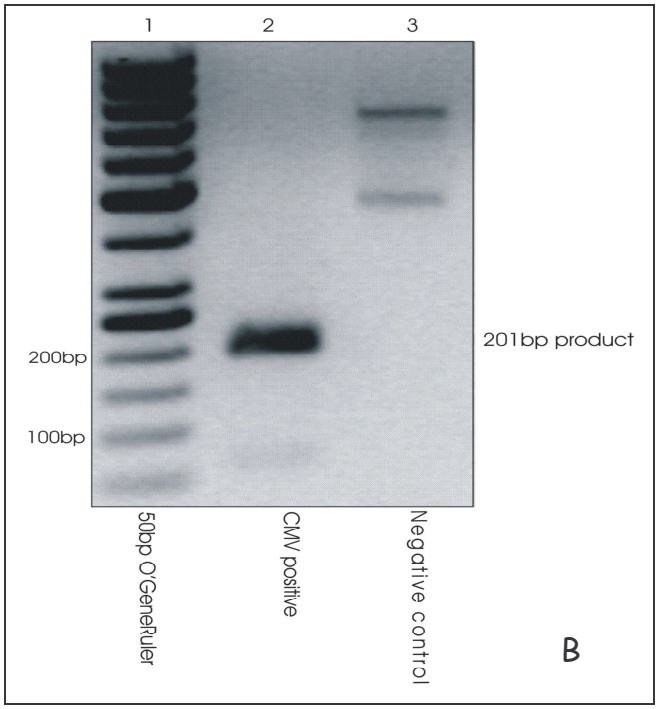

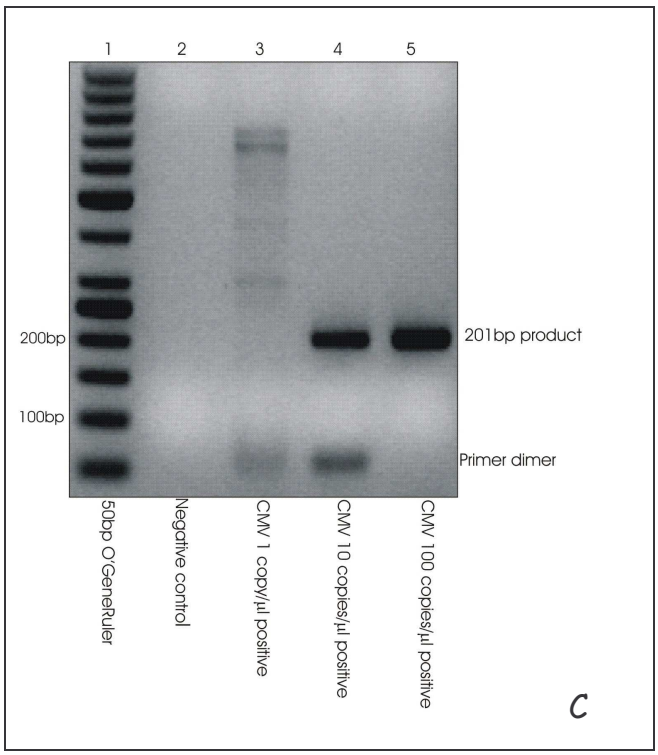

Figure B1: Agarose gel electrophoresis of CMV
(A) Positive control using SYBR Green I; **(B)** Positive control using TaqMan probes; and **(C)** Sensitivity assay performed on plasmids using TaqMan probes.

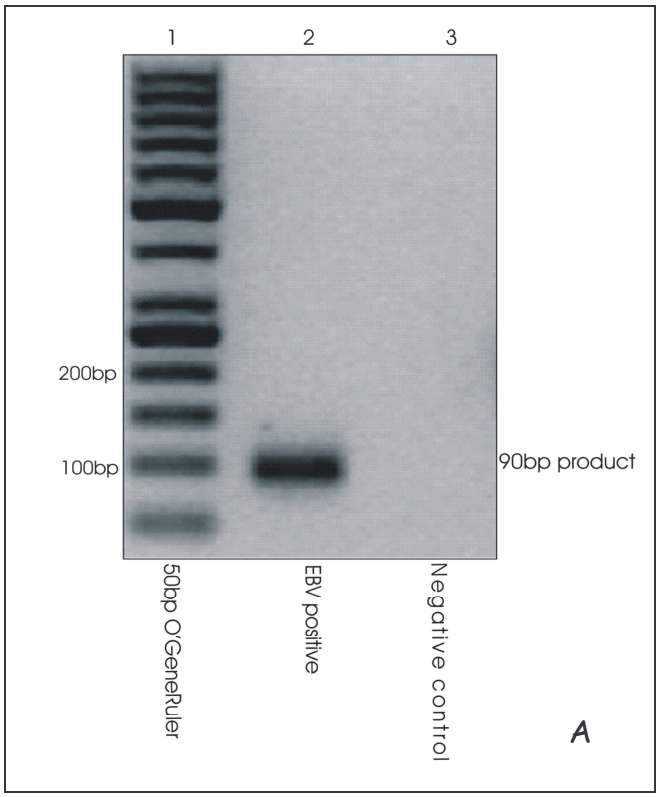

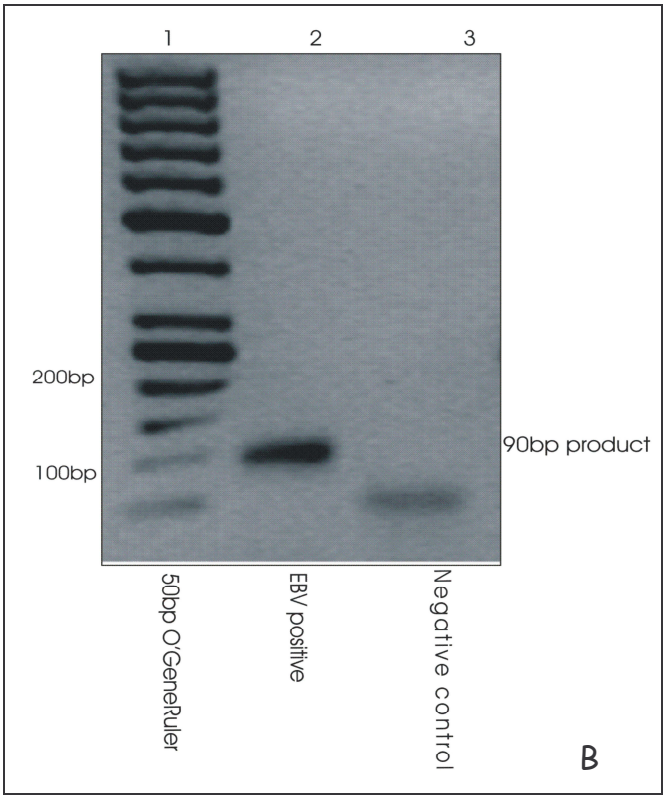

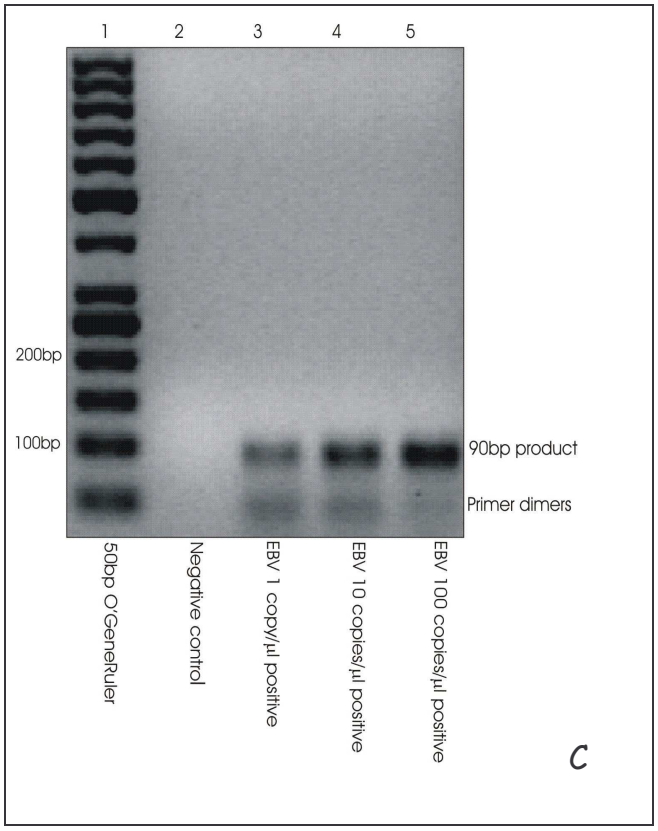

Figure B2: Agarose gel electrophoresis of EBV

(A) Positive control using SYBR Green I; **(B)** Positive control using TaqMan probes; and **(C)** Sensitivity assay performed on plasmids using TaqMan probes.

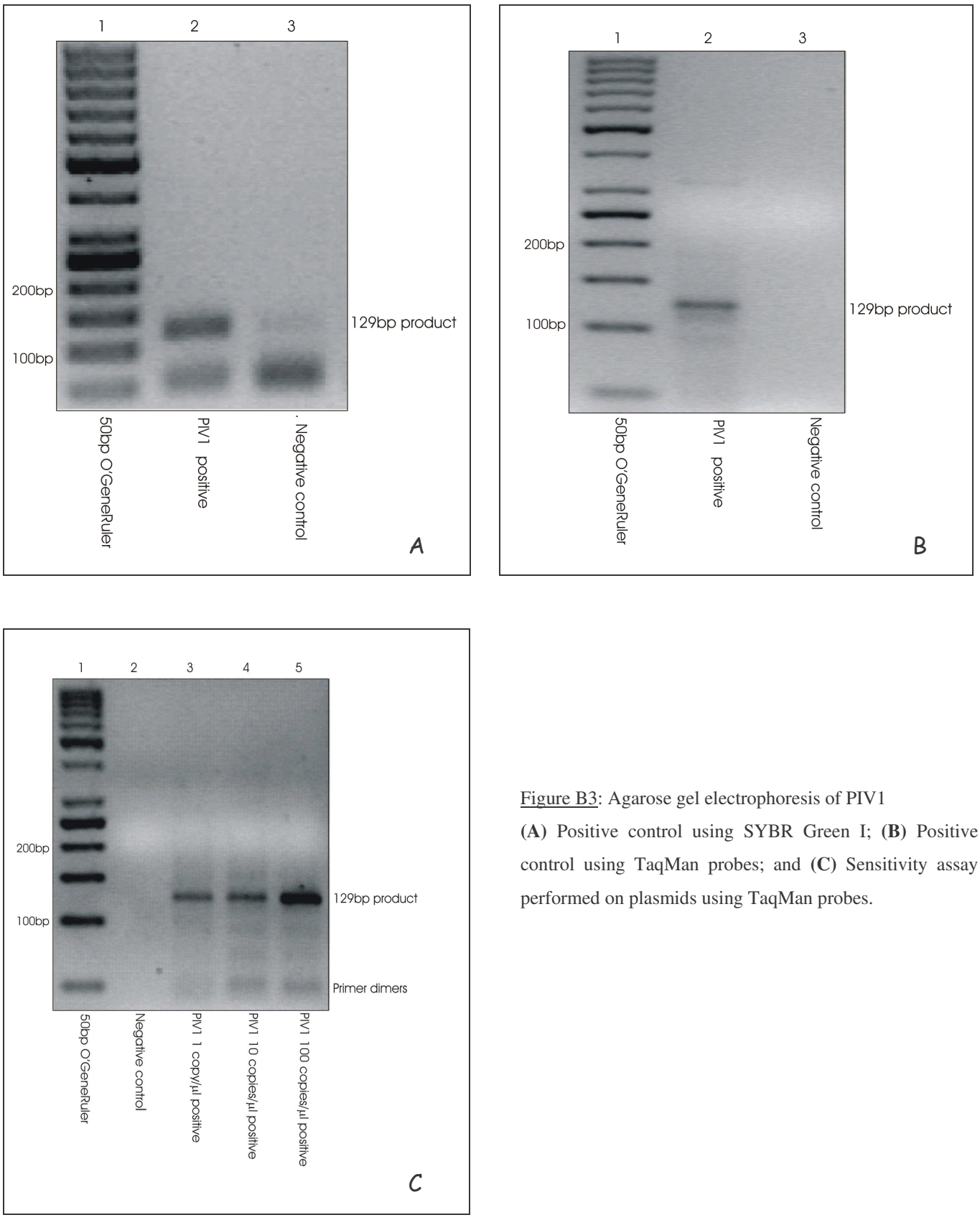

Figure B3: Agarose gel electrophoresis of PIV1

(A) Positive control using SYBR Green I; **(B)** Positive control using TaqMan probes; and **(C)** Sensitivity assay performed on plasmids using TaqMan probes.

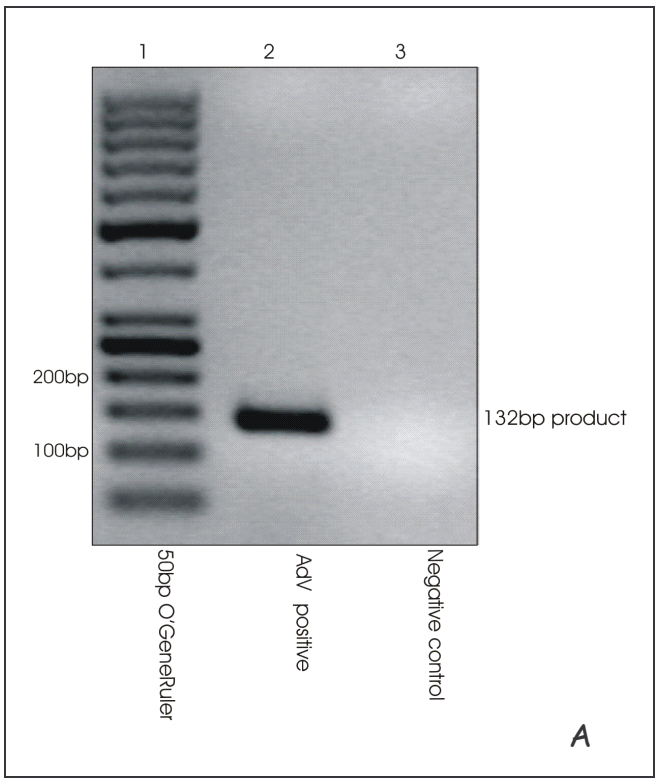

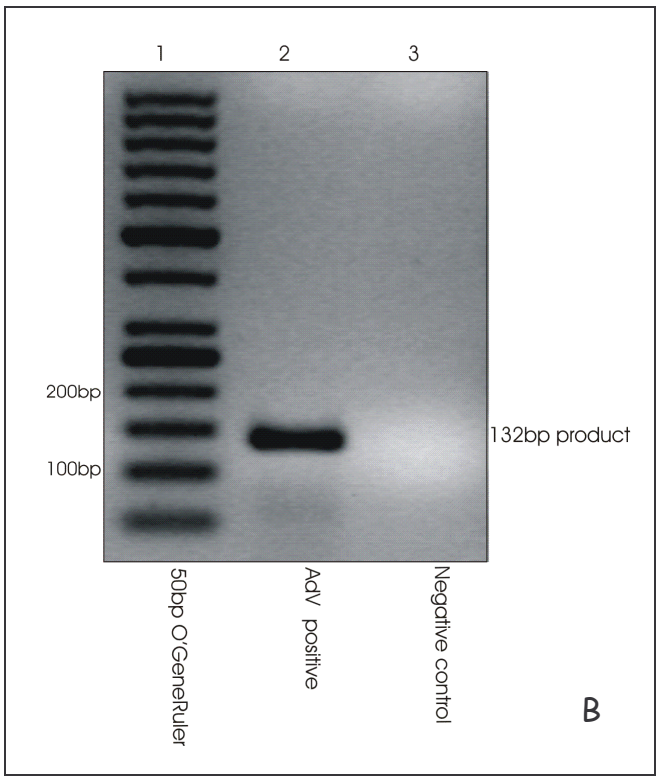

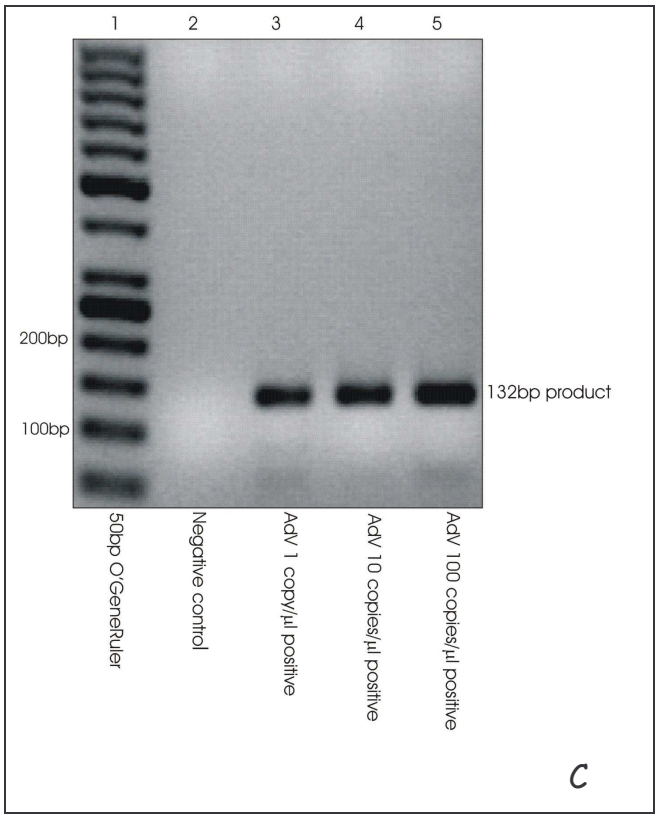

Figure B4: Agarose gel electrophoresis of AdV
(A) Positive control using SYBR Green I; **(B)** Positive control using TaqMan probes; and **(C)** Sensitivity assay performed on plasmids using TaqMan probes.

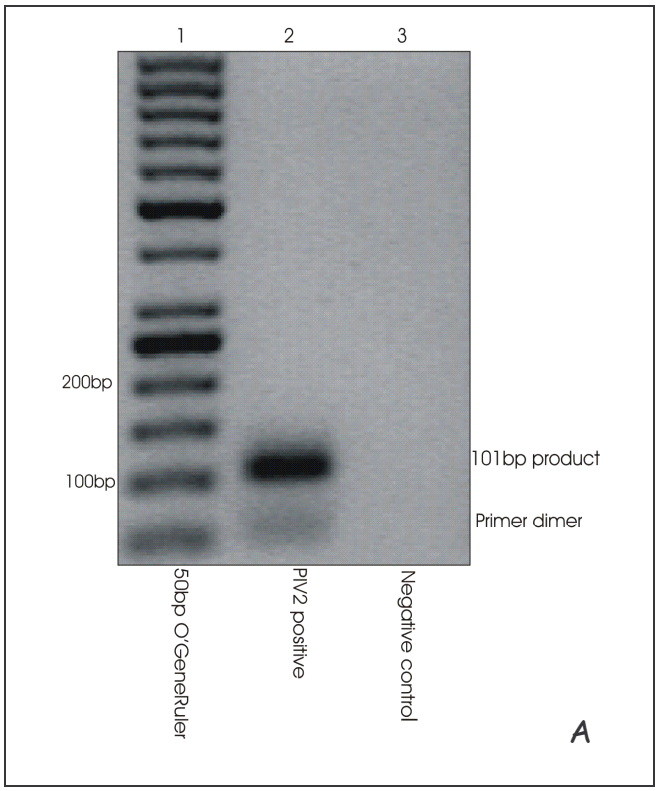

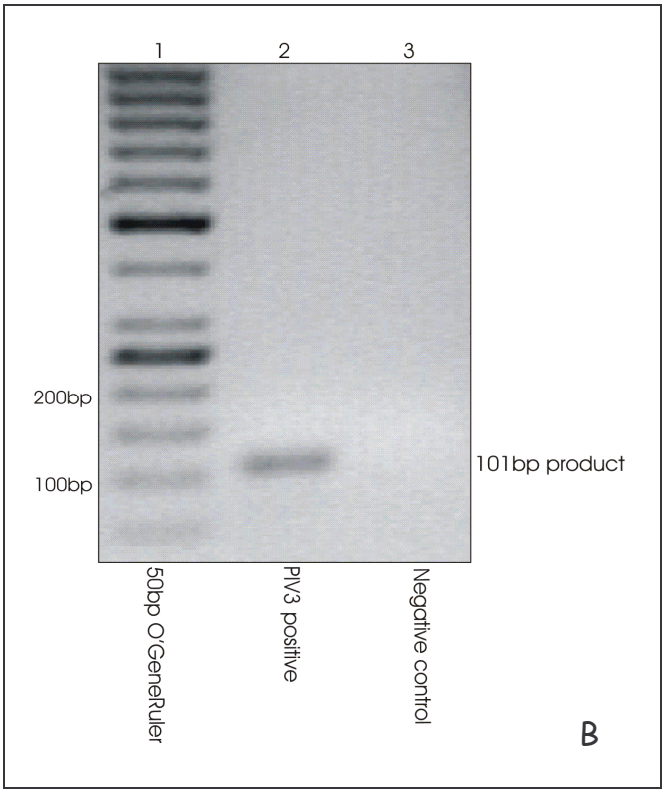

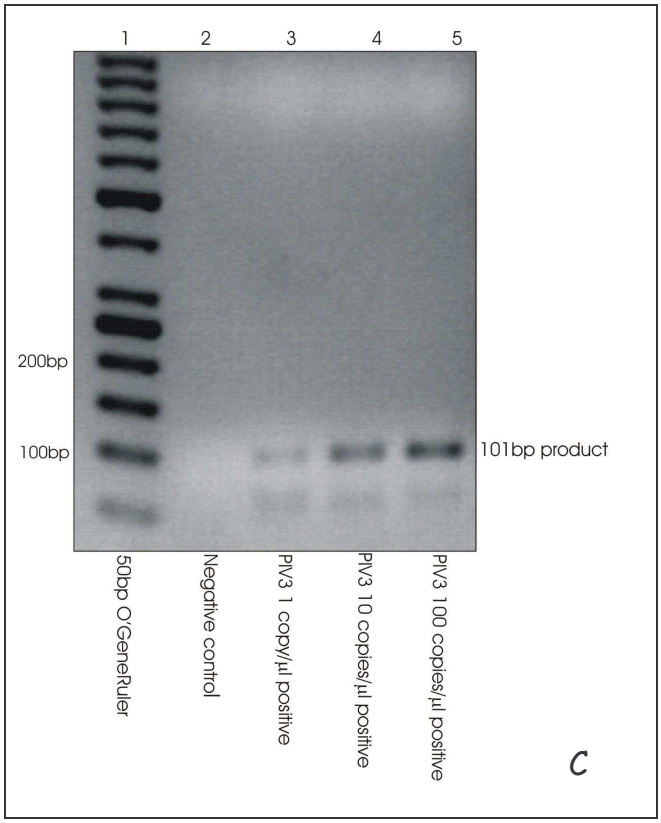

Figure B5: Agarose gel electrophoresis of PIV3

(A) Positive control using SYBR Green I; **(B)** Positive control using TaqMan probes; and **(C)** Sensitivity assay performed on plasmids using TaqMan probes.

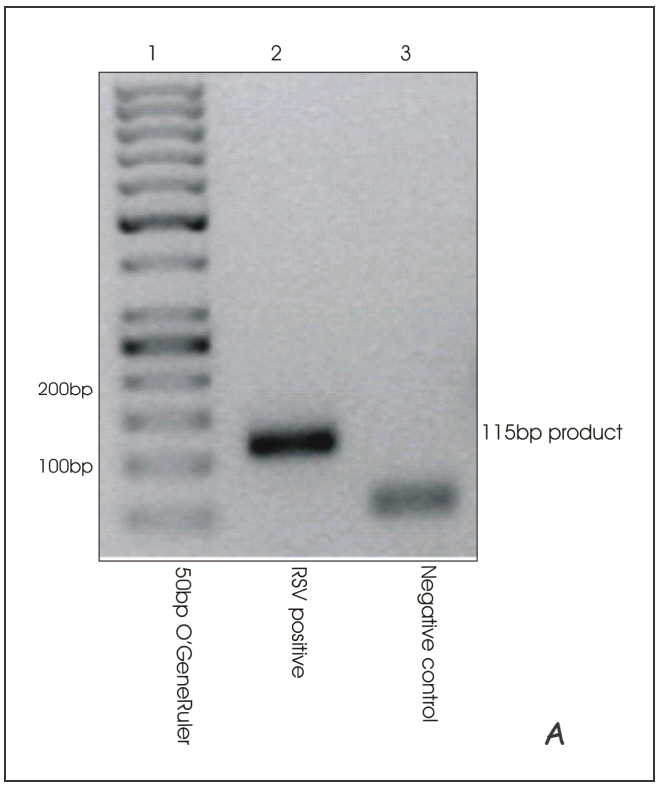

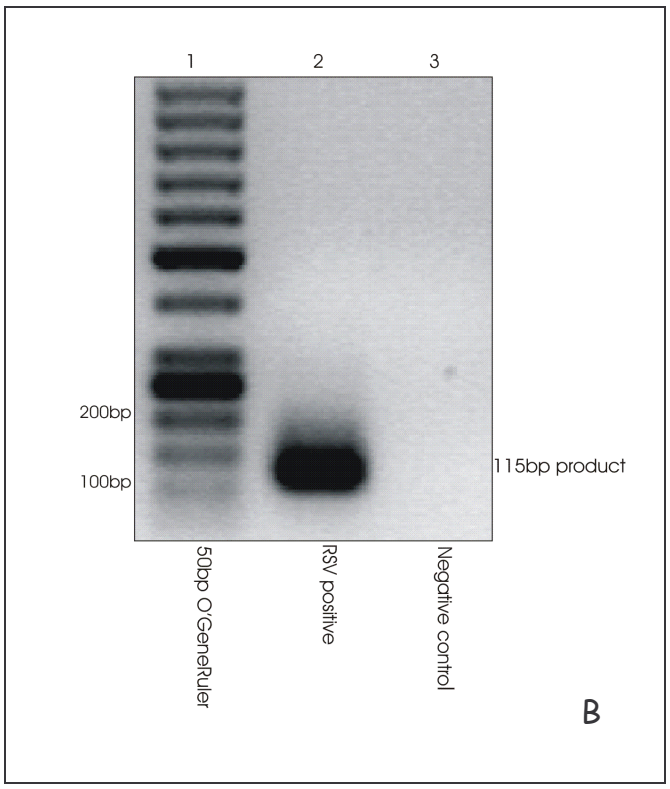

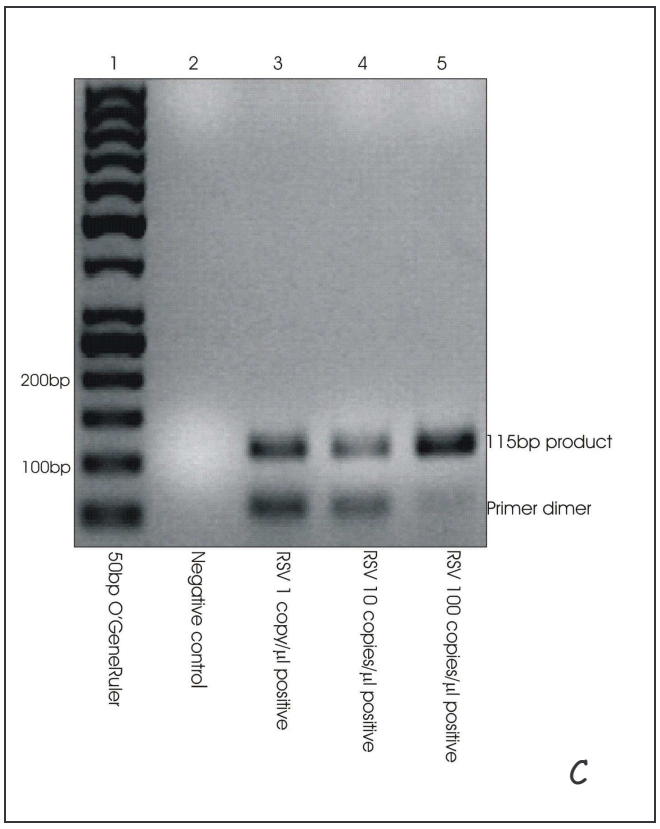

Figure B6: Agarose gel electrophoresis of RSV

(A) Positive control using SYBR Green I; **(B)** Positive control using TaqMan probes; and **(C)** Sensitivity assay performed on plasmids using TaqMan probes.

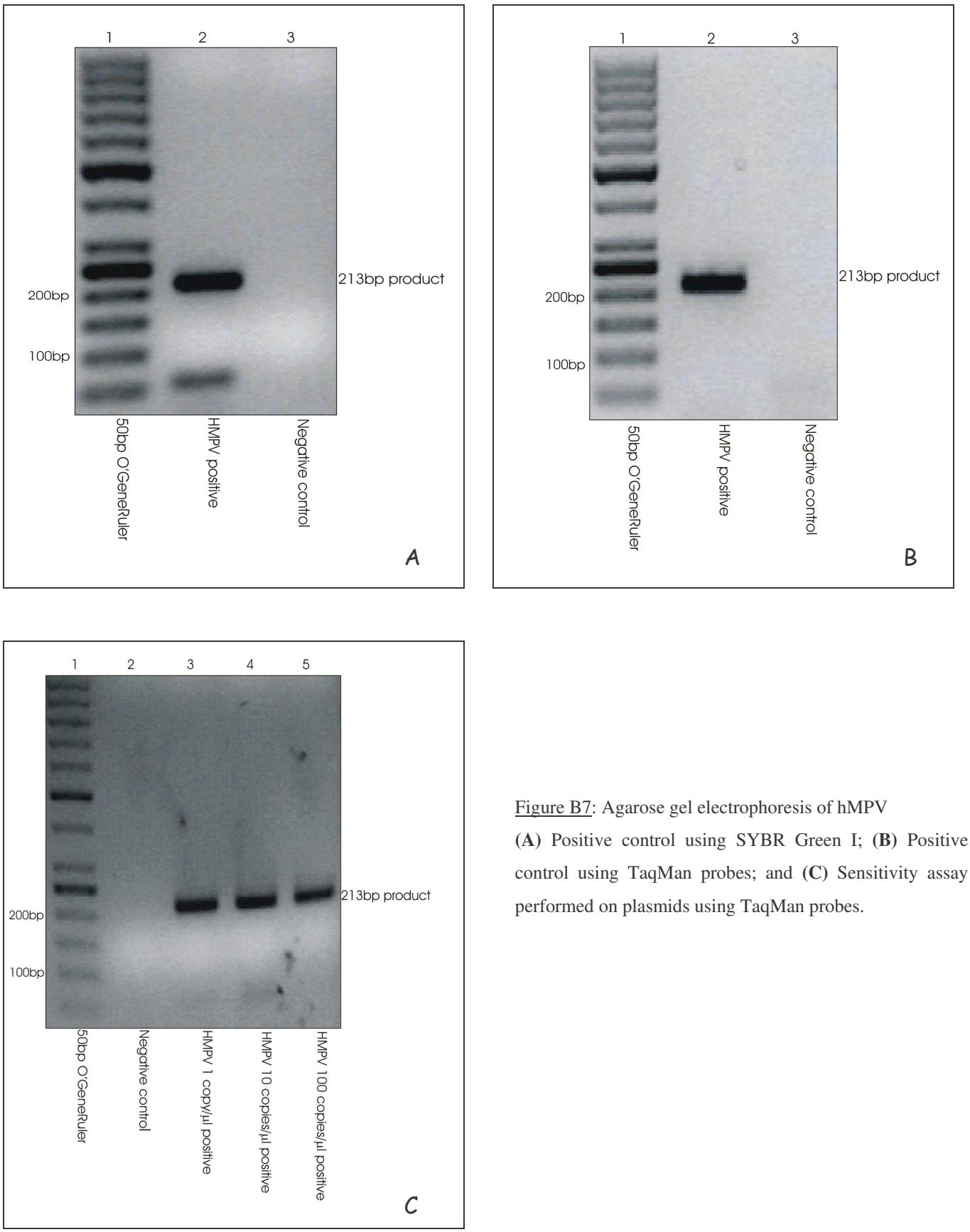

Figure B7: Agarose gel electrophoresis of hMPV

(A) Positive control using SYBR Green I; **(B)** Positive control using TaqMan probes; and **(C)** Sensitivity assay performed on plasmids using TaqMan probes.

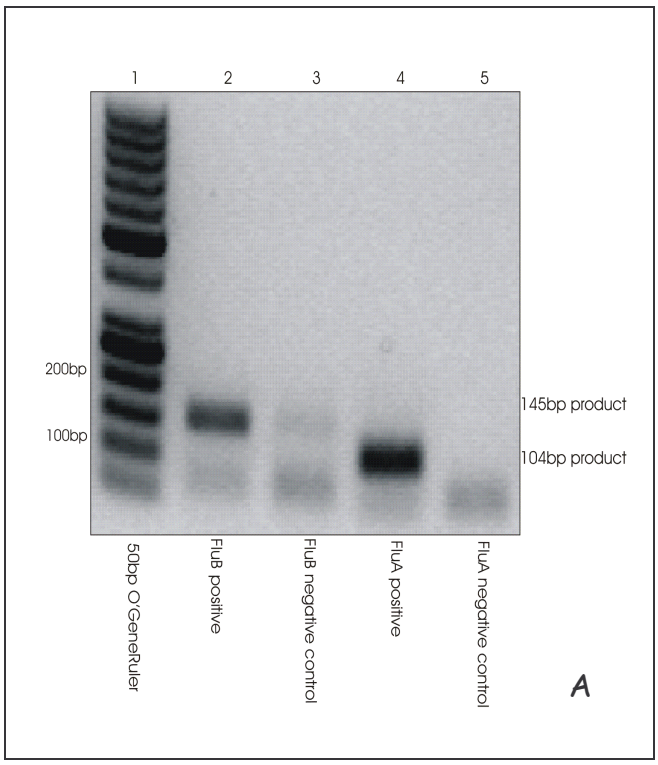
1
2
3
4
5
200bp
100bp
145bp product
104bp product
50bp O'GeneRuler
FluB positive
FluB negative control
FluA positive
FluA negative control
A

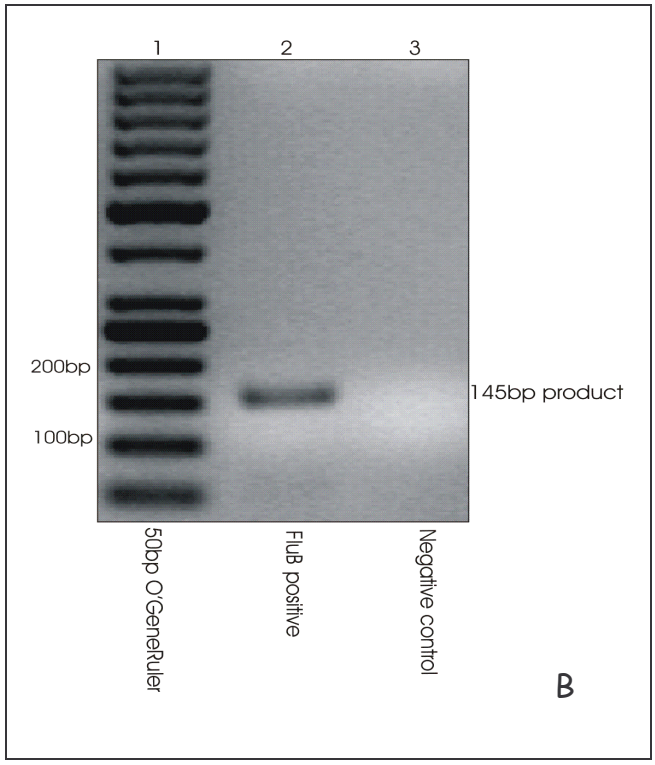
1
2
3
200bp
100bp
145bp product
50bp O'GeneRuler
FluB positive
Negative control
B

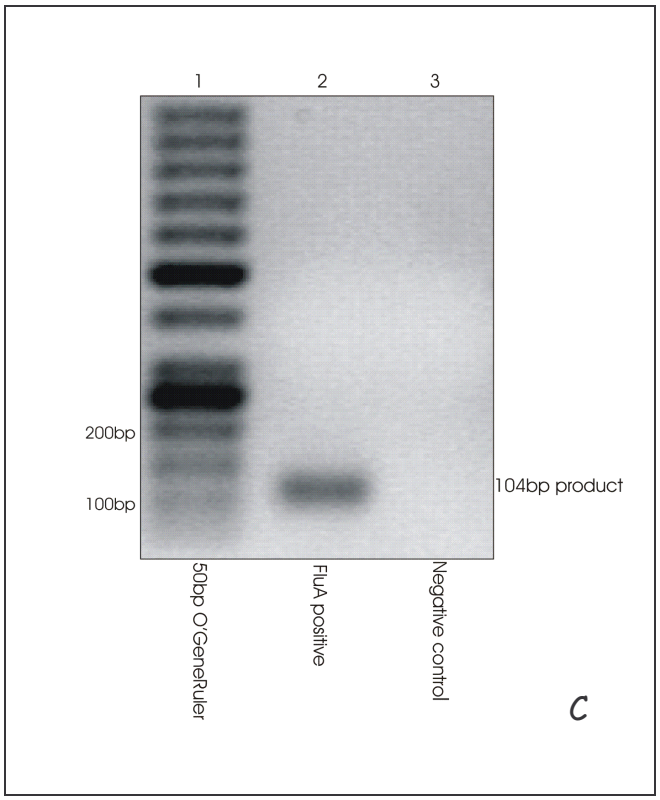
1
2
3
200bp
100bp
104bp product
50bp O'GeneRuler
FluA positive
Negative control
C

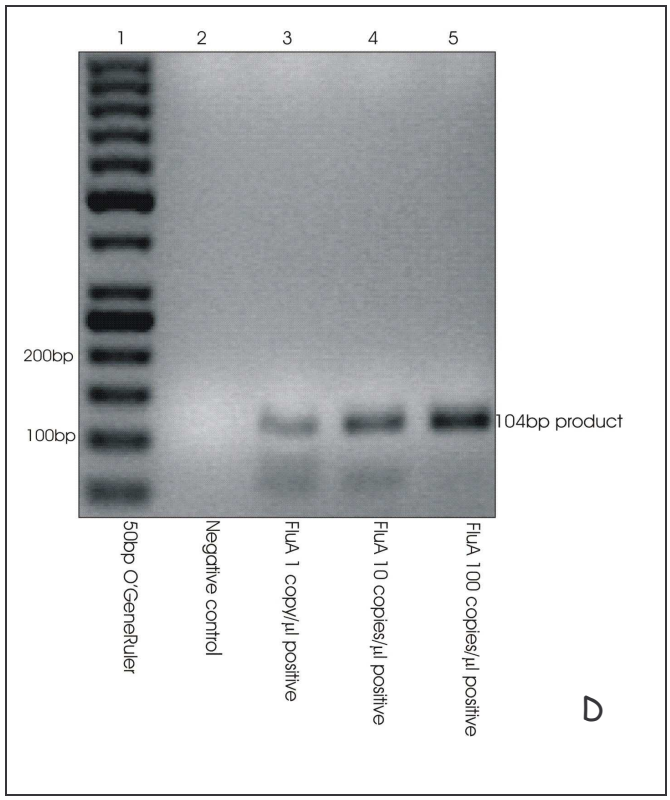
1
2
3
4
5
200bp
100bp
104bp product
50bp O'GeneRuler
Negative control
FluA 1 copy/µl positive
FluA 10 copies/µl positive
FluA 100 copies/µl positive
D

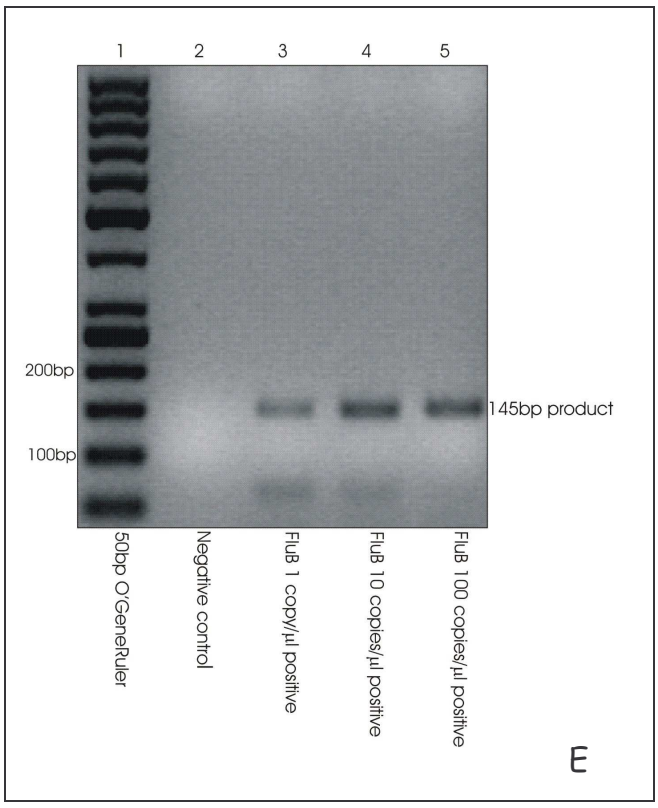

Figure B8: Agarose gel electrophoresis of **(A)** Positive controls of FluA and FluB using SYBR Green I;
(B) Positive control of FluB using TaqMan probes;
(C) Positive control of FluA using TaqMan probes;
(D) Sensitivity assay of FluA performed on plasmids using TaqMan probes; and **(E)** Sensitivity assay of FluB performed on plasmids using TaqMan probes.

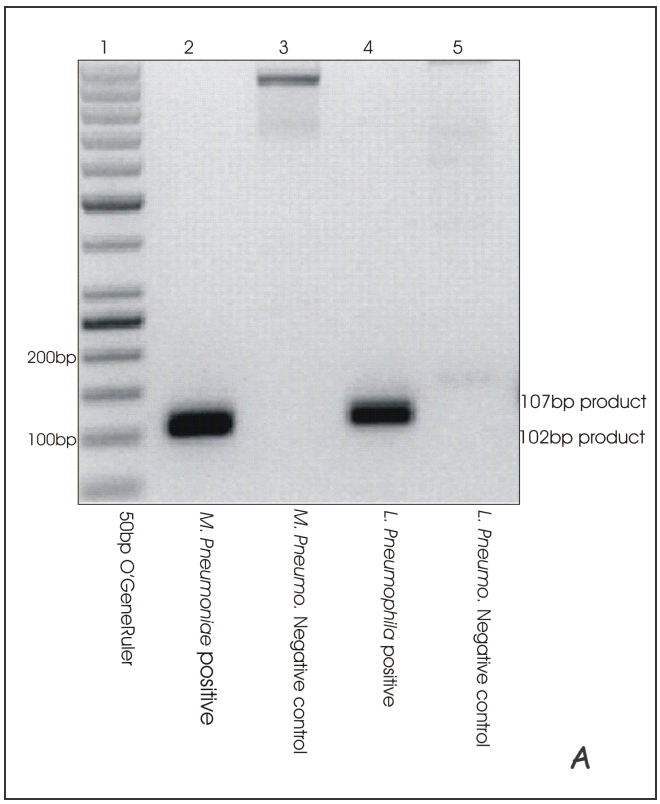
1
2
3
4
5
200bp
100bp
107bp product
102bp product
50bp O'GeneRuler
M. Pneumoniae positive
M. Pneumo. Negative control
L. Pneumophila positive
L. Pneumo. Negative control
A

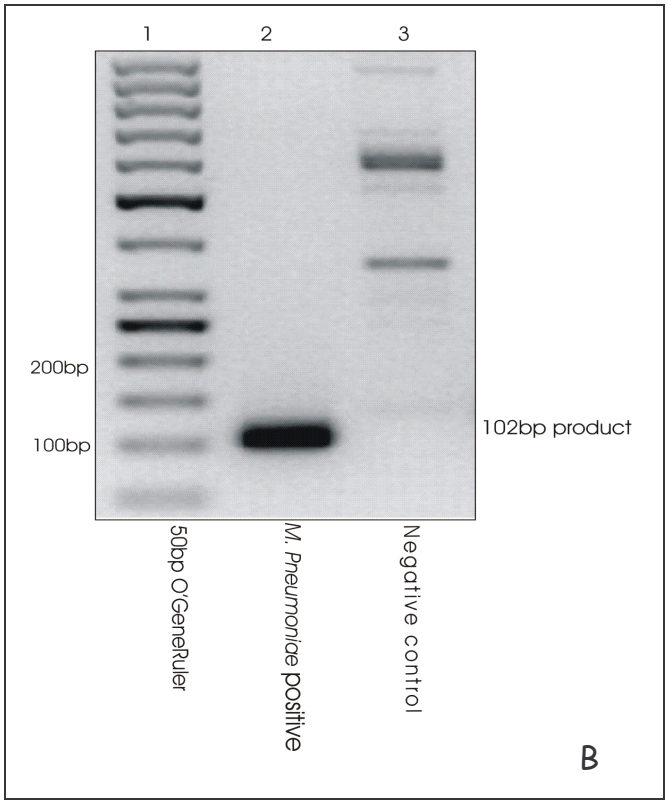
1
2
3
200bp
100bp
102bp product
50bp O'GeneRuler
M. Pneumoniae positive
Negative control
B

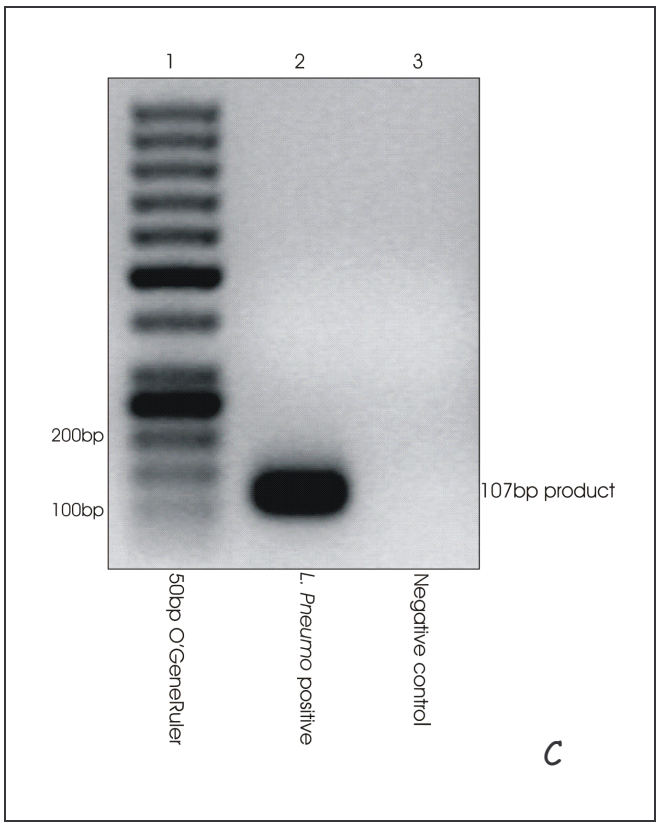
1
2
3
200bp
100bp
107bp product
50bp O'GeneRuler
L. Pneumo positive
Negative control
C

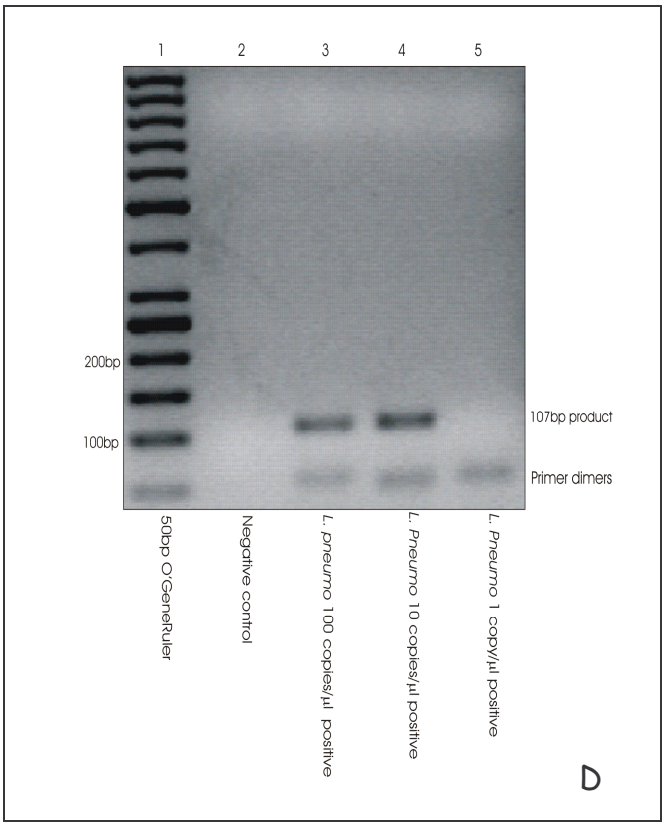
1
2
3
4
5
200bp
100bp
107bp product
Primer dimers
50bp O'GeneRuler
Negative control
L. pneumo 100 copies/µl positive
L. Pneumo 10 copies/µl positive
L. Pneumo 1 copy/µl positive
D

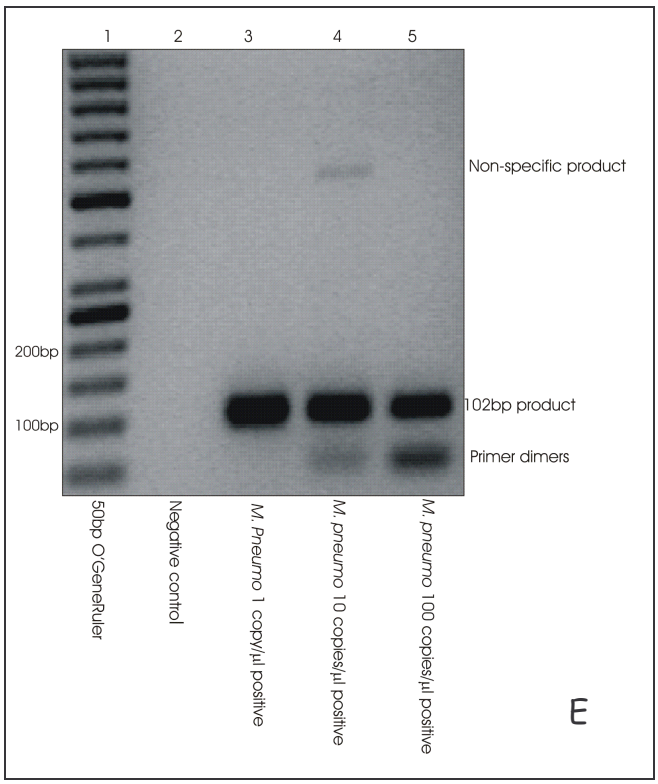

Figure B9: Agarose gel electrophoresis of **(A)** Positive controls of *M. pneumoniae* and *L. pneumophila* using SYBR Green I; **(B)** Positive control of *M. pneumoniae* using TaqMan probes; **(C)** Positive control of *L. pneumophila* using TaqMan probes; **(D)** Sensitivity assay of *L. pneumophila* performed on plasmids using TaqMan probes; and **(E)** Sensitivity assay of *M. pneumoniae* performed on plasmids using TaqMan probes.

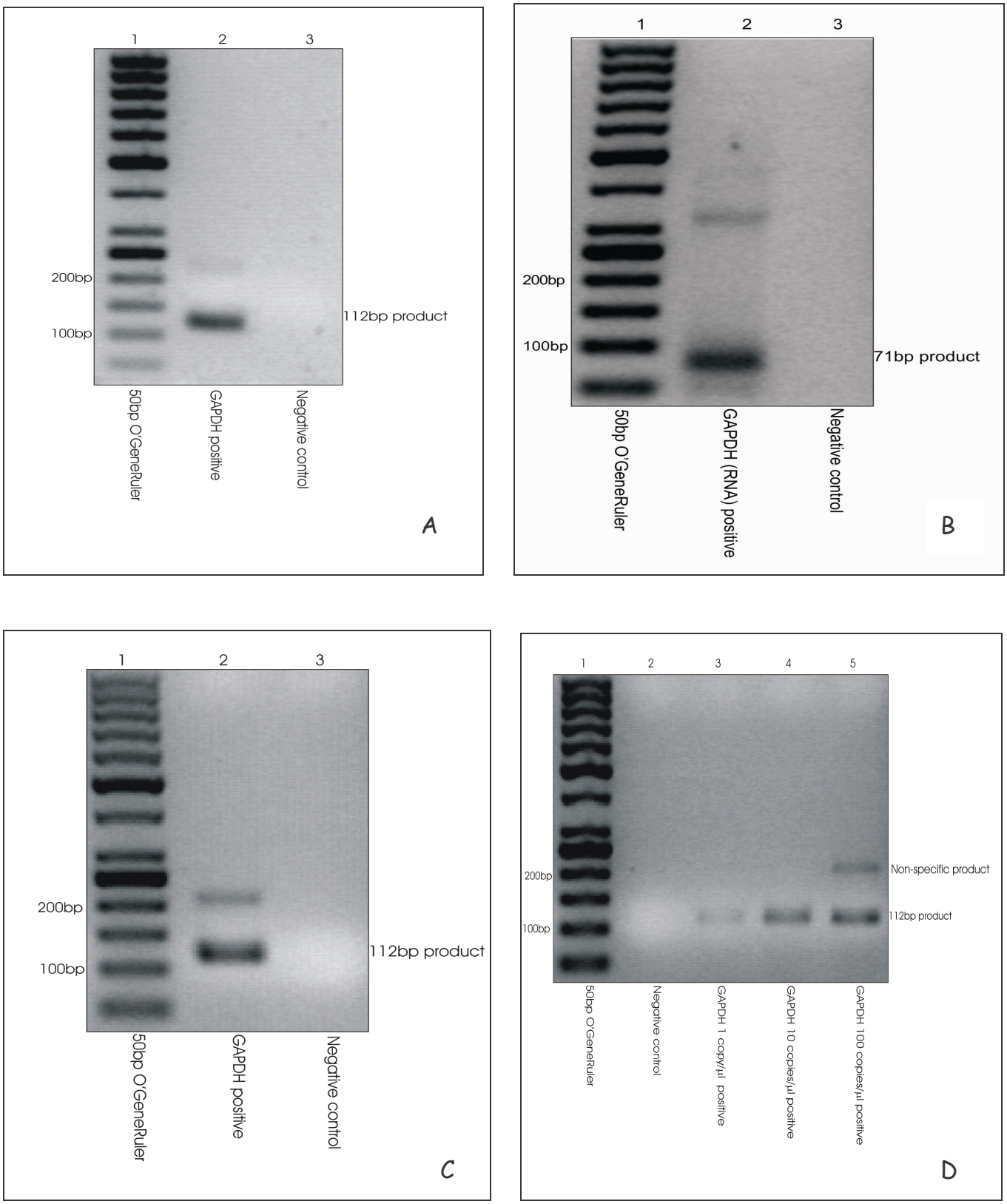

Figure B10: Agarose gel electrophoresis of **(A)** Positive control of GAPDH (DNA) using SYBR Green I; **(B)** Positive control of GAPDH (RNA) using SYBR Green I; **(C)** Positive control of GAPDH (DNA) using TaqMan probes; and **(D)** Sensitivity assay of GAPDH (DNA) performed on plasmids using TaqMan probes.

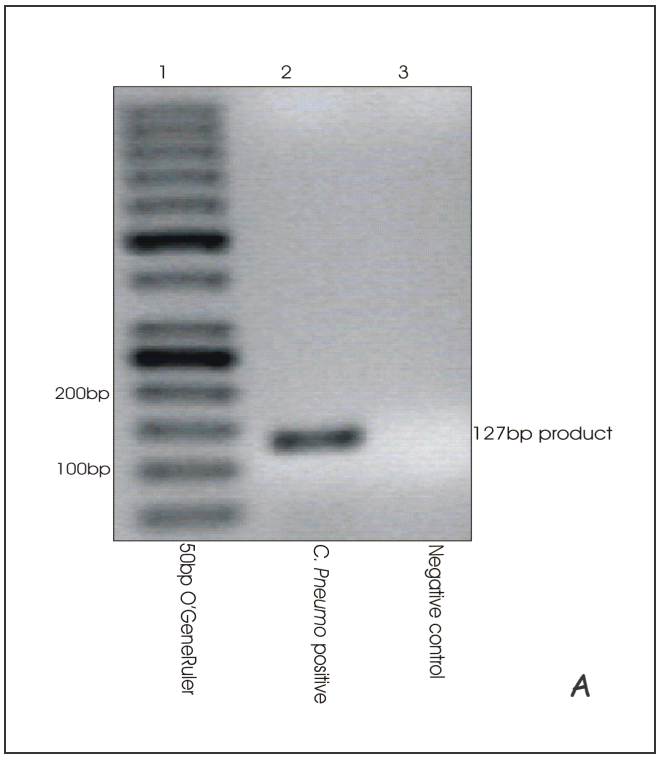

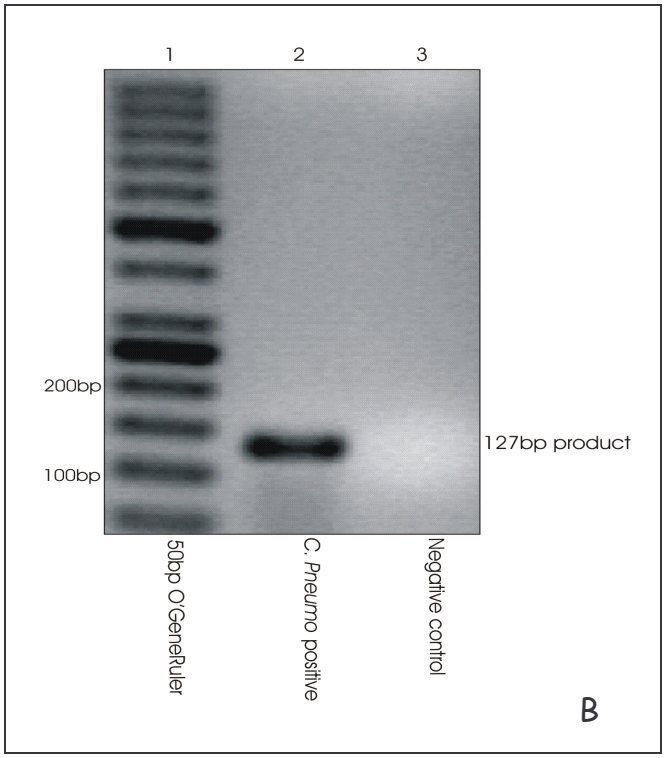

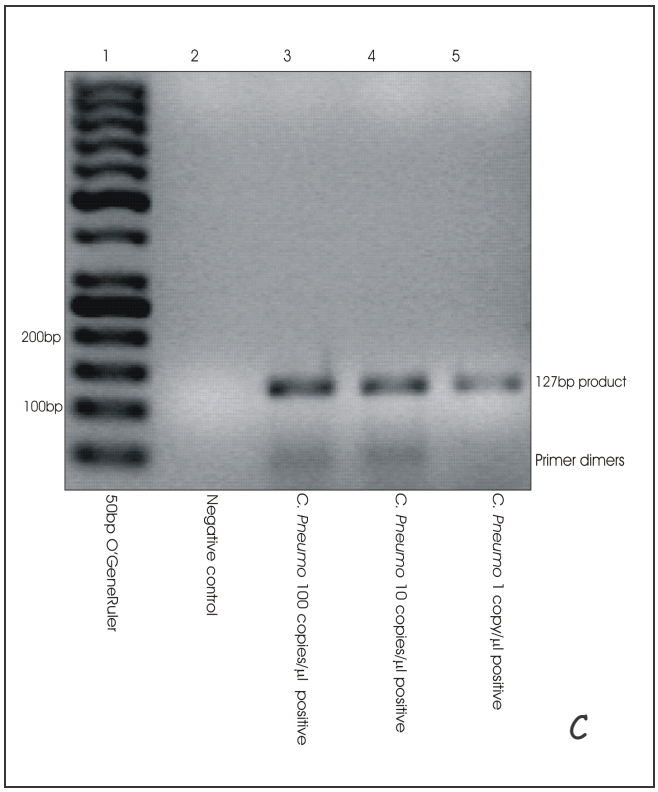

Figure B11: Agarose gel electrophoresis of *C. pneumoniae* **(A)** Positive control using SYBR Green I; **(B)** Positive control using TaqMan probes; and **(C)** Sensitivity assay performed on plasmids using TaqMan probes.

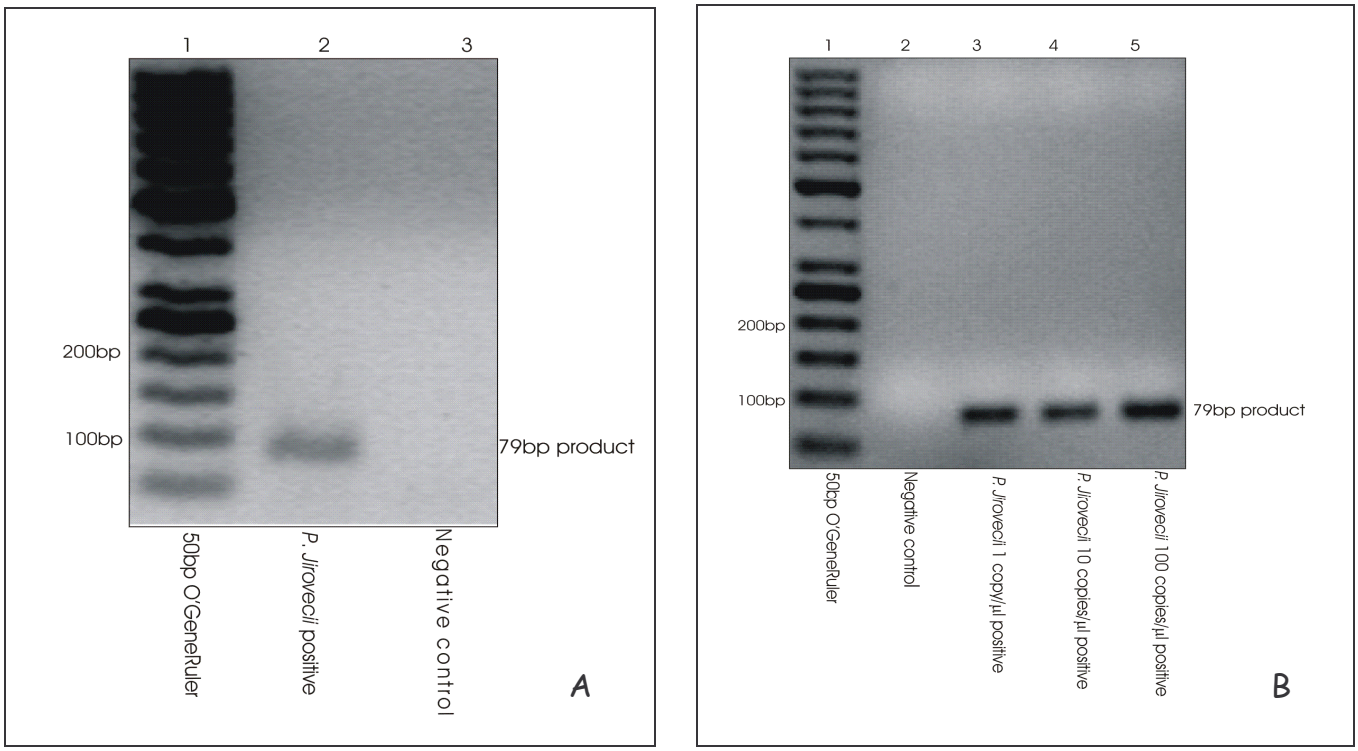

Figure B12: Agarose gel electrophoresis of *P. jirovecii* **(A)** Positive control using SYBR Green I; **(B)** Sensitivity assay performed on plasmids using SYBR Green I.

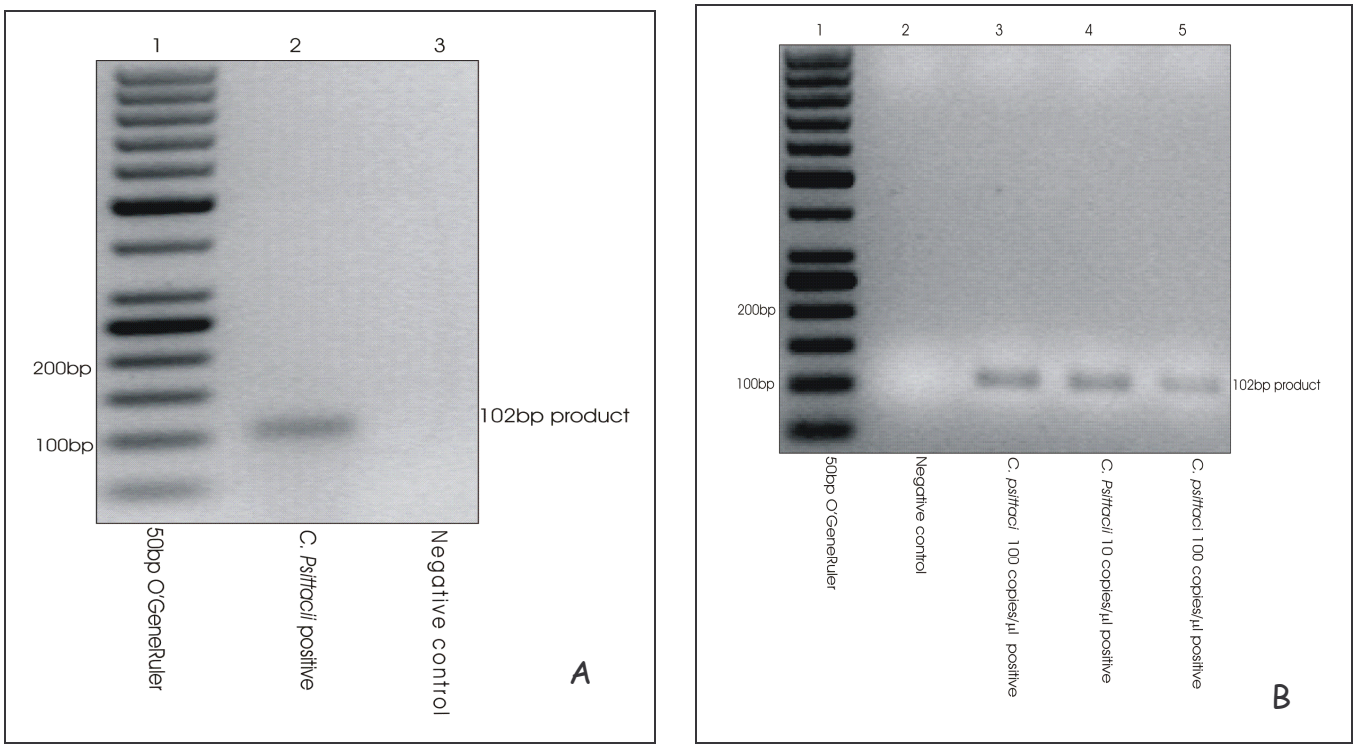

Figure B13: Agarose gel electrophoresis of *C. psittaci* **(A)** Positive control using SYBR Green I; **(B)** Sensitivity assay performed on plasmids using SYBR Green I.

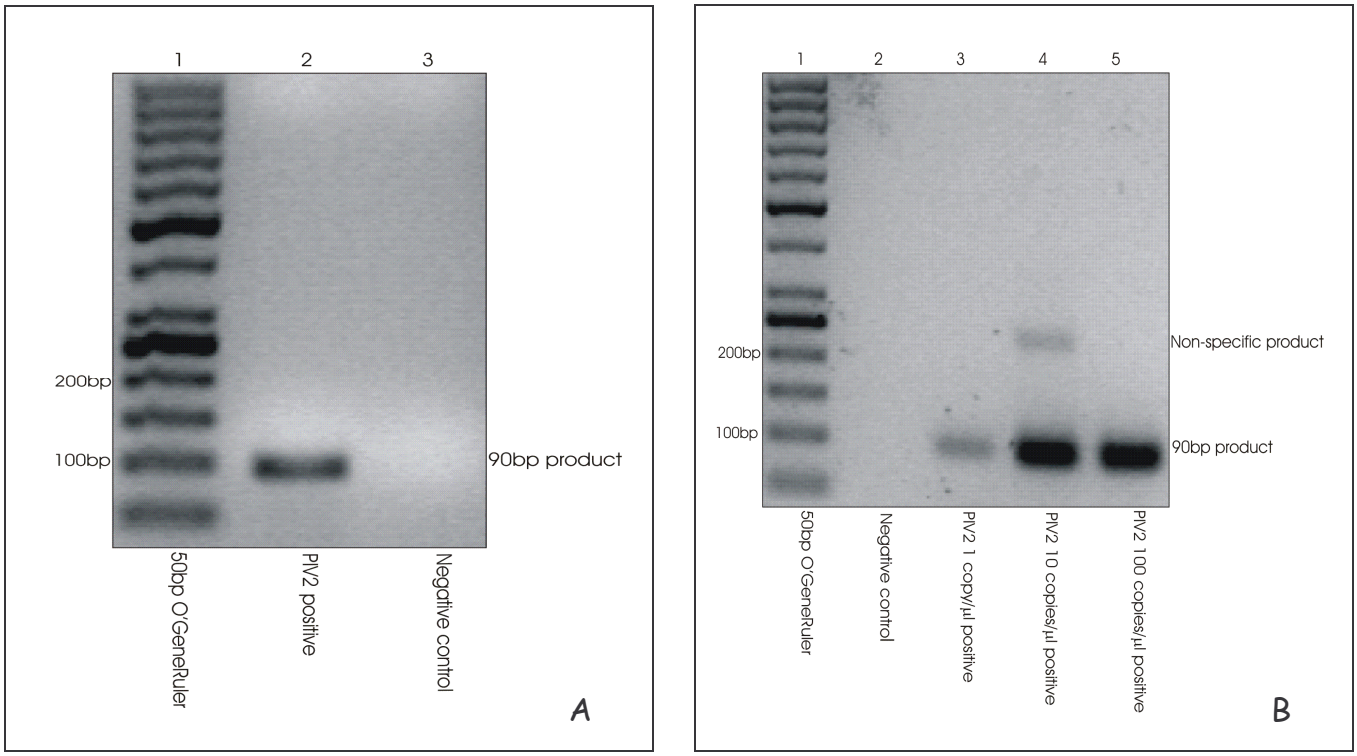

Figure B14: Agarose gel electrophoresis of PIV2 **(A)** Positive control using SYBR Green I; **(B)** Sensitivity assay performed on plasmids using SYBR Green I.

CHAPTER 7: APPENDIX C

7.3.Agarose gels of multiplex real-time PCR reactions: positive controls and sensitivity assays

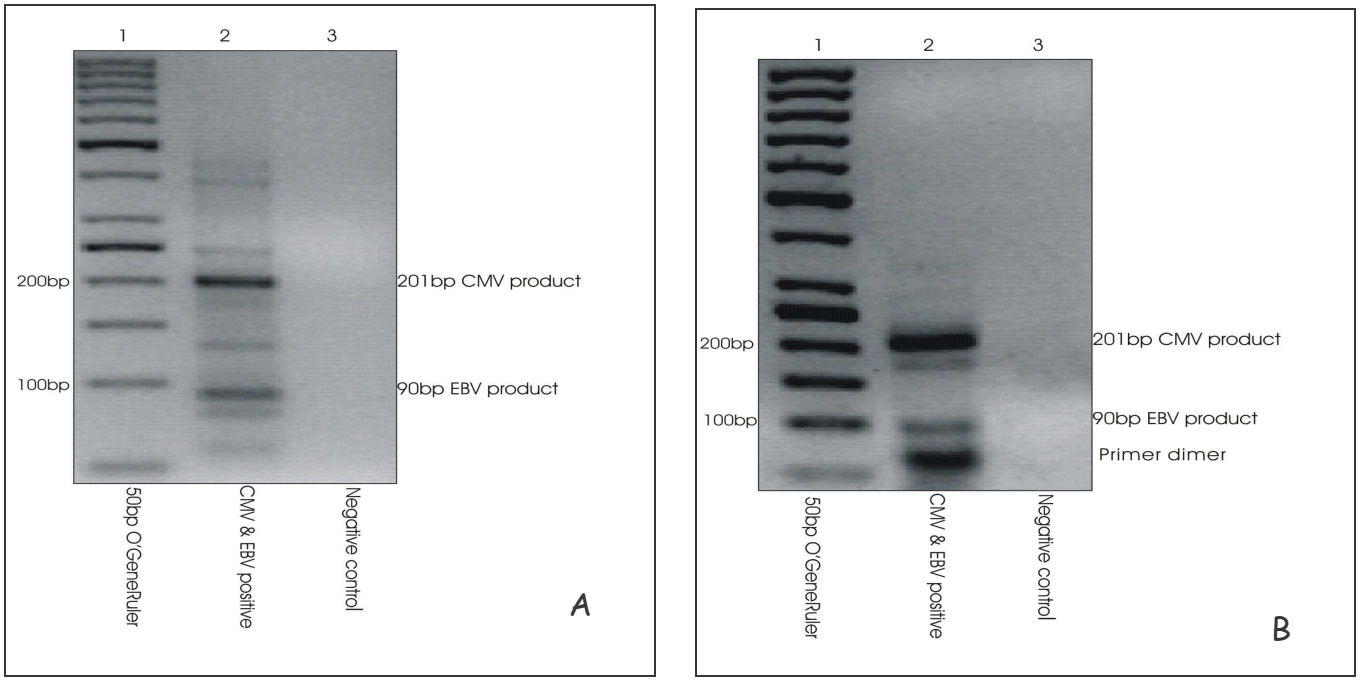

Figure C1: Agarose gel of CMV and EBV multiplex reaction obtained using TaqMan probes on **(A)** Positive controls; **(B)** Plasmids at the lowest detectable concentration.

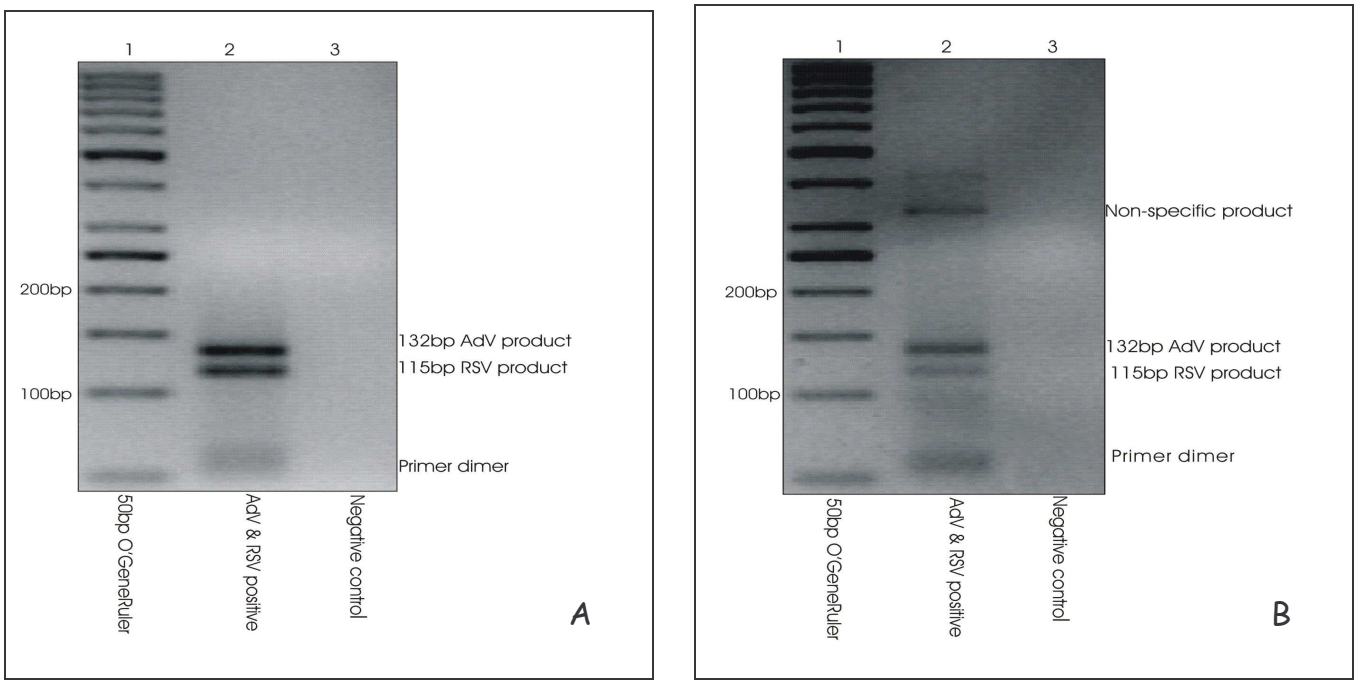

Figure C2: Agarose gel of AdV and RSV multiplex reaction obtained using TaqMan probes on **(A)** Positive controls; **(B)** Plasmids at the lowest detectable concentration.

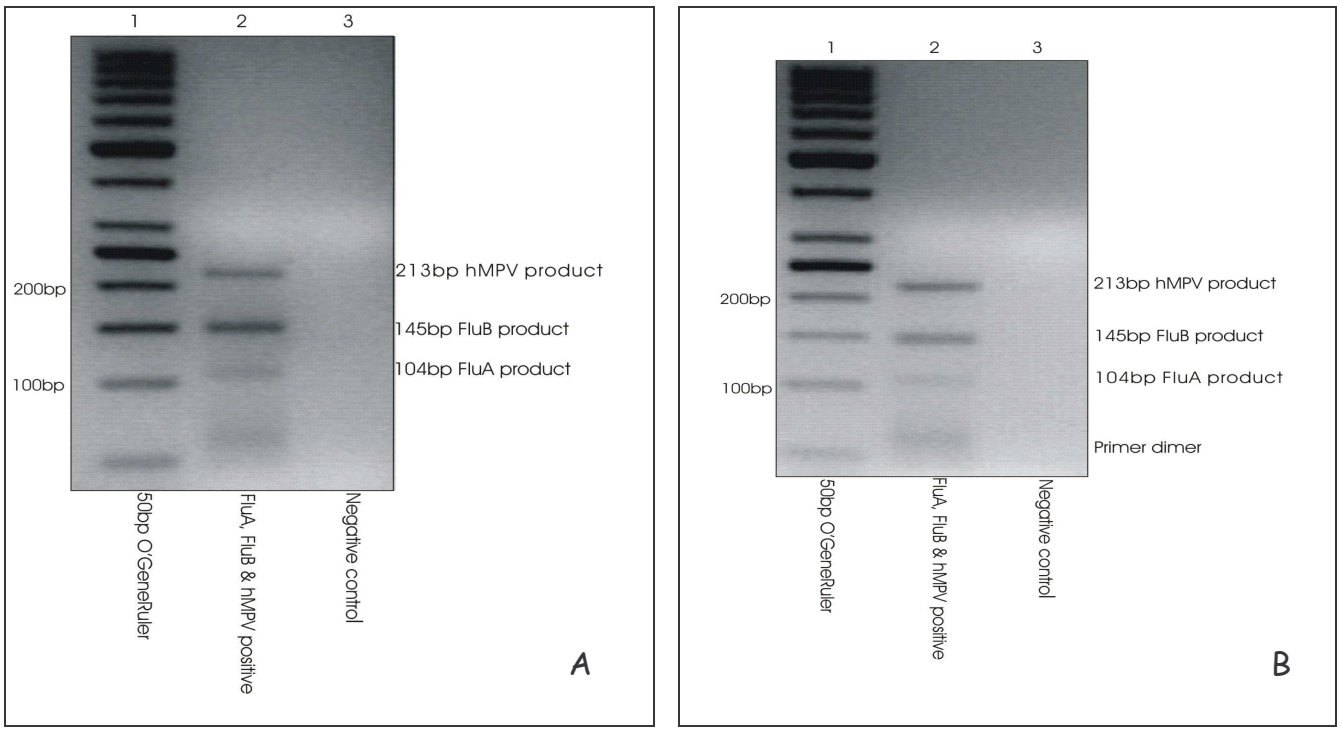

Figure C3: Agarose gel of FluA, FluB and hMPV multiplex reaction obtained using TaqMan probes on **(A)** Positive controls; **(B)** Plasmids at the lowest detectable concentration.

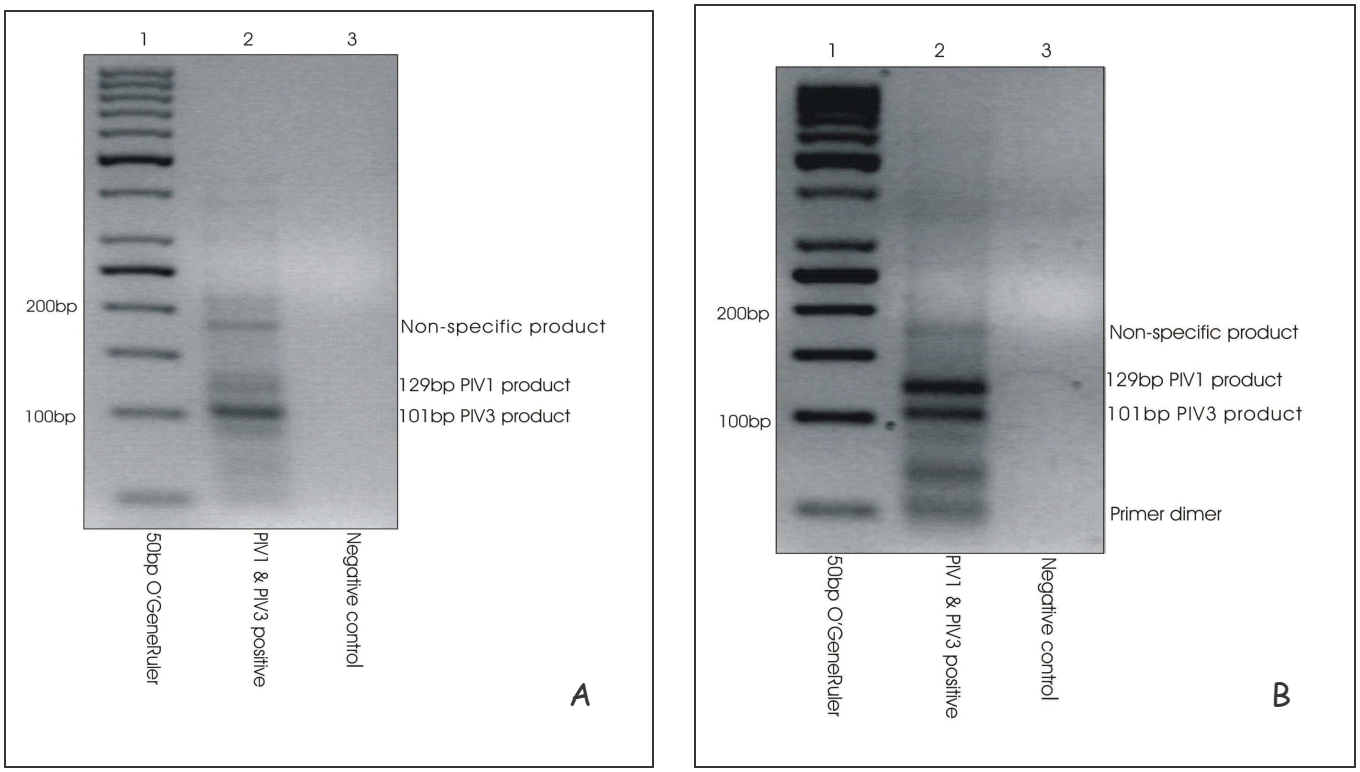

Figure C4: Agarose gel of PIV1 and PIV3 multiplex reaction obtained using TaqMan probes on **(A)** Positive controls; **(B)** Plasmids at the lowest detectable concentration.

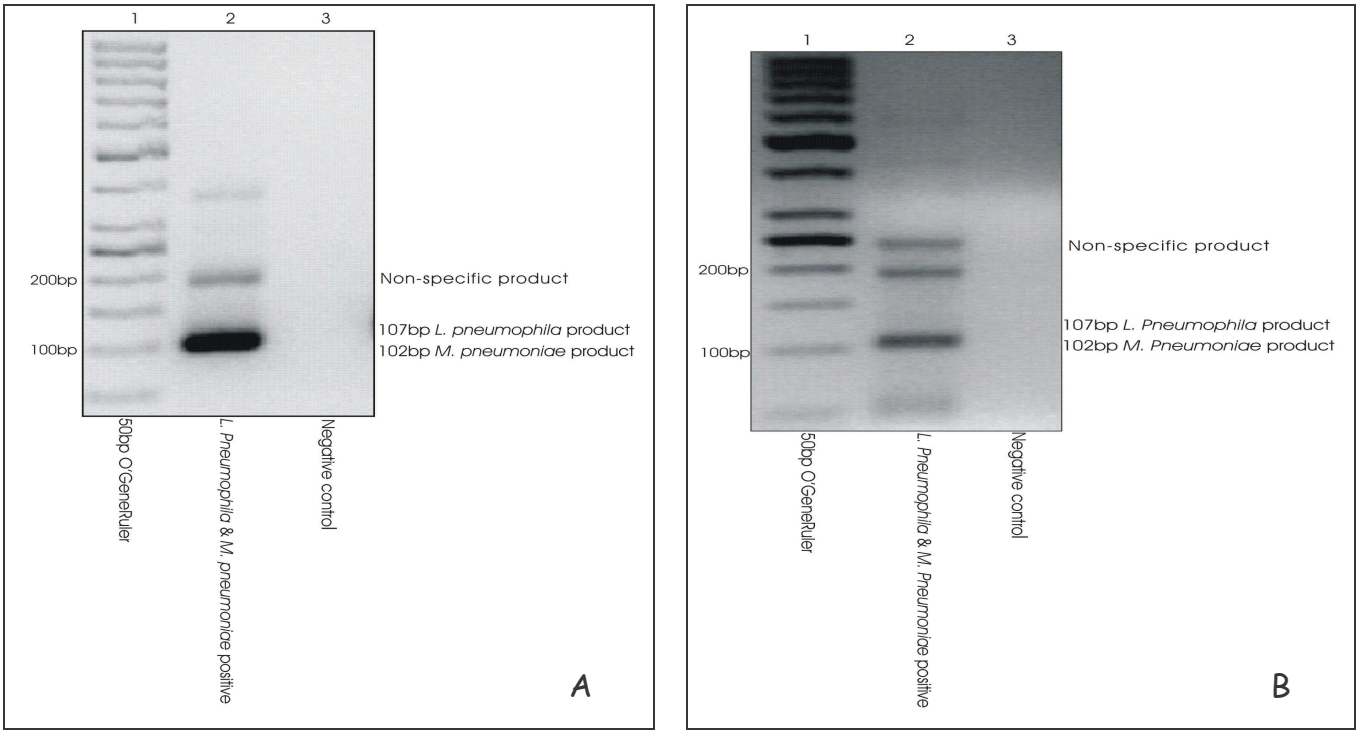

Figure C5: Agarose gel of *L. pneumophila* and *M. pneumoniae* multiplex reaction obtained using TaqMan probes on **(A)** Positive controls; (**B)** Plasmids at the lowest detectable concentration.

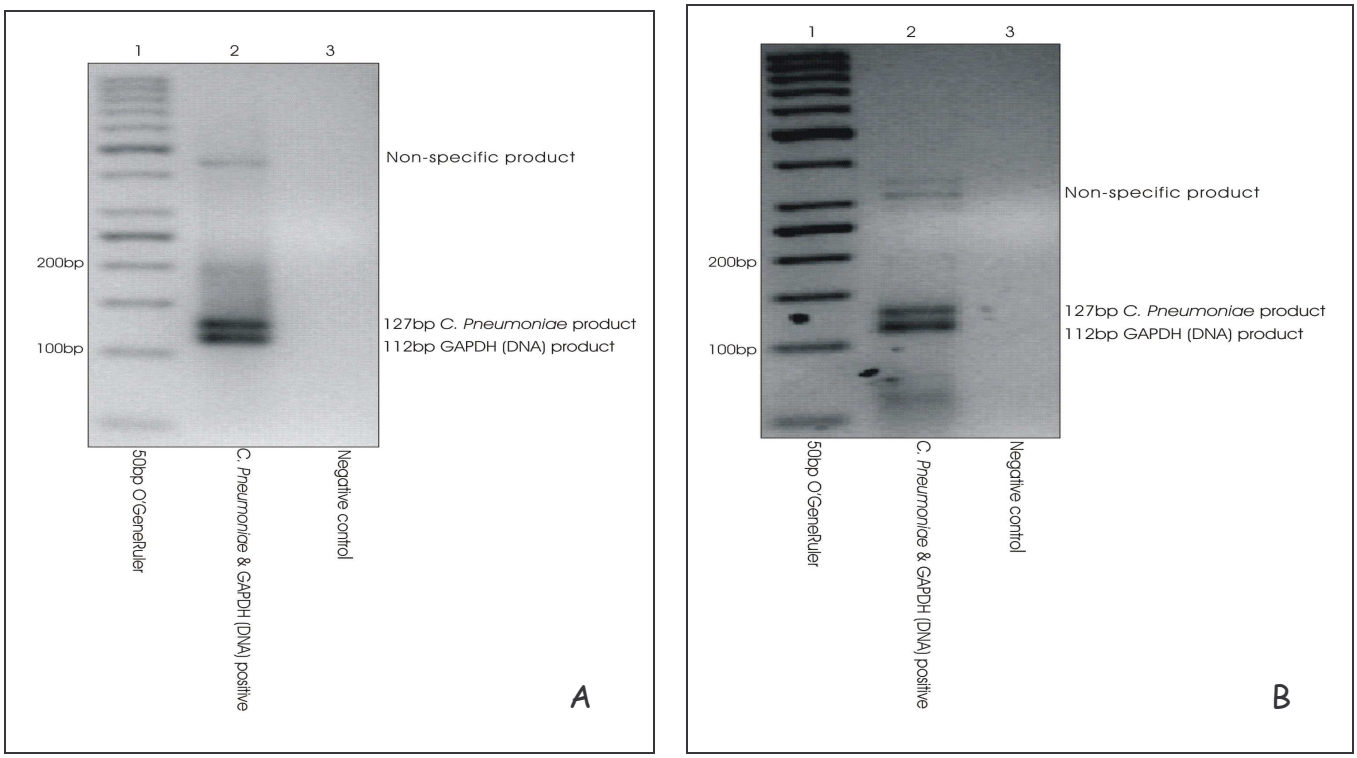

Figure C6: Agarose gel of *C. pneumoniae* and GAPDH (DNA) multiplex reaction obtained using TaqMan probes on **(A)** Positive controls; **(B)** Plasmids at the lowest detectable concentration.

CHAPTER 7: APPENDIX D

7.4. Agarose gels of real-time PCR reactions performed on patient samples and simulations

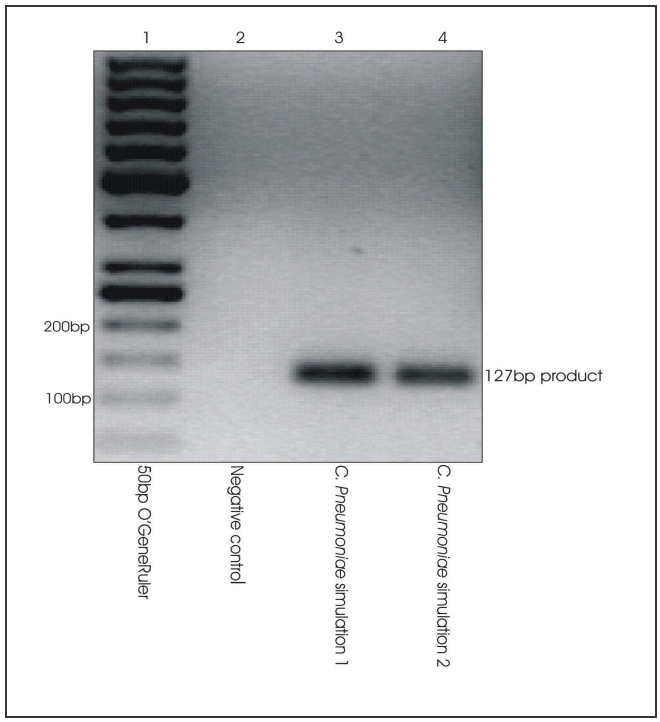

Figure D1: Agarose gel of *C. pneumoniae* real-time PCR product obtained from simulated sputum samples.

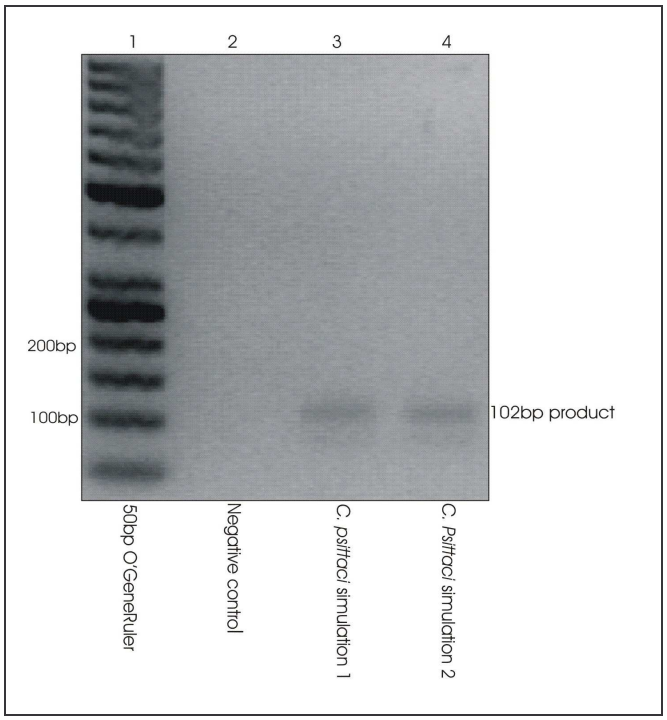

Figure D2: Agarose gel of *C. psittaci* real-time PCR product obtained from simulated sputum samples.

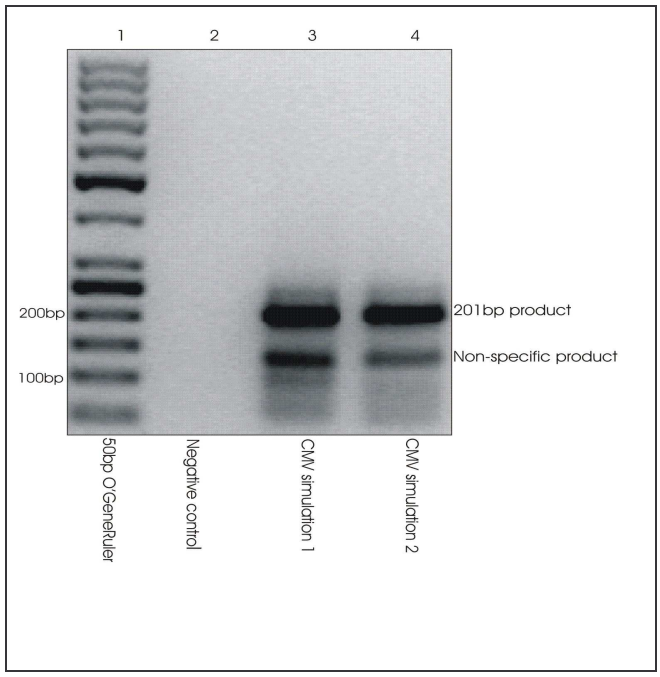

Figure D3: Agarose gel of CMV real-time PCR product obtained from simulated nasopharyngeal swabs.

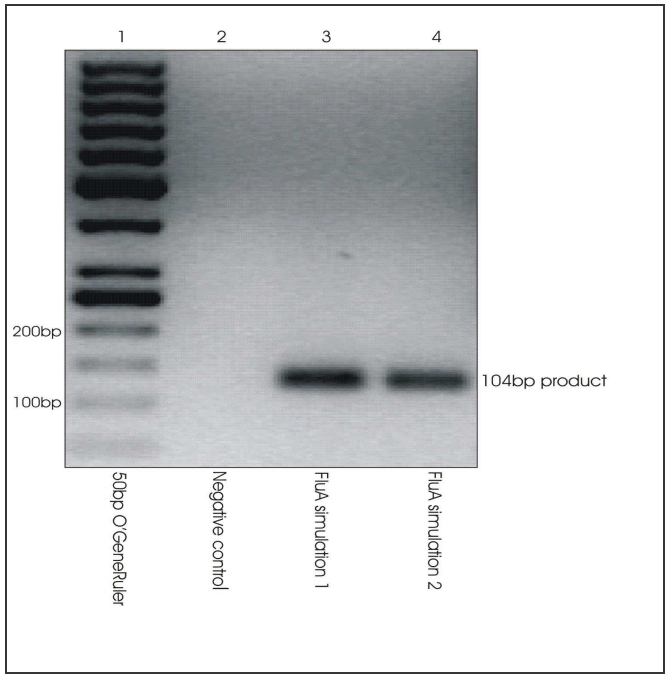

Figure D4: Agarose gel of FluA real-time PCR product obtained from simulated nasopharyngeal swabs.

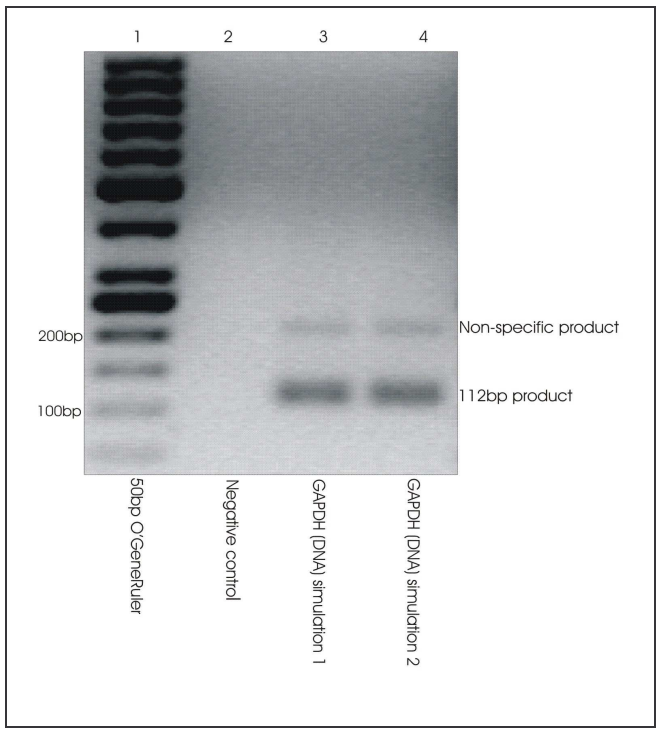

Figure D5: Agarose gel of GAPDH (DNA) real-time PCR product obtained from simulated sputum samples.

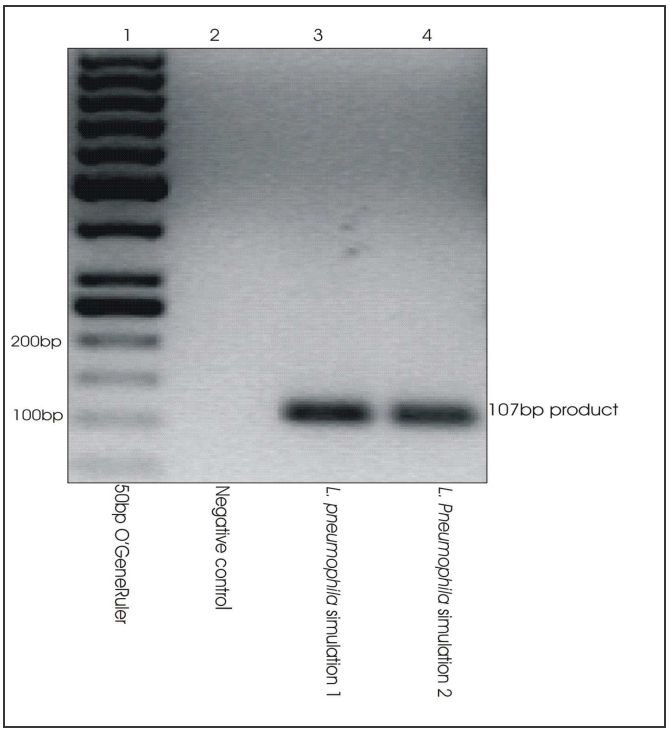

Figure D6: Agarose gel of ***L. pneumophila*** real-time PCR product obtained from simulated sputum samples.

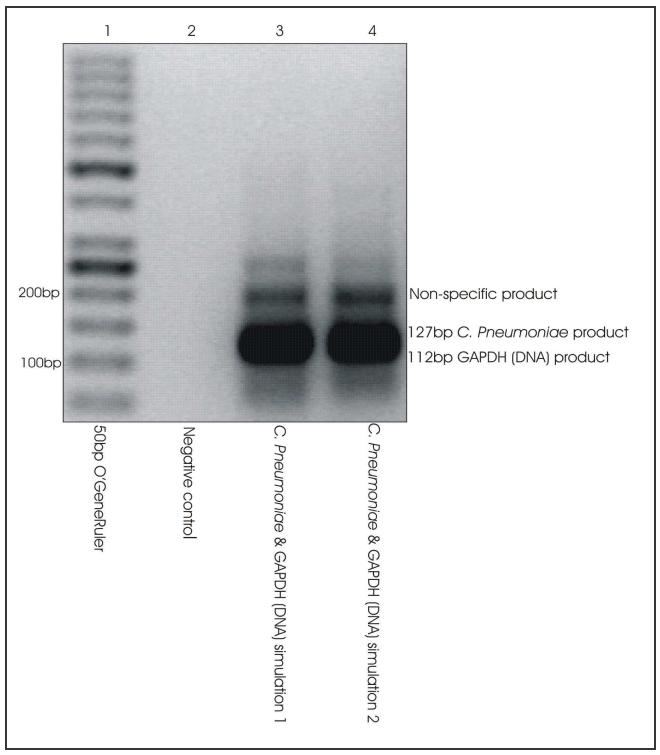

Figure D7: Agarose gel of ***C. pneumoniae*** and GAPDH (DNA) multiplex reaction obtained from simulated sputum samples.

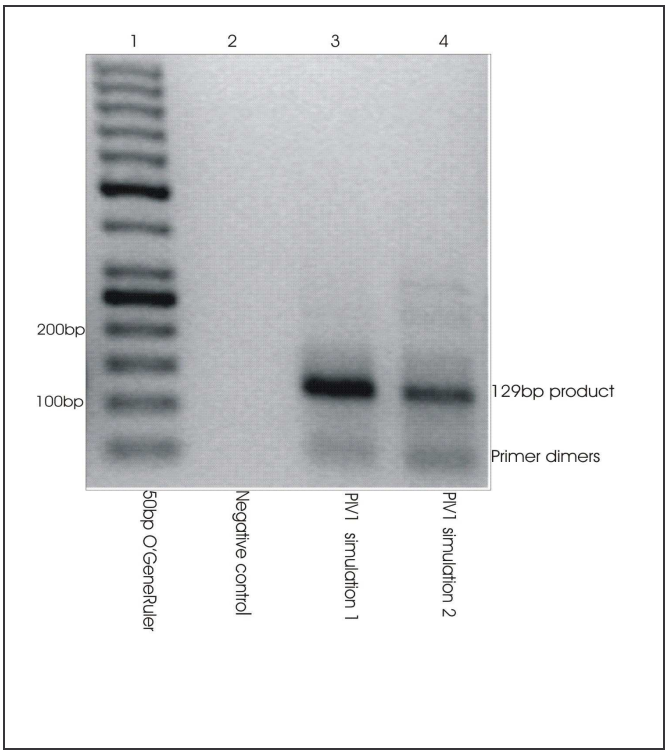

Figure D8: Agarose gel of PIV1 real-time PCR product obtained from simulated nasopharyngeal swabs.

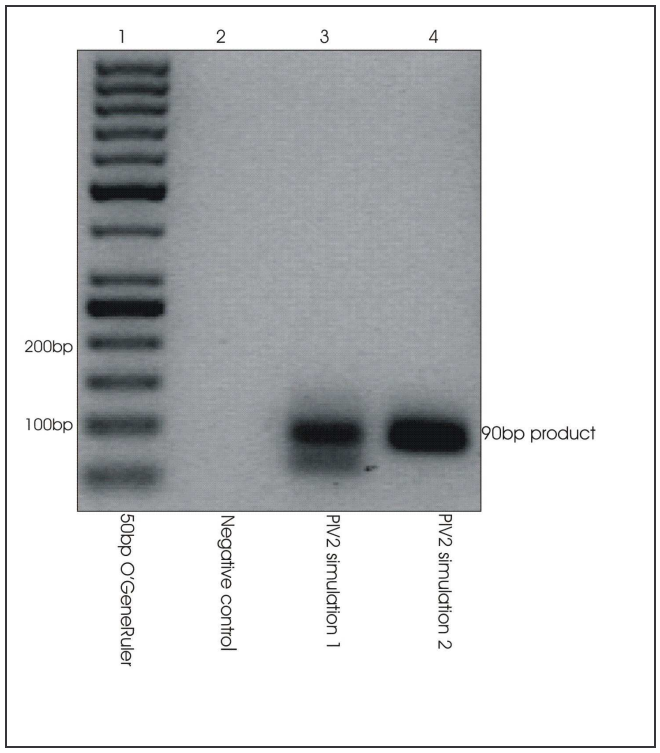

Figure D9: Agarose gel of PIV2 real-time PCR product obtained from simulated nasopharyngeal swabs.

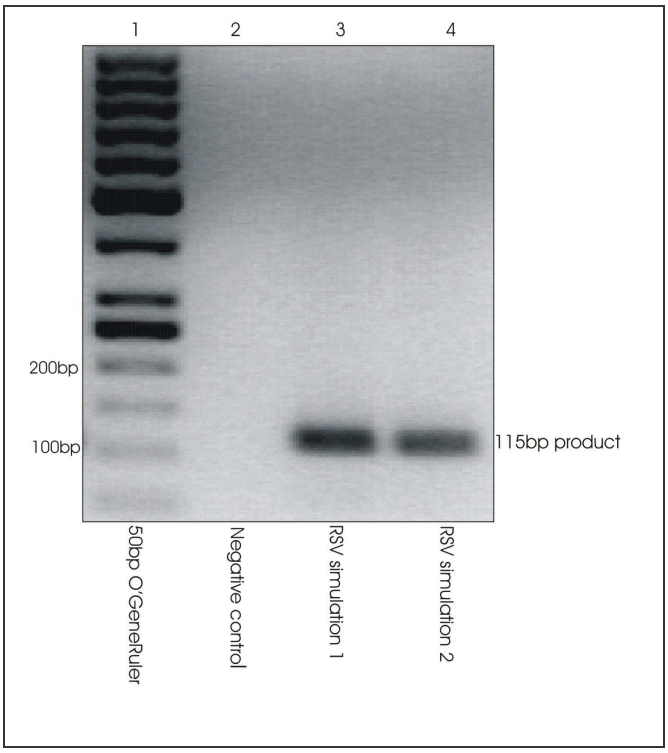

Figure D10: Agarose gel of RSV real-time PCR product obtained from simulated nasopharyngeal swabs.

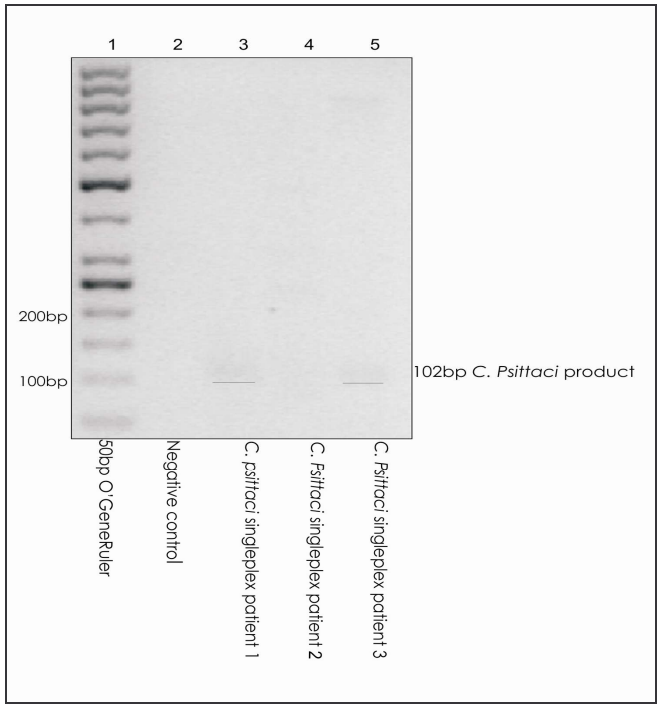

Figure D11: Agarose gel of *C. psittaci* real-time PCR product obtained from CAP patient sputum samples.

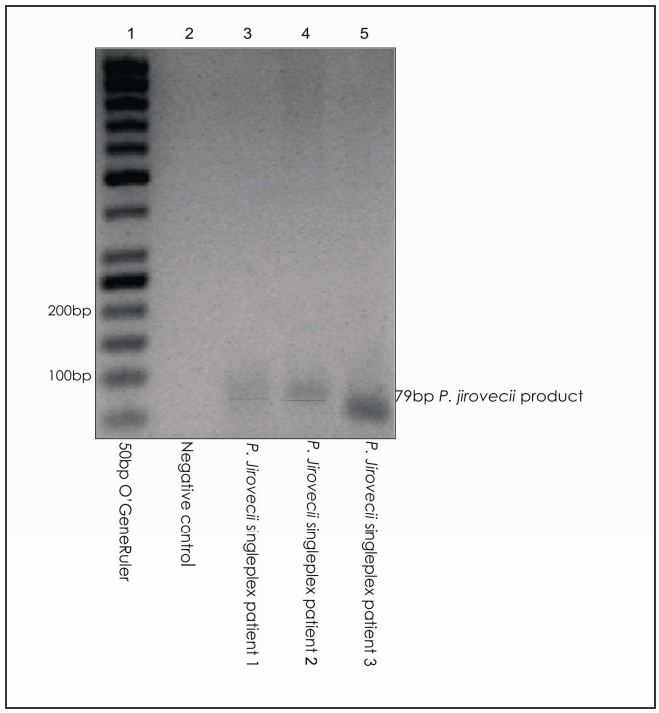

Figure D12: Agarose gel of *P. jirovecii* real-time PCR product obtained from CAP patient sputum samples.

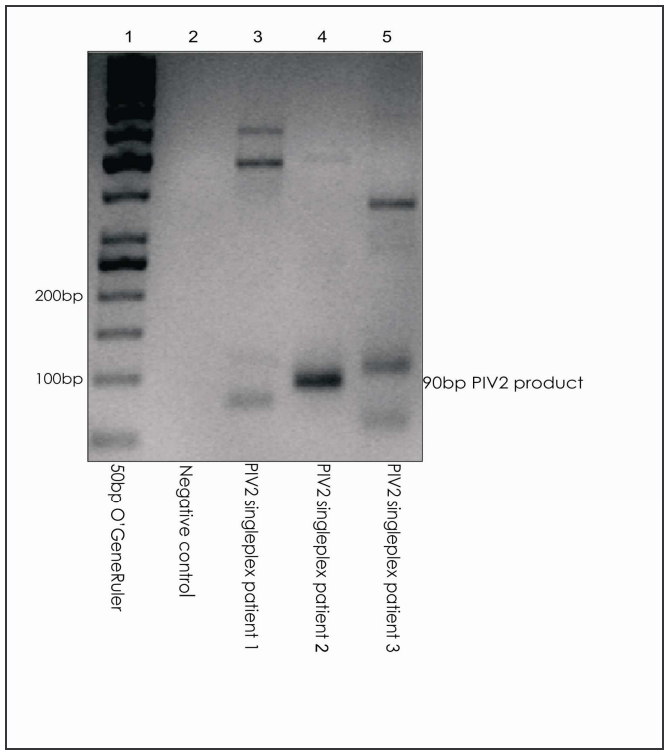

Figure D13: Agarose gel of PIV2 real-time PCR product obtained from CAP patient nasopharyngeal swabs.

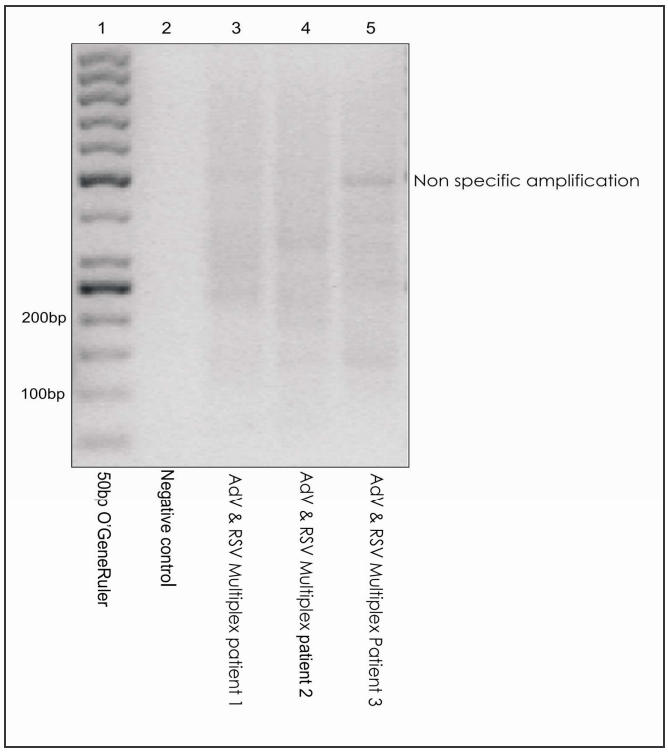

Figure D14: Agarose gel of AdV and RSV multiplex real-time PCR product obtained from CAP patient nasopharyngeal swabs.

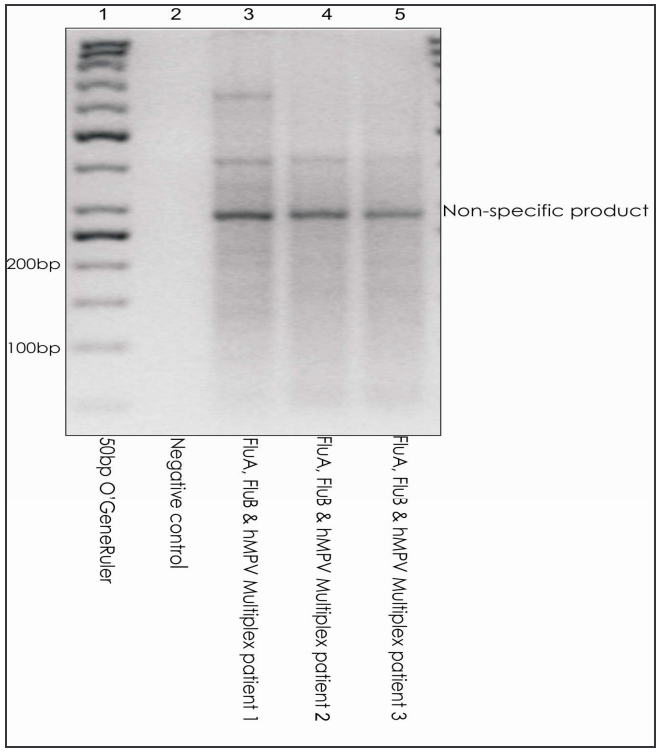

Figure D15: Agarose gel of FluA, FluB and hMPV multiplex real-time PCR product obtained from CAP patient nasopharyngeal swabs.

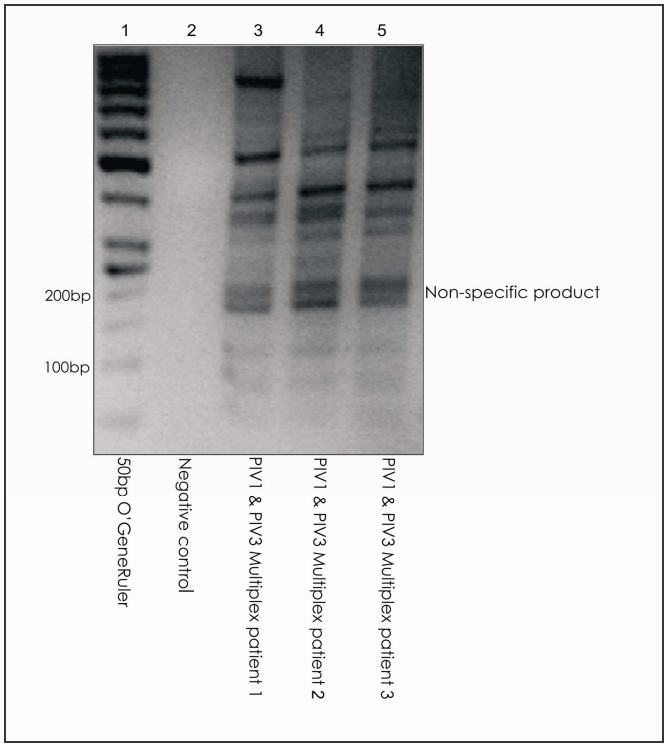

Figure D16: Agarose gel of PIV1 and PIV3 multiplex real-time PCR product obtained from CAP patient nasopharyngeal swabs.

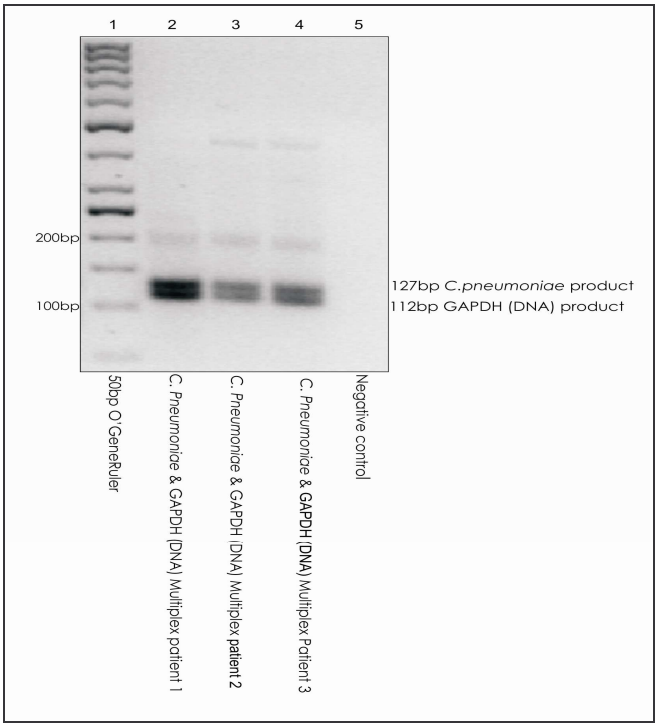

Figure D17: Agarose gel of *C. pneumoniae* and GAPDH (DNA) multiplex real-time PCR product obtained from CAP patient sputum samples.

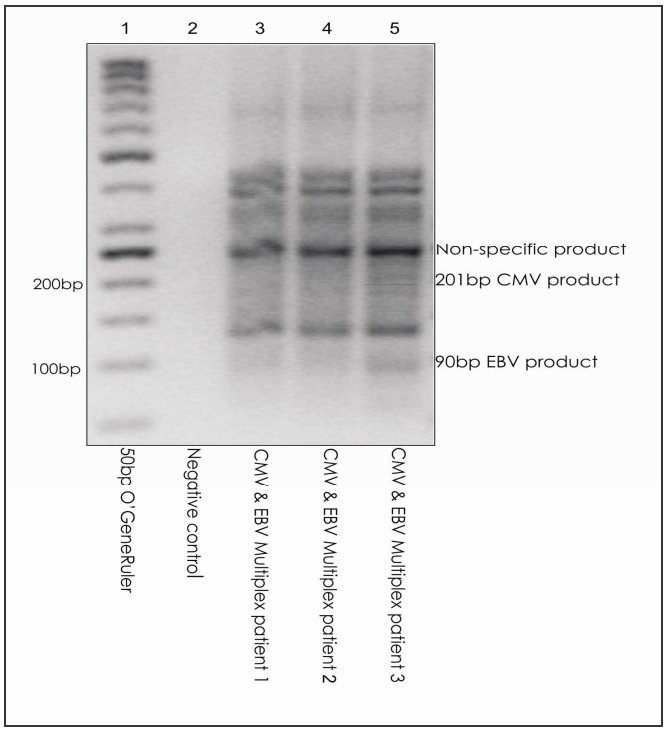

Figure D18: Agarose gel of CMV and EBV multiplex real-time PCR product obtained from CAP patient nasopharyngeal swabs.

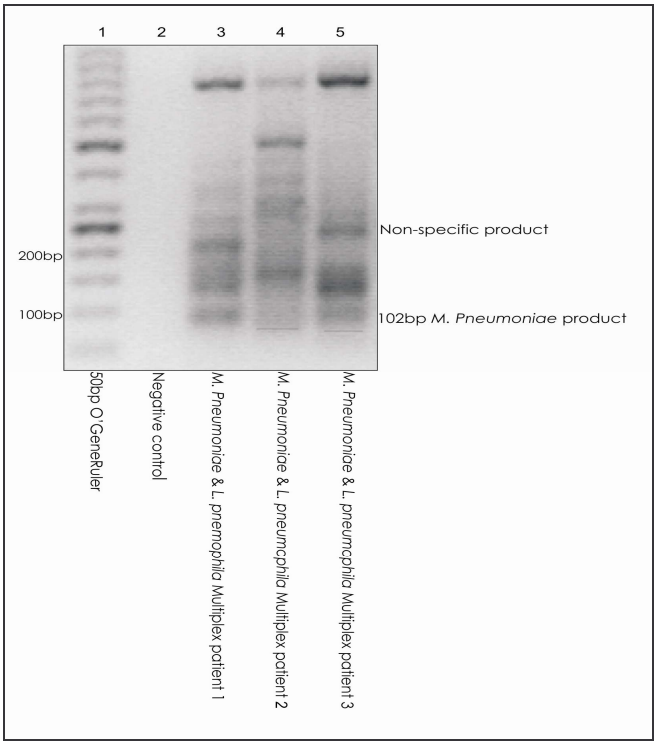

Figure D19: Agarose gel of *M. pneumoniae* and *L. pneumophila* multiplex real-time PCR product obtained from CAP patient sputum samples.

CHAPTER 7: APPENDIX E

7.5. Real-time PCR results for patient samples and simulations

7.5.1. Pathogen detection in simulated samples

7.5.1.1. Singleplex reactions

a. GAPDH (DNA)

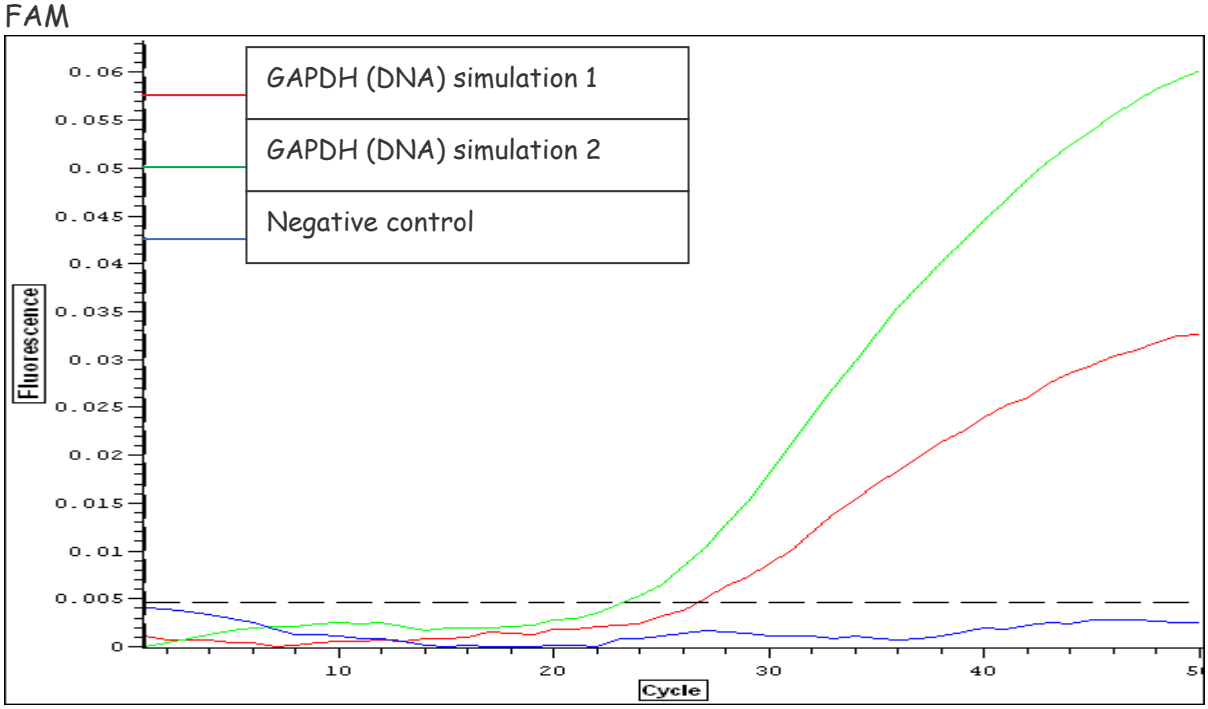

Figure E1: Fluorescence graph of GAPDH (DNA) singleplex reaction performed on nucleic acids extracted from spiked sputum samples. Real-time PCR was carried out in duplicate using TaqMan probes. Shown is a plot of change in fluorescence signal versus cycle number.

b. Influenza A virus

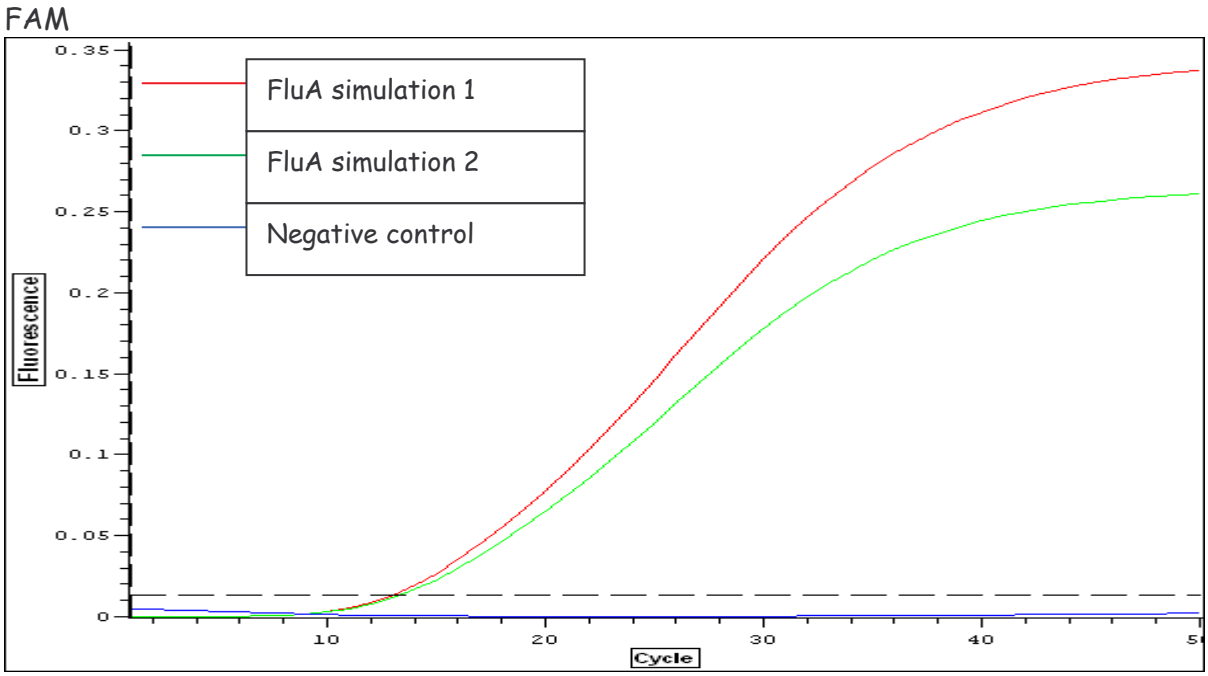

Figure E2: Fluorescence graph of FluA singleplex reaction performed on nucleic acids extracted from spiked nasopharyngeal swabs. Real-time PCR was carried out in duplicate using TaqMan probes. Shown is a plot of change in fluorescence signal versus cycle number.

c. Parainfluenza virus 1

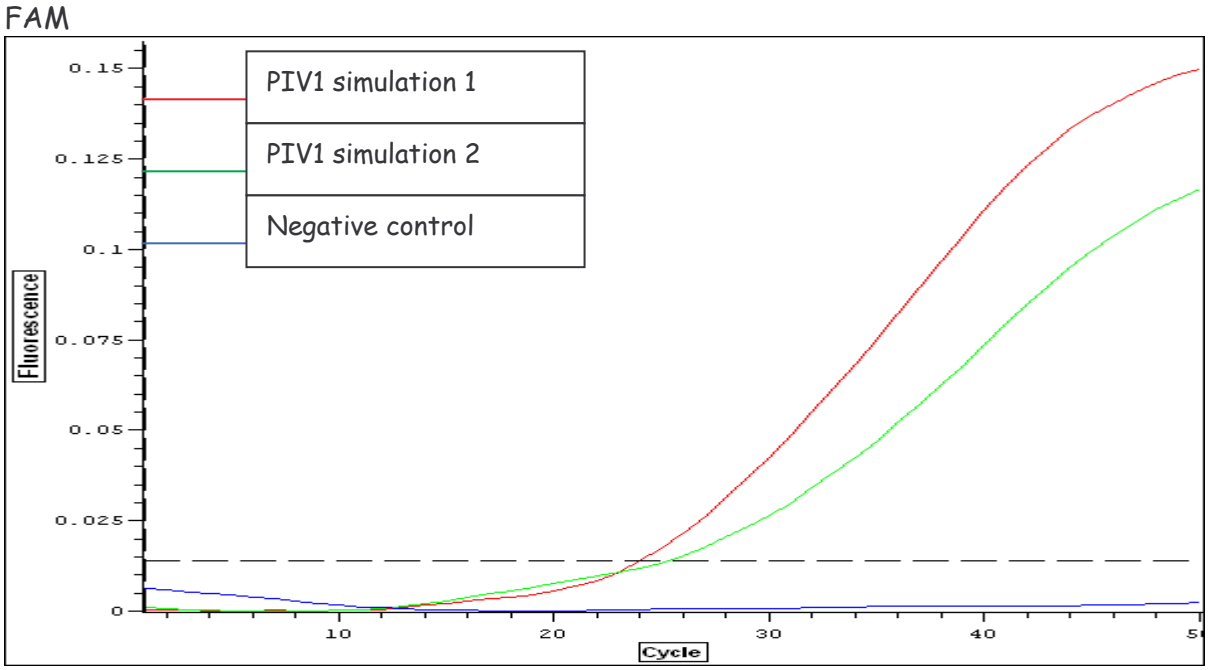

Figure E3: Fluorescence graph of PIV1 singleplex reaction performed on nucleic acids extracted from spiked nasopharyngeal swabs. Real-time PCR was carried out in duplicate using TaqMan probes. Shown is a plot of change in fluorescence signal versus cycle number.

d. Respiratory syncytial virus

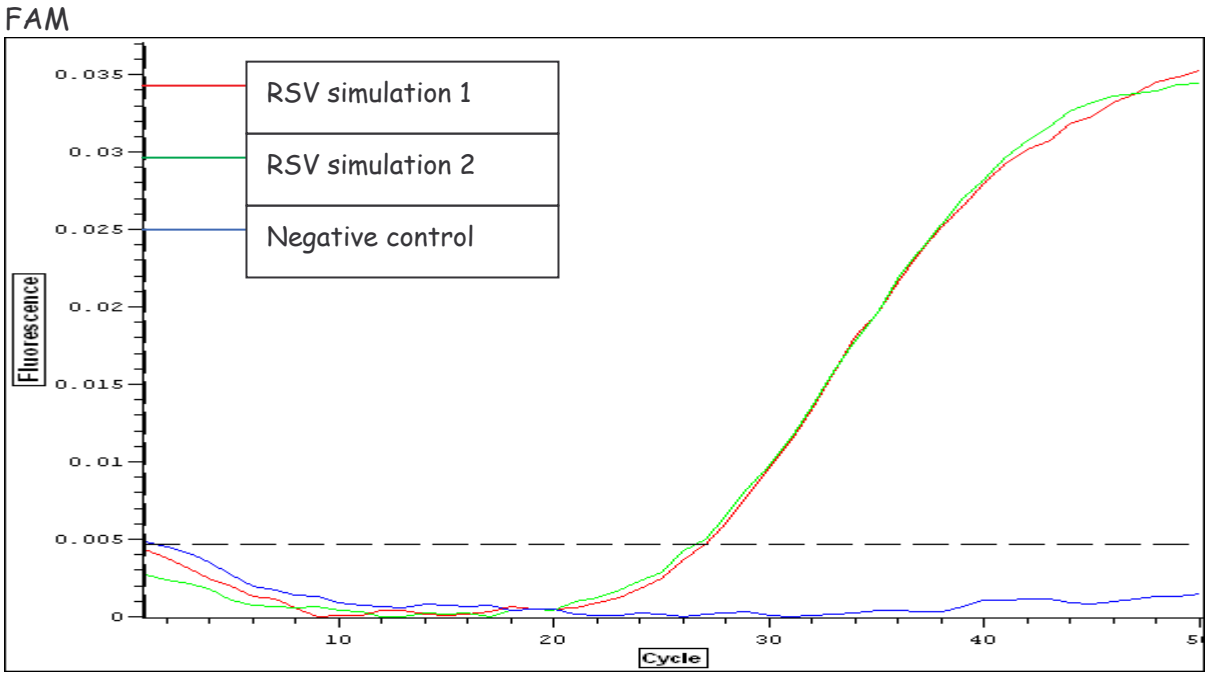

Figure E4: Fluorescence graph of RSV singleplex reaction performed on nucleic acids extracted from spiked nasopharyngeal swabs. Real-time PCR was carried out in duplicate using TaqMan probes. Shown is a plot of change in fluorescence signal versus cycle number.

Cytomegalovirus

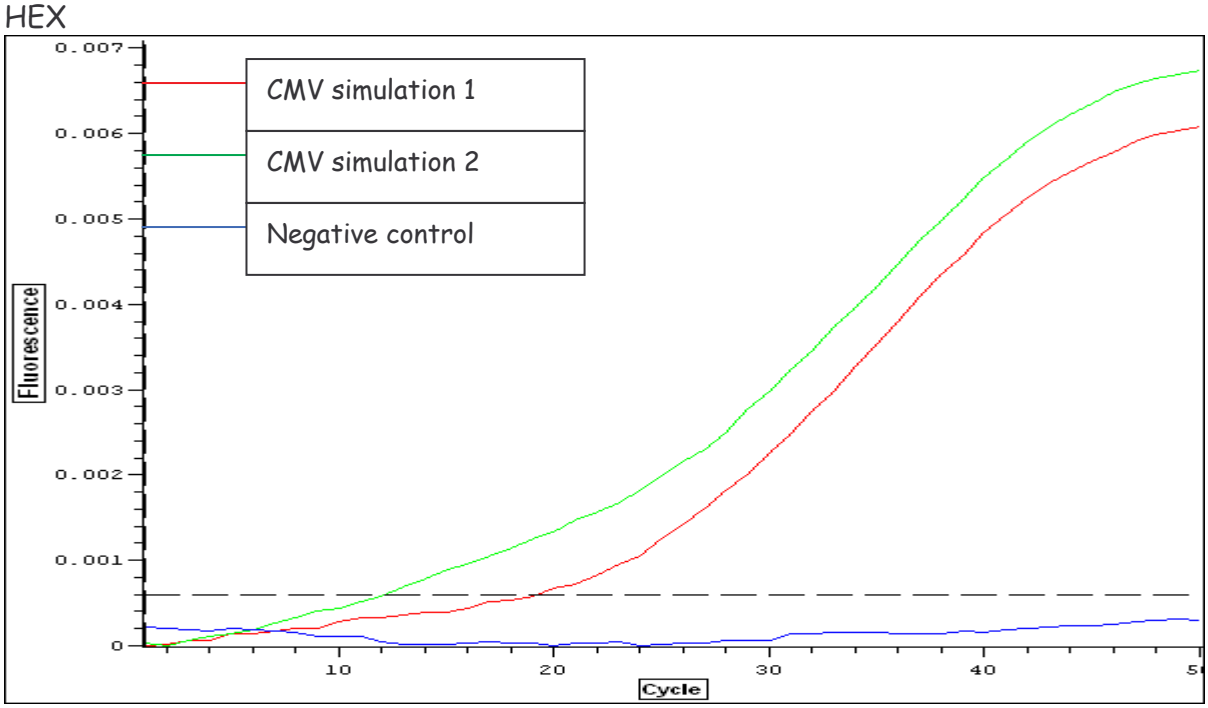

Figure E5: Fluorescence graph of CMV singleplex reaction performed on nucleic acids extracted from spiked nasopharyngeal swabs. Real-time PCR was carried out in duplicate using TaqMan probes. Shown is a plot of change in fluorescence signal versus cycle number.

e. *L. pneumophila*

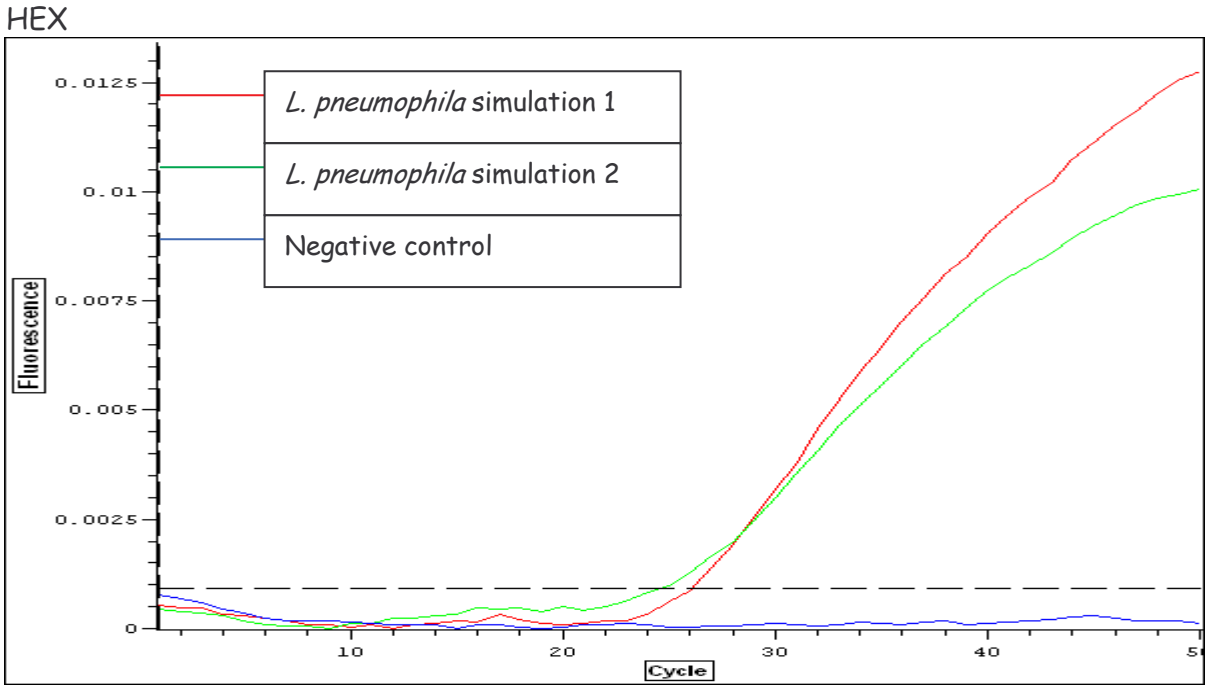

Figure E6: Fluorescence graph of *L. pneumophila* singleplex reaction performed on nucleic acids extracted from spiked sputum samples. Real-time PCR was carried out in duplicate using TaqMan probes. Shown is a plot of change in fluorescence signal versus cycle number.

C. pneumoniae

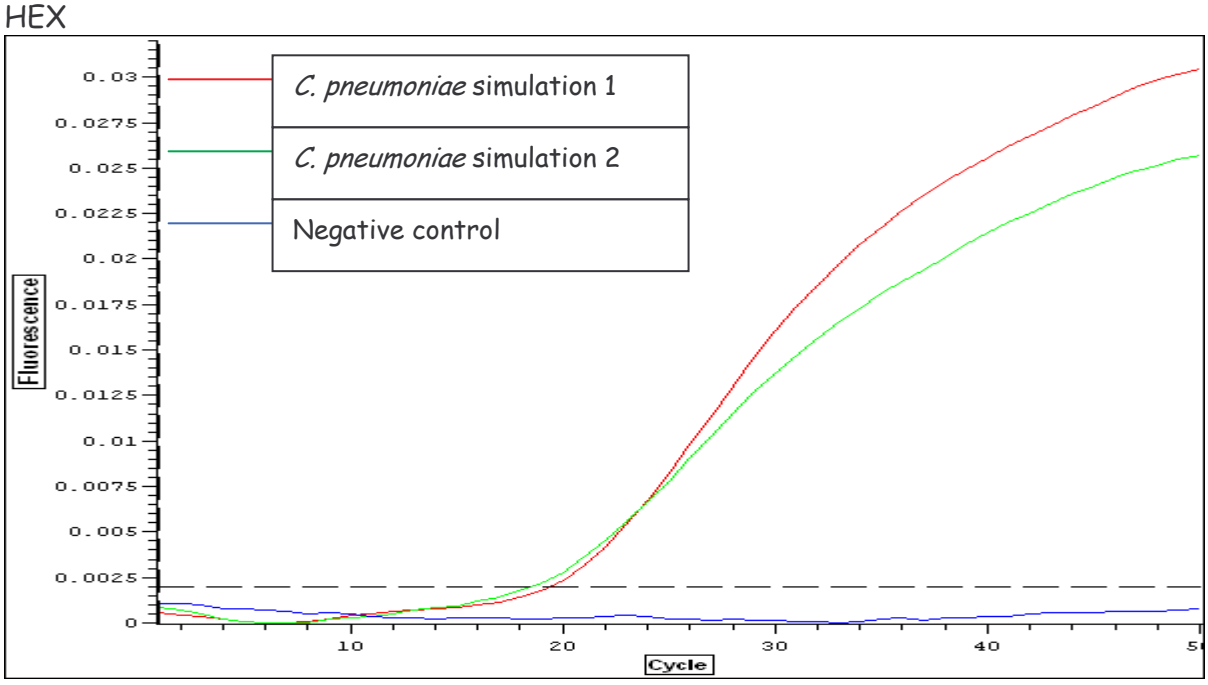

Figure E7: Fluorescence graph of *C. pneumoniae* singleplex reaction performed on nucleic acids extracted from spiked sputum samples. Real-time PCR was carried out in duplicate using TaqMan probes. Shown is a plot of change in fluorescence signal versus cycle number.

f. *C. psittaci*

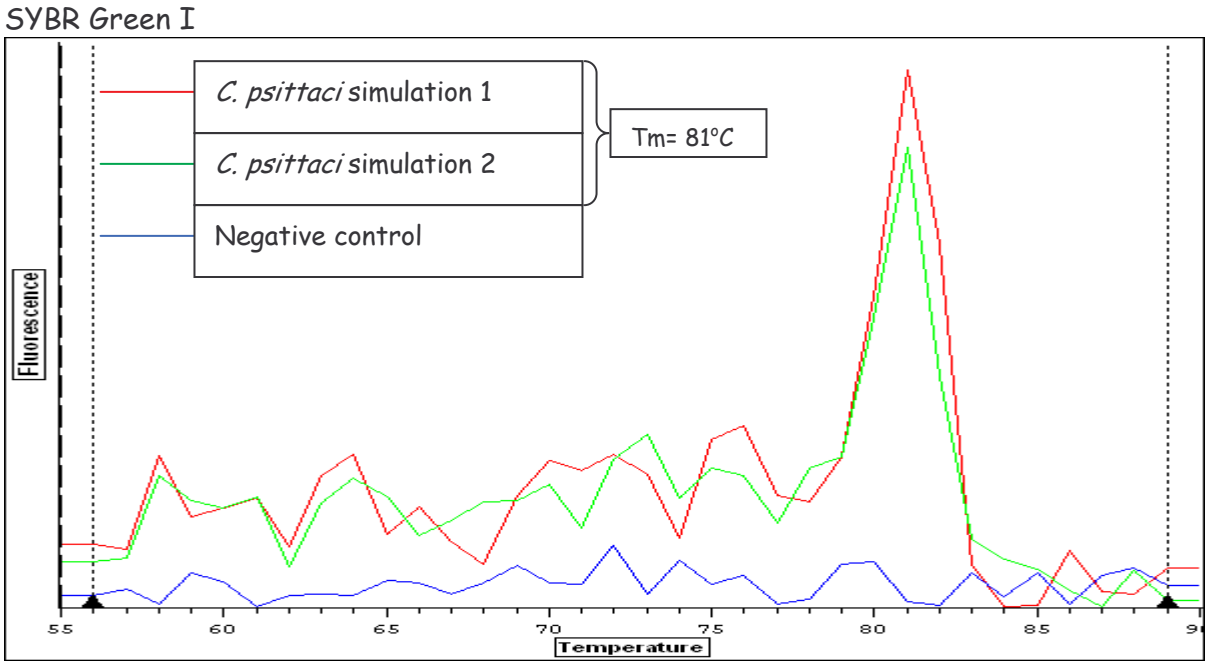

Figure E8: Melting curve analysis of *C. psittaci* singleplex reaction performed on nucleic acids extracted from spiked sputum samples. Real-time PCR was carried out in duplicate using SYBR Green I. The signature melting temperature of *C. psittaci* (81°C) is indicated by the sharp red and green peaks. Shown is a plot of temperature versus fluorescence signal.

g. Parainfluenza virus 2

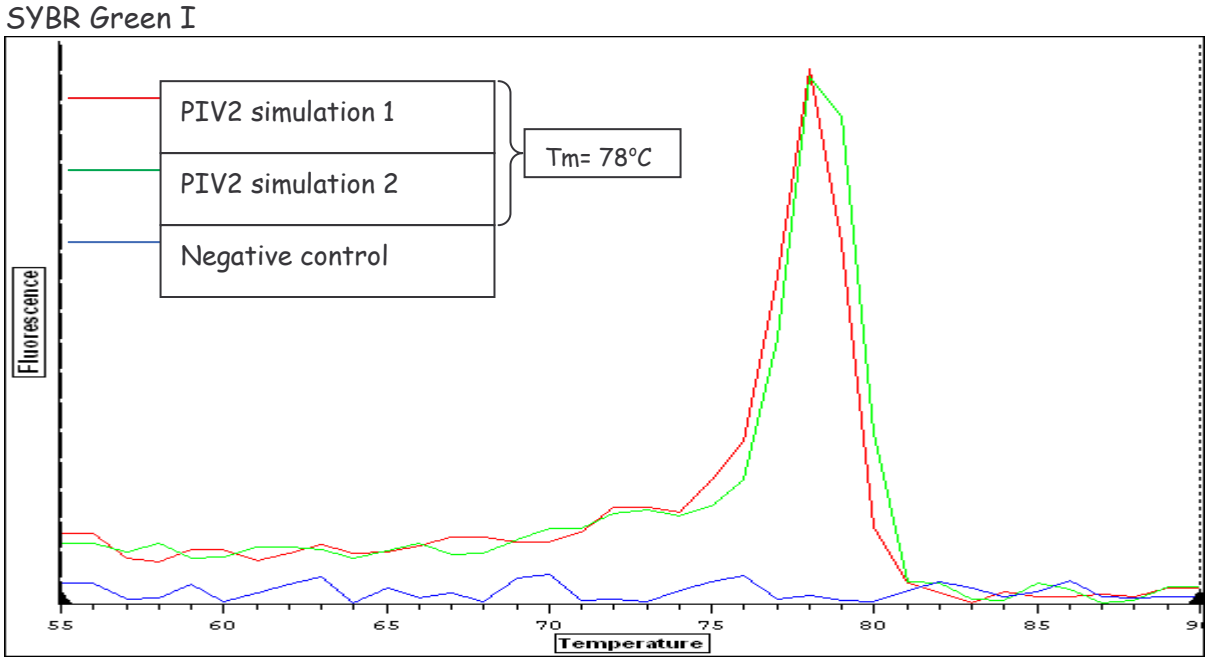

Figure E9: Melting curve analysis of PIV2 singleplex reaction performed on nucleic acids extracted from spiked nasopharyngeal swabs. Real-time PCR was carried out in duplicate using SYBR Green I. The signature melting temperature of PIV2 (78°C) is indicated by the sharp red and green peaks. Shown is a plot of temperature versus fluorescence signal.

7.5.1.2. Multiplex reactions

a. GAPDH (DNA) and *C. pneumoniae*

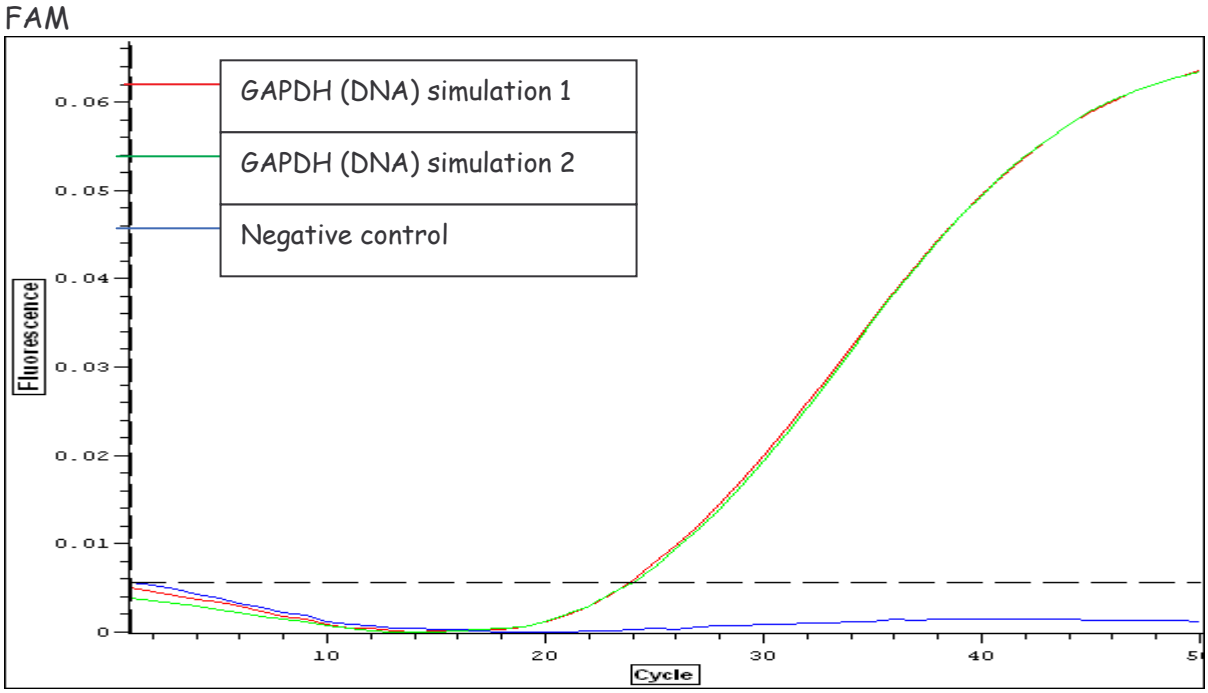

Figure E10a: Fluorescence graph of GAPDH (DNA) multiplex reaction performed on nucleic acids extracted from spiked sputum samples. Real-time PCR was performed in duplicate. Shown is a plot of change in fluorescence signal versus cycle number obtained using TaqMan probes.

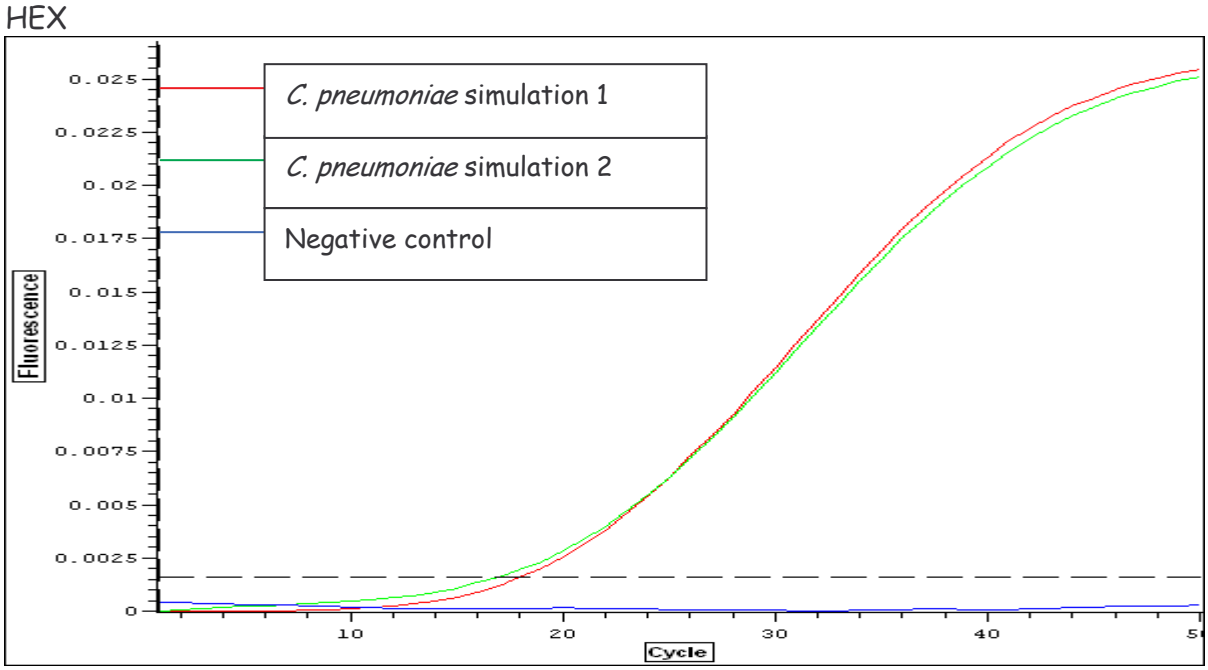

Figure E10b: Fluorescence graph of *C. pneumoniae* multiplex reaction performed on nucleic acids extracted from spiked sputum samples. Real-time PCR was performed in duplicate. Shown is a plot of change in fluorescence signal versus cycle number obtained using TaqMan probes.

7.5.2. Pathogen detection in CAP patient samples

7.5.2.1. Singleplex reactions

a. GAPDH (DNA): Patient sputum samples

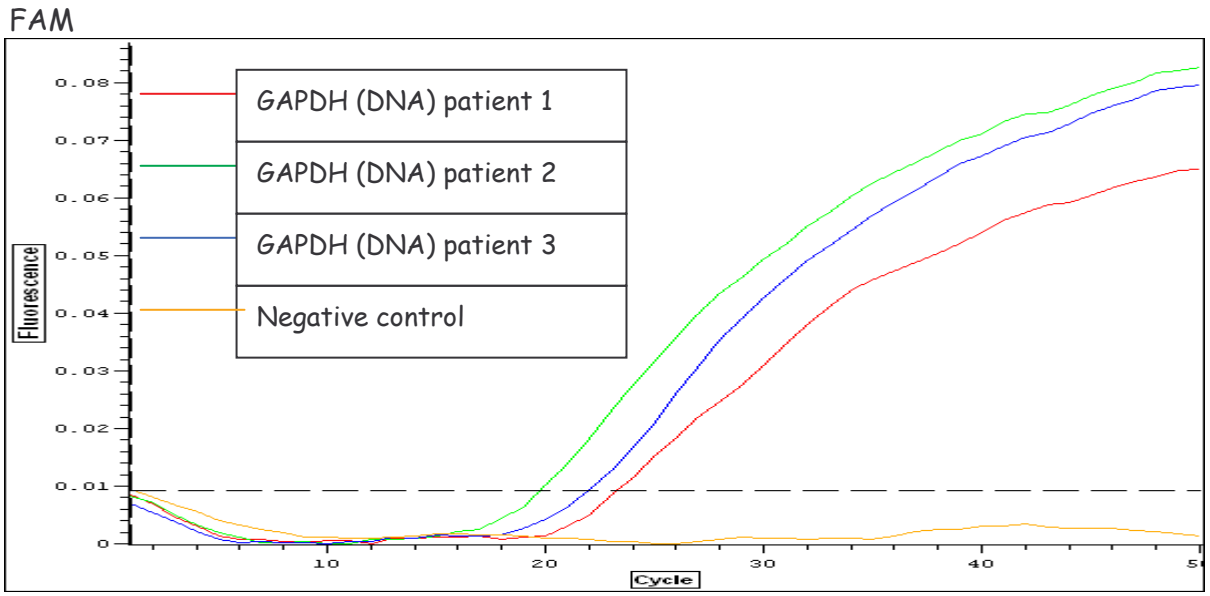

Figure E11: Fluorescence graph of GAPDH (DNA) singleplex reaction performed on nucleic acids extracted from sputum samples taken from CAP patients. Real-time PCR was performed in duplicate using TaqMan probes. Shown is a plot of change in fluorescence signal versus cycle number.

b. GAPDH (DNA): Patient nasopharyngeal swabs

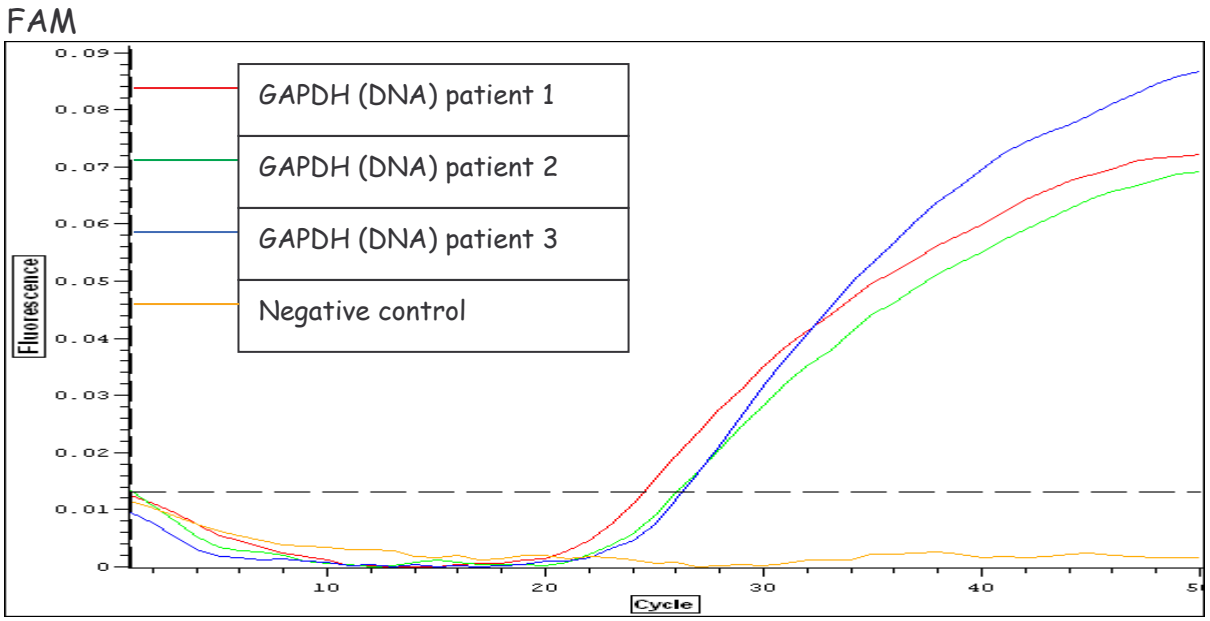

Figure E12: Fluorescence graph of GAPDH (DNA) singleplex reaction performed on nucleic acids extracted from nasopharyngeal swabs taken from CAP patients. Real-time PCR was performed in duplicate using TaqMan probes. Shown is a plot of change in fluorescence signal versus cycle number.

GAPDH (RNA): Patient nasopharyngeal swabs

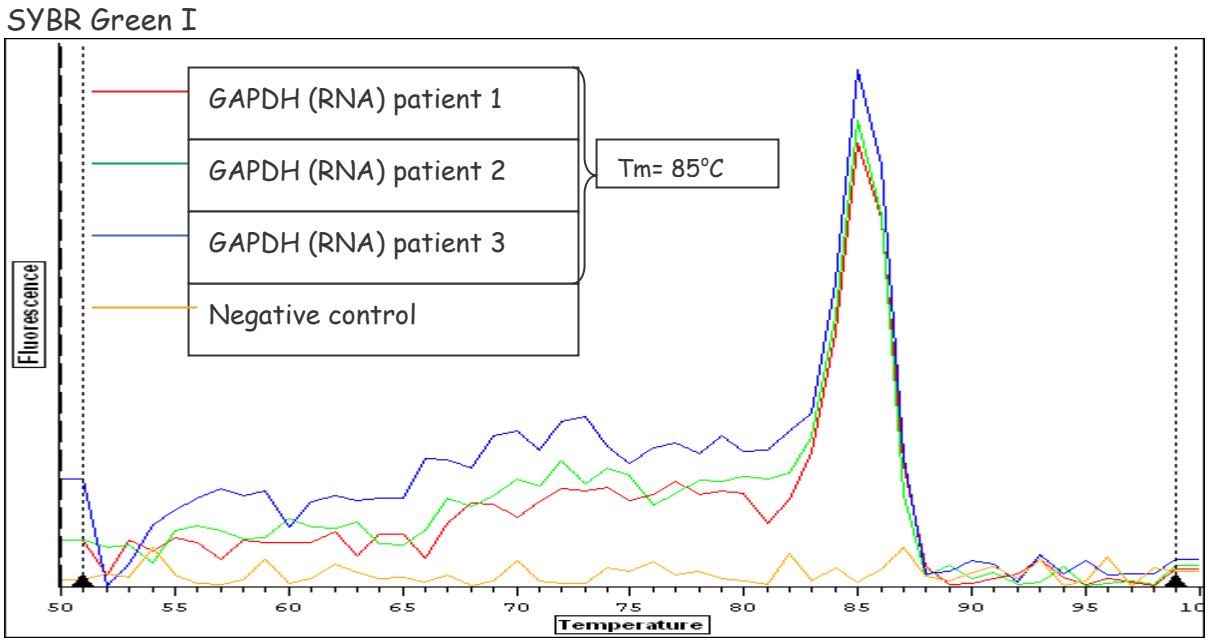

Figure E13: Melting curve analysis of GAPDH (RNA) singleplex reaction performed on nucleic acids extracted from sputum samples taken from CAP patients. Real-time PCR was performed in duplicate using SYBR Green I. Shown is a plot of temperature versus fluorescence signal.

c. *P. jirovecii*

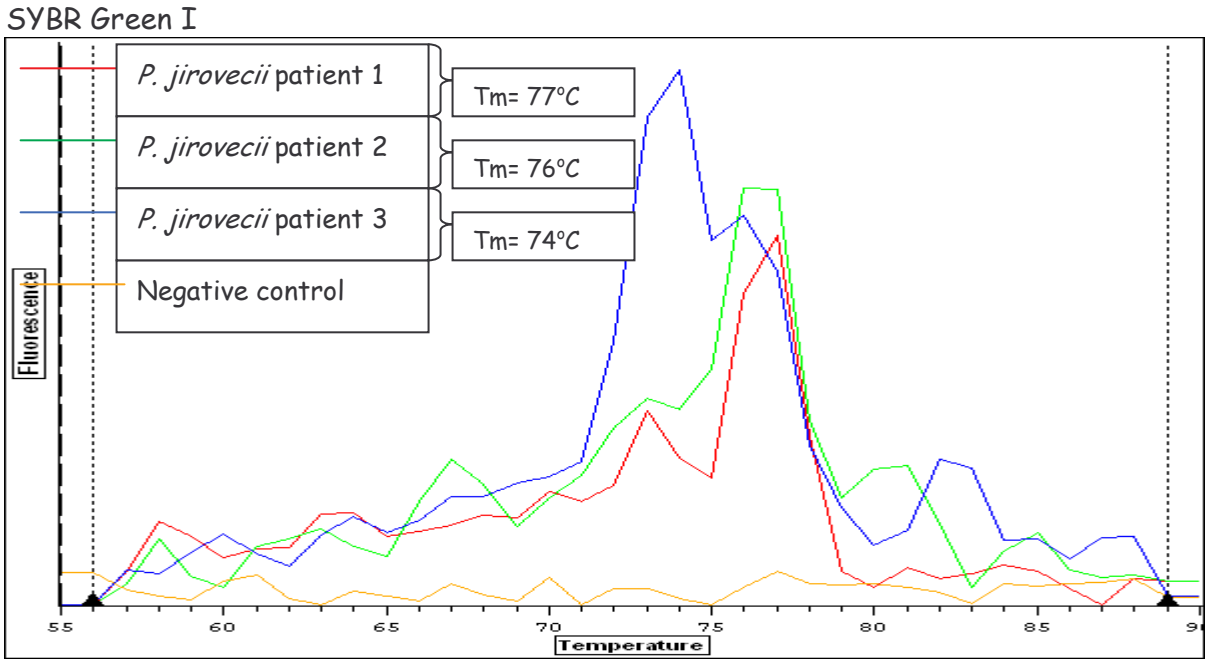

Figure E14: Melting curve analysis of *P. jirovecii* singleplex reaction performed on nucleic acids extracted from sputum samples taken from CAP patients. Real-time PCR was performed in duplicate using SYBR Green I. Shown is a plot of temperature versus fluorescence signal.

d. *C. psittaci*

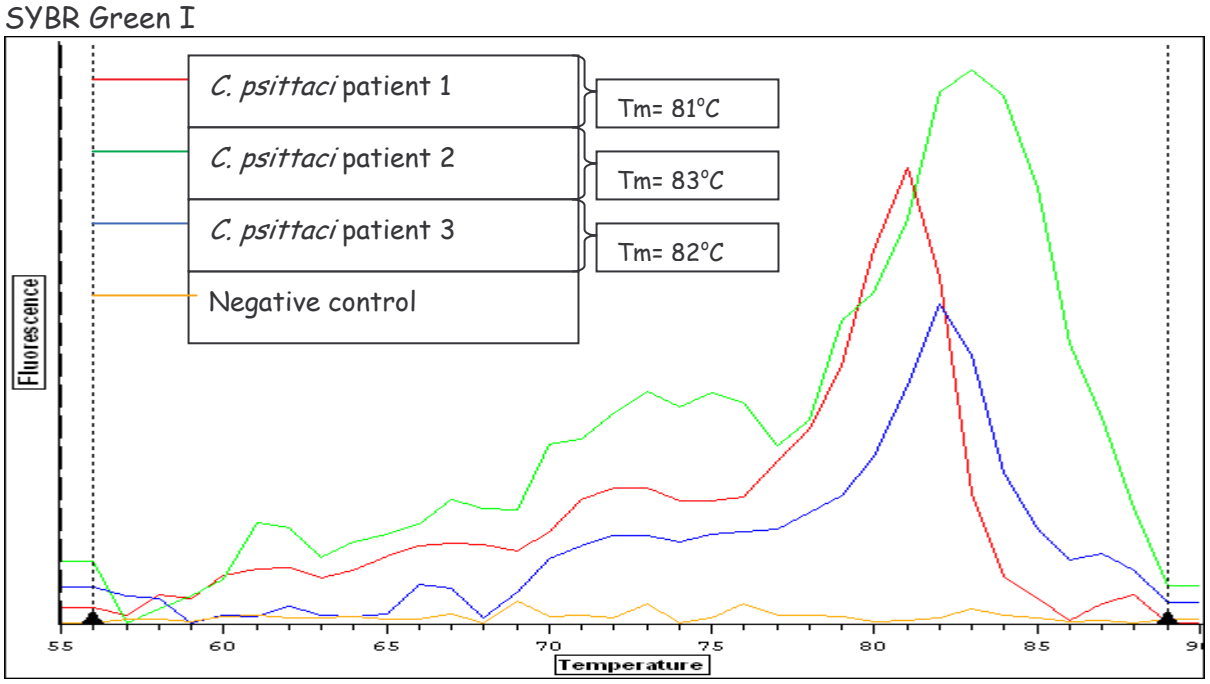

Figure E15: Melting curve analysis of *C. psittaci* singleplex reaction performed on nucleic acids extracted from sputum samples taken from CAP patients. Real-time PCR was performed in duplicate using SYBR Green I. Shown is a plot of temperature versus fluorescence signal.

e. PIV2

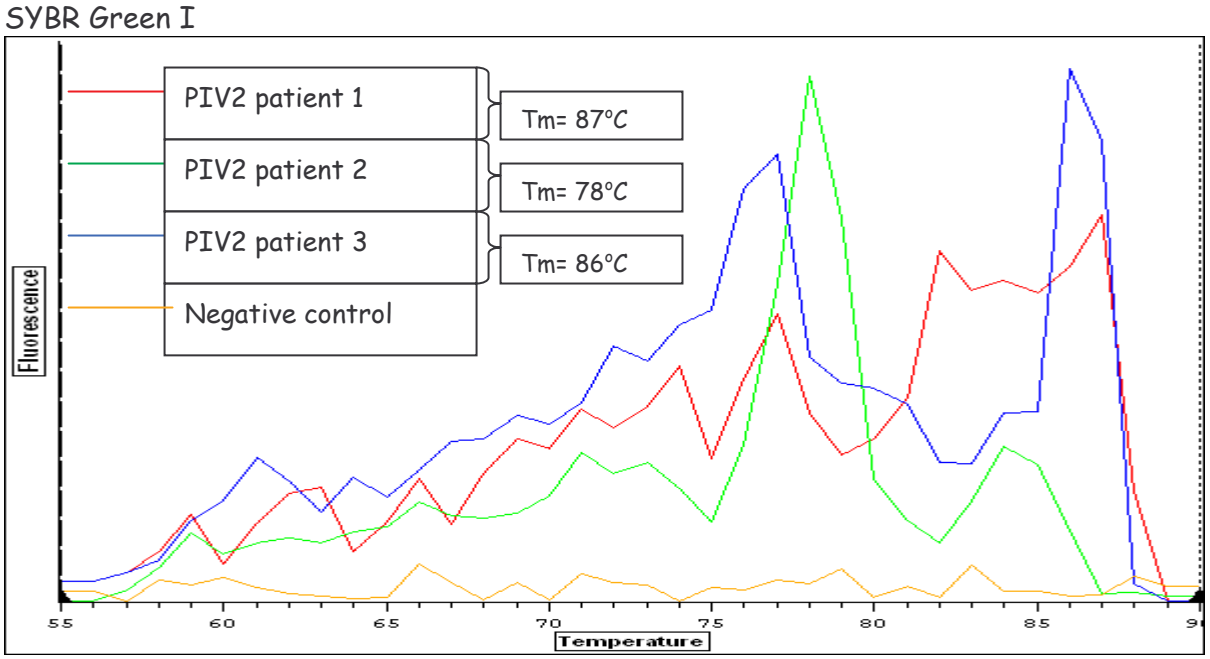

Figure E16: Melting curve analysis of PIV2 singleplex reaction performed on nucleic acids extracted from nasopharyngeal swabs taken from CAP patients. Real-time PCR was performed in duplicate using SYBR Green I. Shown is a plot of temperature versus fluorescence signal.

*7.5.2.2.*Multiplex reactions

a. PIV1 and PIV3

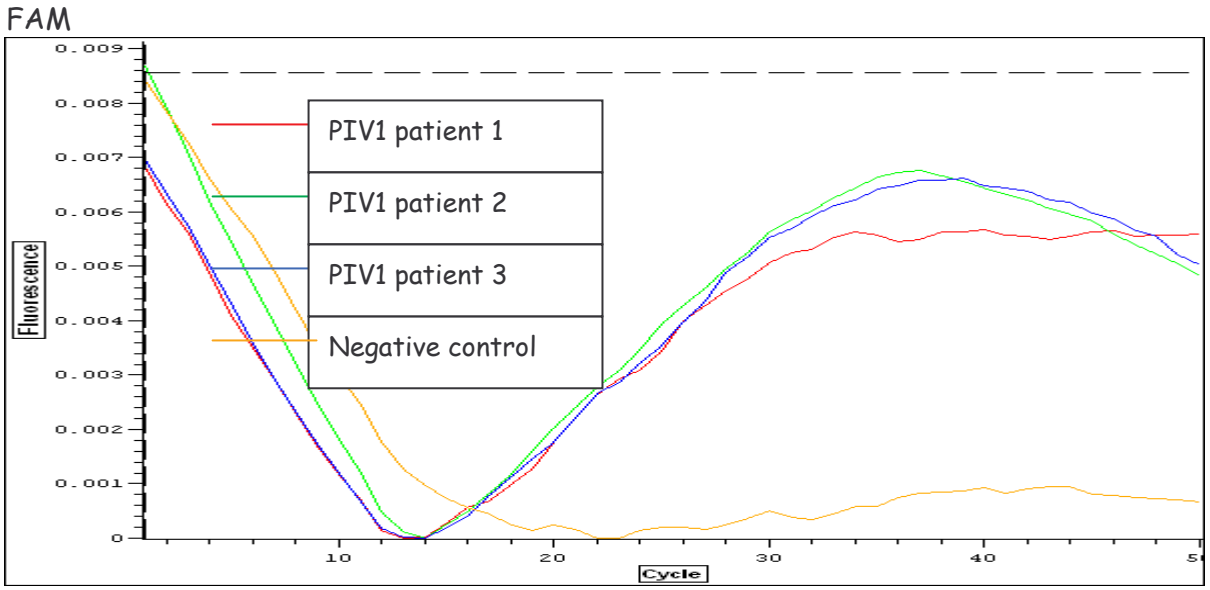

Figure E17a: Fluorescence graph of PIV1 multiplex reaction performed on nucleic acids extracted from nasopharyngeal swabs taken from CAP patients. Shown is a plot of change in fluorescence signal versus cycle number obtained using TaqMan probes.

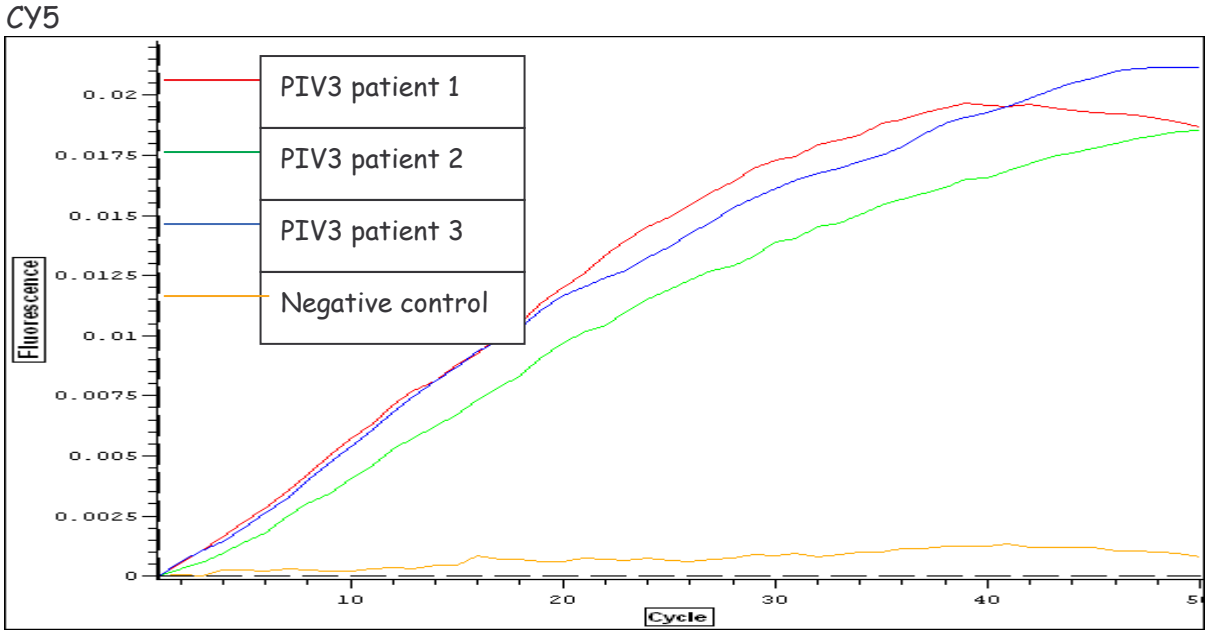

Figure E17b: Fluorescence graph of PIV3 multiplex reaction performed on nucleic acids extracted from nasopharyngeal swabs taken from CAP patients. Shown is a plot of change in fluorescence signal versus cycle number obtained using TaqMan probes.

b. CMV and EBV

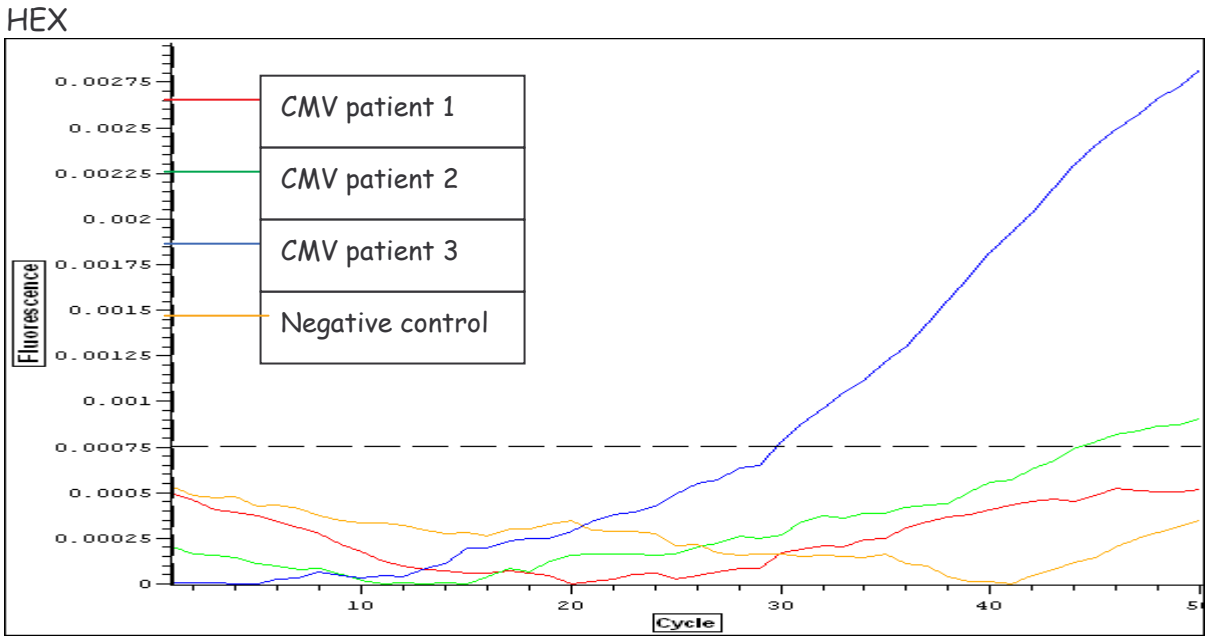

Figure E18a: Fluorescence graph of CMV multiplex reaction performed on nucleic acids extracted from nasopharyngeal swabs taken from CAP patients. Shown is a plot of change in fluorescence signal versus cycle number obtained using TaqMan probes.

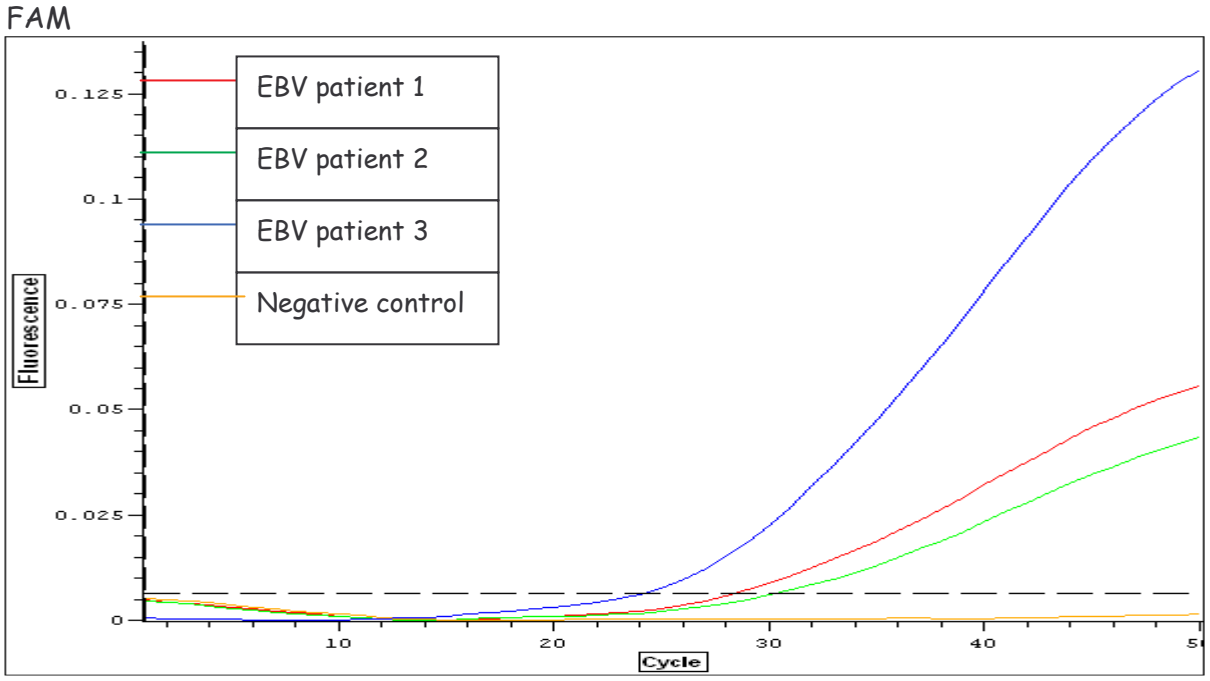

Figure E18b: Fluorescence graph of EBV multiplex reaction performed on nucleic acids extracted from nasopharyngeal swabs taken from CAP patients. Shown is a plot of change in fluorescence signal versus cycle number obtained using TaqMan probes.

c. *M. pneumoniae* and *L. pneumophila*

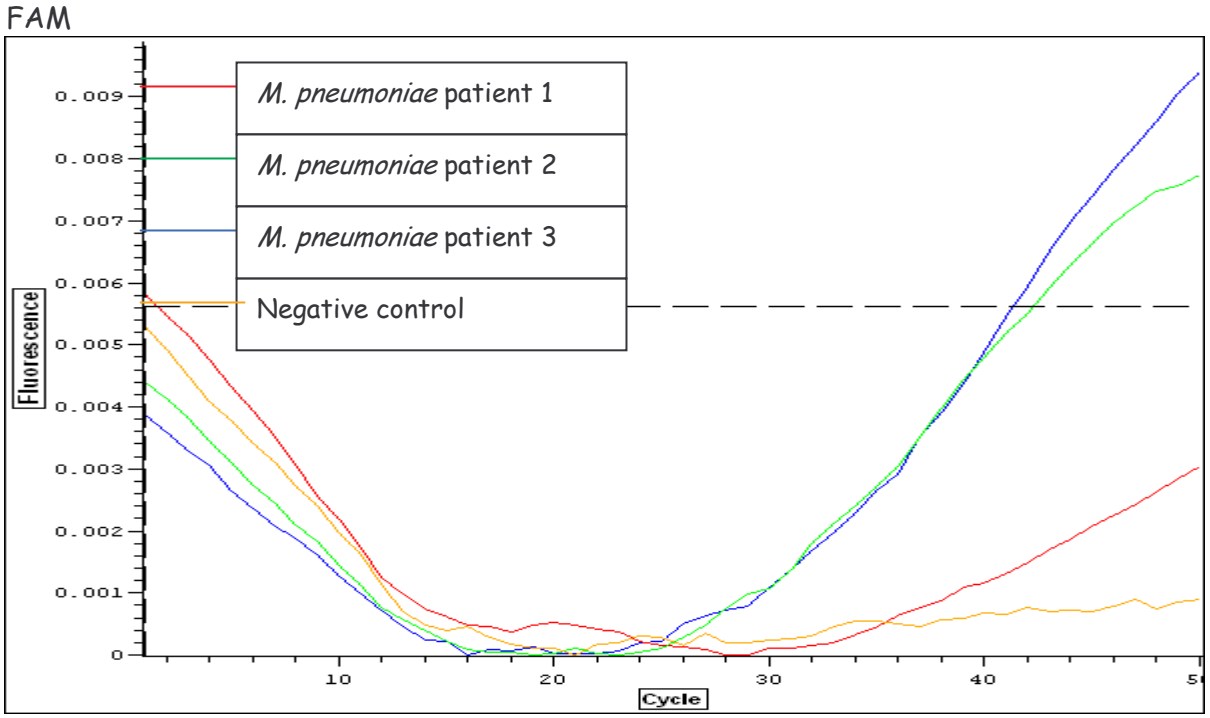

Figure E19a: Fluorescence graph of *M. pneumoniae* multiplex reaction performed on nucleic acids extracted from sputum samples taken from CAP patients. Shown is a plot of change in fluorescence signal versus cycle number obtained using TaqMan probes.

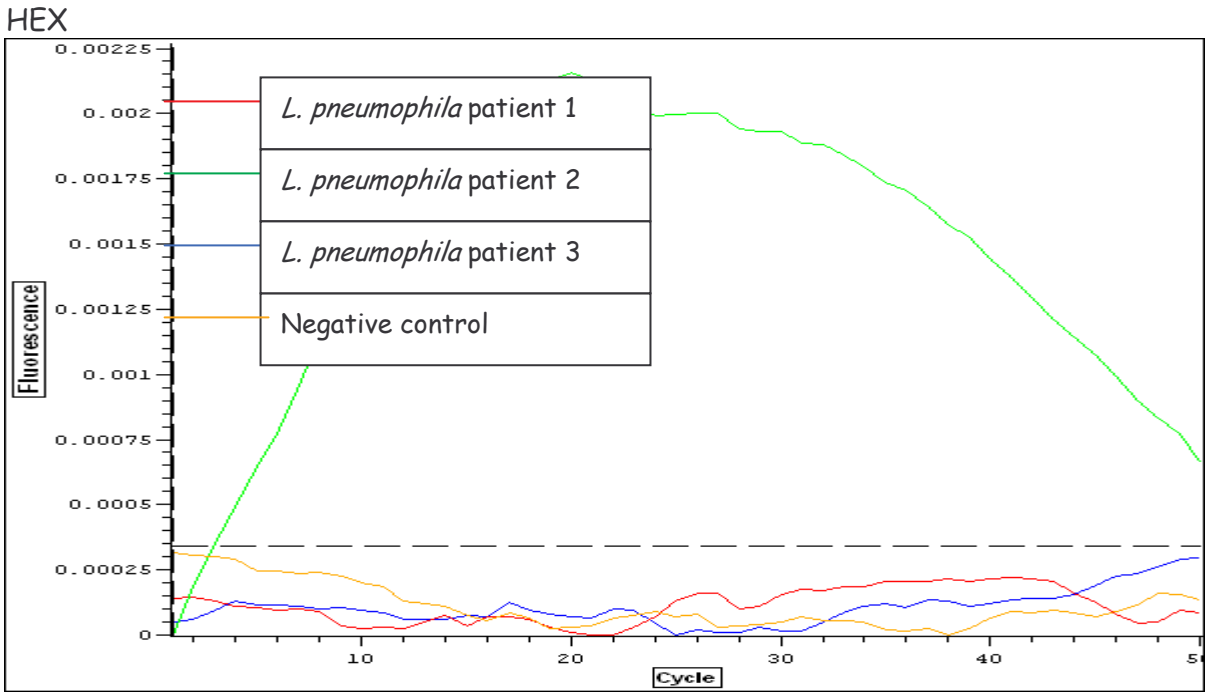

Figure E19b: Fluorescence graph of *L. pneumophila* multiplex reaction performed on nucleic acids extracted from sputum samples taken from CAP patients. Shown is a plot of change in fluorescence signal versus cycle number obtained using TaqMan probes.

d. RSV and AdV

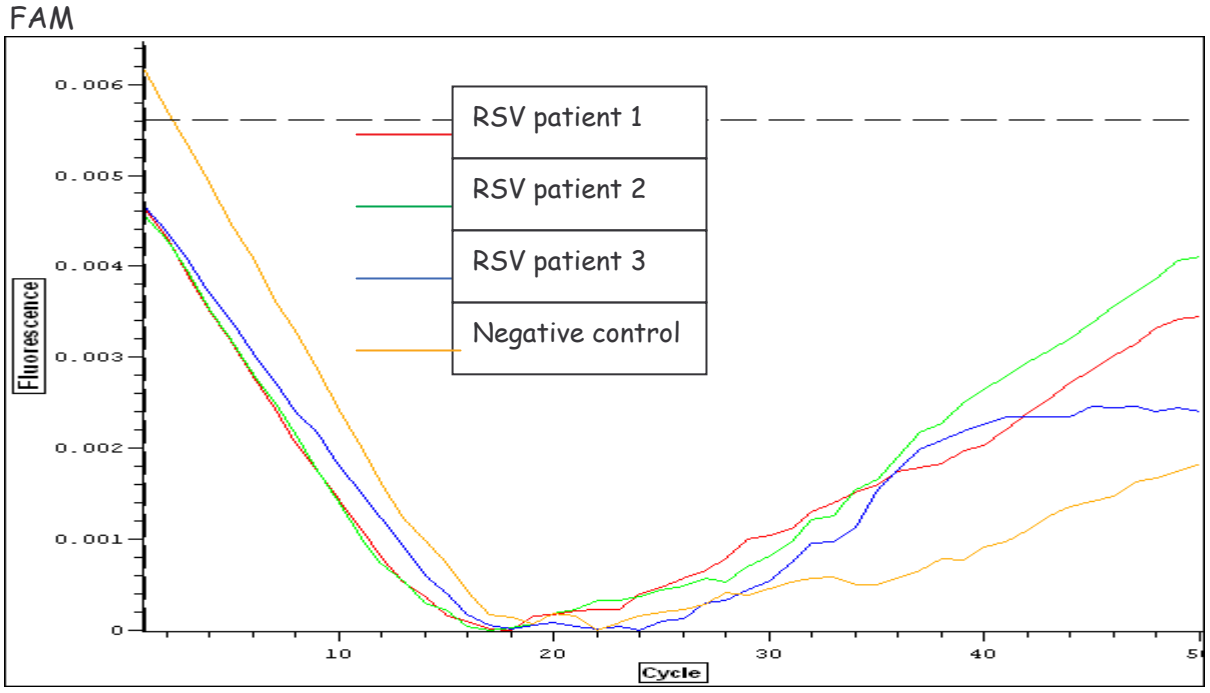

Figure E20a: Fluorescence graph of RSV multiplex reaction performed on nucleic acids extracted from nasopharyngeal swabs taken from CAP patients. Shown is a plot of change in fluorescence signal versus cycle number obtained using TaqMan probes.

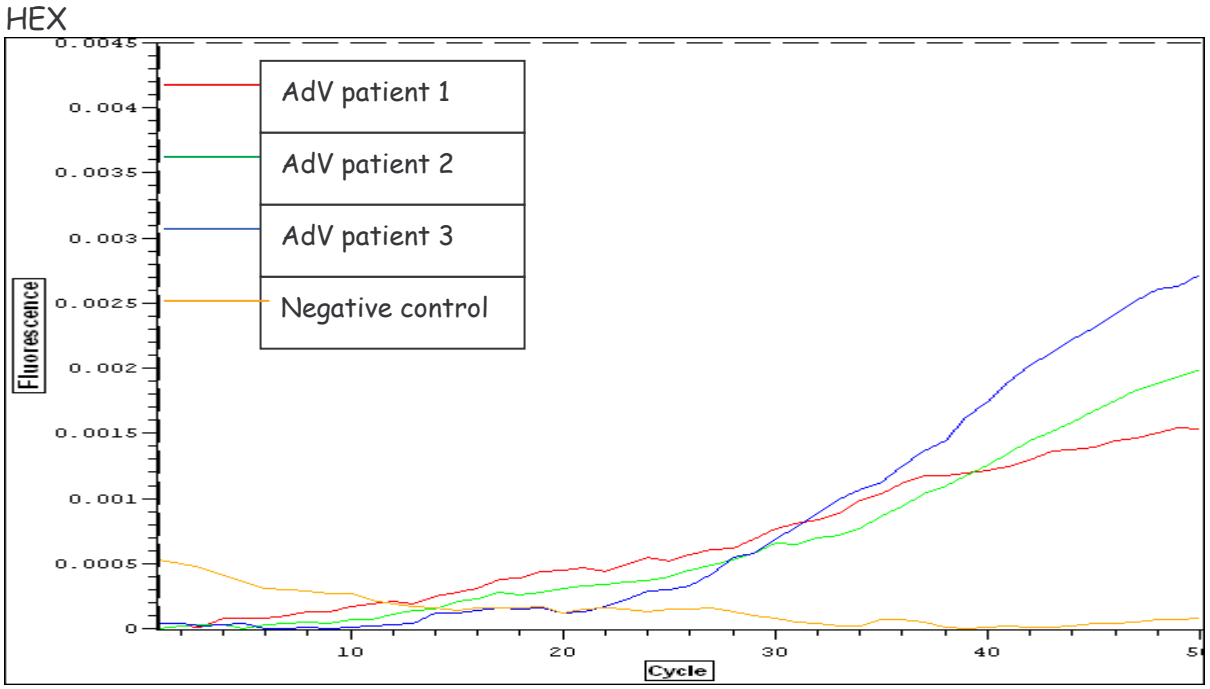

Figure E20b: Fluorescence graph of AdV multiplex reaction performed on nucleic acids extracted from nasopharyngeal swabs taken from CAP patients. Shown is a plot of change in fluorescence signal versus cycle number obtained using TaqMan probes.

e. *C. pneumoniae* and GAPDH (DNA)

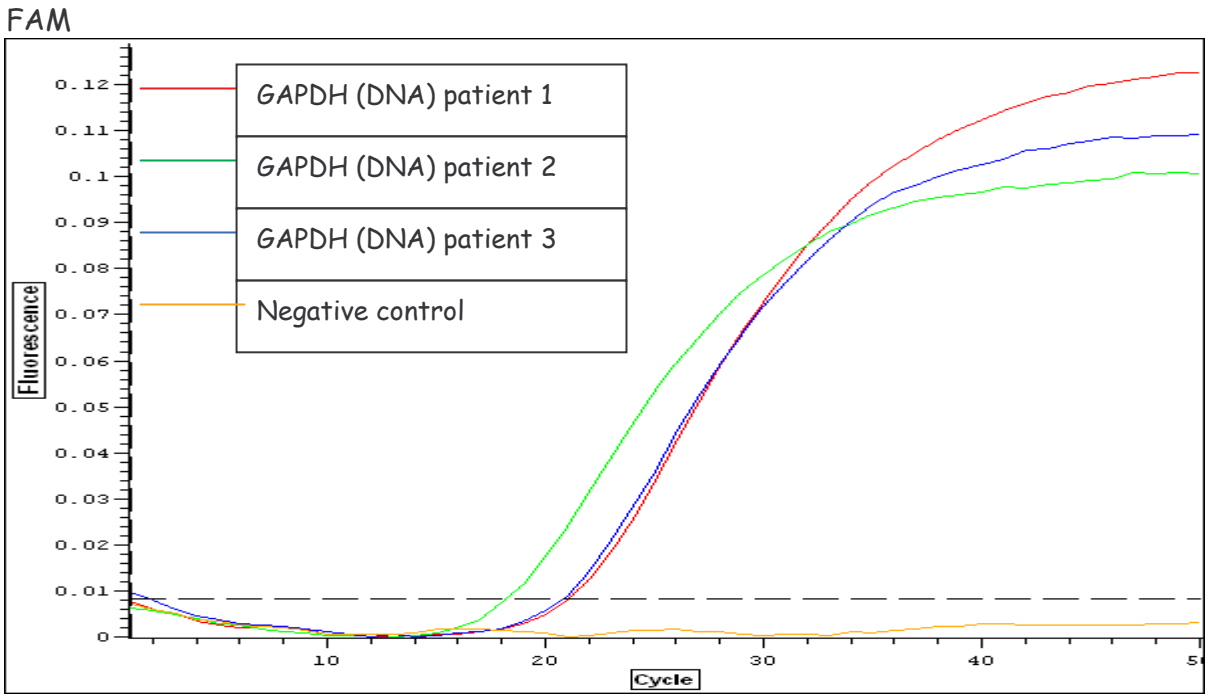

Figure E21a: Fluorescence graph of GAPDH (DNA) multiplex reaction performed on nucleic acids extracted from sputum samples taken from CAP patients. Shown is a plot of change in fluorescence signal versus cycle number obtained using TaqMan probes.

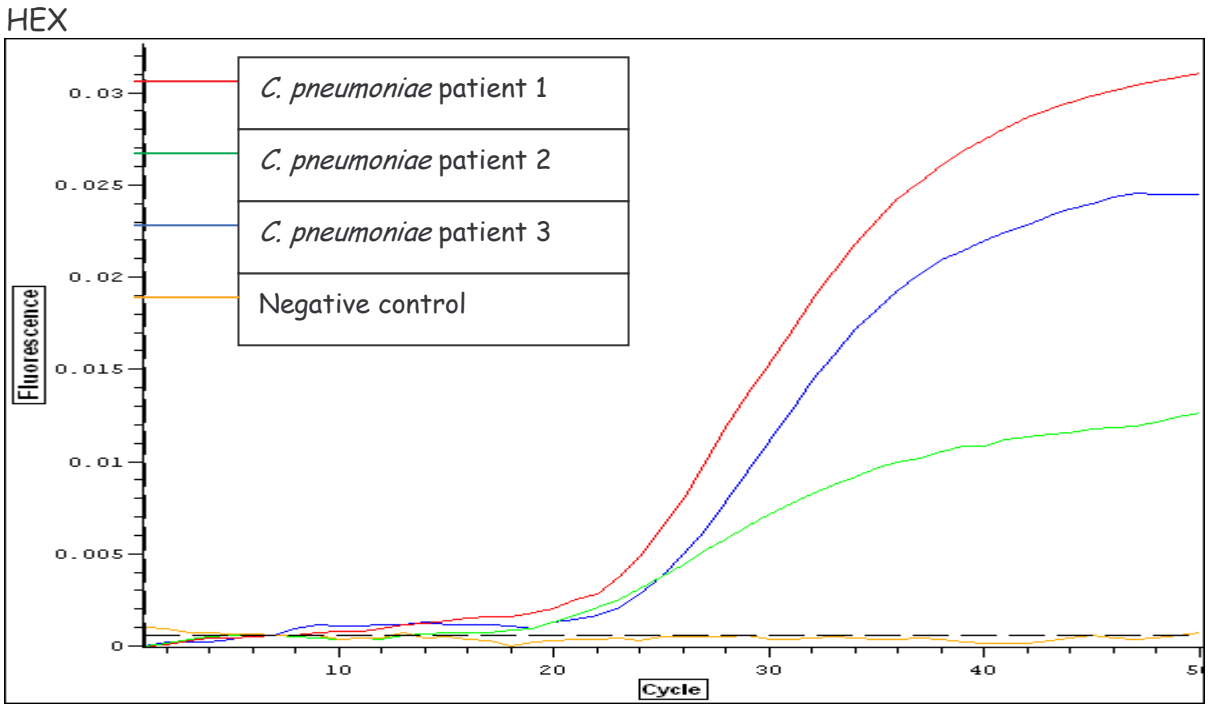

Figure E21b: Fluorescence graph of *C. pneumoniae* multiplex reaction performed on nucleic acids extracted from sputum samples taken from CAP patients. Shown is a plot of change in fluorescence signal versus cycle number obtained using TaqMan probes.

f. FluA, FluB and hMPV

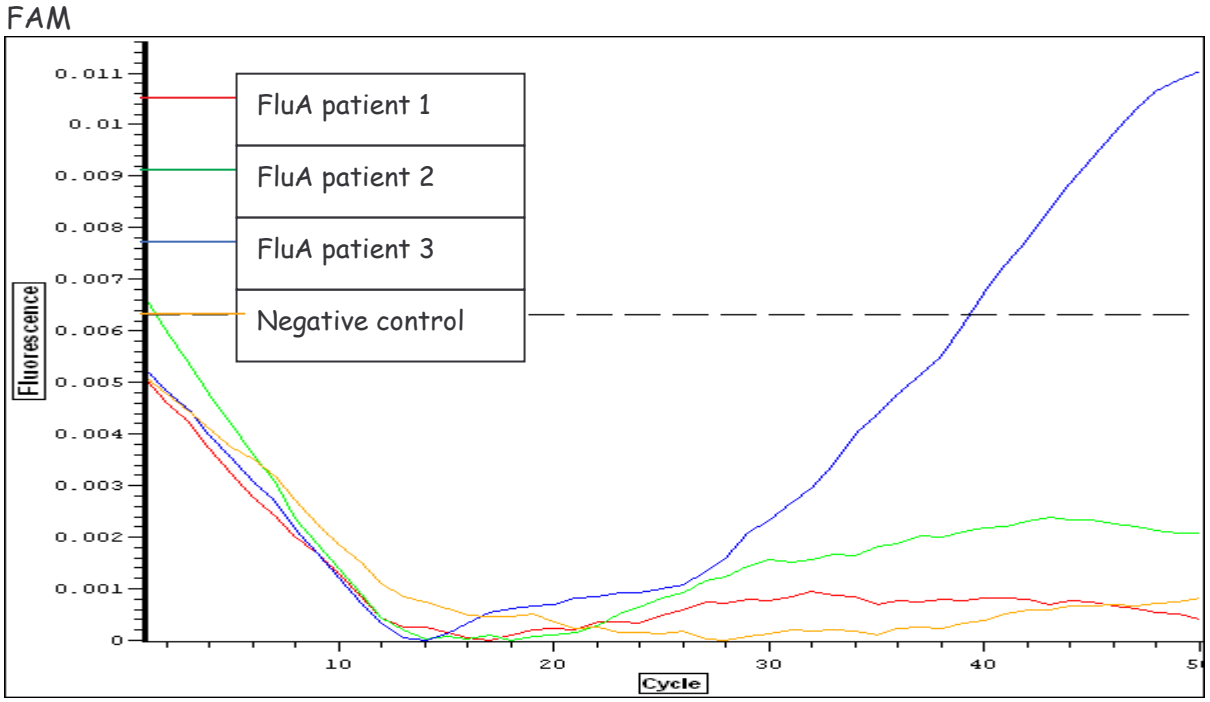

Figure E22a: Fluorescence graph of FluA multiplex reaction performed on nucleic acids extracted from nasopharyngeal swabs taken from CAP patients Shown is a plot of change in fluorescence signal versus cycle number obtained using TaqMan probes.

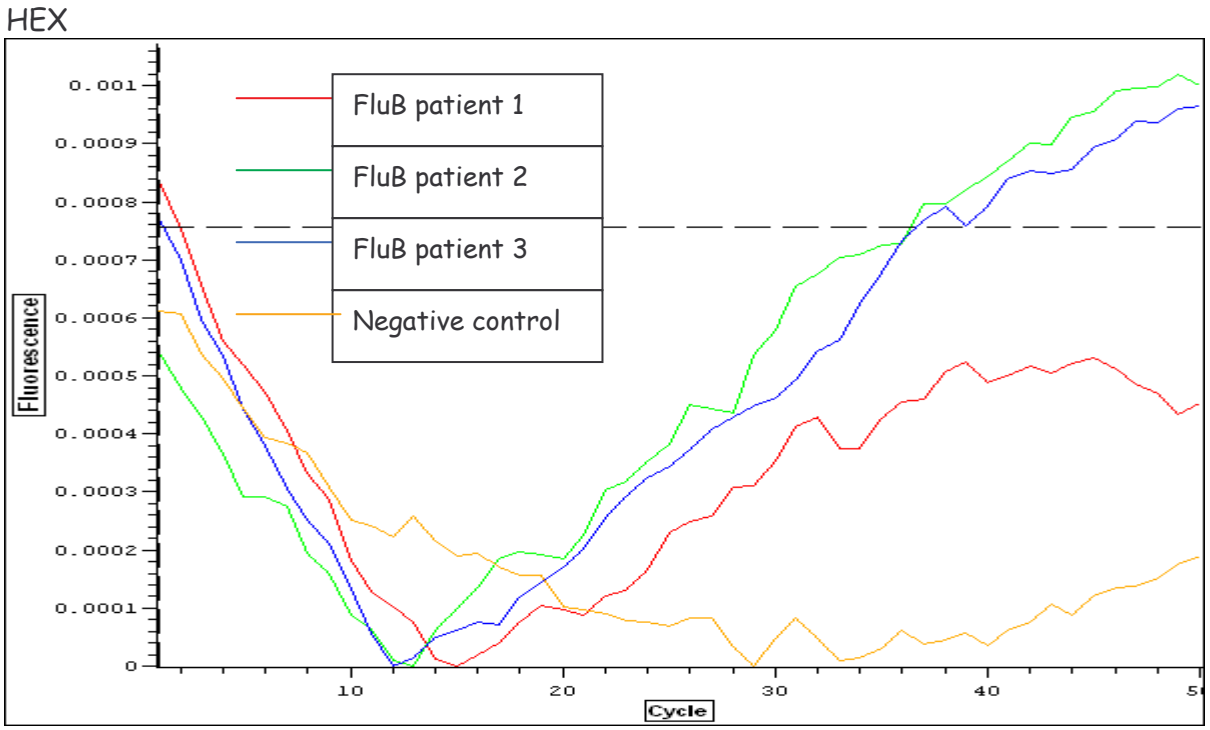

Figure E22b: Fluorescence graph of FluB multiplex reaction performed on nucleic acids extracted from nasopharyngeal swabs taken from CAP patients. Shown is a plot of change in fluorescence signal versus cycle number obtained using TaqMan probes.

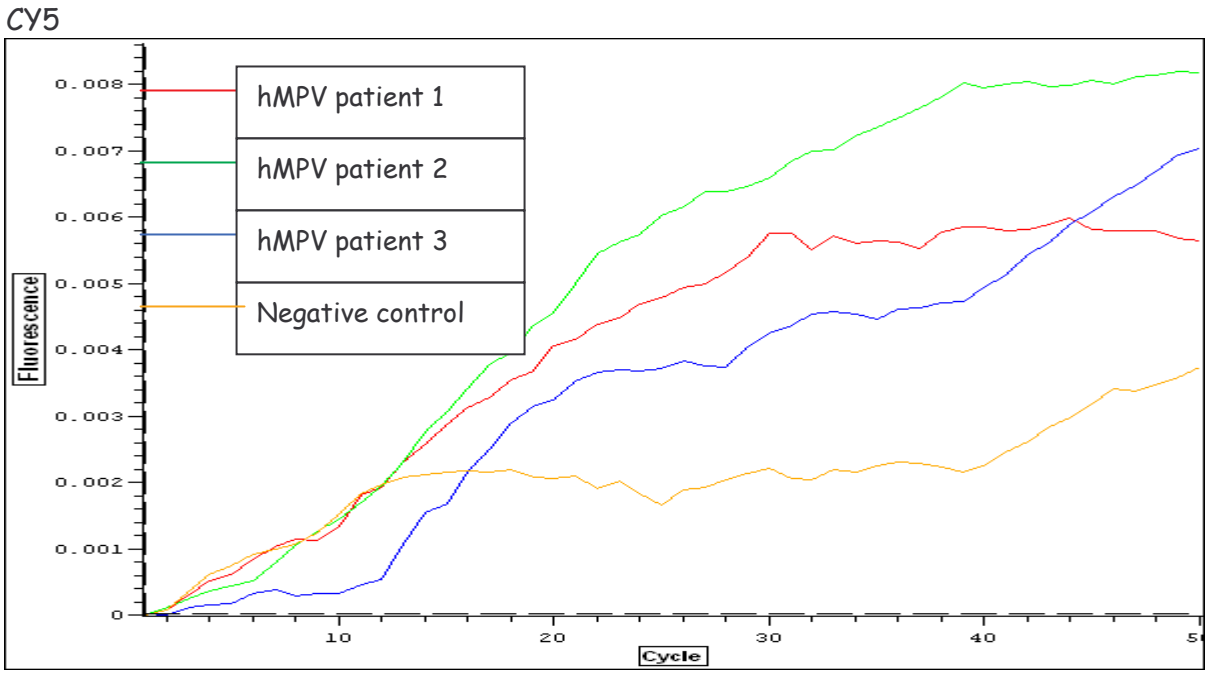

Figure E22c: Fluorescence graph of hMPV multiplex reaction performed on nucleic acids extracted from nasopharyngeal swabs taken from CAP patients. Shown is a plot of change in fluorescence signal versus cycle number obtained using TaqMan probes.

CHAPTER 7: APPENDIX F

UNIVERSITY OF THE WITWATERSRAND, JOHANNESBURG

Division of the Deputy Registrar (Research)

HUMAN RESEARCH ETHICS COMMITTEE (MEDICAL)
R14/49 Perovic

CLEARANCE CERTIFICATE	**PROTOCOL NUMBER M070345**
PROJECT	The Microbial Aetiology of Community-Acquired Pneumonia in Adults in South Africa
INVESTIGATORS	Dr O Perovic
DEPARTMENT	Molecular Medicine & Haem
DATE CONSIDERED	07.03.30
DECISION OF THE COMMITTEE*	APPROVED UNCONDITIONALLY

Unless otherwise specified this ethical clearance is valid for 5 years and may be renewed upon application.

DATE 07.06.14 **CHAIRPERSON** .....
(Professors PE Cleaton-Jones, A Dhai, M Vorster, C Feldman, A Woodiwiss)

*Guidelines for written 'informed consent' attached where applicable

cc: Supervisor : Dr O Perovic

DECLARATION OF INVESTIGATOR(S)

To be completed in duplicate and **ONE COPY** returned to the Secretary at Room 10005, 10th Floor, Senate House, University.
I/We fully understand the conditions under which I am/we are authorized to carry out the abovementioned research and I/we guarantee to ensure compliance with these conditions. Should any departure to be contemplated from the research procedure as approved I/we undertake to resubmit the protocol to the Committee. **I agree to a completion of a yearly progress report.**

PLEASE QUOTE THE PROTOCOL NUMBER IN ALL ENQUIRIES